

**CONTROL OF INDUCTION MOTORS
SUBJECT TO HARD-INPUT
NONLINEARITIES**

BY

HASSAN M. ALABUDIB

A Thesis Presented to the
DEANSHIP OF GRADUATE STUDIES

KING FAHD UNIVERSITY OF PETROLEUM & MINERALS

DHAHRAN, SAUDI ARABIA

1963 ١٣٨٣

In Partial Fulfillment of the
Requirements for the Degree of

MASTER OF SCIENCE

In

ELECTRICAL ENGINEERING

DECEMBER 2017

KING FAHD UNIVERSITY OF PETROLEUM & MINERALS
DHAHRAN 31261, SAUDI ARABIA

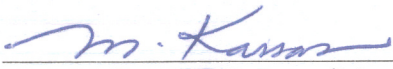
DEANSHIP OF GRADUATE STUDIES

This thesis, written by **HASSAN M. AL-ABUDIB** under the direction of his thesis adviser and approved by his thesis committee, has been presented to and accepted by the Dean of Graduate Studies, in partial fulfillment of the requirements for the degree of **MASTER OF SCIENCE IN ELECTRICAL ENGINEERING**.

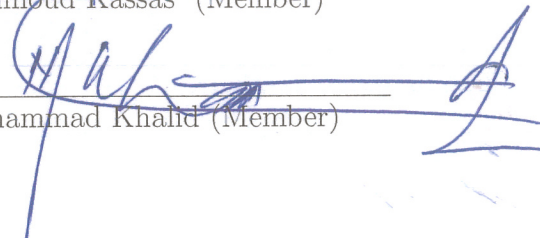
Thesis Committee



Dr. Salim Ibrir (Adviser)



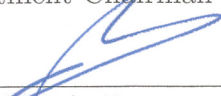
Dr. Mahmoud Kassas (Member)



Dr. Muhammad Khand (Member)



Dr. Ali Ahmad Al-Shaikhi
Department Chairman



Dr. Salam A. Zummo
Dean of Graduate Studies

Date

26/12/17



©Hassan M. Al-Abudib
2017

Dedication

This work is dedicated to my late father, who taught me to seek knowledge, work hard and never give up.

ACKNOWLEDGMENTS

All praise and glory be to Allah almighty, lord of the worlds, who has given me all the guidance, the strength and the support to complete this work. I would never have been able to achieve anything without his help and his countless blessings.

Firstly, I would like to thank King Fahad University of Petroleum and Minerals for offering such a great graduate program and giving me the opportunity to expand my understanding of my field of study and providing such a great facility and atmosphere for knowledge and research.

Also, I would like to thank my adviser Dr. Salim Ibrir for his tremendous help and support for me during my thesis journey. It has been a great honor and privilege to work with him and benefit from his deep knowledge and expertise.

Furthermore, my very sincere thanks and gratitude go to the thesis committee members for participating in evaluating my work and providing me with their valuable comments.

TABLE OF CONTENTS

ACKNOWLEDGEMENT	v
LIST OF TABLES	viii
LIST OF FIGURES	ix
LIST OF ABBREVIATIONS	xvi
ABSTRACT (ENGLISH)	xxiv
ABSTRACT (ARABIC)	xxvi
CHAPTER 1 INTRODUCTION	1
1.1 Introduction to Induction Motors	1
1.1.1 Basics, operation and applications	1
1.1.2 Control objectives and challenges	3
1.1.3 Control approaches	4
1.2 Input Nonlinearity Phenomena	5
1.3 Thesis Objective and Organization	6
CHAPTER 2 LITERATURE REVIEW	9
2.1 Induction Motors Control	9
2.2 Input Nonlinearity Compensation	13
CHAPTER 3 IM SYSTEM MODELING	17
3.1 IM Dynamical Models	17

3.2	IM Model for the Research	23
CHAPTER 4 BACKSTEPPING CONTROLLER DESIGN		25
4.1	Introduction to Adaptive Backstepping	25
4.2	Adaptive Backstepping Controller Design	26
4.3	Simulations and Results	33
CHAPTER 5 IM WITH SYMMETRIC DEAD-ZONE INPUT		51
5.1	Input Nonlinearity Effect	51
5.2	Symmetric Dead-zone Modeling	53
5.3	Controller Design for Symmetric Dead-zone Input	55
5.4	Simulations and Results	61
CHAPTER 6 IM WITH ASYMMETRIC DEAD-ZONE INPUT		80
6.1	Asymmetric Dead-zone Modeling	80
6.2	Controller Design for Asymmetric Dead-zone Input	83
6.3	Simulations and Results	90
CHAPTER 7 IM WITH BACKLASH INPUT		109
7.1	Backlash Modeling and Controller Design	110
7.2	Simulations and Results	114
CHAPTER 8 IM WITH BOUC-WEN HYSTERESIS INPUT		132
8.1	Bouc-Wen Hysteresis Modeling and Controller Design	132
8.2	Simulations and Results	140
CHAPTER 9 CONCLUSION AND FUTURE WORK		158
REFERENCES		161
VITAE		170

LIST OF TABLES

4.1	Induction Motor rated Specifications and Parameters (for simulation part 1)	35
4.2	Induction Motor rated Specifications and Parameters (for simulation part 2)	35
8.1	Bouc-Wen hysteresis boundedness conditions	139

LIST OF FIGURES

1.1	Examples of induction motors	3
3.1	(A,B,C) Phasor representation with the corresponding <i>a-b</i> stationary frame of reference representation	20
3.2	Visual description of Park transformation	22
4.1	Speed tracking performance of IM (with $T_L = 0$) against constant, ramp and sinusoidal reference trajectory respectively.	36
4.2	Applied control input voltages of IM (with $T_L = 0$) against various constant references.	37
4.3	Applied control input voltages of IM (with $T_L = 0$) against ramp and sinusoid references respectively.	38
4.4	Magnetic flux components of IM (with $T_L = 0$) for various constant references.	39
4.5	Magnetic flux components of IM (with $T_L = 0$) for ramp and sinusoid references respectively.	40
4.6	Current components of IM (with $T_L = 0$) for various constant references.	41
4.7	Current components of IM (with $T_L = 0$) for ramp and sinusoid references respectively.	42
4.8	Speed tracking performance of IM (with $T_L = 1$ [Nm]) against constant, ramp and sinusoidal reference trajectory respectively. . .	43
4.9	Applied control input voltages of IM (with $T_L = 1$ [Nm]) against various constant references.	44

4.10	Applied control input voltages of IM (with $T_L = 1$ [Nm]) against ramp and sinusoid references respectively.	45
4.11	Magnetic flux components of IM (with $T_L = 1$ [Nm]) for various constant references.	46
4.12	Magnetic flux components of IM (with $T_L = 1$ [Nm]) for ramp and sinusoid references respectively.	47
4.13	Current components of IM (with $T_L = 1$ [Nm]) for various constant references.	48
4.14	Current components of IM (with $T_L = 1$ [Nm]) for ramp and sinusoid references respectively.	49
4.15	Load torque adaptive parameter \hat{T}_L performance for constant, ramp and sinusoid references respectively.	50
5.1	Speed tracking performance of IM (with dead-zone/backlash inputs nonlinearities respectively) against constant reference with no applied compensation.	52
5.2	Applied control input voltages (u_1 and u_2) of IM in cases of dead-zone input and backlash input respectively with no applied compensation.	53
5.3	Symmetric dead-zone nonlinearity	54
5.4	Speed tracking performance of IM (with $T_L = 0$) against constant, ramp and sinusoidal reference trajectory respectively (symmetric dead-zone case).	63
5.5	Applied control input voltages of IM (with $T_L = 0$) against various constant references (symmetric dead-zone case).	64
5.6	Applied control input voltages of IM (with $T_L = 0$) against ramp and sinusoid references respectively (symmetric dead-zone case).	65
5.7	Magnetic flux components of IM (with $T_L = 0$) for various constant references (symmetric dead-zone case).	66

5.8	Magnetic flux components of IM (with $T_L = 0$) for ramp and sinusoid references respectively (symmetric dead-zone case).	67
5.9	Current components of IM (with $T_L = 0$) for various constant references (symmetric dead-zone case).	68
5.10	Current components of IM (with $T_L = 0$) for ramp and sinusoid references respectively (symmetric dead-zone case).	69
5.11	Adaptive parameter \hat{m} performance for constant, ramp and sinusoid references respectively (symmetric dead-zone case).	70
5.12	Speed tracking performance of IM (with $T_L = 1$ [Nm]) against constant, ramp and sinusoidal reference trajectory respectively (symmetric dead-zone case).	71
5.13	Applied control input voltages of IM (with $T_L = 1$ [Nm]) against various constant references (symmetric dead-zone case).	72
5.14	Applied control input voltages of IM (with $T_L = 1$ [Nm]) against ramp and sinusoid references respectively (symmetric dead-zone case).	73
5.15	Magnetic flux components of IM (with $T_L = 1$ [Nm]) for various constant references (symmetric dead-zone case).	74
5.16	Magnetic flux components of IM (with $T_L = 1$ [Nm]) for ramp and sinusoid references respectively (symmetric dead-zone case).	75
5.17	Current components of IM (with $T_L = 1$ [Nm]) for various constant references (symmetric dead-zone case).	76
5.18	Current components of IM (with $T_L = 1$ [Nm]) for ramp and sinusoid references respectively (symmetric dead-zone case).	77
5.19	Load torque adaptive parameter \hat{T}_L performance for constant, ramp and sinusoid references respectively (symmetric dead-zone case).	78
5.20	Adaptive parameter \hat{m} performance for constant, ramp and sinusoid references respectively (symmetric dead-zone case).	79
6.1	Asymmetric dead-zone nonlinearity	81

6.2	Speed tracking performance of IM (with $T_L = 0$) against constant, ramp and sinusoidal reference trajectory respectively (asymmetric dead-zone case).	92
6.3	Applied control input voltages of IM (with $T_L = 0$) against various constant references (asymmetric dead-zone case).	93
6.4	Applied control input voltages of IM (with $T_L = 0$) against ramp and sinusoid references respectively (asymmetric dead-zone case).	94
6.5	Magnetic flux components of IM (with $T_L = 0$) for various constant references (asymmetric dead-zone case).	95
6.6	Magnetic flux components of IM (with $T_L = 0$) for ramp and sinusoid references respectively (asymmetric dead-zone case).	96
6.7	Current components of IM (with $T_L = 0$) for various constant references (asymmetric dead-zone case).	97
6.8	Current components of IM (with $T_L = 0$) for ramp and sinusoid references respectively (asymmetric dead-zone case).	98
6.9	Adaptive parameter $\hat{\rho}$ performance for constant, ramp and sinusoid references respectively (asymmetric dead-zone case).	99
6.10	Speed tracking performance of IM (with $T_L = 1$ [Nm]) against constant, ramp and sinusoidal reference trajectory respectively (asymmetric dead-zone case).	100
6.11	Applied control input voltages of IM (with $T_L = 1$ [Nm]) against various constant references (asymmetric dead-zone case).	101
6.12	Applied control input voltages of IM (with $T_L = 1$ [Nm]) against ramp and sinusoid references respectively (asymmetric dead-zone case).	102
6.13	Magnetic flux components of IM (with $T_L = 1$ [Nm]) for various constant references (asymmetric dead-zone case).	103
6.14	Magnetic flux components of IM (with $T_L = 1$ [Nm]) for ramp and sinusoid references respectively (asymmetric dead-zone case).	104

6.15	Current components of IM (with $T_L = 1$ [Nm]) for various constant references (asymmetric dead-zone case).	105
6.16	Current components of IM (with $T_L = 1$ [Nm]) for ramp and sinusoid references respectively (asymmetric dead-zone case).	106
6.17	Load torque adaptive parameter \hat{T}_L performance for constant, ramp and sinusoid references respectively (asymmetric dead-zone case).	107
6.18	Adaptive parameter $\hat{\rho}$ performance for constant, ramp and sinusoid references respectively (asymmetric dead-zone case).	108
7.1	Backlash nonlinearity	112
7.2	Speed tracking performance of IM (with $T_L = 0$) against constant, ramp and sinusoidal reference trajectory respectively (backlash case).	115
7.3	Applied control input voltages of IM (with $T_L = 0$) against various constant references (backlash case).	116
7.4	Applied control input voltages of IM (with $T_L = 0$) against ramp and sinusoid references respectively (backlash case).	117
7.5	Magnetic flux components of IM (with $T_L = 0$) for various constant references (backlash case).	118
7.6	Magnetic flux components of IM (with $T_L = 0$) for ramp and sinusoid references respectively (backlash case).	119
7.7	Current components of IM (with $T_L = 0$) for various constant references (backlash case).	120
7.8	Current components of IM (with $T_L = 0$) for ramp and sinusoid references respectively (backlash case).	121
7.9	Adaptive parameter \hat{h} performance for constant, ramp and sinusoid references respectively (backlash case).	122
7.10	Speed tracking performance of IM (with $T_L = 1$ [Nm]) against constant, ramp and sinusoidal reference trajectory respectively (backlash case).	123

7.11	Applied control input voltages of IM (with $T_L = 1$ [Nm]) against various constant references (backlash case).	124
7.12	Applied control input voltages of IM (with $T_L = 1$ [Nm]) against ramp and sinusoid references respectively (backlash case).	125
7.13	Magnetic flux components of IM (with $T_L = 1$ [Nm]) for various constant references (backlash case).	126
7.14	Magnetic flux components of IM (with $T_L = 1$ [Nm]) for ramp and sinusoid references respectively (backlash case).	127
7.15	Current components of IM (with $T_L = 1$ [Nm]) for various constant references (backlash case).	128
7.16	Current components of IM (with $T_L = 1$ [Nm]) for ramp and sinusoid references respectively (backlash case).	129
7.17	Load torque adaptive parameter \hat{T}_L performance for constant, ramp and sinusoid references respectively (backlash case).	130
7.18	Adaptive parameter \hat{h} performance for constant, ramp and sinusoid references respectively (backlash case).	131
8.1	An example of Bouc-Wen hysteresis	133
8.2	Speed tracking performance of IM (with $T_L = 0$) against constant, ramp and sinusoidal reference trajectory respectively (Bouc-Wen hysteresis case).	141
8.3	Applied control input voltages of IM (with $T_L = 0$) against various constant references (Bouc-Wen hysteresis case).	142
8.4	Applied control input voltages of IM (with $T_L = 0$) against ramp and sinusoid references respectively (Bouc-Wen hysteresis case).	143
8.5	Magnetic flux components of IM (with $T_L = 0$) for various constant references (Bouc-Wen hysteresis case).	144
8.6	Magnetic flux components of IM (with $T_L = 0$) for ramp and sinusoid references respectively (Bouc-Wen hysteresis case).	145

8.7	Current components of IM (with $T_L = 0$) for various constant references (Bouc-Wen hysteresis case).	146
8.8	Current components of IM (with $T_L = 0$) for ramp and sinusoid references respectively (Bouc-Wen hysteresis case).	147
8.9	Adaptive parameter \hat{g} performance for constant, ramp and sinusoid references respectively (Bouc-Wen hysteresis case).	148
8.10	Speed tracking performance of IM (with $T_L = 1$ [Nm]) against constant, ramp and sinusoidal reference trajectory respectively (Bouc-Wen hysteresis case).	149
8.11	Applied control input voltages of IM (with $T_L = 1$ [Nm]) against various constant references (Bouc-Wen hysteresis case).	150
8.12	Applied control input voltages of IM (with $T_L = 1$ [Nm]) against ramp and sinusoid references respectively (Bouc-Wen hysteresis case).	151
8.13	Magnetic flux components of IM (with $T_L = 1$ [Nm]) for various constant references (Bouc-Wen hysteresis case).	152
8.14	Magnetic flux components of IM (with $T_L = 1$ [Nm]) for ramp and sinusoid references respectively (Bouc-Wen hysteresis case).	153
8.15	Current components of IM (with $T_L = 1$ [Nm]) for various constant references (Bouc-Wen hysteresis case).	154
8.16	Current components of IM (with $T_L = 1$ [Nm]) for ramp and sinusoid references respectively (Bouc-Wen hysteresis case).	155
8.17	Load torque adaptive parameter \hat{T}_L performance for constant, ramp and sinusoid references respectively (Bouc-Wen hysteresis case).	156
8.18	Adaptive parameter \hat{g} performance for constant, ramp and sinusoid references respectively (Bouc-Wen hysteresis case).	157

LIST OF ABBREVIATIONS

α	Load torque adaptive law's constant
α_l	Defined function in backlash definition
α_r	Defined function in backlash definition
α_s	Defined function in backlash definition
β	Defined constant in Bouc-Wen hysteresis definition
δ	Asymmetric dead-zone parameter adaptive law's constant
ϵ_1	Defined constant
ϵ_2	Defined constant
η	Bounded perturbation function for symmetric dead-zone case
η_{max}	Upper bound of the perturbation function for symmetric dead-zone case
Γ	Asymmetric dead-zone function
γ	Symmetric dead-zone parameter adaptive law's constant
$\hat{\rho}$	Adaptive parameter for asymmetric dead-zone case

\hat{g}	Adaptive parameter for Bouc-Wen hysteresis case
\hat{h}	Adaptive parameter for backlash case
\hat{m}	Adaptive parameter for symmetric dead-zone case
\hat{T}_L	Adaptive parameter associated with load torque
λ	Defined constant in Bouc-Wen hysteresis definition
λ_a, x_2	Magnetic flux component a in stationary frame of reference
λ_b, x_3	Magnetic flux component b in stationary frame of reference
λ_d	Magnetic flux component d in rotating frame of reference
λ_q	Magnetic flux component q in rotating frame of reference
μ	Coefficient of Friction
ν	Defined constant in Bouc-Wen hysteresis definition
Ω	Defined quantity for load torque adaptive law
ω, x_1	Induction motor angular speed
ω_s	Induction motor synchronous speed
Φ	Defined quantity for symmetric dead-zone adaptive law
ϕ	Backstepping virtual feedback
Ψ	Defined quantity for asymmetric dead-zone adaptive law
ψ	Defined quantity
ρ	Maximum value of $q(t)$
ρ_{max}	Maximum value of ρ

σ	Defined constant for IM model
τ	Backlash parameter adaptive law's constant
Θ	Set of $z(0)$ that satisfy certain conditions
θ	The angle of the rotor flux
$\tilde{\rho}$	Estimation error associated with asymmetric dead-zone parameter
\tilde{h}	Estimation error associated with backlash parameter
\tilde{m}	Estimation error associated with symmetric dead-zone parameter
\tilde{T}_L	Estimation error associated with load torque
Υ	Defined quantity
φ	Defined constant
ϱ	Bounded function for backlash case
ϑ	Bounded perturbation function for backlash case
ϑ_{max}	Upper bound of the perturbation function for backlash case
ξ	Bounded perturbation function for asymmetric dead-zone case
ξ_{max}	Upper bound of the perturbation function for asymmetric dead-zone case
ζ	Defined function in Bouc-Wen hysteresis definition
ζ_{max}	Upper bound of the perturbation function for Bouc-Wen hysteresis case
A	Defined constant in Bouc-Wen hysteresis definition

B	Backlash function
b	Symmetric dead-zone break point value
b_l	Asymmetric dead-zone left break point value
b_{max}	Dead-zone parameter's maximum
b_{min}	Dead-zone parameter's minimum
b_r	Asymmetric dead-zone right break point value
c_1	Defined backstepping constant
c_2	Defined backstepping constant
D	Symmetric dead-zone function
d	Backlash parameter
d_{max}	Backlash parameter's maximum
d_{min}	Backlash parameter's minimum
e_1	Speed Tracking error
e_2	Defined system error
F	Friction force
G	Defined positive constant in Bouc-Wen hysteresis definition
g	Defined constant in Bouc-Wen hysteresis definition
g_{max}	Bouc-Wen hysteresis parameter's maximum
g_{min}	Bouc-Wen hysteresis parameter's minimum
h	Backlash slope

H_{BW}	Bouc-Wen hysteresis function
h_{max}	Backlash maximum slope
h_{min}	Backlash minimum slope
i_A	Stator current component (phase A)
i_a, x_4	Stator current component a in stationary frame of reference
i_B	Stator current component (phase B)
i_b, x_5	Stator current component b in stationary frame of reference
i_C	Stator current component (phase C)
i_d	Stator current component d in rotating frame of reference
i_q	Stator current component q in rotating frame of reference
I_s	Stator current in complex form
J	Induction motor mechanical inertia
K	Defined constant in Bouc-Wen hysteresis model
k_0	Defined constant in IM simplified model
k_1	Defined constant in IM simplified model
k_2	Defined constant in IM simplified model
k_3	Defined constant in IM simplified model
k_4	Defined constant in IM simplified model
k_5	Defined constant in IM simplified model
k_6	Defined constant in IM simplified model

k_7	Defined constant in IM simplified model
L_m	Mutual inductance
L_r	Rotor inductance
L_s	Stator inductance
m	Symmetric dead-zone slope
m_l	Asymmetric dead-zone left slope
m_{max}	Dead-zone maximum slope
m_{min}	Dead-zone minimum slope
m_r	Asymmetric dead-zone right slope
n	Defined constant in Bouc-Wen hysteresis definition
n_p	Defined constant in IM model
q	Defined function of asymmetric dead-zone parameters
Q_1	Defined constant
Q_2	Defined constant
r	Reference trajectory function
R_r	Rotor resistance
R_s	Stator resistance
S	Defined quantity
T	Simulation Time period
t	Time

T_{Lmax}	External load torque maximum value
T_{Lmin}	External load torque minimum value
T_L	External load torque
u	Generic input
u_s	Defined constant in backlash definition
V	Lyapunov function of the system
v	Selected quantity
V_1	Backstepping first stage Lyapunov function
v_a, u_1	Input voltage component a in stationary frame of reference
v_b, u_2	Input voltage component b in stationary frame of reference
v_d	Input voltage component d in stationary frame of reference
v_q	Input voltage component q in stationary frame of reference
W	Defined positive quantity
W_ϵ	Defined positive quantity
y_a	Component a of v, λ or i in a-b stationary frame
y_b	Component b of v, λ or i in a-b stationary frame
y_d	Component d of v, λ or i in d-q rotating frame
y_q	Component q of v, λ or i in d-q rotating frame
z	Defined function in Bouc-Wen hysteresis definition
z_0	Defined constant

z_1

Defined constant

THESIS ABSTRACT

NAME: Hassan M. Al-Abudib

TITLE OF STUDY: Control of Induction Motors Subject to Hard-Input Non-linearities

MAJOR FIELD: Electrical Engineering

DATE OF DEGREE: December 2017

Induction motor is a very essential component in many applications due to its various important and useful features. However, because of its complicated dynamics, induction motor control is not a trivial task. In the two recent decades, many studies have been devoted to tackle this problem, aiming to achieve some control objectives such as angular speed regulation, magnetic flux regulation, fault detection and energy consumption optimization. Consequently, many control techniques have been presented as solutions to this problem. The objective of this thesis is to construct an angular speed tracking controller for a voltage-controlled induction motor subject to unknown input nonlinearities. These nonlinearities include symmetric/asymmetric dead-zones, backlash as well as Bouc-Wen hysteresis. In addition, the controller is designed to compensate for unknown external load torque

applied to the induction motor rotor. In order to accomplish these objectives, the adaptive backstepping mechanism is utilized to design the controller to achieve the desired outcome. Furthermore, an extensive induction motor simulations are performed with the developed controller against a variety of reference inputs including constant, ramp and sinusoid. The results shall prove design validity by achieving a bounded-error trajectory tracking.

ملخص الرسالة

الاسم الكامل: حسن محمد علي آل أبوديب
عنوان الرسالة: التحكم بالمحركات الحثية الخاضعة لمدخلات غير الخطية
التخصص: هندسة كهربائية
تاريخ الدرجة العلمية: ديسمبر 2017

يتمتع المحرك الحثي بالعديد من الخواص المميزة والتي تجعله مفيدة جداً في الكثير من التطبيقات المختلفة. إلا أن التحكم بالمحرك الحثي ليس بالمهمة السهلة بسبب تعقيد نمودجه الرياضي. في العقدين الأخيرين تم تكريس العديد من الدراسات التي تهدف إلى تحقيق بعض أهداف التحكم بالمحرك الحثي من قبيل التحكم بسرعة دوران المحرك، تنظيم التدفق المغناطيسي وتحسين استهلاك الطاقة، ونتيجة لذلك تم تقديم العديد من تقنيات التحكم الجديدة في هذا المجال. الهدف من هذه الرسالة هو استنباط وحدة تحكم لتتبع سرعة الدوران للمحرك الحثي (الذي يمكن التحكم به من خلال فرق الجهد الكهربائي) الخاضع لمدخلات غير خطية ومجهولة المعاملات. هذه المدخلات تشمل المناطق الميتة المتناظرة وغير المتناظرة، تباطؤ رد الفعل وتباطؤ بوك ون. وبالإضافة إلى ذلك، تم تصميم وحدة التحكم للتعويض عن عزم الدوران الخارجي غير المعروف والمتصل بمحرك الحث. من أجل تحقيق هذه الأهداف تم إعمال آلية التكيف الخلفية لتصميم التحكم اللازم للمحرك. وعلاوة على ذلك، تم إجراء محاكاة واسعة لأداء محرك الحث مع وحدة التحكم المقترحة لمجموعة متنوعة من المدخلات المرجعية بما في ذلك الثابت والمنحدر والجيبي.

CHAPTER 1

INTRODUCTION

Before exploring the details of this work, it is important to have some preliminary background about the subject's keywords; induction motors and input nonlinearities. This chapter is dedicated to provide an overview of both topics in a nutshell and then, to present the thesis main objective and the work organization for next chapters.

1.1 Introduction to Induction Motors

1.1.1 Basics, operation and applications

The induction motor (IM) is an electromechanical device that converts electrical energy to mechanical energy by means of electromagnetic induction. It can be either single phase or three-phase. It consists of two main parts:

(1) The stator, the stationary part which supplies the IM with power. It consists of three main parts; the frame, the core and the winding.

(2) The rotor, the rotating component of the IM to which the mechanical load is connected through a shaft. It can be made of laminated steel core with evenly spaced conductor bars as in squirrel-cage rotor. The core can also be cylindrical made from laminated steel but with slots to hold the three-phase windings as in wound rotor. In both cases, bars/windings are permanently short-circuited.

The operation of the IM can be summarized as follows:

AC power is supplied to the stator windings. The resulting electrical current creates a magnetic field in the air gap between the stator and the rotor. In this context, the synchronous speed ω_s is defined as the rotating speed of the magnetic field. Because the supplied power is alternating, magnetic flux is changing as well. Based on Faraday's law and Lenz's law of electromagnetic induction, current is induced in the rotor's windings/bars in the direction opposing the change in the magnetic flux. So, by Lorentz law, the magnetic field interacts with the induced current in the rotor, producing a torque causing it to rotate in the direction of the field. Note that as the rotor gains more speed, the change in magnetic flux drops down so does the magnitude of the rotor's induced current. As the rotor speed approaches ω_s , there will be no induced current in the rotor. Once this point is reached, the rotor speed drops down due to friction since no Lorentz force is exerted. Finally, the change in the rotor speed causes a change in the magnetic flux and thus current induction takes place again in the rotor and the cycle repeats. As a result, IM rotor speed cannot exceed the synchronous speed ω_s , hence the name asynchronous motor [1].

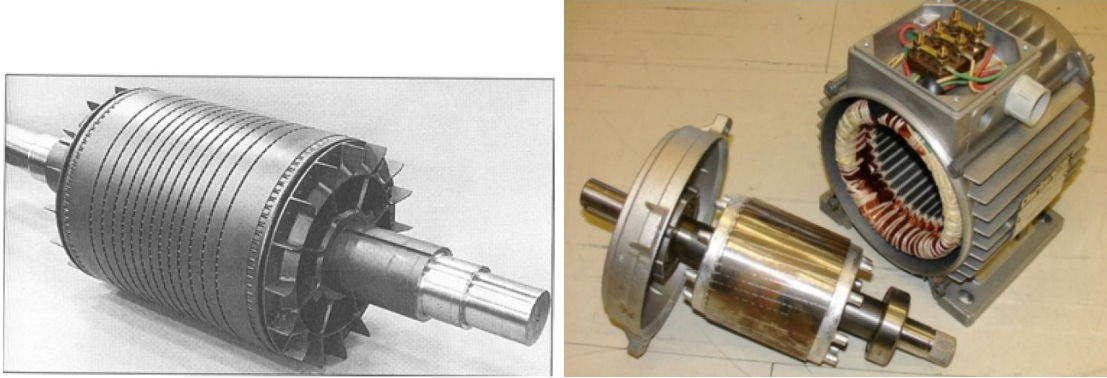


Figure 1.1: Examples of induction motors

IM has a number of interesting features including power/mass ratio, low moment of inertia, low torque ripple, low cost, small size, robustness, simple construction and easy maintenance. Because of these useful features, IM has been an essential part in wide areas of applications such as actuators, air conditioning/heating equipments, pump equipments, conveyor systems, electric vehicles, appliances, ...etc [2, 3, 4].

1.1.2 Control objectives and challenges

Since IM is a crucial component in many applications, IM control problem has become one of the major concerns. Each application needs a certain IM operational performance, which requires achieving specific control goals. These goals include power consumption optimization, IM speed tracking/regulation, fault detection and flux regulation. However, IM control is not an easy problem. IM model has a multi-variable coupled nonlinear dynamics. Some model parameters are time-varying. In addition, some states (speed, flux) are not accessible for measurements with cheap and reliable sensors [3, 5]. The load torque is usu-

ally uncertain and has to be accounted for in the controller design. In short, the combination of control objectives and model complexity makes the control problem more and more challenging. Thus, many researches have been motivated to propose solutions to this problem.

1.1.3 Control approaches

In the recent decades, there has been a great number of researches focusing on IM control. Consequently, a significant progress has been made that led to introducing new techniques. These IM control approaches/trends can be summarized by the following schemes [4]:

Scalar control: This approach is used for applications with low cost/ low performance IM drives. It is done by adjusting the magnitude/frequency of either the current or the voltage source. Examples of this approach includes slip frequency control and V/f control.

Vector control: In contrast to scalar approach, vector control is used for expensive high performance applications. The approach controls the magnitude/phase of the voltage or the current vector. Examples of this approach include field orientation control (FOC) as well as direct torque control (DTC). In these techniques, the aim is to reduce the complex nonlinear system structure to a linear form. Both techniques are very successful IM control methods.

Speed sensorless control: In this scheme, estimation algorithms are utilized to eliminate the need for speed/position sensors. such algorithms involve lengthy

computations based on the system parameters in addition to the terminal voltages/currents.

Intelligent control: Such as fuzzy logic and neural network methods. These techniques are becoming more common among IM control studies. They proved to be very helpful when dealing with complicated nonlinear systems with parameters variations (such as IM system) and help simplify very complex computations.

Backstepping control: This technique has shown to be useful in IM control and a number of researches adopted it. The dynamical structure of the IM system is suited for applying such technique. It is also applied in the controller design of this project.

1.2 Input Nonlinearity Phenomena

Many different electrical and mechanical industrial applications (such as DC motors, servomotors, tubular linear motors, piezoelectric stages, sensors, amplifiers, gears, hydraulic actuators, mechanical connections ...etc) experience some of input nonlinearity phenomena during their operations [6, 7, 8, 9]. These nonlinearities are caused by imperfect system components in most of the cases [10]. They can be either static as dead-zones or dynamic as backlash and hysteresis, each of which having different behaviors. For instance, the dead-zone is a memoryless phenomenon that results in insensitivity towards input in specific region of operation. Thus, the input has no effect on the system within this region. On the other hand, backlash or hysteresis can cause input delays in addition to input

insensitivity as in dead-zones as well as having dynamic input/output nature. In addition, the parameters that characterize these nonlinearities (static or dynamic) are usually poorly known or completely unknown.

Such phenomena lead to system performance degradation. It might result in undesired output behavior, such as delays, oscillations, limit cycles [11] and even system instability [12]. This issue poses even a bigger problem in systems with high precision control [13]. It is worth mentioning that a nonlinearity such as dead-zone even with small region of operation can have a very serious effect on the system's output and can lead to a very undesirable control accuracy. Therefore, input nonlinearity behavior has to be resolved completely in order to avoid these problems.

1.3 Thesis Objective and Organization

As stated previously, IM's are very important for many different applications because of their valuable features. However, IM control is a difficult task due to the model complexity and it is still an open research area. Many studies have contributed to this subject by introducing new techniques and solving new problems. In this thesis, the objective is to design and simulate a feedback controller to the IM system to force the angular speed to follow specific known trajectory functions (constant, ramp and sinusoid). The IM system in this problem is subjected to static/dynamic input nonlinearities including; symmetric dead-zone, asymmetric dead-zone, backlash and Bouc-Wen hysteresis. Each of these nonlinearities in-

roduced at the system's input has unknown parameters. In addition to input nonlinearity uncertainty, the IM system is operating while being connected to some unknown external load torque. The feedback controller is designed according to the mechanism of adaptive backstepping. Such method has shown to be a very powerful and successful tool to control nonlinear systems with uncertainties. The designed controller shall be able to accomplish the desired tracking target and simultaneously compensate for the effect of uncertain input nonlinearity and unknown external torque. The aim is to achieve trajectory tracking with bounded-error, which is a sufficient practical goal.

The scope of the thesis is organized as follows: chapter two provides a literature survey of recent published works related to methods for IM control and input nonlinearity compensation. Next is chapter three which introduces different models of IM and present the selected model for this project. In chapter four, the IM speed tracking backstepping controller is designed. Chapter five discusses the effect of input nonlinearity, introduces symmetric dead-zone nonlinearity and modifies the controller developed in the previous chapter. The modification is aimed to compensate for the effect of the symmetric dead-zone. In chapter six the asymmetric dead-zone nonlinearity is introduced and the controller is re-designed accordingly. Backlash models and control are presented in chapter seven. In chapter eight, Bouc-Wen hysteresis model and control are discussed. All controllers developed are simulated using MATLAB SIMULINK. The simulation results are plotted and displayed at the end of each corresponding chapter. Finally, the thesis is

concluded in chapter nine along with a discussion of possible future work.

CHAPTER 2

LITERATURE REVIEW

The review of relevant materials consists of two parts; reviewing current IM control methods and reviewing of input nonlinearity compensation techniques.

2.1 Induction Motors Control

IM control using scalar method has been very popular and practical for many applications. The method aims to keep the voltage to frequency ratio V/f as a constant quantity in order to maintain the magnetic flux of the motor. One of the most important advantages of this approach is its simplicity. Such an approach does not require complex hardware to be applied and can be implemented at low cost. The disadvantage of this method, however, is its mediocre outcome performance. Study [14] is an example of this method enhanced version. It works for industrial applications that do not require very precise control output. In addition, it introduces a slip compensation technique that does not require neither speed sensing or flux estimations. Another example can be seen in [15], where

a scalar neural network IM control scheme is proposed. The scheme uses new way for speed estimation using space vector modulation by a scalar control technique. In research [16], a scalar IM control approach with fuzzy control system is presented. The system utilizes an embedded digital signal processor (DSP) to implement the control scheme to keep the ratio of the IM source voltage-frequency constant.

On the other hand, the most famous method for IM control is vector control, which includes field oriented control (FOC) and direct torque control (DTC). The idea in field oriented control scheme is to use the appropriate transformation to decouple the field producing current and the torque producing current. Based on the method to obtain rotor flux orientation, FOC can be either direct by developing a method to sense the rotor flux or indirect by flux estimation. This method is widely used in literature [1]. References [17] and [18] are some examples of applying FOC. On the other hand, DTC method as the name suggests, is a mechanism to directly control the torque and the stator flux. This is done by utilizing a hysteresis controller based on bang-bang control method. Knowledge of stator variables plays a major role in the controller design. Such a method is favored by many researches due to its fast torque response time [1]. Some examples of studies based on IM DTC can be seen in [19, 20] and [21].

In addition to the above methods, many of the recent works of IM controller development are based on intelligent control techniques schemes. The techniques are sometimes combined with vector control or scalar control techniques as al-

ready mentioned previously. The followings are examples of fuzzy/neural network (NN) techniques. In [16] IM speed was controlled using a compact embedded fuzzy control system, which uses speed error and speed error variations to modify the voltage of a pulse width modulator inverter. In [22], a fuzzy credit-assigned cerebellar model articulation technique (FCA-CMA) was employed to design the IM speed sensorless controller. This method uses a multi-estimator that performs a real-time accurate estimation of the speed regardless of any variations in the parameters. The multi-estimator is utilized by the FCA-CMA controller in the learning process to ensure speed faster convergence. Also, in [17], Takagi-Sugeno (T-S) fuzzy model was used to develop an integral fuzzy controller. It uses a fuzzy observer to estimate the rotor flux. The control design uses a Linear Matrix Inequality (LMI) approach to achieve H_∞ tracking performance. In addition, [23] proposes a new fuzzy vector control approach of IM. This approach solves the coupling problem in the IM model by using the inverse version of the model. In [24], the IM speed tracking controller is a self-tuning Multiresolution wavelet-fuzzy based. The speed error between the actual and the set is resolved into different frequency components by a discrete wavelet transformation. The gain of the controller is calculated by a fuzzy self-tuning algorithm. Furthermore, the controller can follow an adaptive supervisory fuzzy-cerebellar model articulation scheme as in [20]. The method is model-free. The controller is both learning and approximating the system dynamics as well as tuning the tracking error to a specified bound. In [15], the controller objective is achieved by using a scalar

control scheme based on neural network technique. A reference model neuro-fuzzy sliding mode based controller is proposed in [25]. The speed error is used to train its connective weights. In [26], a back propagation network algorithm is used to train a linear NN. This network is used in a model reference adaptive system to construct the IM controller, which is applied both in simulation and prediction modes.

Backstepping is a strong tool to control nonlinear systems such as IM dynamical model. Also, it is of a particular interest to this research as it shall be seen in the proposed controller design in the coming chapters. So, it is worth mentioning that a number of researchers developed the IM controller based on backstepping schemes, combined with one or two of previously discussed methods. For example, a sensorless robust observer-based backstepping IM controller is proposed in [27]. To cope with system uncertainties and perturbations, an FOC method was combined with the controller. In [28], the author used output feedback adaptive backstepping control technique, incorporated with a sliding mode flux observer. The controller drives the output asymptotically towards the reference input. Also, in study [29], a speed sensorless backstepping controller was employed to stabilize the error in the flux and in the torque, backed up by fast search methods to increase efficiency. In paper [3], the authors tried to set a global mechanism to deal with the IM control problem. The proposed controller is nonlinear adaptive multi-loop backstepping based with multiple control objectives, including speed regulation and flux optimization. The objectives' performances have been mea-

sured by applying tools from Lyapunov stability and averaging theory.

2.2 Input Nonlinearity Compensation

Many studies tackled the problem of input nonlinearity applied to various systems. The methods employed to develop a compensating controller can be summarised in three main approaches [30]. The first approach is to build the inverse model of the nonlinearity. This is done by utilizing the exact, the approximate or the adaptive form of the inverse model. Originally, this approach can be traced back to [31, 32] and [33]. Many examples of this method can be seen in the recent studies. For instance, [34] and [35] both use fuzzy-based adaptive backstepping technique to control strict-feedback nonlinear systems with unknown dead-zone input by developing the adaptive inverse model. In [36], the inverse model method is used to construct a robust/adaptive precision motion controller for electrical drive systems having unknown input dead-zones. Another example is seen in [9] in which this approach is used to compensate for the asymmetric dead-zone input applied at a class of nonlinear dynamic systems. In this method, an indirect parameter estimation algorithm is used to obtain estimates of the input dead-zone parameters with high accuracy. Similarly, this approach can be used to compensate for systems with unknown backlash input as well as other types of hysteresis. For example, an inverse backlash model based robust compensation method is developed to control a class of nonlinear system with unknown symmetric backlash input in [37] and asymmetric backlash as in [38]. In [39], a modified inverse Bouc-Wen

model based dynamical control technique is proposed to handle rate-dependent hysteresis in Piezoelectric actuators. Employing this method results in a real-time online hysteresis compensation. Another example of Bouc-Wen hysteresis compensation is seen in [40], where a class of uncertain nonlinear systems with input hysteresis is considered. The developed method constructs a perfect inverse of the hysteresis which is utilized with an adaptive backstepping controller. The outcome shows that such a technique can result in asymptotic stability and transient behavior improvement. Another class of nonlinear systems with Bouc-Wen hysteresis compensation is presented in [41]. Again, the inverse approach is applied with adaptive neural algorithm. It results in semiglobal uniform ultimate boundedness of the outcome.

The second approach tackles the problem using adaptive and robust control techniques without attempting to build any inverse models, in contrast to the first approach. This method might capitalize in convex-optimization tools to deal with the input nonlinearities, being a dead-zone or a hysteresis. The followings are some examples of dead-zone input compensation in the literature. In paper [13], an adaptive control of nonlinear systems with non-symmetric dead-zone inputs has been discussed. The method requires minimum knowledge about the dead-zone bounds. It results in bounded signals and bounded-error trajectory tracking. Also, in [6], the author developed an adaptive controller to stabilize a class of nonlinear feedforward systems with unknown symmetric/non-symmetric dead-zone inputs. The technique is based on invariant manifold approach supported by an

adaptive/robust compensation method. In [42], an adaptive iterative learning NN based method to control a class of time varying nonlinear system with unknown dead-zone input was introduced. The method used Lyapunov-like composite energy function to prove the convergence of the system's output to the desired trajectory. In addition, adaptive fuzzy control schemes of nonlinear systems with an unknown dead-zone input were presented in [43] for pure-feedback stochastic systems, in [8] for strict-feedback nonlinear systems using backstepping and in [44] for a class of uncertain multi-input multi-output (MIMO) chaotic systems. In addition, the followings are examples for the compensation controllers of systems with backlash and Bouc-Wen hysteresis the literature. An unknown backlash input Timoshenko beam vibration control using adaptive boundary control algorithm is presented in [45]. Also, [46] discusses the issue of stability/stablization of linear systems with unknown backlash input and designed a stabilizing controller based on convex optimizations tools. In [30], the author developed a generalized strategy to design a compensation controller for a class of feedforward nonlinear system subjected to an uncertain backlash hysteresis input. To illustrate its performance, the method was applied to a non-minimum phase mechanical system which then was accompanied by real-time experiments and numerical simulations. Other recent researches are devoted to backlash-like hysteresis input compensation using adaptive fuzzy control methods as in [47] or adaptive NN techniques as in [48]. In [49], the compensation of a class of time-varying nonlinear system in a non-strict-feedback form with unknown direction Bouc-Wen hysteresis is discussed.

The compensation uses adaptive/neural techniques to ensure practical stability of the system where tracking errors stay within a reasonable neighbourhood of the origin. Other research [50] utilizes an adaptive backstepping mechanism and Nussbaum gain approach to compensate for Bouc-Wen hysteresis input in a type of nonlinear systems with parametric uncertainties to achieve asymptotic tracking performance.

The third approach is based on replacing the non-smooth input nonlinearity by a smooth input function. This function provides a reliable estimate version of the actual nonlinearity. This approach can be seen in [51] which provides a NN strategy to approximate piecewise continuous function with finite number of discontinuities.

Now, the method to be developed in this research follows the second approach, i.e., without the development of the nonlinearity inverse model. Unlike the method in [13], this method relies only on one adaptation parameter dedicated for input nonlinearity compensation. There is another adaptive parameter in the method. However, it is utilized to compensate for another problem, i.e., the unknown external torque effect. The method shall result in construction of a feedback that achieves "practical" stability. Both the development and the proof of stability are done simultaneously in one stage thanks to the method of adaptive backstepping introduced later in the coming chapters. In principle, the method can provide a precise mechanism to compensate for any dead-zone/backlash/Bouc-Wen hysteresis input nonlinearities effect with any parameters values.

CHAPTER 3

IM SYSTEM MODELING

IM system has a number of models available in the literature. Different models can be useful for different IM applications. The sole purpose of this chapter is to present the IM dynamical model that suits this research.

3.1 IM Dynamical Models

Before introducing any mathematical models for IM, it is important to know the conditions under which such models are precise and actually represent the operation of actual IM device. The next assumption introduces these conditions.

Assumption 1. The IM models to be discussed in this chapter and studied throughout this work are valid under the following conditions:

- 1) The equivalent magnetic circuit is fully linearized.
- 2) Iron and stray losses can be neglected.
- 3) The air gap magnetomotive force (mmf) is a sinusoidal function.
- 4) The three-phase distributed windings are balanced and symmetrical.

In case of balanced three-phase IM, the following current relation holds:

$$i_A + i_B + i_C = 0, \quad (3.1)$$

where i_A , i_B , i_C are the three-phase current components and A , B , C are defined as the three-phase 120-degree separated complex phase axes. The stator current I_s is defined in complex representation as [52]:

$$I_s = \frac{2}{3}(i_A + e^{j2\pi/3}i_B + e^{j4\pi/3}i_C). \quad (3.2)$$

Now, the three-phase IM system can be transformed into a two-phase system. This process reduces the number of stator current components from three (i_A , i_B , i_C) to two orthogonal components (i_a , i_b), where a , b are stationary reference points. This process is known as Clarke transformation. This results in the transformation to what can be referred to as a - b stationary frame of reference. Below equation describes the process [53]:

$$\begin{bmatrix} i_a \\ i_b \end{bmatrix} = \begin{bmatrix} \frac{2}{3} & -\frac{1}{3} & -\frac{1}{3} \\ 0 & \frac{\sqrt{3}}{3} & -\frac{\sqrt{3}}{3} \end{bmatrix} \begin{bmatrix} i_A \\ i_B \\ i_C \end{bmatrix}. \quad (3.3)$$

In addition, this transformation can be reversed as follows:

$$\begin{bmatrix} i_A \\ i_B \\ i_C \end{bmatrix} = \begin{bmatrix} 1 & 0 \\ -\frac{1}{2} & \frac{\sqrt{3}}{2} \\ -\frac{1}{2} & -\frac{\sqrt{3}}{2} \end{bmatrix} \begin{bmatrix} i_a \\ i_b \end{bmatrix}. \quad (3.4)$$

The dynamics of this model can be described by the following fifth order coupled nonlinear system [54]:

$$\begin{aligned} \dot{\omega} &= \frac{n_p L_m}{J L_r} (\lambda_a i_b - \lambda_b i_a) - \frac{F}{J} - \frac{T_L}{J} \\ \dot{\lambda}_a &= -\frac{R_r}{L_r} \lambda_a - \omega \lambda_b + \frac{R_r L_m}{L_r} i_a \\ \dot{\lambda}_b &= -\frac{R_r}{L_r} \lambda_b + \omega \lambda_a + \frac{R_r L_m}{L_r} i_b \\ \dot{i}_a &= -\left(\frac{R_s}{\sigma} + \frac{L_m^2 R_r}{\sigma L_r^2}\right) i_a + \frac{L_m R_r}{\sigma L_r^2} \lambda_a + \frac{L_m}{\sigma L_r} \omega \lambda_b + \frac{1}{\sigma} v_a \\ \dot{i}_b &= -\left(\frac{R_s}{\sigma} + \frac{L_m^2 R_r}{\sigma L_r^2}\right) i_b + \frac{L_m R_r}{\sigma L_r^2} \lambda_b - \frac{L_m}{\sigma L_r} \omega \lambda_a + \frac{1}{\sigma} v_b, \end{aligned} \quad (3.5)$$

where ω denotes the IM rotor angular speed in $[rad/s]$, λ_a, λ_b denote the components of the rotor flux in $[Wb]$, i_a, i_b denote the components of stator current in $[A]$, v_a, v_b denote the stator input voltages in $[V]$ and F, T_L denote friction force and external torque in $[Nm]$ respectively. In addition, let $J, L_r, L_s, L_m, R_r, R_s$ denote mechanical inertia in $[Kg \cdot m^2]$, rotor, stator and mutual inductances in $[H]$, rotor and stator resistances in $[\Omega]$, respectively. Note that F, n_p and σ are

defined as follow (μ denotes the coefficient of friction in $[Kg \cdot m^2/s]$):

$$\begin{aligned}
 F &= \mu \omega, \\
 n_p &= \frac{3}{2}(\text{pole pairs}), \\
 \sigma &= L_s - \frac{L_m^2}{L_r}.
 \end{aligned} \tag{3.6}$$

In addition to the stationary two-phase system, there is another important two-

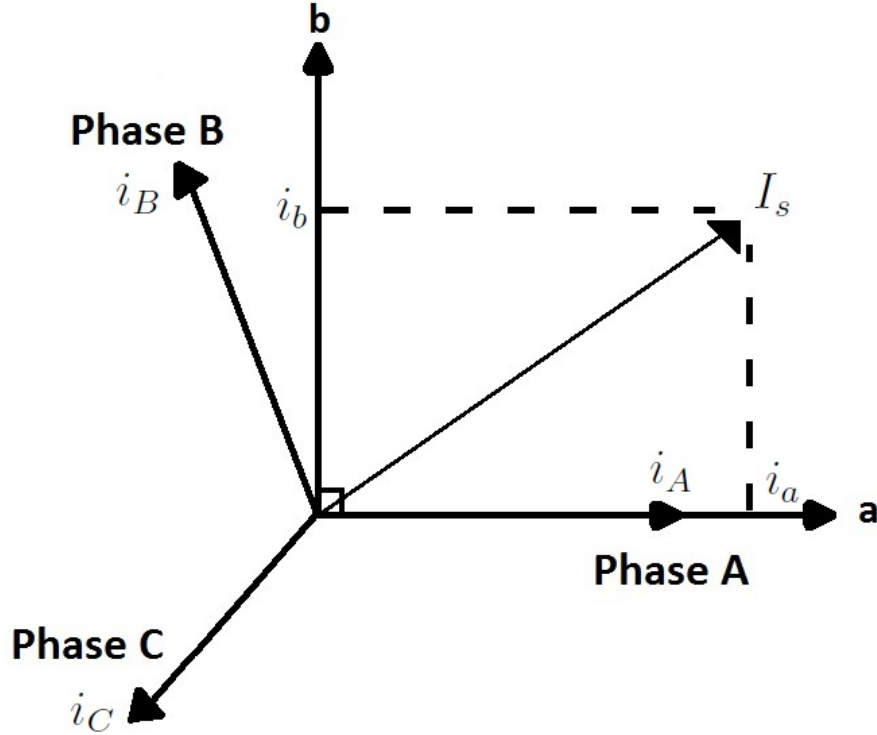


Figure 3.1: (A,B,C) Phasor representation with the corresponding a - b stationary frame of reference representation

phase orthogonal representation of the IM dynamics in rotational coordinates or d - q frame of reference. To transform the IM system from a - b stationary to d - q rotational synchronous frame of reference, Park transformation is applied. The

following equation describes the operation [55]:

$$\begin{bmatrix} y_d \\ y_q \end{bmatrix} = \begin{bmatrix} \cos(\theta) & \sin(\theta) \\ -\sin(\theta) & \cos(\theta) \end{bmatrix} \begin{bmatrix} y_a \\ y_b \end{bmatrix}, \quad (3.7)$$

where y represents either the current i , the flux λ or the voltage v component in the specified frame of reference whereas θ represents the angle of the rotor flux. Note that, the motor synchronous speed ω_s is the time derivative of θ , that is:

$$\dot{\theta} = \omega_s. \quad (3.8)$$

In addition, the inverse transformation is obtained as follows:

$$\begin{bmatrix} y_a \\ y_b \end{bmatrix} = \begin{bmatrix} \cos(\theta) & -\sin(\theta) \\ \sin(\theta) & \cos(\theta) \end{bmatrix} \begin{bmatrix} y_d \\ y_q \end{bmatrix}. \quad (3.9)$$

By utilizing the transformation described by (3.7) and the state variables in (3.5), the IM system model in the d - q frame of reference can be represented by the

following system of dynamical equations:

$$\begin{aligned}
 \dot{\omega} &= \frac{n_p L_m}{J L_r} (\lambda_d i_q - \lambda_q i_d) - \frac{F}{J} - \frac{T_L}{J} \\
 \dot{\lambda}_d &= -\frac{R_r}{L_r} \lambda_d + (\omega_s - \omega) \lambda_q + \frac{R_r L_m}{L_r} i_d \\
 \dot{\lambda}_q &= -\frac{R_r}{L_r} \lambda_q - (\omega_s - \omega) \lambda_d + \frac{R_r L_m}{L_r} i_q \\
 \dot{i}_d &= -\left(\frac{R_s}{\sigma} + \frac{L_m^2 R_r}{\sigma L_r^2}\right) i_d + \frac{L_m R_r}{\sigma L_r^2} \lambda_d + \frac{L_m}{\sigma L_r} \omega \lambda_q + \omega_s i_q + \frac{1}{\sigma} v_d \\
 \dot{i}_q &= -\left(\frac{R_s}{\sigma} + \frac{L_m^2 R_r}{\sigma L_r^2}\right) i_q + \frac{L_m R_r}{\sigma L_r^2} \lambda_q - \frac{L_m}{\sigma L_r} \omega \lambda_d - \omega_s i_d + \frac{1}{\sigma} v_q.
 \end{aligned} \tag{3.10}$$

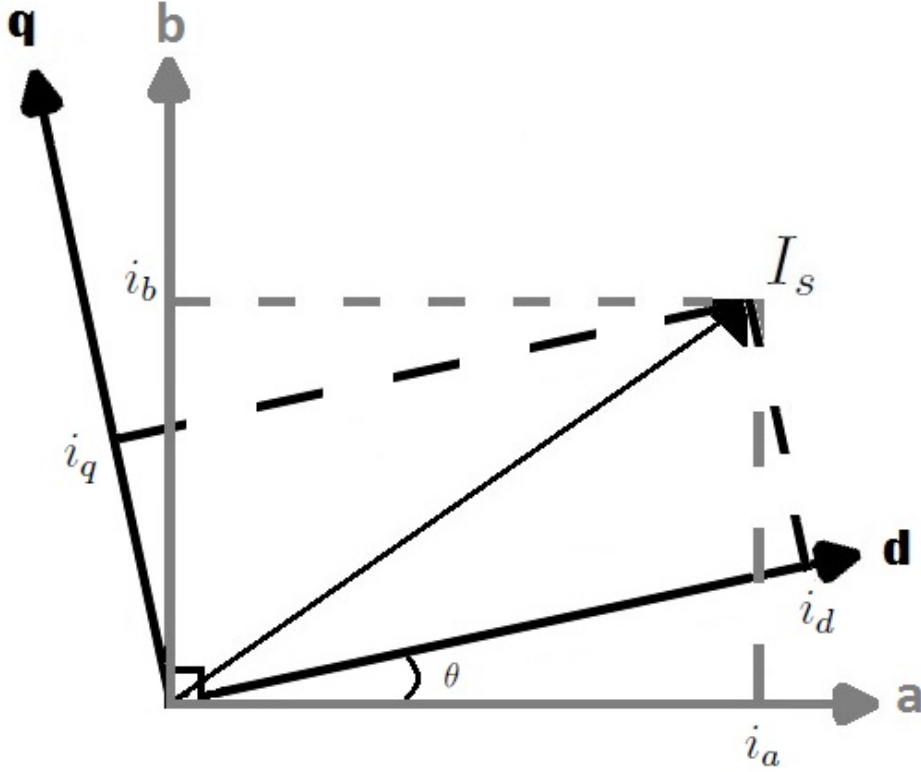


Figure 3.2: Visual description of Park transformation

3.2 IM Model for the Research

Throughout this study, the stationary IM model is considered. In order to achieve the same results -which are explored in next chapters- with other models, the appropriate transformation should be applied. Before advancing any further with the selected model (3.5), the following assumption is very essential to note.

Assumption 2. All systems parameters (resistances, inductances, moment of inertia, coefficient of friction and number of pole pairs) are assumed to be known constants. Also, system state variables (rotor speed, flux and current) are all assumed to be available for measurements. Note that in real life implementation IM magnetic flux is mostly not measurable needs to be estimated.

In order to simplify the model, define the following constants:

$$\begin{aligned} k_0 &= \frac{\mu}{J}, k_1 = \frac{n_p L_m}{J L_r}, k_2 = \frac{R_r}{L_r}, k_3 = \frac{R_r L_m}{L_r}, \\ k_4 &= \left(\frac{R_s}{\sigma} + \frac{L_m^2 R_r}{\sigma L_r^2} \right), k_5 = \frac{L_m R_r}{\sigma L_r^2}, k_6 = \frac{L_m}{\sigma L_r}, k_7 = \frac{1}{\sigma}. \end{aligned} \quad (3.11)$$

To make the model even more convenient, rename the state variables $(\omega, \lambda_a, \lambda_b, i_a, i_b)$ to $(x_1, x_2, x_3, x_4, x_5)$ respectively. Also, rename the system inputs (v_a, v_b) to (u_1, u_2) respectively. The IM dynamical model after

simplification, becomes:

$$\begin{aligned} \dot{x}_1 &= -k_0x_1 + k_1(x_2x_5 - x_3x_4) - \frac{T_L}{J} \\ \dot{x}_2 &= -k_2x_2 - x_1x_3 + k_3x_4 \\ \dot{x}_3 &= -k_2x_3 + x_1x_2 + k_3x_5 \\ \dot{x}_4 &= -k_4x_4 + k_5x_2 + k_6x_1x_3 + k_7u_1 \\ \dot{x}_5 &= -k_4x_5 + k_5x_3 - k_6x_1x_2 + k_7u_2. \end{aligned} \tag{3.12}$$

Throughout this work, the IM system described by the dynamical model (3.12) is used both in design and simulation.

CHAPTER 4

BACKSTEPPING CONTROLLER DESIGN

As stated earlier, the objective is to design an IM tracking control feedback that compensates for the system's uncertainties caused by both the input nonlinearity and the external load torque. In this chapter, the method of adaptive backstepping is introduced. This mechanism is utilized throughout this work to achieve the desired control objective.

4.1 Introduction to Adaptive Backstepping

Backstepping is a control technique that is based on Lyapunov stability theory and LaSalle-Yoshizawa theorem [56]. The technique is very-well known and has proven to be an excellent tool for nonlinear systems control. It is a systematic approach to break down a complex nonlinear system into simpler subsystems and recursively develop a "virtual feedback controller" for each subsystem as a func-

tion of the system's state variables, which helps in constructing the final control input to the original system. More specifically, in each stage, a subsystem virtual control is chosen, which is utilized as reference for the next subsystem design and so on. Controller development is done simultaneously with the construction of the system's Lyapunov function $V(x)$ which consists of the sum of the Lyapunov functions of each individual subsystem. Upon reaching the final stage, $V(x)$ is completely constructed and the original system input can be selected according to the desired control objective. Adaptive control methods and backstepping technique can easily be combined together to form the adaptive backstepping mechanism. This is done by modifying system Lyapunov function $V(x)$ to minimize the unknown parameter estimations' errors. The parameter adaptive laws can be developed simultaneously with backstepping design procedures. Thus, the new controller is a backstepping static feedback that is dependent on the parameter estimates. These estimates are updated continuously via dynamic update laws [52].

4.2 Adaptive Backstepping Controller Design

Consider the IM system (3.12) and define \hat{T}_L as the adaptive parameter associated with the external load torque T_L and the corresponding error \tilde{T}_L as:

$$\tilde{T}_L = T_L - \hat{T}_L. \quad (4.1)$$

Assumption 3. T_L is an unknown constant with known positive boundaries T_{Lmin} and T_{Lmax} , such that $T_{Lmin} \leq T_L \leq T_{Lmax}$.

Define the errors e_1, e_2 as:

$$\begin{aligned} e_1 &= x_1 - r, \\ e_2 &= \dot{e}_1 + \frac{\tilde{T}_L}{J}, \end{aligned} \quad (4.2)$$

where $r(t)$ is a known bounded differentiable reference trajectory. Taking the derivatives, the below system is obtained:

$$\begin{aligned} \dot{e}_1 &= e_2 - \frac{\tilde{T}_L}{J}, \\ \dot{e}_2 &= -k_0(k_1x_2x_5 - k_1x_3x_4 - k_0x_1) + k_1x_5(-k_2x_2 + k_3x_4 \\ &\quad - x_1x_3) - k_1x_4(-k_2x_3 + k_3x_5 + x_1x_2) - k_1x_3(k_6x_1x_3 \\ &\quad - k_4x_4 + k_5x_2 + k_7u_1) + k_1x_2(-k_6x_1x_2 - k_4x_5 \\ &\quad + k_5x_3 + k_7u_2) + \frac{\dot{\tilde{T}}_L}{J} + k_0\frac{T_L}{J} - \ddot{r}. \end{aligned} \quad (4.3)$$

The IM control design approach can be summarized as follows:

In order to drive IM speed according to a reference trajectory, the tracking error has to be minimized. Thus, the design ultimate objective is to stabilize this error. The first step is to apply backstepping technique to come up with a stabilizing controller for the error system in (4.3). The feedback must have an adaptive component to cope with the external torque effect. The next step is to tackle the same problem but after introducing input nonlinearities (dead-zone or hystere-

sis) to the system. Again, to account for the system's uncertainties, additional adaptive laws shall be introduced to update the feedback accordingly. In short, the control feedback development is done in two stages; without and with input nonlinearities respectively. The first stage is done in this chapter while the second stage is to be completed in next chapters.

Back to system (4.3). Following the backstepping procedures, the control input is chosen such that the time derivative of the system's Lyapunov function is negative definite, that is $\dot{V} \leq 0$. Let:

$$V_1 = \frac{1}{2}e_1^2 \geq 0. \quad (4.4)$$

Taking the derivative, results in:

$$\dot{V}_1 = e_1\dot{e}_1 = e_1(e_2 - \frac{\tilde{T}_L}{J}). \quad (4.5)$$

Set the virtual feedback $\phi = -c_1e_1$, c_1 being a selected positive constant:

$$\begin{aligned} \dot{V}_1 &= e_1(e_2 - \frac{\tilde{T}_L}{J}) = e_1\phi + e_1(e_2 - \frac{\tilde{T}_L}{J} - \phi) \\ &= -c_1e_1^2 + e_1(e_2 + c_1e_1) - e_1\frac{\tilde{T}_L}{J}. \end{aligned} \quad (4.6)$$

Now, consider the Lyapunov function:

$$V = V_1 + \frac{1}{2}(e_2 + c_1e_1)^2 + \frac{1}{2\alpha}\tilde{T}_L^2 \geq 0, \quad (4.7)$$

where α is a selected positive constant. The function can be differentiated as follows:

$$\begin{aligned}
\dot{V} &= \dot{V}_1 + (e_2 + c_1 e_1)(\dot{e}_2 + c_1 \dot{e}_1) + \frac{1}{\alpha} \tilde{T}_L \dot{\tilde{T}}_L \\
&= -c_1 e_1^2 + e_1(e_2 + c_1 e_1) - \frac{e_1}{J} \tilde{T}_L + \frac{1}{\alpha} \tilde{T}_L \dot{\tilde{T}}_L \\
&\quad + (e_2 + c_1 e_1)(\dot{e}_2 + c_1 \dot{e}_1) \\
&= -c_1 e_1^2 - c_2 (e_2 + c_1 e_1)^2 - \tilde{T}_L \left(\frac{e_1}{J} - \frac{\dot{\tilde{T}}_L}{\alpha} \right) \\
&\quad + (e_2 + c_1 e_1)(\dot{e}_2 + (1 + c_1 c_2) e_1 + (c_1 + c_2) e_2 - c_1 \frac{\tilde{T}_L}{J}), \tag{4.8}
\end{aligned}$$

where c_2 is a selected positive constant. Define Υ and W as follow:

$$\begin{aligned}
\Upsilon &= ((1 + c_1 c_2) e_1 + (c_1 + c_2) e_2 - k_0 (k_1 x_2 x_5 - k_1 x_3 x_4 \\
&\quad - k_0 x_1) + k_1 x_5 (-k_2 x_2 + k_3 x_4 - x_1 x_3) - k_1 x_4 (-k_2 x_3 \\
&\quad + k_3 x_5 + x_1 x_2) - k_1 x_3 (k_5 x_2 - k_4 x_4 + k_6 x_1 x_3) \\
&\quad + k_1 x_2 (k_5 x_3 - k_4 x_5 - k_6 x_1 x_2) - \ddot{r}) \\
&= \dot{e}_2 + (1 + c_1 c_2) e_1 + (c_1 + c_2) e_2 - \frac{\dot{\tilde{T}}_L}{J} - k_0 \frac{T_L}{J} \\
&\quad + k_1 k_7 x_3 u_1 - k_1 k_7 x_2 u_2, \tag{4.9}
\end{aligned}$$

$$W = c_1 e_1^2 + c_2 (e_2 + c_1 e_1)^2 \geq 0. \tag{4.10}$$

Substitute (4.9) and (4.10) in (4.8) and simplify to get:

$$\begin{aligned} \dot{V} = & -W + (e_2 + c_1 e_1) \left(\Upsilon - \frac{\dot{\hat{T}}_L}{J} + k_0 \frac{T_L}{J} - c_1 \frac{\tilde{T}_L}{J} \right) \\ & - k_1 k_7 x_3 u_1 + k_1 k_7 x_2 u_2 - \tilde{T}_L \left(\frac{e_1}{J} + \frac{\dot{\hat{T}}_L}{\alpha} \right). \end{aligned} \quad (4.11)$$

Note that:

$$\dot{\hat{T}}_L = -\dot{\tilde{T}}_L. \quad (4.12)$$

By manipulating (4.11), the below is obtained:

$$\begin{aligned} \dot{V} = & -W + (e_2 + c_1 e_1) \left(\Upsilon - \frac{\dot{\hat{T}}_L}{J} + \frac{k_0}{J} (T_L - \tilde{T}_L) \right) \\ & - k_1 k_7 x_3 u_1 + k_1 k_7 x_2 u_2 - \tilde{T}_L \left(\frac{e_1}{J} + \frac{\dot{\hat{T}}_L}{\alpha} \right) \\ & + \left(\frac{c_1 - k_0}{J} \right) (e_2 + c_1 e_1). \end{aligned} \quad (4.13)$$

Now, let the dynamics of the adaptive parameter \hat{T}_L be defined by the following projection law:

$$\dot{\hat{T}}_L = Proj(\hat{T}_L, \Omega) = \begin{cases} -\alpha \Omega & \text{if; } T_{Lmin} < \hat{T}_L < T_{Lmax}, \\ & \text{or; } \hat{T}_L = T_{Lmax} \text{ and } \Omega > 0, \\ & \text{or; } \hat{T}_L = T_{Lmin} \text{ and } \Omega < 0, \\ 0 & \text{Otherwise,} \end{cases} \quad (4.14)$$

where Ω is defined as:

$$\Omega = \frac{1}{J}(e_1 + (c_1 - k_0)(e_2 + c_1 e_1)). \quad (4.15)$$

This projection law ensures that the adaptive parameter \hat{T}_L stays within specified boundaries for all $t \geq 0$. Furthermore, by applying this law, the below inequality is guaranteed:

$$-\tilde{T}_L \left(\frac{e_1}{J} + \frac{\dot{\hat{T}}_L}{\alpha} + \left(\frac{c_1 - k_0}{J} \right) (e_2 + c_1 e_1) \right) \leq 0. \quad (4.16)$$

For simplicity, let:

$$\psi = \Upsilon - \frac{\dot{\hat{T}}_L}{J} + \frac{k_0}{J} \hat{T}_L. \quad (4.17)$$

From (4.13), applying the adaptive law (4.14) and making use of the result (4.16) and the definition (4.17), the below result is obtained:

$$\dot{V} \leq -W + (e_2 + c_1 e_1)(\psi - k_1 k_7 x_3 u_1 + k_1 k_7 x_2 u_2). \quad (4.18)$$

The following control inputs shall be used:

$$u_1 = \frac{x_3 \psi}{k_1 k_7 (x_2^2 + x_3^2)}, \quad u_2 = \frac{-x_2 \psi}{k_1 k_7 (x_2^2 + x_3^2)}. \quad (4.19)$$

Note that the magnitude of the IM rotor flux $\sqrt{x_2^2 + x_3^2}$ is assumed to be a positive quantity. Clearly, using the control inputs (4.19) in (4.18), yields the following result:

$$\dot{V} \leq -W. \quad (4.20)$$

From (4.20), by LaSalle theorem, the proposed controller ensures global asymptotic stability of the states in the dynamical system (4.3). Thus, for any initial condition $x_1(0) \in \mathbb{R}$:

$$\lim_{t \rightarrow \infty} x_1(t) - r(t) = 0. \quad (4.21)$$

4.3 Simulations and Results

In this section, the IM system is simulated with the control feedback developed in the previous section. The simulation is conducted using MATLAB SIMULINK and consists of two parts; without and with the effect of external torque T_L . For the first part, the objective is to test the controller in absence of any external factors that affect the system performance. So, the assumption is that T_L is known to be zero, which eliminates the need to apply the torque adaptive law (4.14). The selected IM system specifications for the first part are presented in table 4.1 [54], whereas the specifications for the second part are shown in table 4.2 [27]. Both simulation scenarios are done with a set of three known reference trajectories; constant, ramp and sinusoid. The initial conditions are set as $\{x_1(0) = 0 \text{ [rad/s]}, x_2(0) = 0.1 \text{ [Wb]}, x_3(0) = 0.1 \text{ [Wb]}, x_4(0) = 0 \text{ [A]}, x_5(0) = 0 \text{ [A]}\}$. The simulation time is $T = 10 \text{ [s]}$ and backstepping controller constants are selected as $\{c_1 = 1, c_2 = 21\}$. The references chosen for this part are $\{r(t)_{constant} = 60, 80, 100, r(t)_{ramp} = 8t, r(t)_{sine} = 80\sin(t)\}$. The results of the simulation are shown in figures 4.1-4.7. As it can be seen from figure 4.1, the controller has succeeded to achieve references tracking with very good performance. The rise time of the trajectory is at max 2.3[s] as in the constant reference cases, and very insignificant in case of ramp and sine references. Also, the applied feedback stays within a range of $(-5[V], 5[V])$ throughout simulation time, as shown in figures 4.2 and 4.3. Note that the input voltage for ramp tracking is expected to be increasing since the reference itself is increasing in magnitude. In

addition, figures 4.4-4.7 depict the rest of the state variables of the system. As seen from these figures, all states are bounded throughout the simulation time. Overall, the control feedback achieved a decent trajectory tracking performance. The second part of the simulation treats the case of non-zero load torque exerted on the IM system. The reference functions are selected as $\{r(t)_{constant} = 80, 100, 120, r(t)_{ramp} = 8t, r(t)_{sine} = 80\sin(t)\}$. The initial conditions are kept the same with an additional condition for the adaptive parameter $\hat{T}_L = 0$ [Nm]. The actual load applied to the system is set as $T_L = 1$ [Nm] with a maximum bound of $T_{Lmax} = 100$ [Nm]. The simulation time is set as $T = 20$ [s] and backstepping controller constants are selected as $\{c_1 = 1, c_2 = 31\}$. The results of the simulation are shown in figures 4.8-4.15. From figure 4.8, the feedback has successfully achieved tracking of various constants, ramp and sinusoidal references. The rise time is reached in less than 5s in the worst case scenario and almost instantaneous in best cases. This performance is inferior compared to the first part of the simulation in 4.1 which is expected. In addition, control feedback performance is seen in plots 4.9 and 4.10. The outcome is bounded in the range $(-60[V], 60[V])$, which does not exceed or even come close the rated value of 220V. Furthermore, figures 4.11-4.15 are plots for the other state variables of the system. As shown, all states are bounded throughout the simulation time. In general, the controller perform in satisfactory manner based on illustrated results.

Table 4.1: Induction Motor rated Specifications and Parameters (for simulation part 1)

Rated Specifications	
Pole Pairs	3
Voltage	120 [V]
Current	3.4 [A]
Power	400 [W]
Speed	157 [rad/s]
IM Parameters	
R_s	2.85 [Ω]
R_r	4.0 [Ω]
L_s	0.19667 [H]
L_r	0.19667 [H]
L_m	0.1886 [H]
J	0.001 [$Kg \cdot m^2$]
μ	0.0002 [$Kg \cdot m^2/s$]

Table 4.2: Induction Motor rated Specifications and Parameters (for simulation part 2)

Rated Specifications	
Pole Pairs	2
Voltage	220 [V]
Current	7.5 [A]
Power	1500 [W]
Speed	149.7 [rad/s]
IM Parameters	
R_s	1.633 [Ω]
R_r	0.93 [Ω]
L_s	0.142 [H]
L_r	0.076 [H]
L_m	0.099 [H]
J	0.0111 [$Kg \cdot m^2$]
μ	0.00222 [$Kg \cdot m^2/s$]

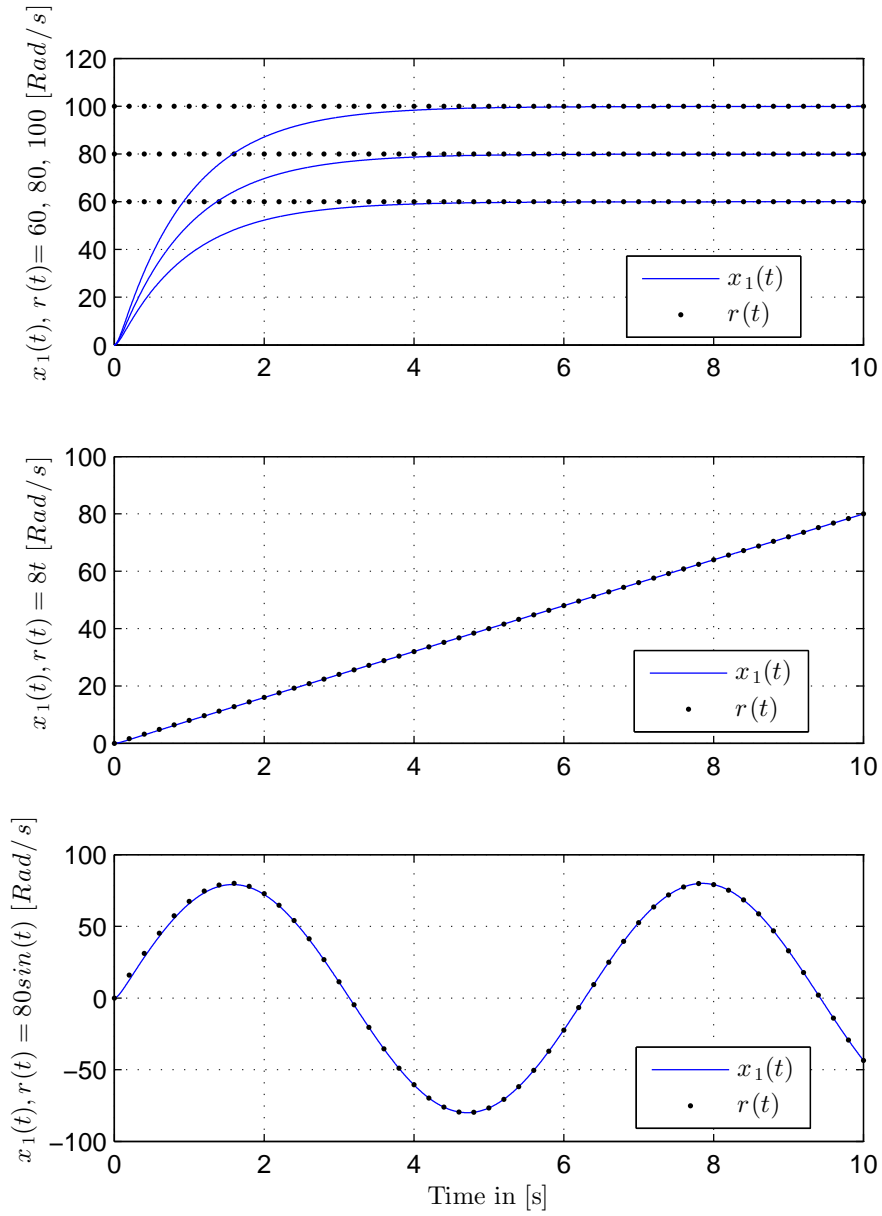


Figure 4.1: Speed tracking performance of IM (with $T_L = 0$) against constant, ramp and sinusoidal reference trajectory respectively.

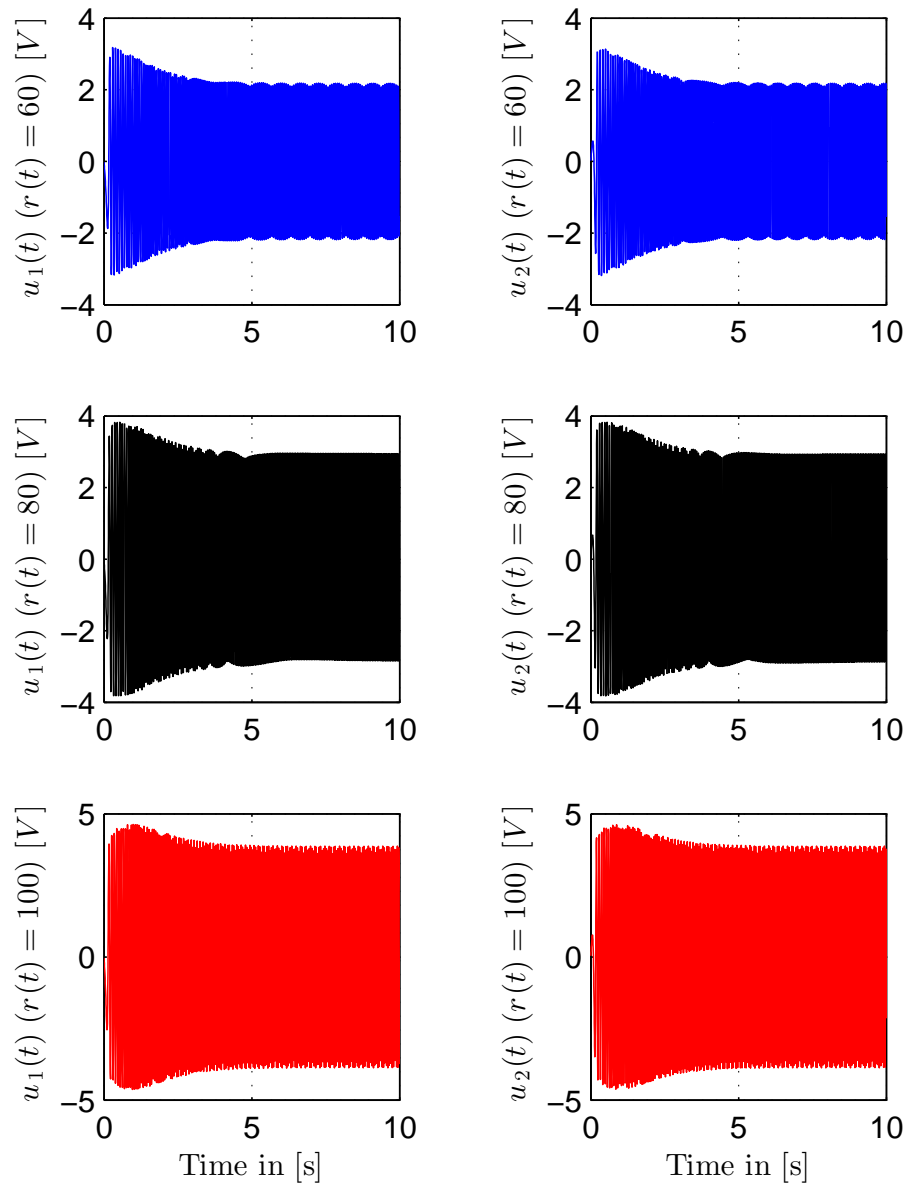


Figure 4.2: Applied control input voltages of IM (with $T_L = 0$) against various constant references.

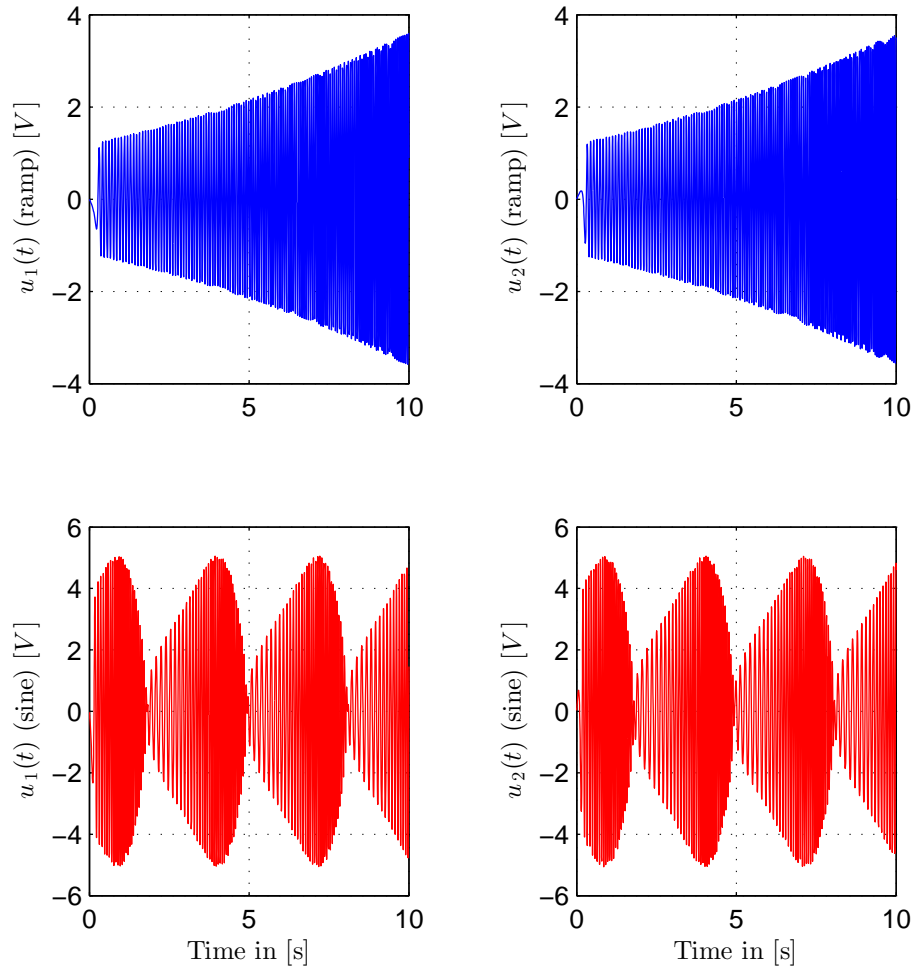


Figure 4.3: Applied control input voltages of IM (with $T_L = 0$) against ramp and sinusoid references respectively.

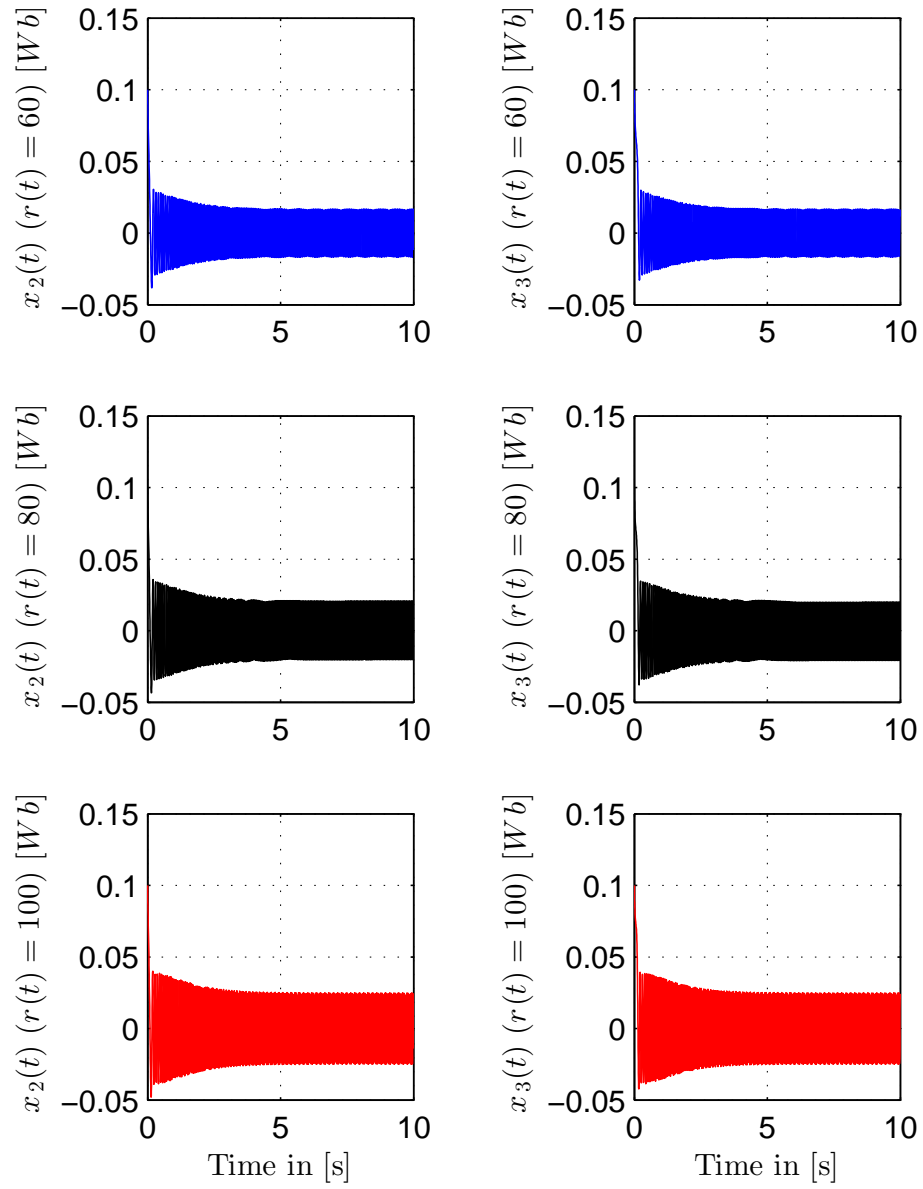


Figure 4.4: Magnetic flux components of IM (with $T_L = 0$) for various constant references.

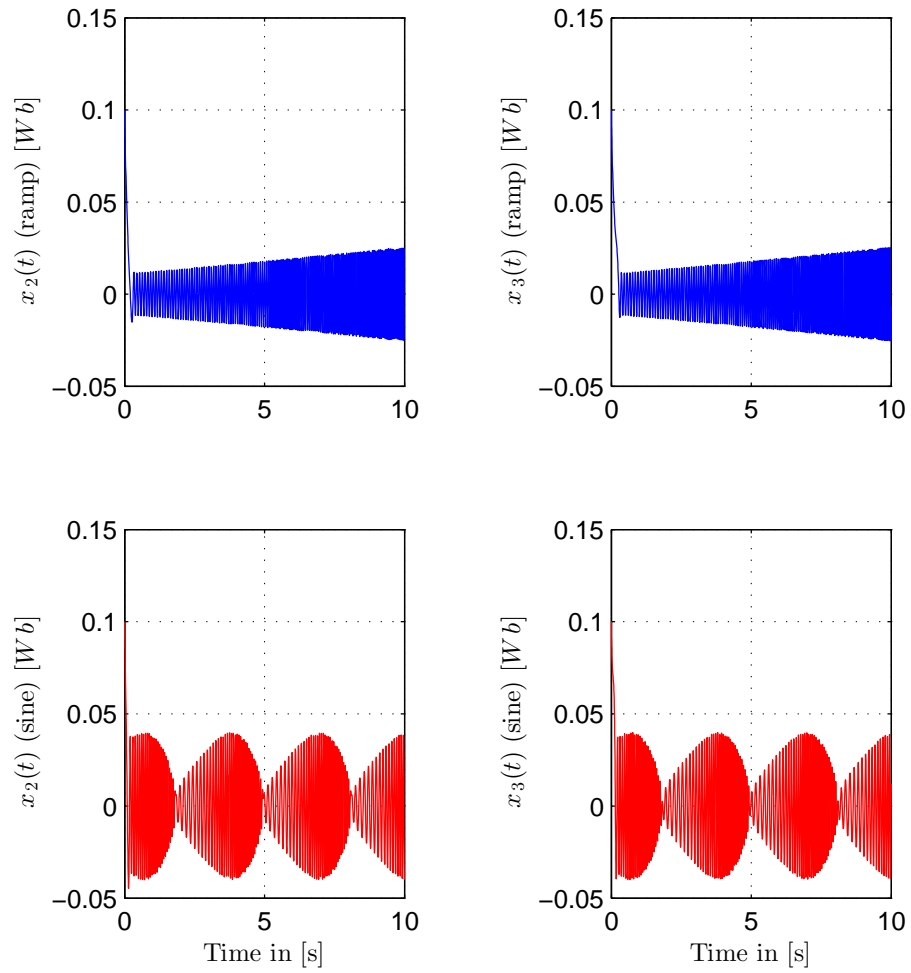


Figure 4.5: Magnetic flux components of IM (with $T_L = 0$) for ramp and sinusoid references respectively.

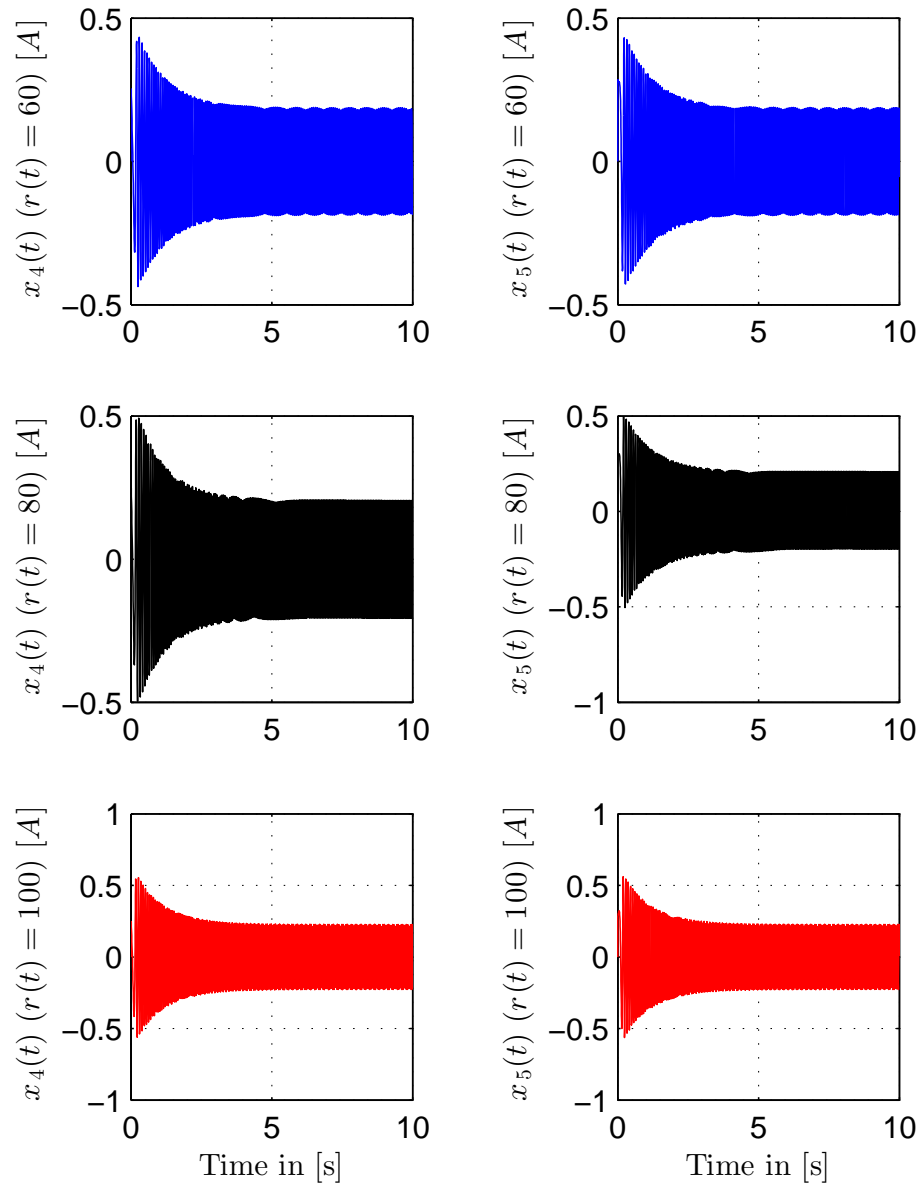


Figure 4.6: Current components of IM (with $T_L = 0$) for various constant references.

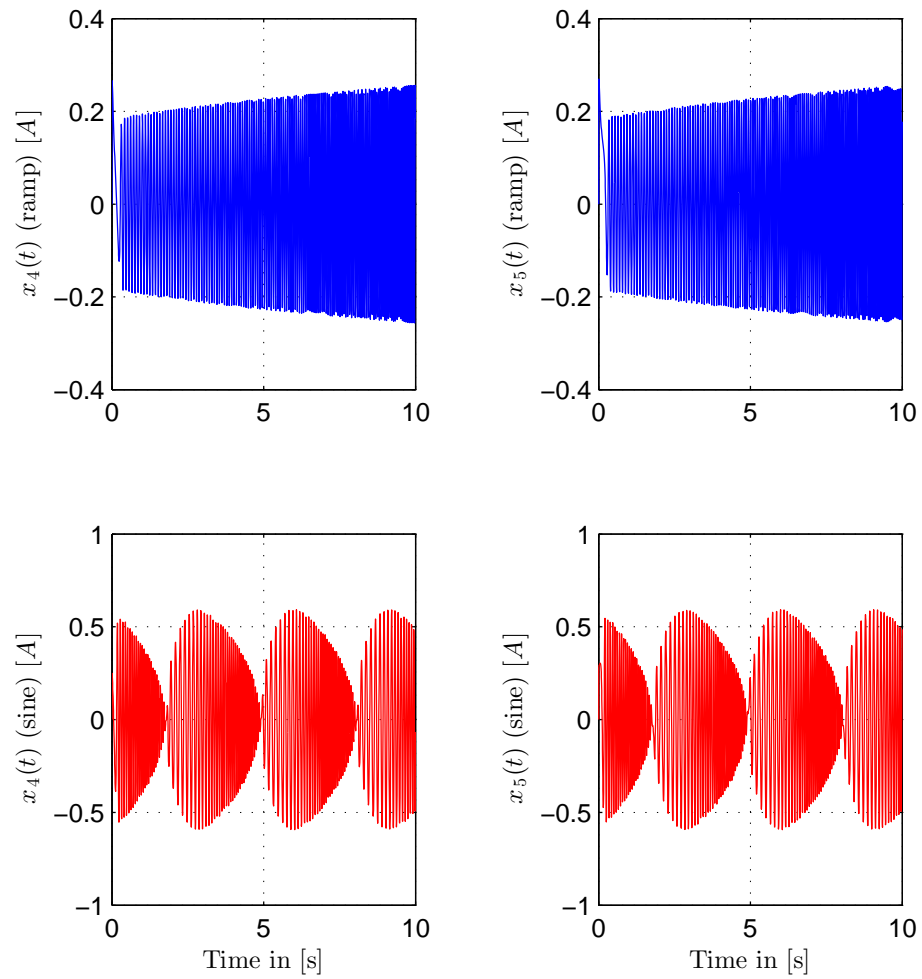


Figure 4.7: Current components of IM (with $T_L = 0$) for ramp and sinusoid references respectively.

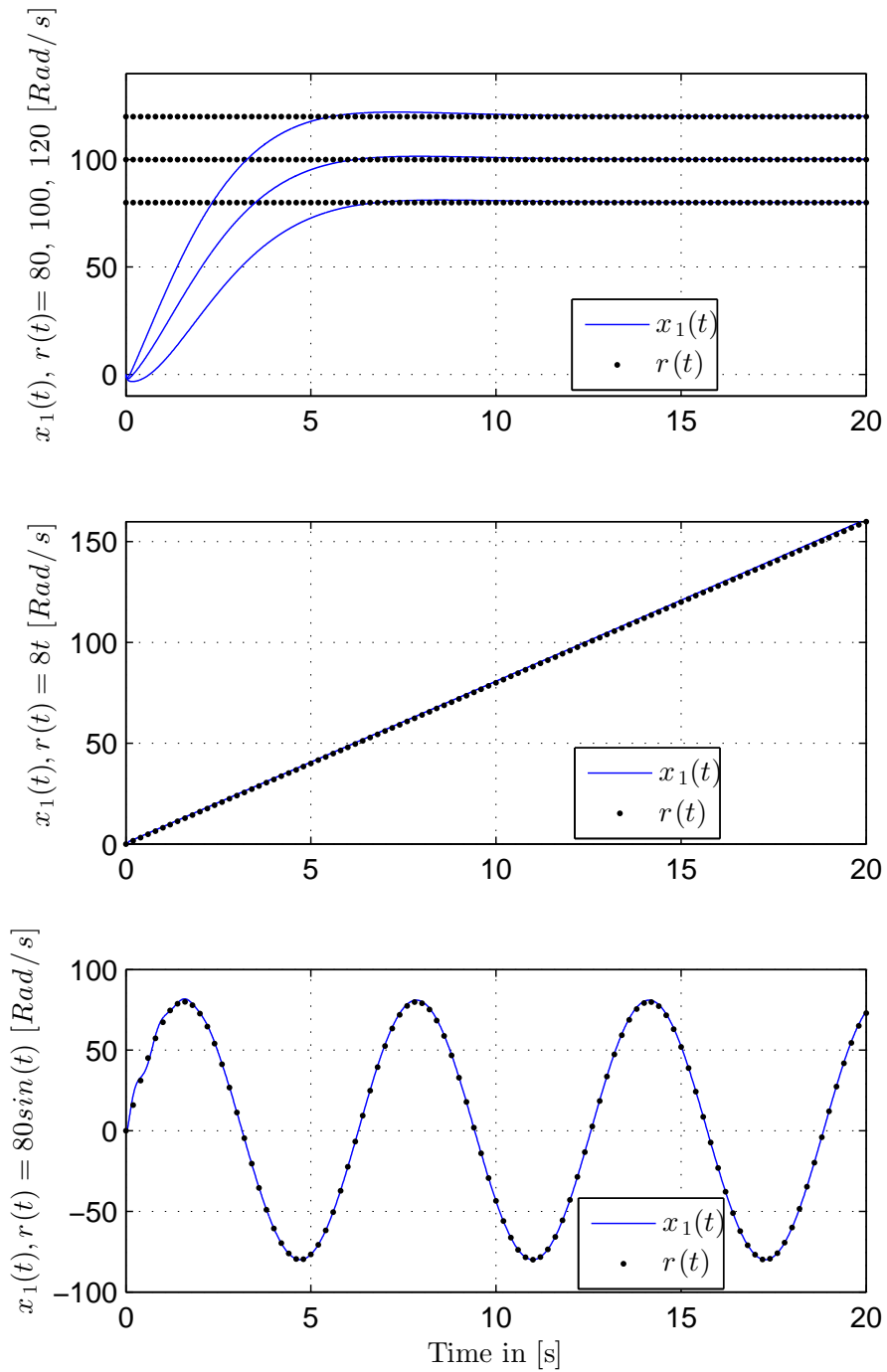


Figure 4.8: Speed tracking performance of IM (with $T_L = 1$ [Nm]) against constant, ramp and sinusoidal reference trajectory respectively.

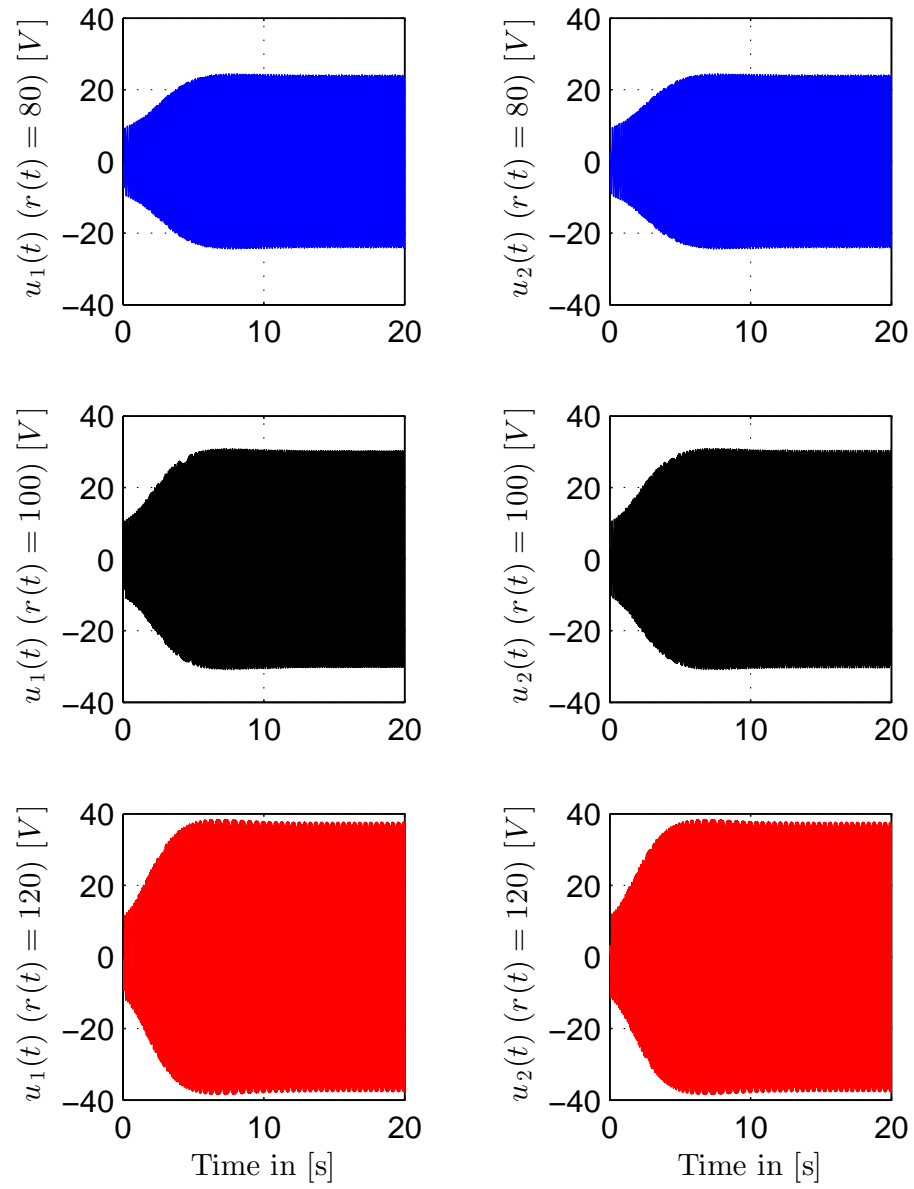


Figure 4.9: Applied control input voltages of IM (with $T_L = 1$ [Nm]) against various constant references.

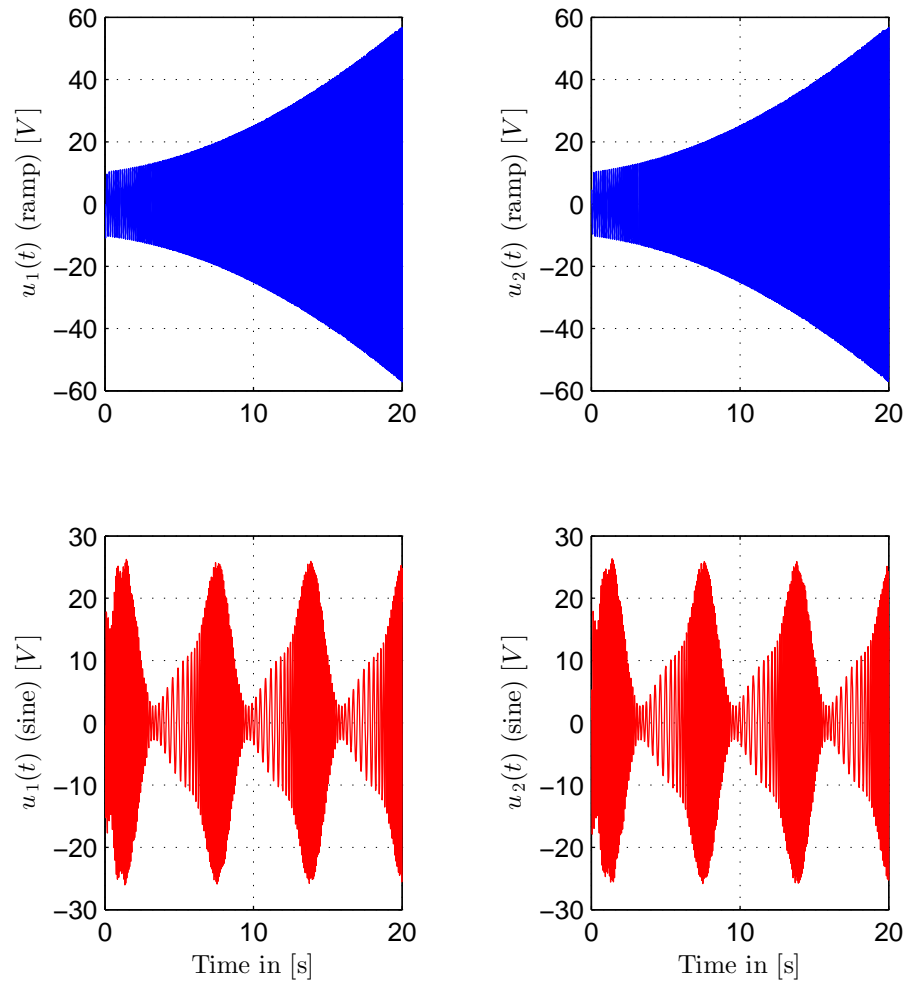


Figure 4.10: Applied control input voltages of IM (with $T_L = 1$ [Nm]) against ramp and sinusoid references respectively.

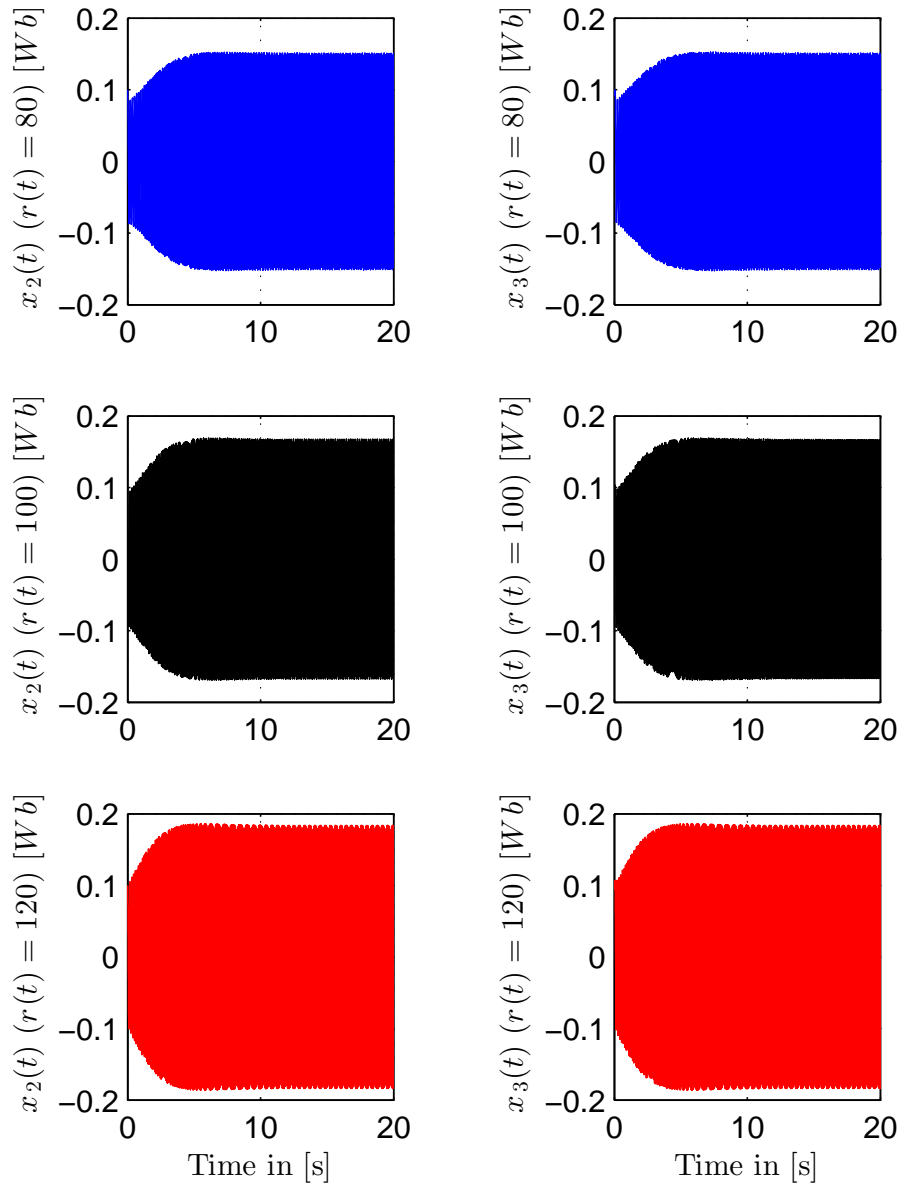


Figure 4.11: Magnetic flux components of IM (with $T_L = 1$ [Nm]) for various constant references.

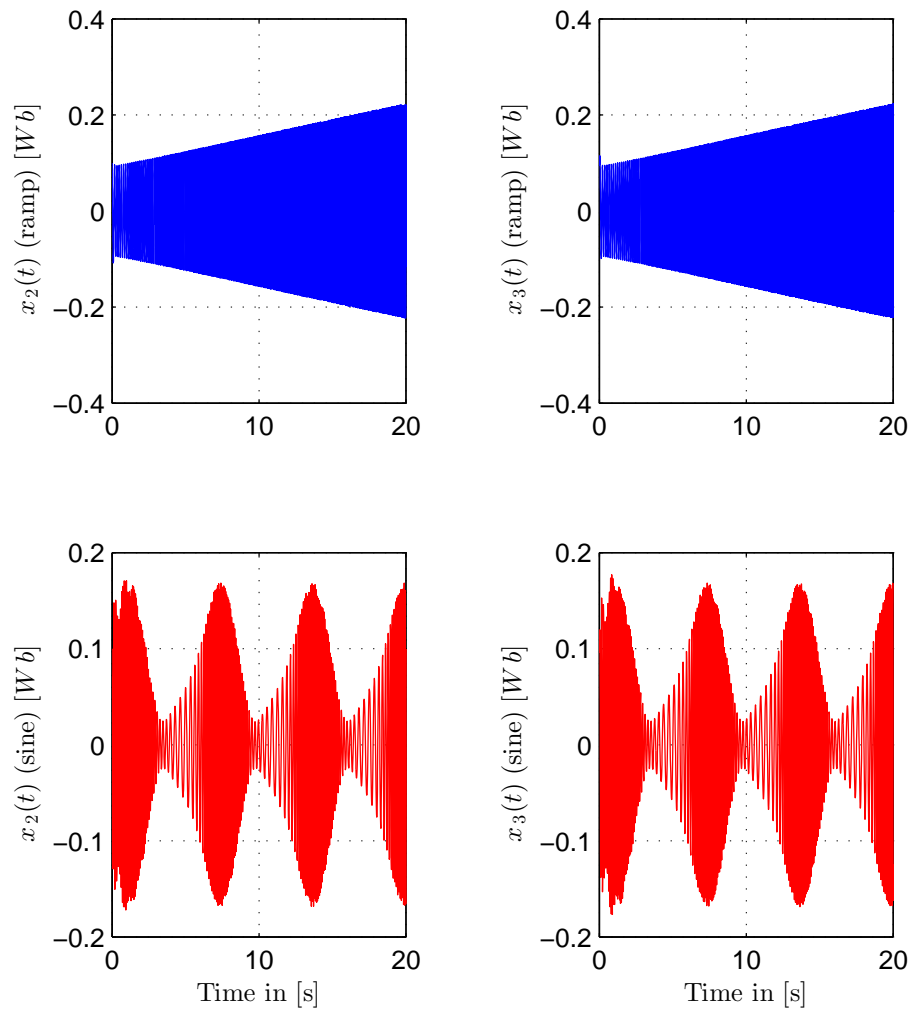


Figure 4.12: Magnetic flux components of IM (with $T_L = 1$ [Nm]) for ramp and sinusoid references respectively.

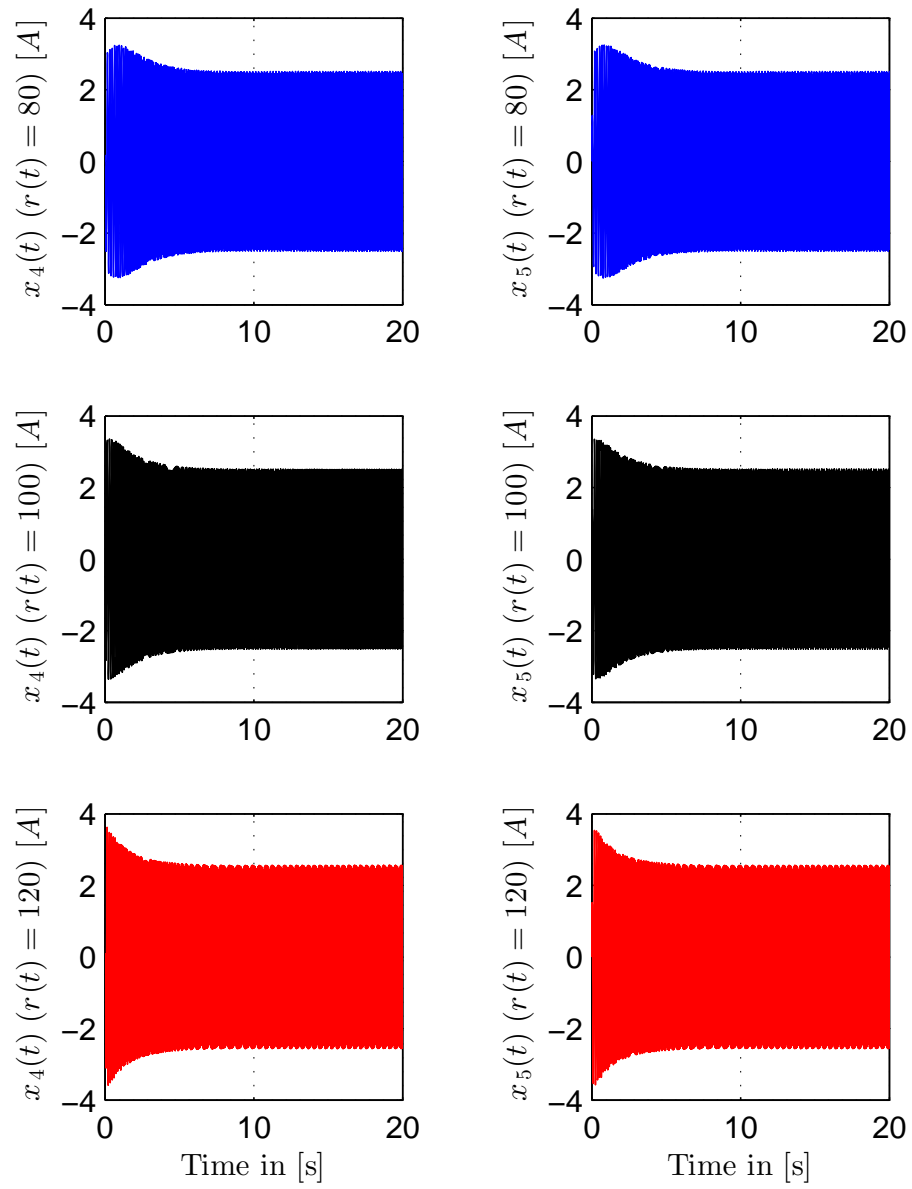


Figure 4.13: Current components of IM (with $T_L = 1$ [Nm]) for various constant references.

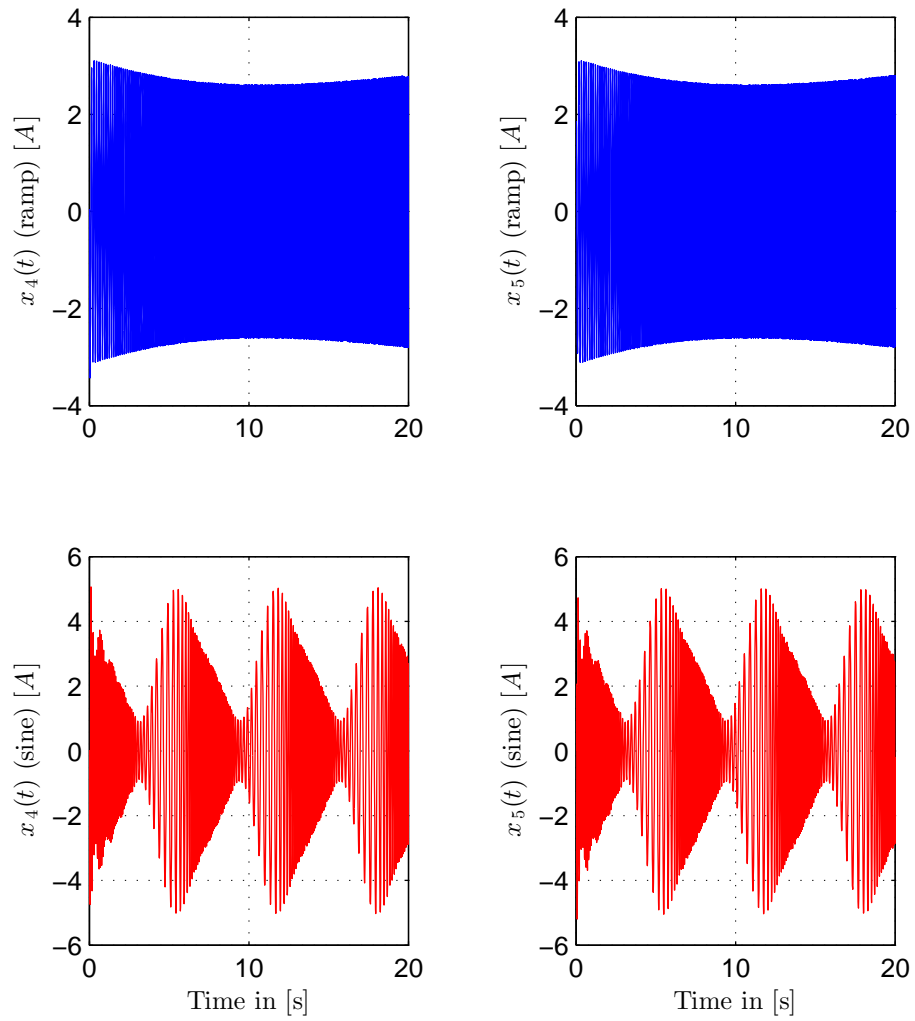


Figure 4.14: Current components of IM (with $T_L = 1$ [Nm]) for ramp and sinusoid references respectively.

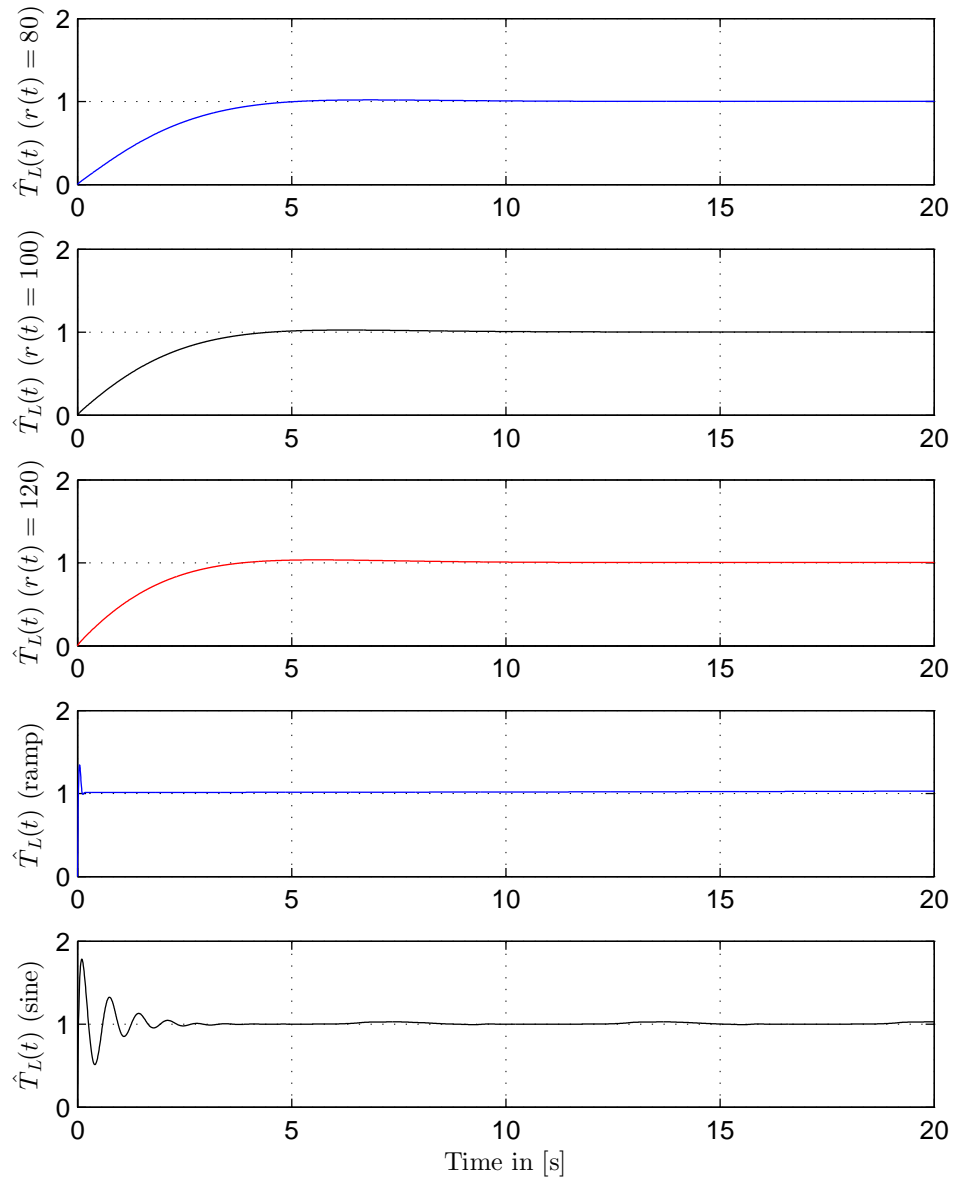


Figure 4.15: Load torque adaptive parameter \hat{T}_L performance for constant, ramp and sinusoid references respectively.

CHAPTER 5

IM WITH SYMMETRIC DEAD-ZONE INPUT

5.1 Input Nonlinearity Effect

Now, consider the system (3.12) and apply the feedback developed in the previous chapter (4.19). This time assume that the system's inputs (u_1, u_2) are subjected to some nonlinearities such as dead-zone or backlash. The presence of any of these nonlinearities (even with very small parameters) can have a very devastating effect on the controller performance. Figure 5.1 shows the IM speed tracking performance after introducing dead-zone and backlash (respectively) in the system input, while figure 5.2 depicts the applied voltages in both cases. Clearly, the feedback has significantly failed to even come close the desired reference function. The nonlinearities applied in these scenarios are very limited in range, yet, effective enough to sabotage the controller performance. Thus, the feedback has to be

revisited and updated to account for such damaging effects.

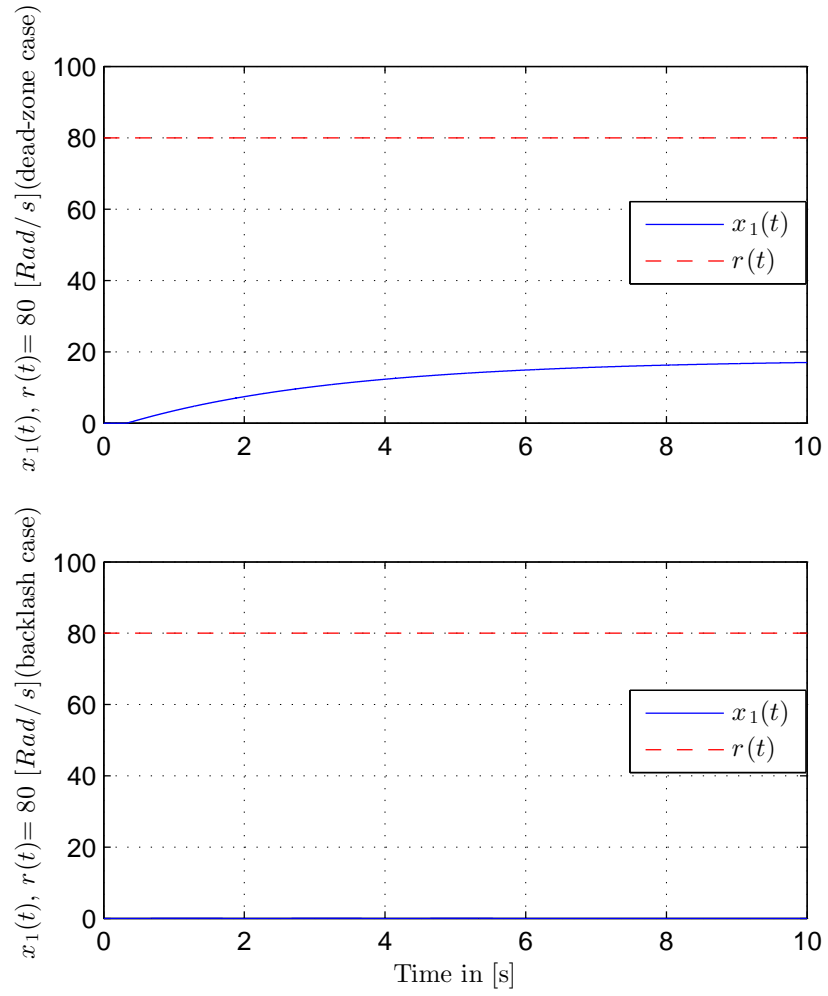


Figure 5.1: Speed tracking performance of IM (with dead-zone/backlash inputs nonlinearities respectively) against constant reference with no applied compensation.

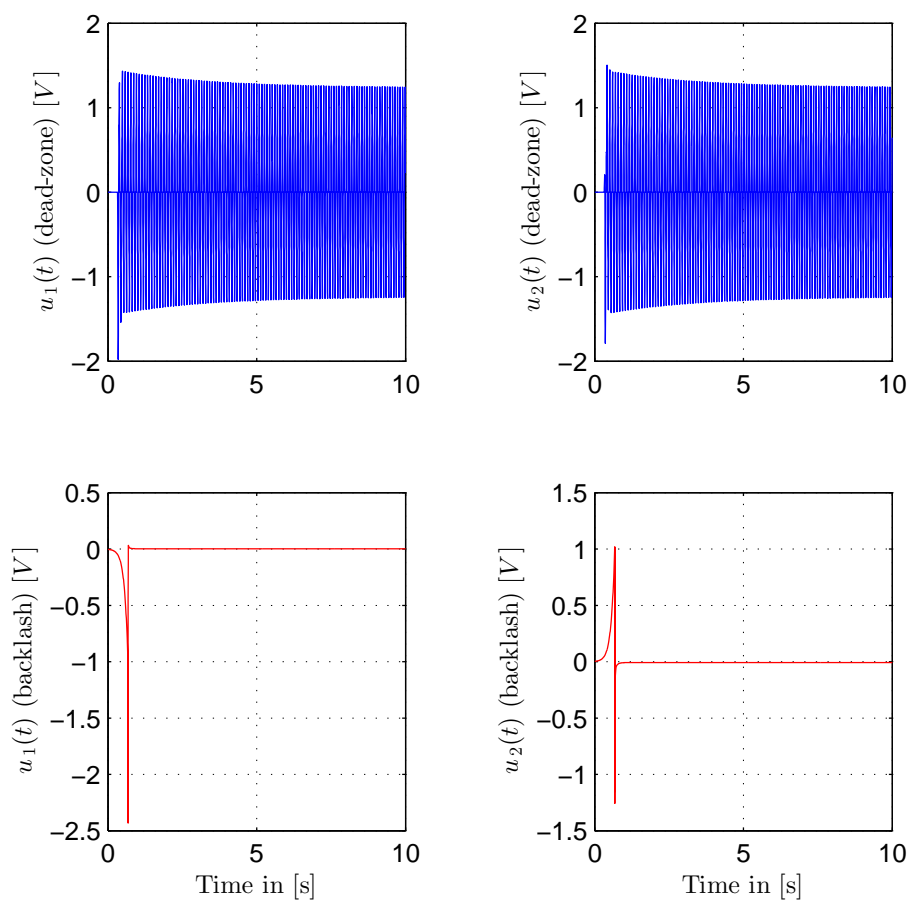


Figure 5.2: Applied control input voltages (u_1 and u_2) of IM in cases of dead-zone input and backlash input respectively with no applied compensation.

5.2 Symmetric Dead-zone Modeling

The symmetric dead-zone nonlinearity $D(\cdot)$ for a scalar input u is defined as [6]:

$$D(u) = \begin{cases} m(u - b) & \text{if; } u > b, \\ 0 & \text{if; } -b \leq u \leq b, \\ m(u + b) & \text{if; } u < -b, \end{cases} \quad (5.1)$$

where m, b are unknown positive and upper bounded constants. That is, there exist $b_{min}, b_{max}, m_{min}$ and m_{max} such that:

$$b_{min} \leq b \leq b_{max} \text{ and } m_{min} \leq m \leq m_{max}. \quad (5.2)$$

$D(u)$ can also be represented alternatively as follows [6]:

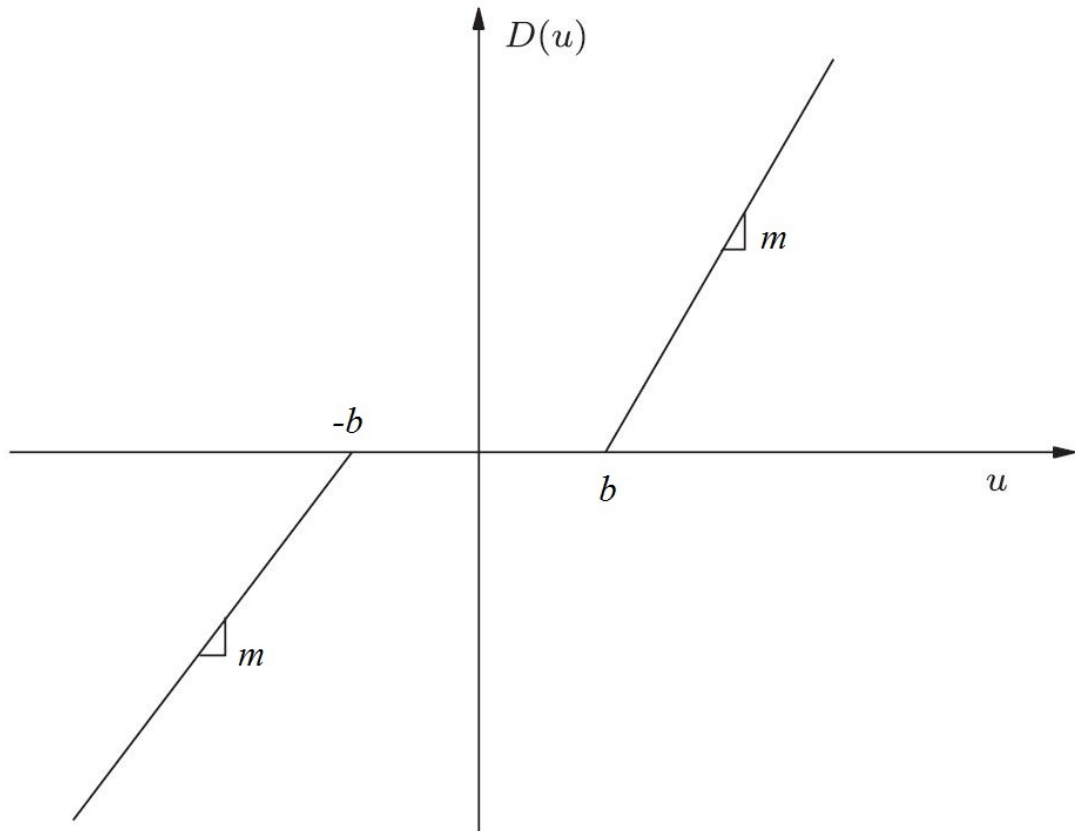


Figure 5.3: Symmetric dead-zone nonlinearity

$$D(u) = mu + \eta(u), \quad (5.3)$$

where $\eta(u)$ is a bounded perturbation function with a maximum bound of $\eta_{max} = b_{max}m_{max}$, which has the following definition:

$$\eta(u) = \begin{cases} -mb & \text{if; } u > b, \\ -mu & \text{if; } -b \leq u \leq b, \\ mb & \text{if; } u < -b. \end{cases} \quad (5.4)$$

Assumption 4. Dead-zone parameters boundaries, i.e., $b_{min}, b_{max}, m_{min}, m_{max}$ and η_{max} are all assumed to be known positive constants. This claim is justified since having some knowledge about the parameters' boundaries seems to be a very natural assumption in engineering practice.

5.3 Controller Design for Symmetric Dead-zone

Input

Now, suppose that the inputs applied to the IM stator (u_1, u_2) experience unknown symmetric dead-zone behavior. Consequently, the effective IM system inputs are replaced by $(D(u_1), D(u_2))$. Let \hat{m} be the adaptive control parameter. Define the error \tilde{m} as:

$$\tilde{m} = \frac{1}{m} - \hat{m}. \quad (5.5)$$

The system Lyapunov function in (4.7) is updated to account for dead-zone parameter compensation as follows:

$$V = V_1 + \frac{1}{2}(e_2 + c_1 e_1)^2 + \frac{1}{2\alpha} \tilde{T}_L^2 + \frac{1}{2\gamma} m \tilde{m}^2 \geq 0, \quad (5.6)$$

where γ is a selected positive constant. Now, taking the time derivative and utilizing (4.18) result in:

$$\begin{aligned} \dot{V} = & -W + (e_2 + c_1 e_1)(\psi + k_1 k_7 x_2 D(u_2) - k_1 k_7 x_3 D(u_1)) \\ & + \frac{1}{\gamma} m \tilde{m} \dot{\tilde{m}}. \end{aligned} \quad (5.7)$$

Choose the inputs to be:

$$u_1 = \frac{-\hat{m} x_3 (-\psi + v)}{k_1 k_7 (x_2^2 + x_3^2)}, \quad u_2 = \frac{\hat{m} x_2 (-\psi + v)}{k_1 k_7 (x_2^2 + x_3^2)}. \quad (5.8)$$

Substituting (5.3) and (5.8) in (5.7), results in:

$$\begin{aligned} \dot{V} = & -W + (e_2 + c_1 e_1) \left(\psi + k_1 k_7 x_2 \left(m \frac{\hat{m} x_2 (-\psi + v)}{k_1 k_7 (x_2^2 + x_3^2)} \right. \right. \\ & \left. \left. + \eta(u_2) \right) - k_1 k_7 x_3 \left(m \frac{-\hat{m} x_3 (-\psi + v)}{k_1 k_7 (x_2^2 + x_3^2)} + \eta(u_1) \right) \right) \\ & + \frac{1}{\gamma} m \tilde{m} \dot{\tilde{m}}. \end{aligned} \quad (5.9)$$

Note that:

$$\begin{aligned}
m\hat{m} &= m\left(\frac{1}{m} - \tilde{m}\right) = 1 - m\tilde{m}, \\
\dot{\tilde{m}} &= -\dot{\hat{m}}.
\end{aligned} \tag{5.10}$$

Manipulating (5.9) and using (5.10), \dot{V} can be bounded as:

$$\begin{aligned}
\dot{V} &\leq -W + (e_2 + c_1e_1)(\psi + k_1k_7x_2\left(\frac{(1 - m\tilde{m})x_2(-\psi + v)}{k_1k_7(x_2^2 + x_3^2)}\right) \\
&\quad - k_1k_7x_3\left(-\frac{(1 - m\tilde{m})x_3(-\psi + v)}{k_1k_7(x_2^2 + x_3^2)}\right)) \\
&\quad + k_1k_7|(e_2 + c_1e_1)x_3\eta(u_1)| + k_1k_7|(e_2 + c_1e_1)x_2\eta(u_2)| \\
&\quad - \frac{1}{\gamma}m\tilde{m}\dot{\hat{m}}.
\end{aligned} \tag{5.11}$$

Note that $k_1, k_7 > 0$. Now, using the fact that $|xy| \leq |x||y|$ for any $x, y \in \mathbb{R}$ and with some simplifications, the inequality is reduced to:

$$\begin{aligned}
\dot{V} &\leq -W + (e_2 + c_1e_1)v + k_1k_7|e_2 + c_1e_1||x_3||\eta(u_1)| \\
&\quad + k_1k_7|e_2 + c_1e_1||x_2||\eta(u_2)| - \frac{1}{\gamma}m\tilde{m}\dot{\hat{m}} \\
&\quad - m\tilde{m}(-\psi + v)(e_2 + c_1e_1).
\end{aligned} \tag{5.12}$$

Now, set the adaptive parameter dynamics according to the following projection

law:

$$\dot{\hat{m}} = Proj(\hat{m}, \Phi) = \begin{cases} -\gamma \Phi & \text{if; } \frac{1}{m_{max}} < \hat{m} < \frac{1}{m_{min}}, \\ & \text{or; } \hat{m} = \frac{1}{m_{min}} \text{ and } \Phi > 0, \\ & \text{or; } \hat{m} = \frac{1}{m_{max}} \text{ and } \Phi < 0, \\ 0 & \text{Otherwise,} \end{cases} \quad (5.13)$$

where Φ is defined as:

$$\Phi = (-\psi + v)(e_2 + c_1 e_1). \quad (5.14)$$

This update law ensures that the adaptive parameter \hat{m} stays within previously specified boundaries in (5.2) for all $t \geq 0$ and satisfies the below inequality:

$$-\frac{1}{\gamma} m \tilde{m} \dot{\hat{m}} - m \tilde{m} (-\psi + v)(e_2 + c_1 e_1) \leq 0, \quad (5.15)$$

which entails that:

$$\begin{aligned} \dot{V} \leq & -W + (e_2 + c_1 e_1)v + k_1 k_7 |e_2 + c_1 e_1| |x_3| |\eta(u_1)| \\ & + k_1 k_7 |e_2 + c_1 e_1| |x_2| |\eta(u_2)|. \end{aligned} \quad (5.16)$$

Now, set v as follows:

$$v = -\frac{(k_1 k_7 (|x_2| + |x_3|) \eta_{max})^2 (e_2 + c_1 e_1)}{k_1 k_7 (|x_2| + |x_3|) \eta_{max} |e_2 + c_1 e_1| + \epsilon_1 (e_2 + c_1 e_1)^2 + \epsilon_2}, \quad (5.17)$$

where ϵ_1 is a small constant satisfies $0 \leq \epsilon_1 < c_2$, and ϵ_2 is a sufficiently small chosen positive constant. Note that by setting v as above, the need to utilize the signum function $sgn(e_2 + c_1 e_1)$ is eliminated. Using such a function can cause many problems such as chattering and switching problems, due to its discontinuity nature. Substituting for v in (5.16), it becomes:

$$\begin{aligned} \dot{V} \leq & -W + k_1 k_7 |e_2 + c_1 e_1| (|x_3| |\eta(u_1)| + |x_2| |\eta(u_2)|) \\ & - \frac{(k_1 k_7 (|x_2| + |x_3|) \eta_{max} (e_2 + c_1 e_1))^2}{k_1 k_7 (|x_2| + |x_3|) \eta_{max} |e_2 + c_1 e_1| + \epsilon_1 (e_2 + c_1 e_1)^2 + \epsilon_2}. \end{aligned} \quad (5.18)$$

Consider the below inequality for any Y , $\epsilon \in \mathbb{R}$ ($\epsilon \neq -|Y|$):

$$-\frac{Y^2}{|Y| + \epsilon} \leq -|Y| + \epsilon. \quad (5.19)$$

Utilizing the inequality (5.19), by setting:

$$\begin{aligned} Y &= k_1 k_7 (|x_2| + |x_3|) \eta_{max} (e_2 + c_1 e_1) \\ \epsilon &= \epsilon_1 (e_2 + c_1 e_1)^2 + \epsilon_2, \end{aligned} \quad (5.20)$$

the following inequality is deduced:

$$\begin{aligned}
& - \frac{(k_1 k_7 (|x_2| + |x_3|) \eta_{max} (e_2 + c_1 e_1))^2}{k_1 k_7 (|x_2| + |x_3|) \eta_{max} |e_2 + c_1 e_1| + \epsilon_1 (e_2 + c_1 e_1)^2 + \epsilon_2} \\
& \leq -k_1 k_7 (|x_2| + |x_3|) \eta_{max} |e_2 + c_1 e_1| + \epsilon_1 (e_2 + c_1 e_1)^2 + \epsilon_2. \tag{5.21}
\end{aligned}$$

Using (5.21) in (5.18) results in the following:

$$\begin{aligned}
\dot{V} & \leq -W + \epsilon_2 + k_1 k_7 |e_2 + c_1 e_1| |x_3| (|\eta(u_1)| - \eta_{max}) \\
& \quad + k_1 k_7 |e_2 + c_1 e_1| |x_2| (|\eta(u_2)| - \eta_{max}) + \epsilon_1 (e_2 + c_1 e_1)^2, \tag{5.22}
\end{aligned}$$

which implies next result:

$$\dot{V} \leq -W_\epsilon + \epsilon_2, \tag{5.23}$$

where W_ϵ is set as:

$$W_\epsilon = c_1 e_1^2 + (c_2 - \epsilon_1) (e_2 + c_1 e_1)^2 \geq 0. \tag{5.24}$$

This concludes the controller development. Note that by achieving (5.23) with ϵ_2 being small enough, the proposed feedback can ensure "practical stability" which guarantees tracking with error boundedness.

5.4 Simulations and Results

In this section, symmetric dead-zones are attached to the inputs to the previously simulated IM model. The dead-zone nonlinearity has the following parameters $\{m = 7, m_{min} = 0.01, m_{max} = 10, b = 2.5, \eta_{max} = 25\}$. The simulation -as in previous section- consists of two parts; without and with the effect of load torque, making use of the IM parameters tables 4.1 and table 4.2 in each part respectively. In addition, the system state variables are starting from the same set of initial conditions introduced in previous chapter. Also, the reference functions -in both parts- are similar to the set introduced previously. The first part of the simulation is done with the feedback derived in section 5.3, assuming that T_L is known to be zero thereby eliminating the use of the adaptive law (4.14). In this scenario, the adaptive parameter is initialized as $\hat{m}(0) = 0.05$. And finally, simulation time is chosen to be $T = 10$ [s]. The simulation outcome shows that tracking is achieved with very close accuracy. According to figure 5.4, the IM speed reaches more than 90% of the target value in less than 2.4s for constant references. As for ramp and sine references, the rise time is almost negligible. Also, note that the applied feedback shown in figures 5.5-5.6 for all cases are bounded in magnitude, within the low range (-2V, 2V). Figures 5.7-5.11 display the rest of state variables obtained from the simulation. All states exhibit a reasonable behavior and stay below rating values specified in table 4.1. This proves that the designed feedback has successfully compensated for the dead-zone input nonlinearity of the system, while achieving bounded-error trajectory tracking of various references.

The second part treats the case of existing external load torque. In this scenario, the IM rotor is attached to a constant load of $T_L = 1$ [Nm]. The system states are initialized similar to the previous part. In addition, the initial condition of the torque adaptive parameter is set as $\hat{T}_L(0) = 0.01$ [Nm]. The simulation time is $T = 20$ [s] and backstepping constants are set as $\{c_1 = 1, c_2 = 31\}$. The performance of the adaptive controller against several reference functions is shown in figure 5.12. The rise time is reached before 5s in worst cases (constant references) and in less than 1s in the best case (with some negligible transient oscillations). As for the control feedback, the results prove that applied voltages stays within a boundary of ± 12 [V] as depicted in figures 5.13 and 5.14. The other state variables of the IM system in addition to both adaptive parameters are plotted in figures 5.15-5.20. All are bounded throughout the simulation time. Comparing the results of this chapter to the previous chapter, there are no noticeable differences in the outcome of the controller. The rise time is very close in both cases and the transient behavior is very similar, But there seems to be a difference in the range of the voltage applied in both cases (refer to figures 4.2-4.3, 5.5-5.6 and figures 4.9-4.10, 5.13-5.14). However, this difference is understandable. It originates from the fact that the feedback introduced in this chapter is scaled by the magnitude of the adaptive parameter \hat{m} . Since the dead-zone in the simulation magnifies the input by a factor of $m = 7$, the adaptive parameter (seen in figures 5.11 and 5.20) counter the effect of the parameter m by reducing the applied voltages. In conclusion, the simulations outcomes verify the validity of the proposed controller.

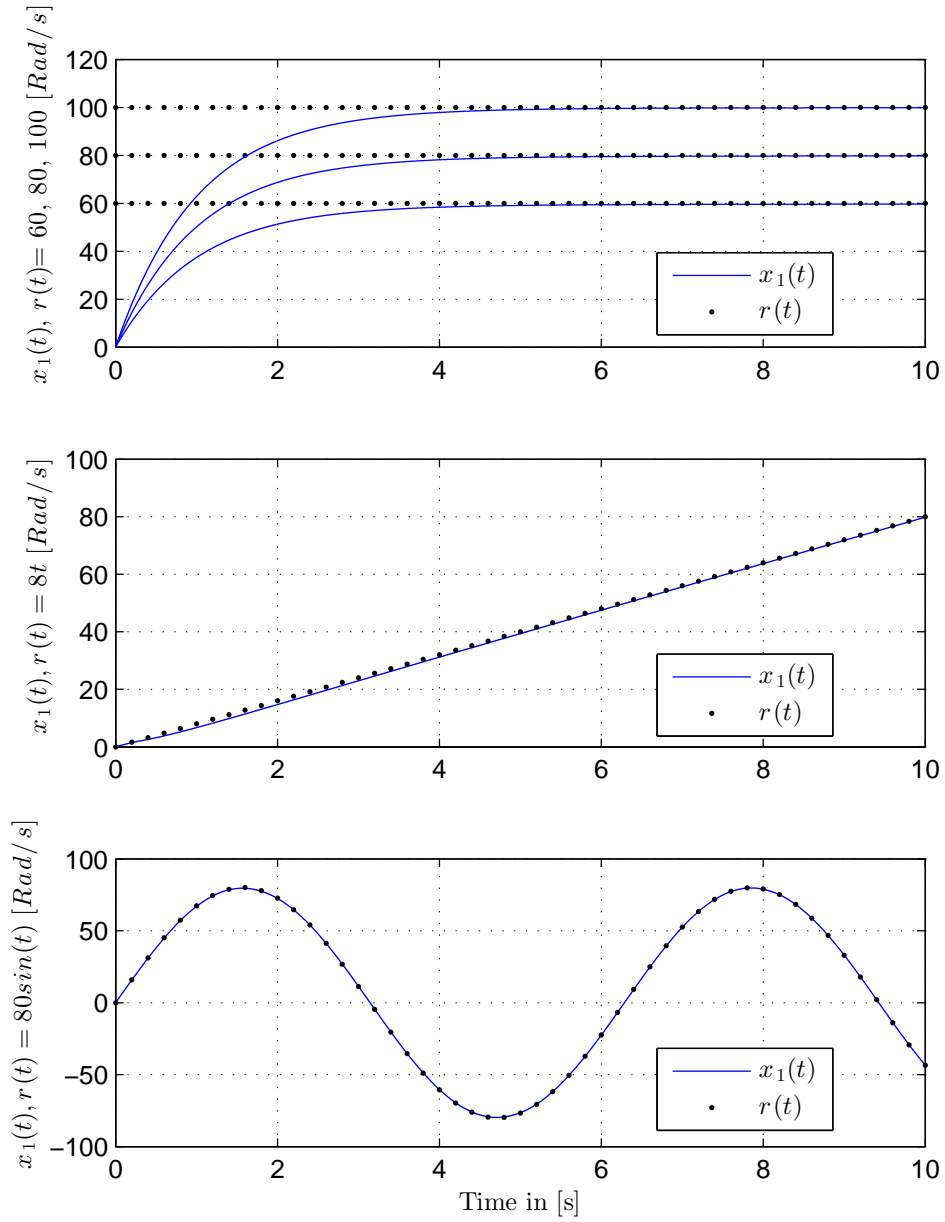


Figure 5.4: Speed tracking performance of IM (with $T_L = 0$) against constant, ramp and sinusoidal reference trajectory respectively (symmetric dead-zone case).

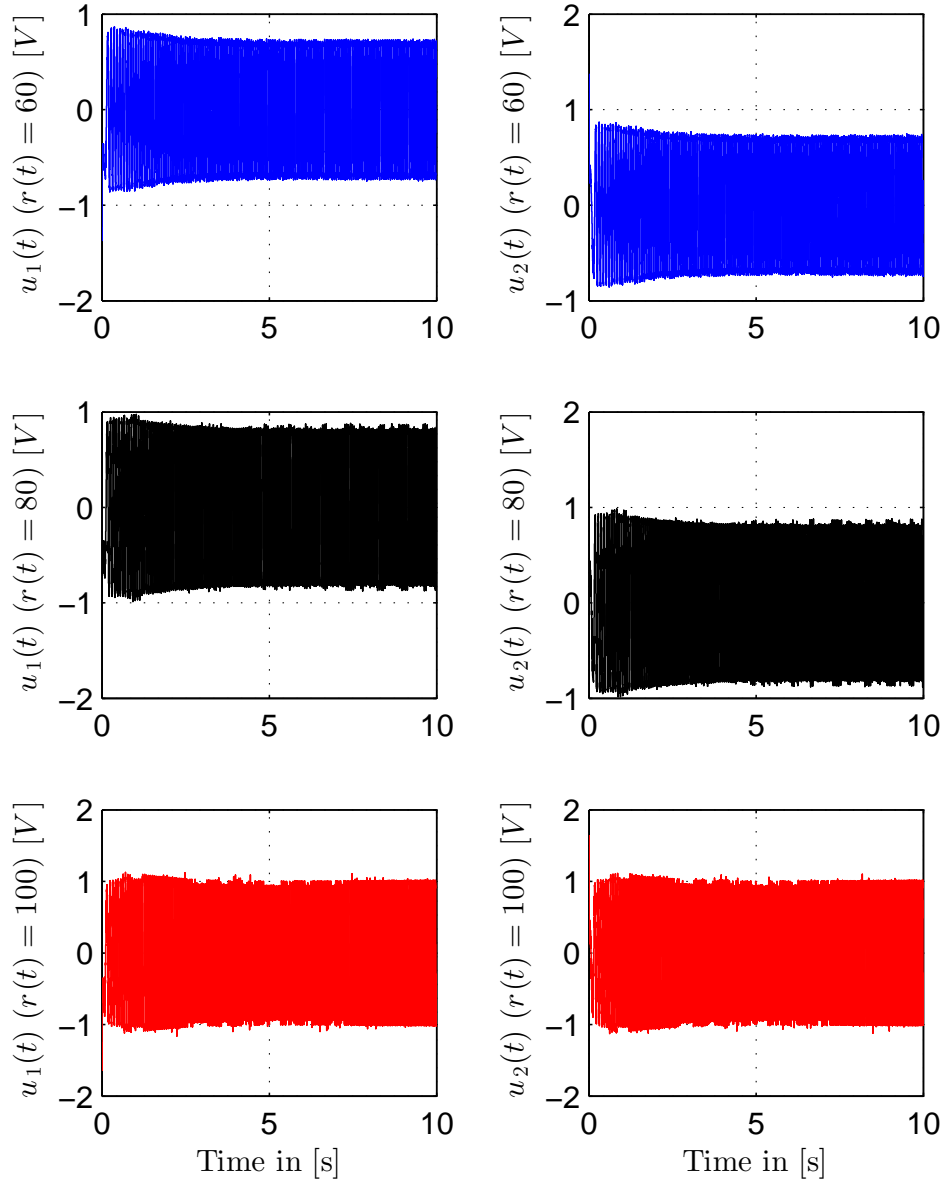


Figure 5.5: Applied control input voltages of IM (with $T_L = 0$) against various constant references (symmetric dead-zone case).

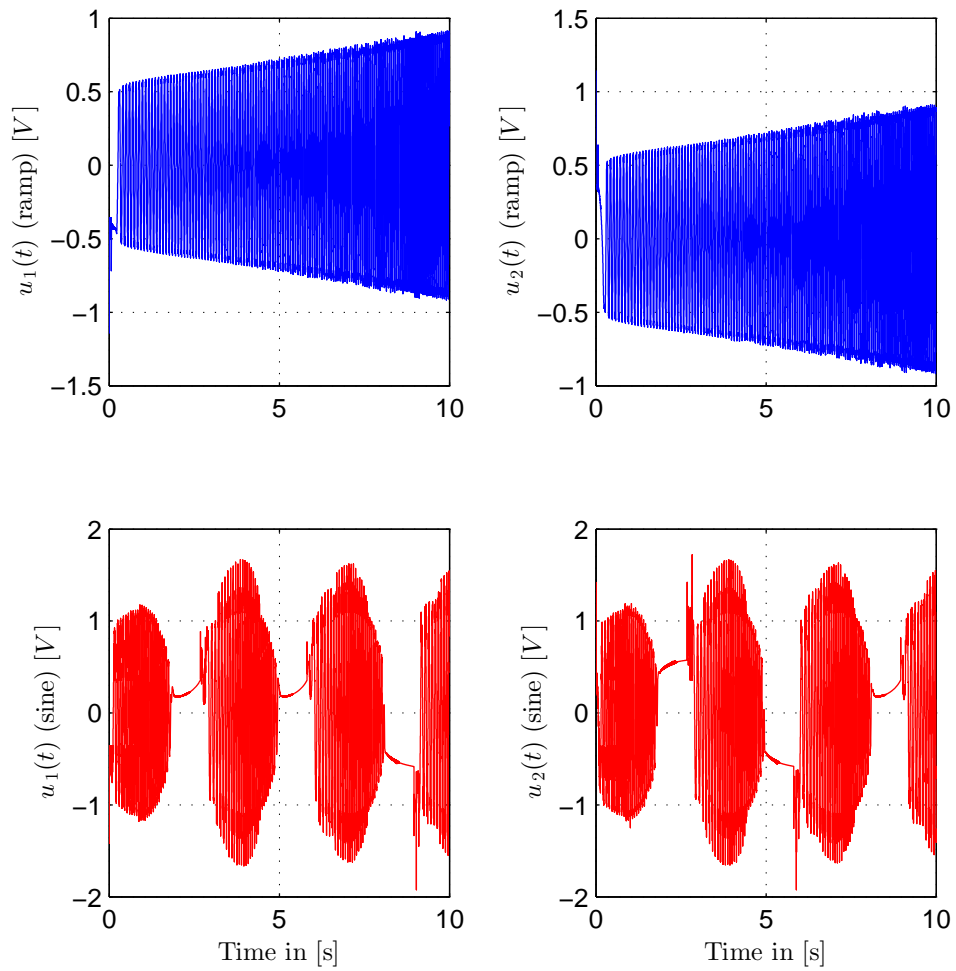


Figure 5.6: Applied control input voltages of IM (with $T_L = 0$) against ramp and sinusoid references respectively (symmetric dead-zone case).

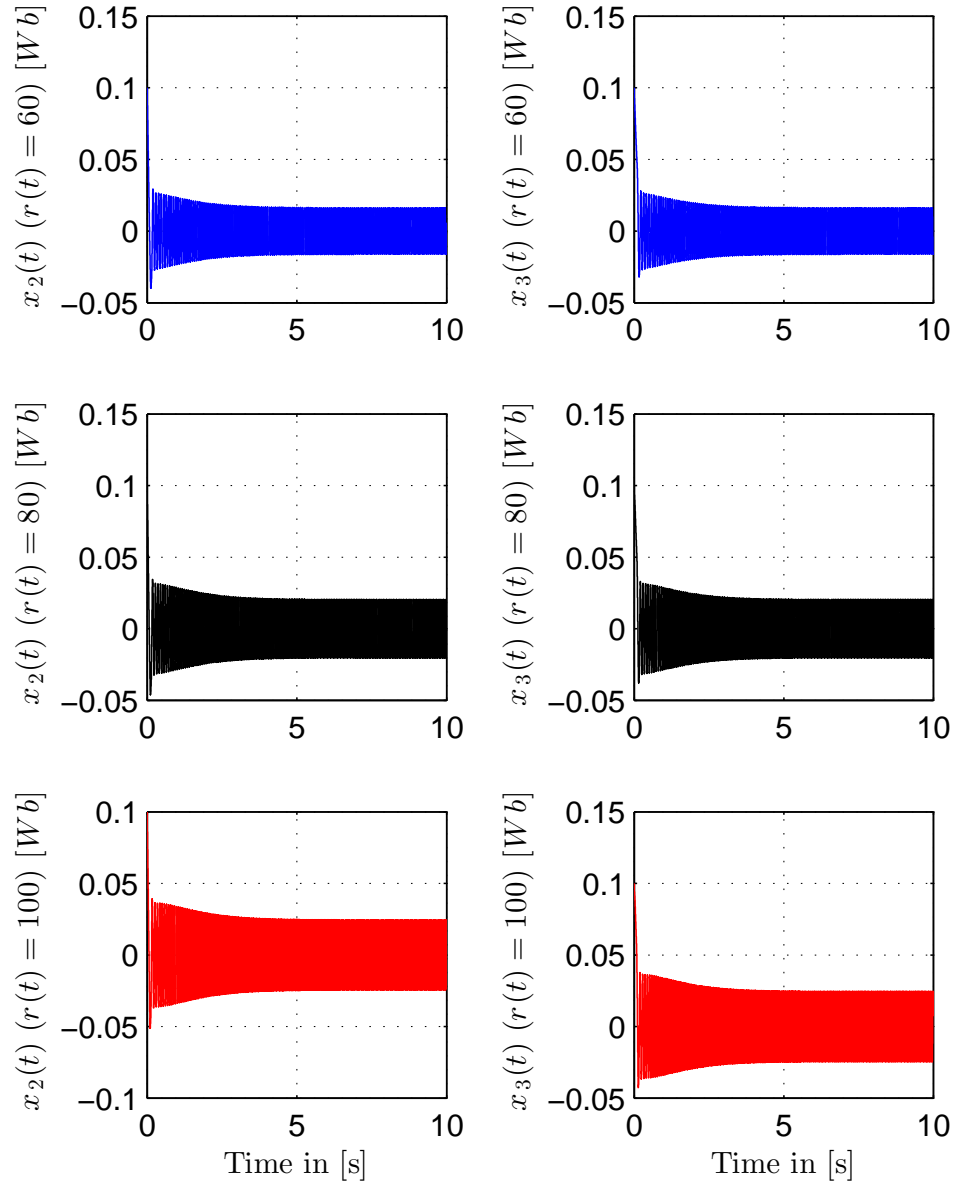


Figure 5.7: Magnetic flux components of IM (with $T_L = 0$) for various constant references (symmetric dead-zone case).

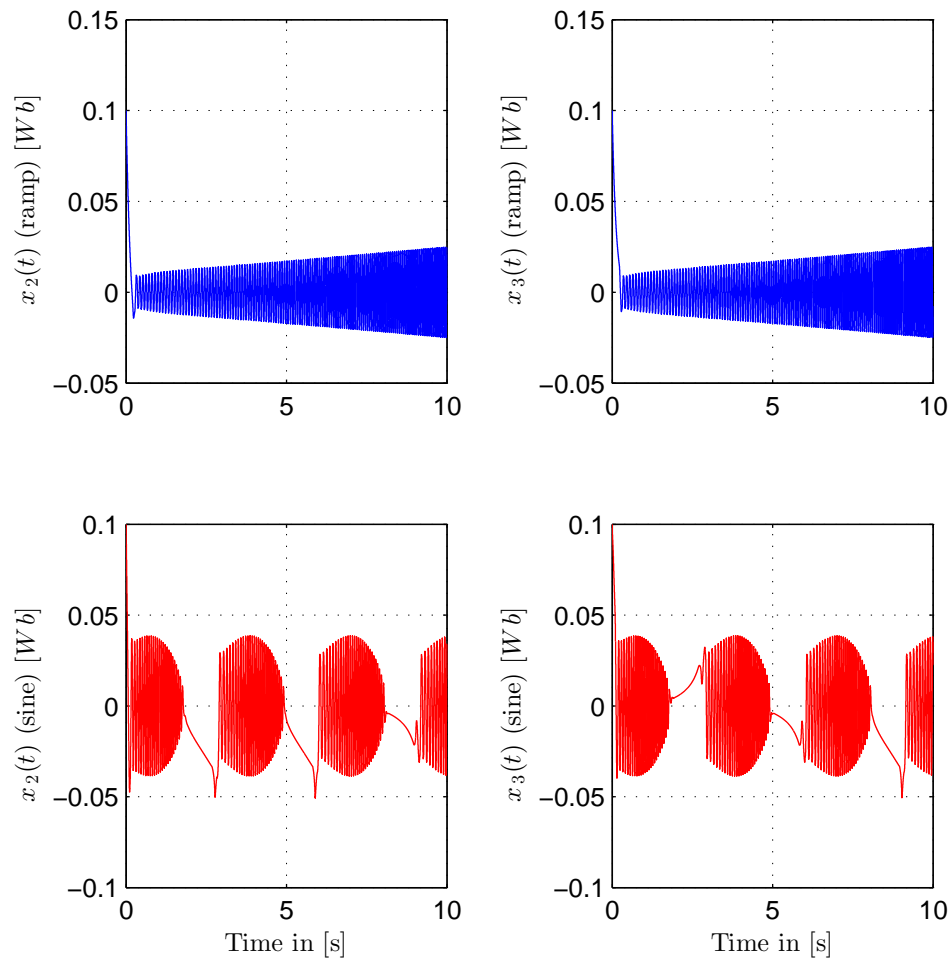


Figure 5.8: Magnetic flux components of IM (with $T_L = 0$) for ramp and sinusoid references respectively (symmetric dead-zone case).

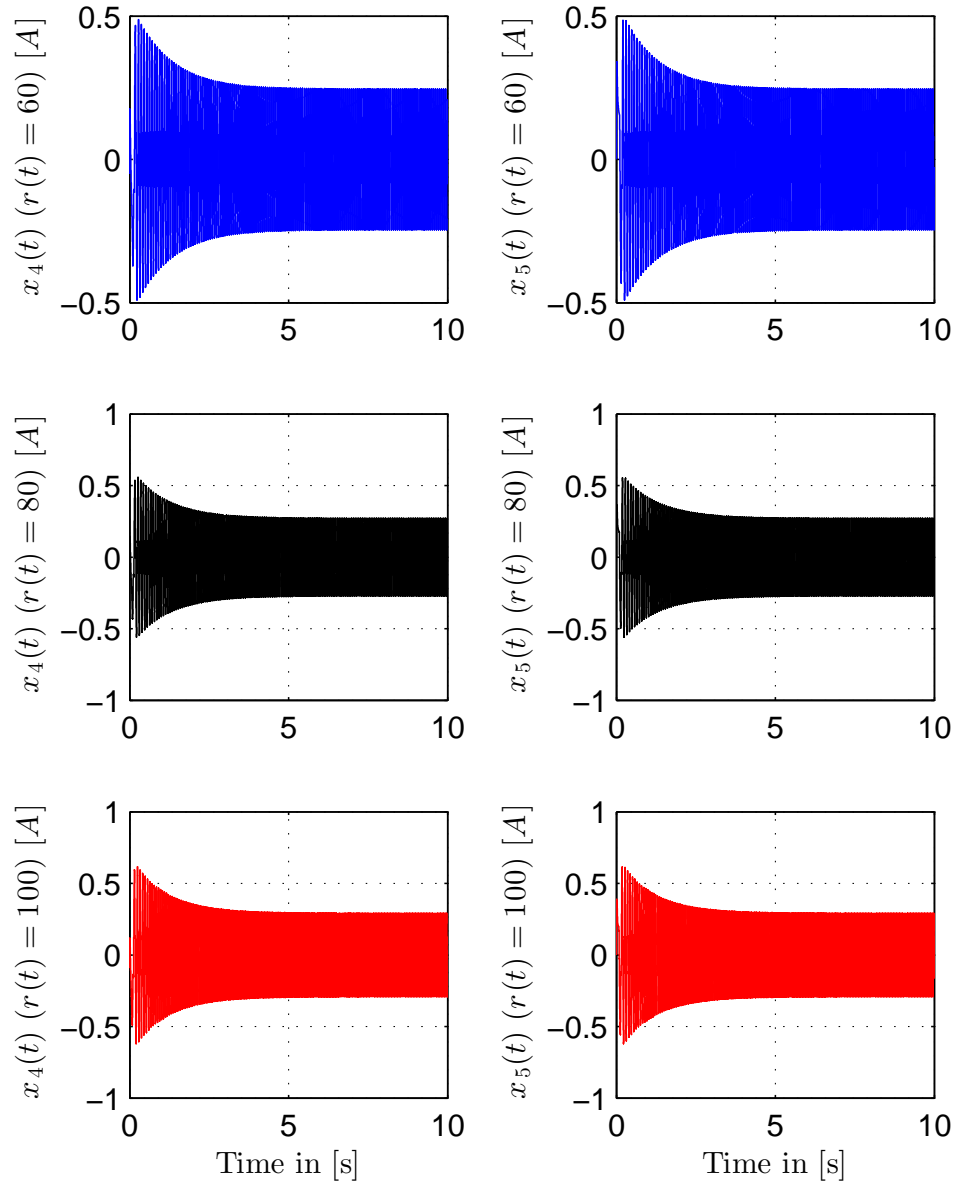


Figure 5.9: Current components of IM (with $T_L = 0$) for various constant references (symmetric dead-zone case).

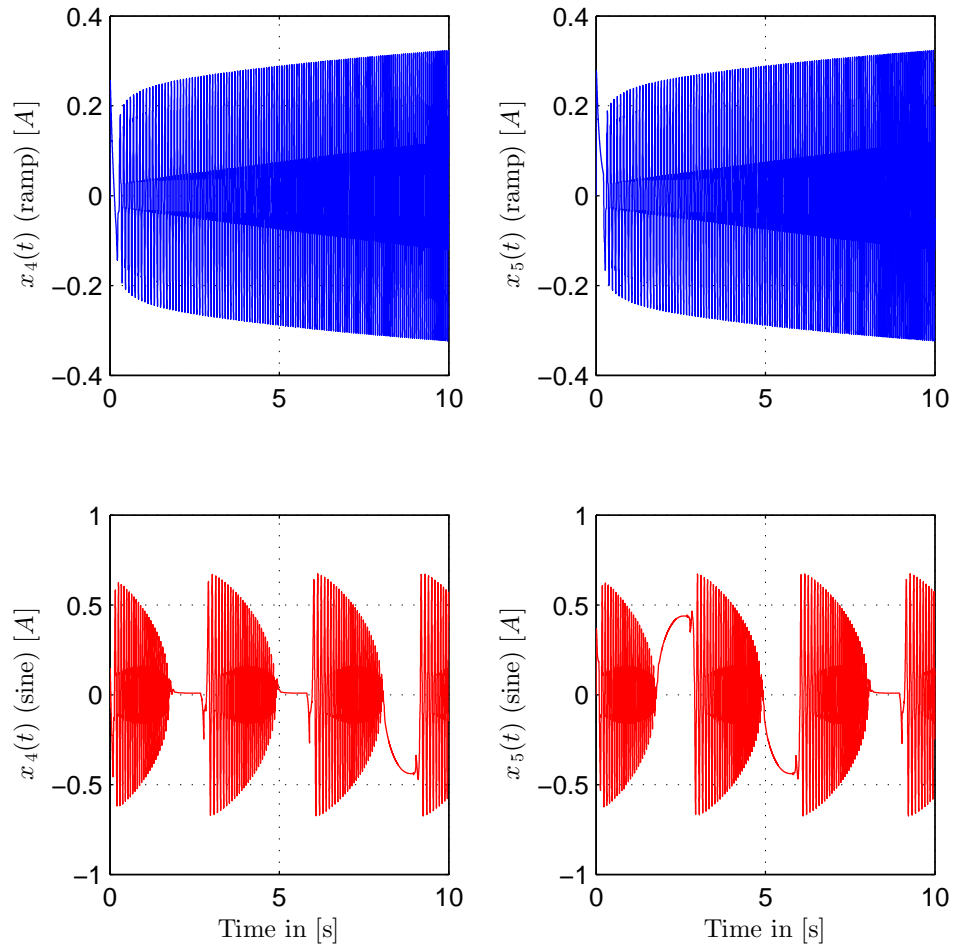


Figure 5.10: Current components of IM (with $T_L = 0$) for ramp and sinusoid references respectively (symmetric dead-zone case).

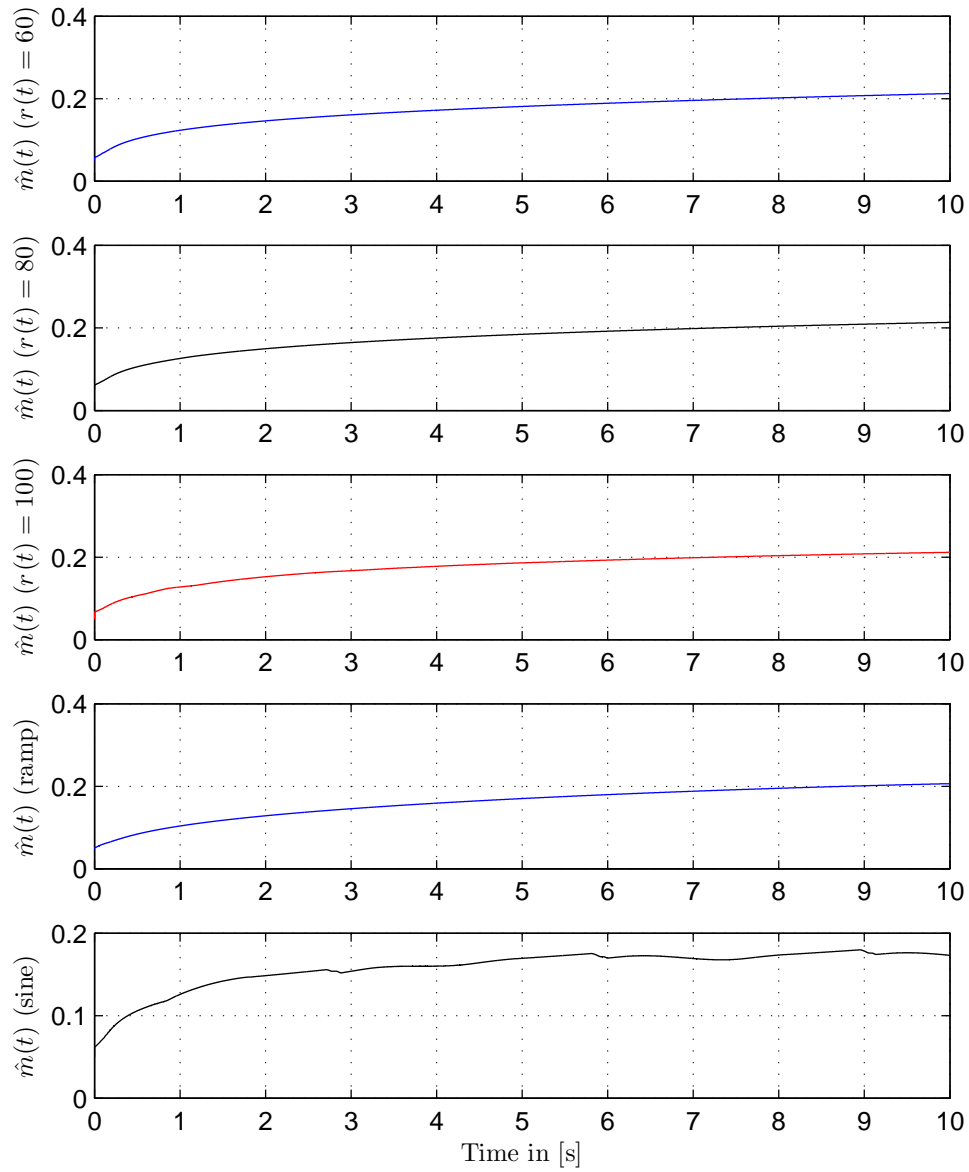


Figure 5.11: Adaptive parameter \hat{m} performance for constant, ramp and sinusoid references respectively (symmetric dead-zone case).

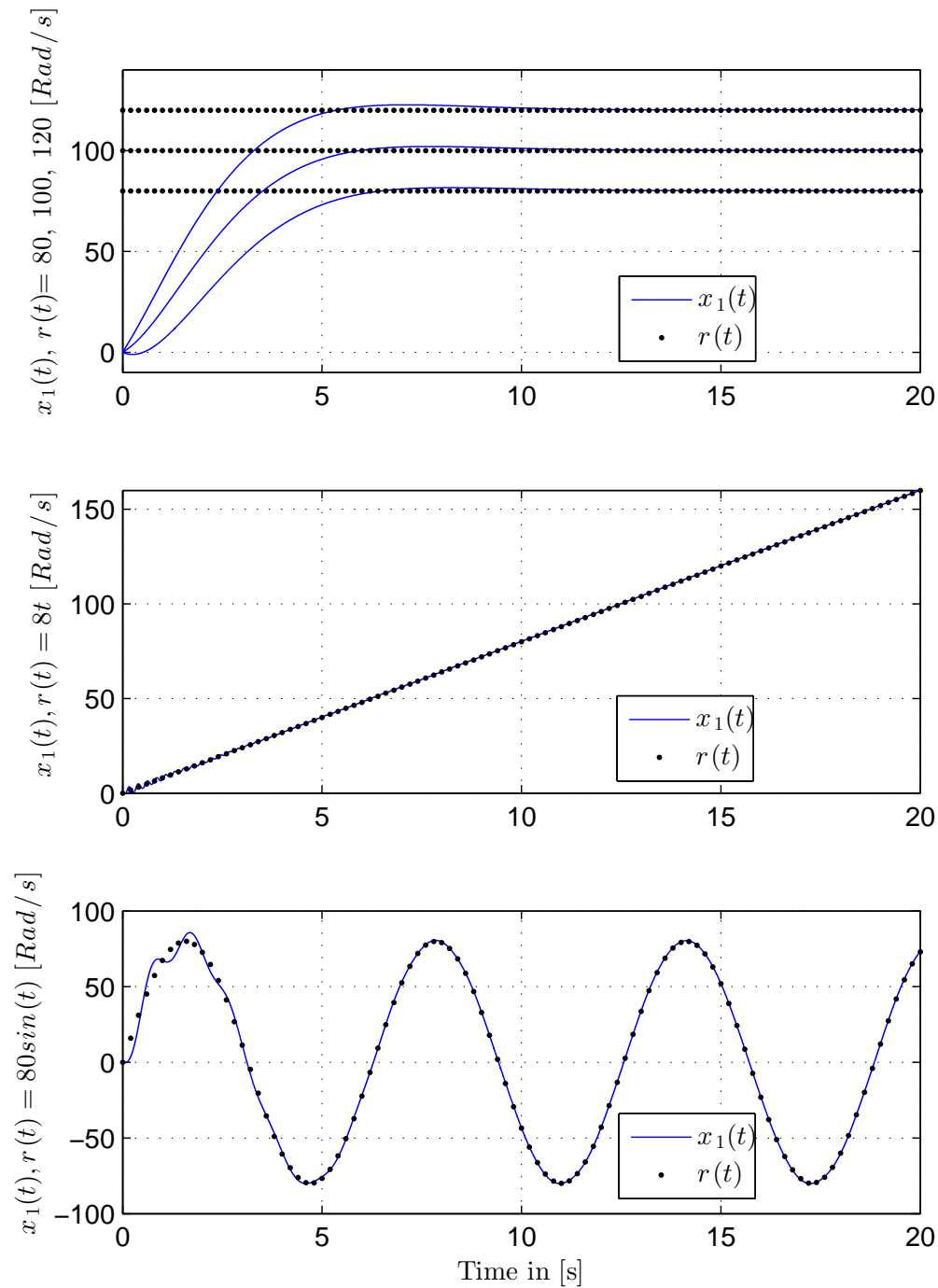


Figure 5.12: Speed tracking performance of IM (with $T_L = 1$ [Nm]) against constant, ramp and sinusoidal reference trajectory respectively (symmetric dead-zone case).

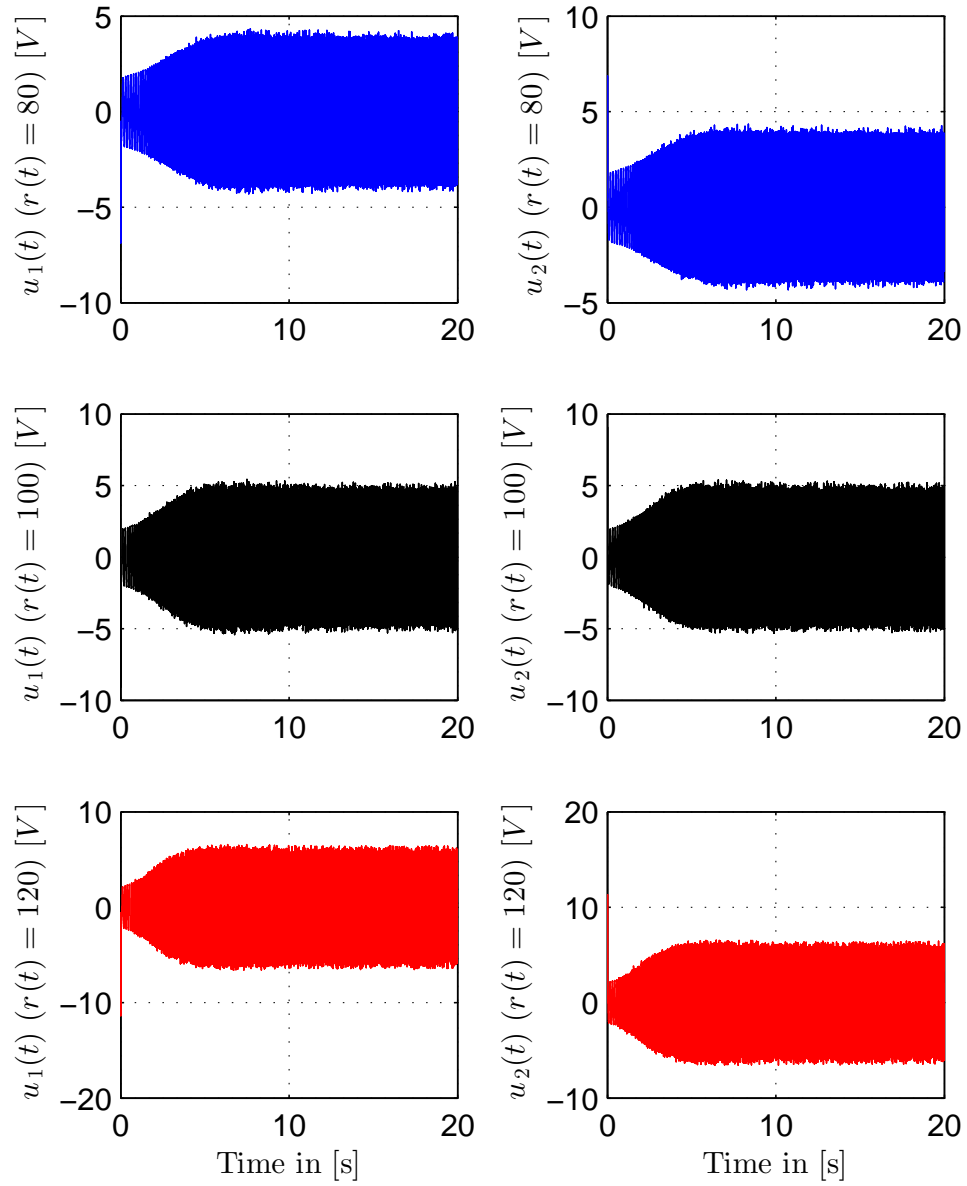


Figure 5.13: Applied control input voltages of IM (with $T_L = 1$ [Nm]) against various constant references (symmetric dead-zone case).

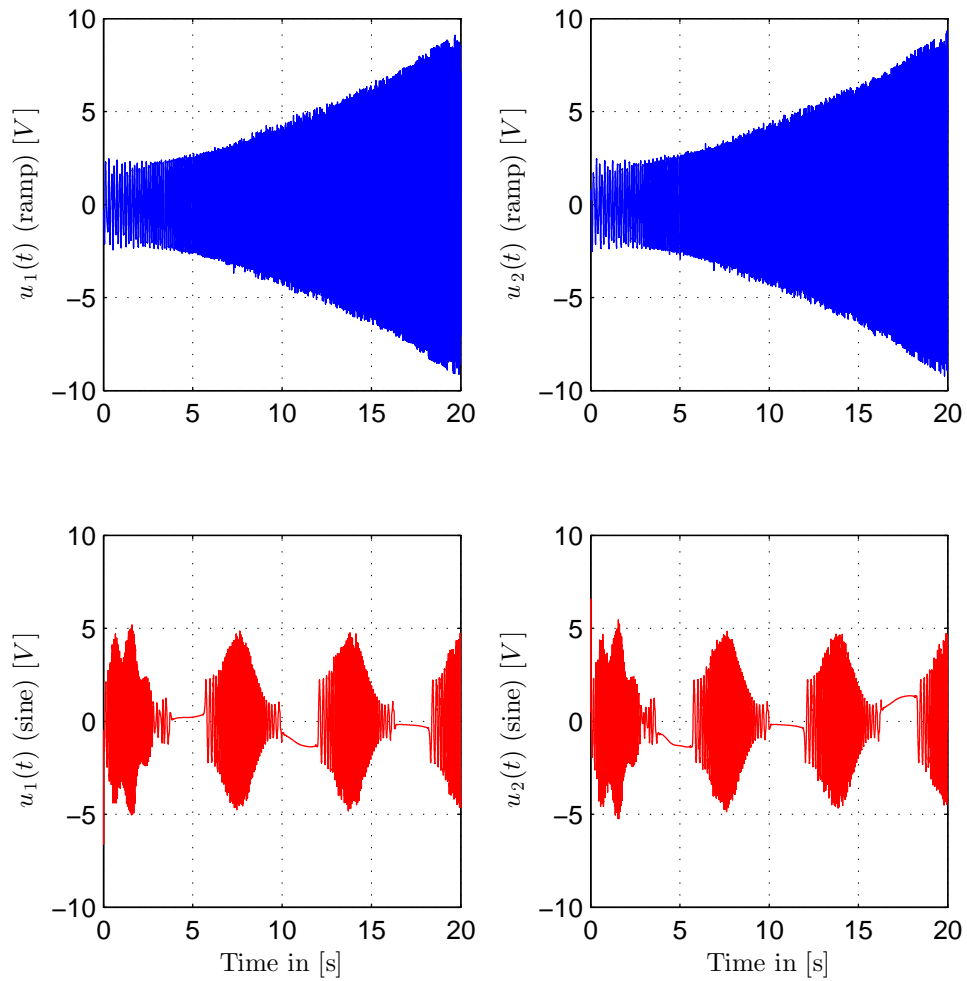


Figure 5.14: Applied control input voltages of IM (with $T_L = 1$ [Nm]) against ramp and sinusoid references respectively (symmetric dead-zone case).

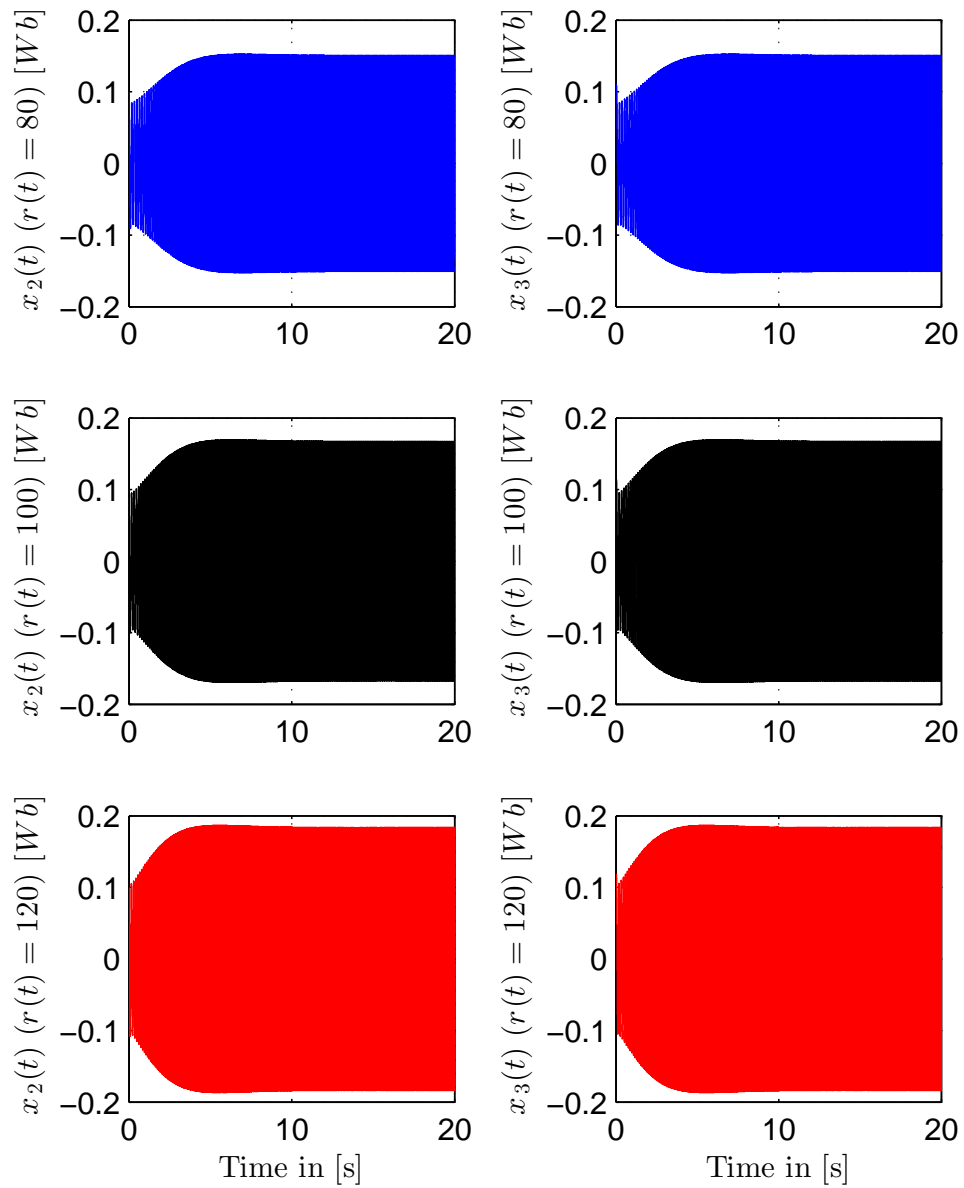


Figure 5.15: Magnetic flux components of IM (with $T_L = 1$ [Nm]) for various constant references (symmetric dead-zone case).

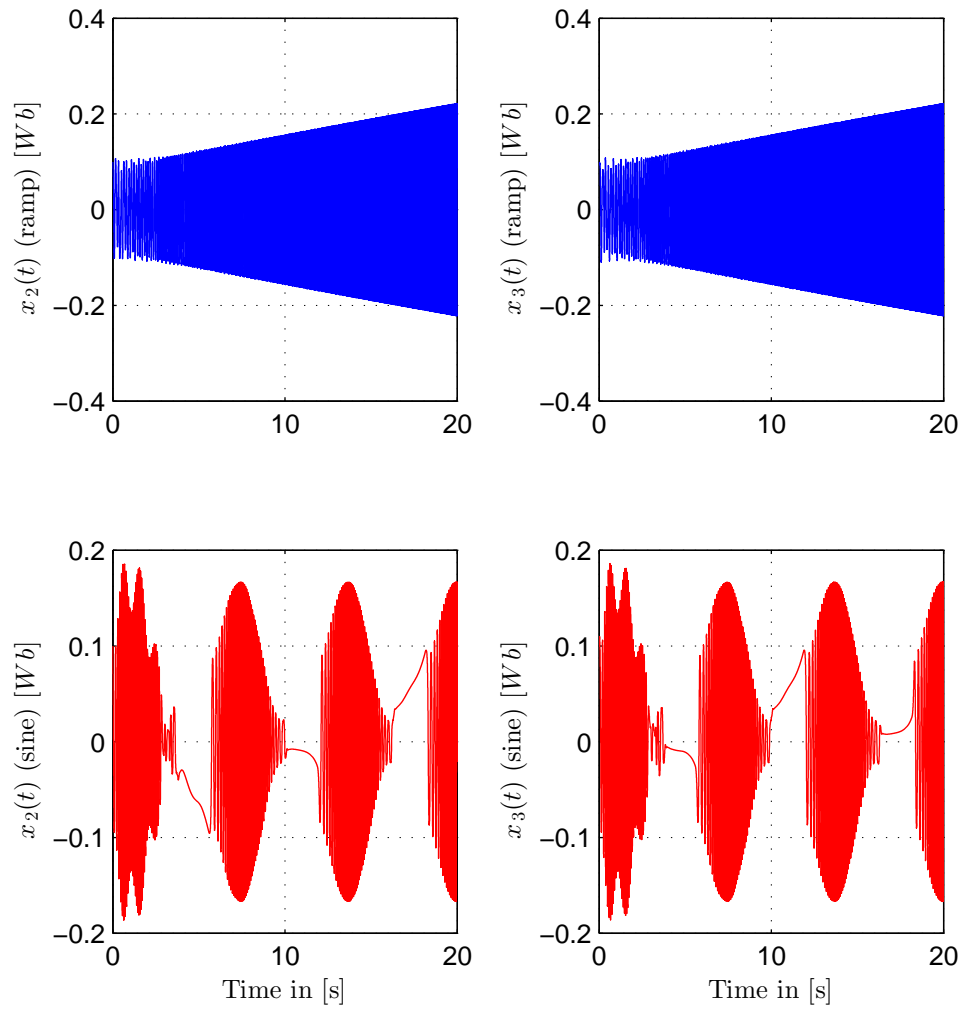


Figure 5.16: Magnetic flux components of IM (with $T_L = 1$ [Nm]) for ramp and sinusoid references respectively (symmetric dead-zone case).

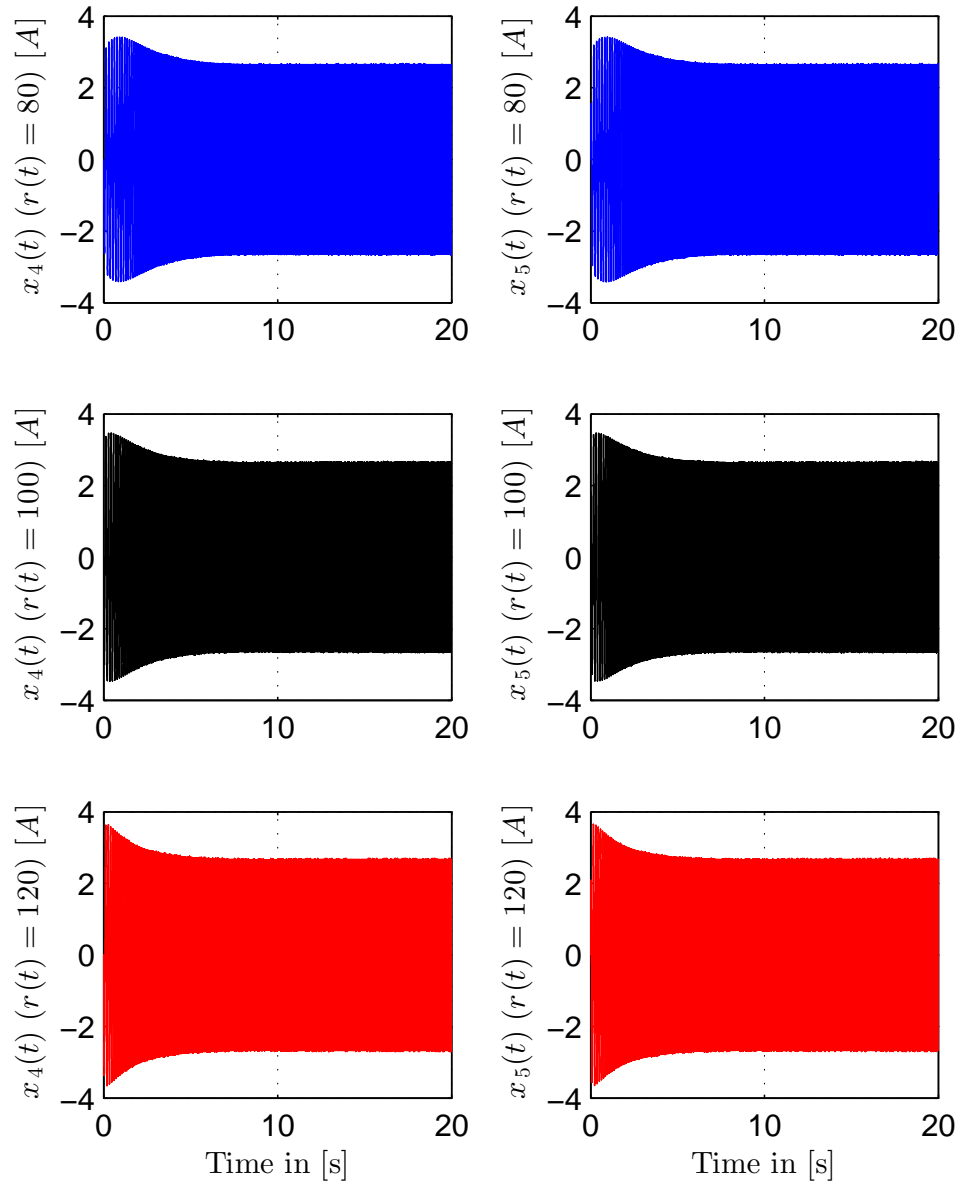


Figure 5.17: Current components of IM (with $T_L = 1$ [Nm]) for various constant references (symmetric dead-zone case).

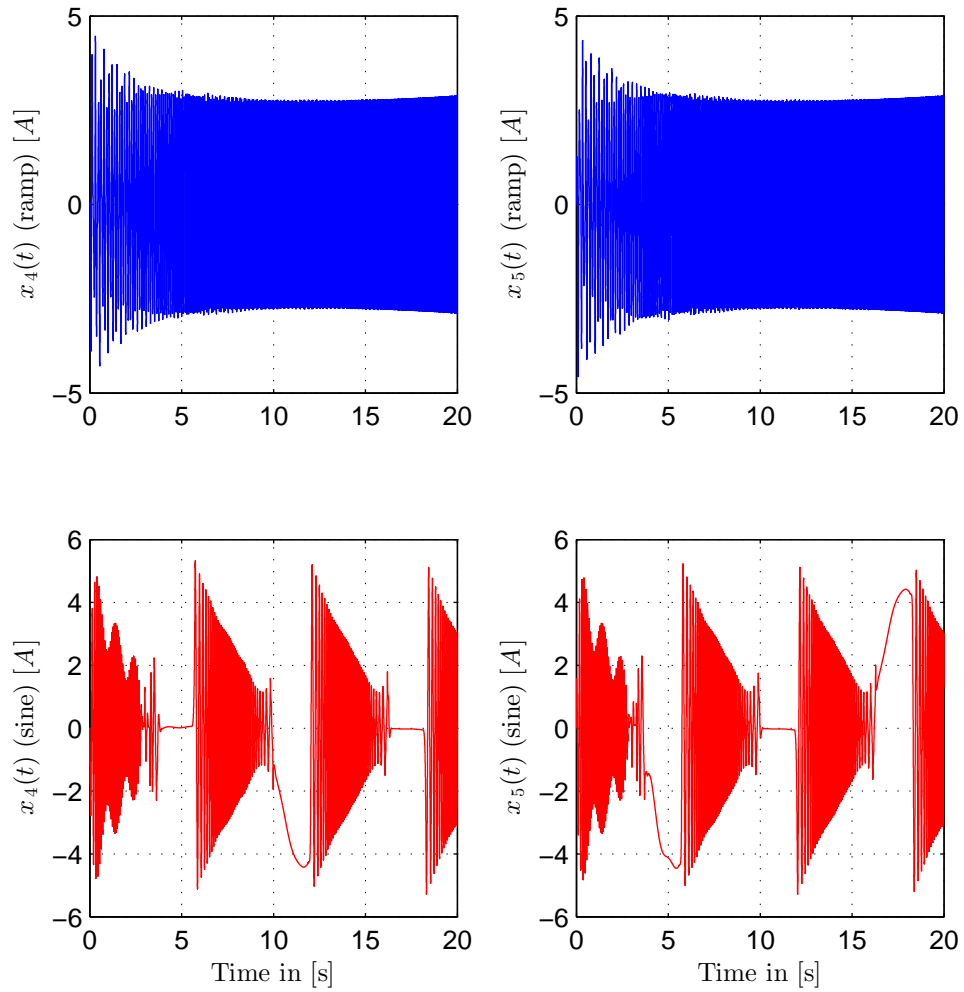


Figure 5.18: Current components of IM (with $T_L = 1$ [Nm]) for ramp and sinusoid references respectively (symmetric dead-zone case).

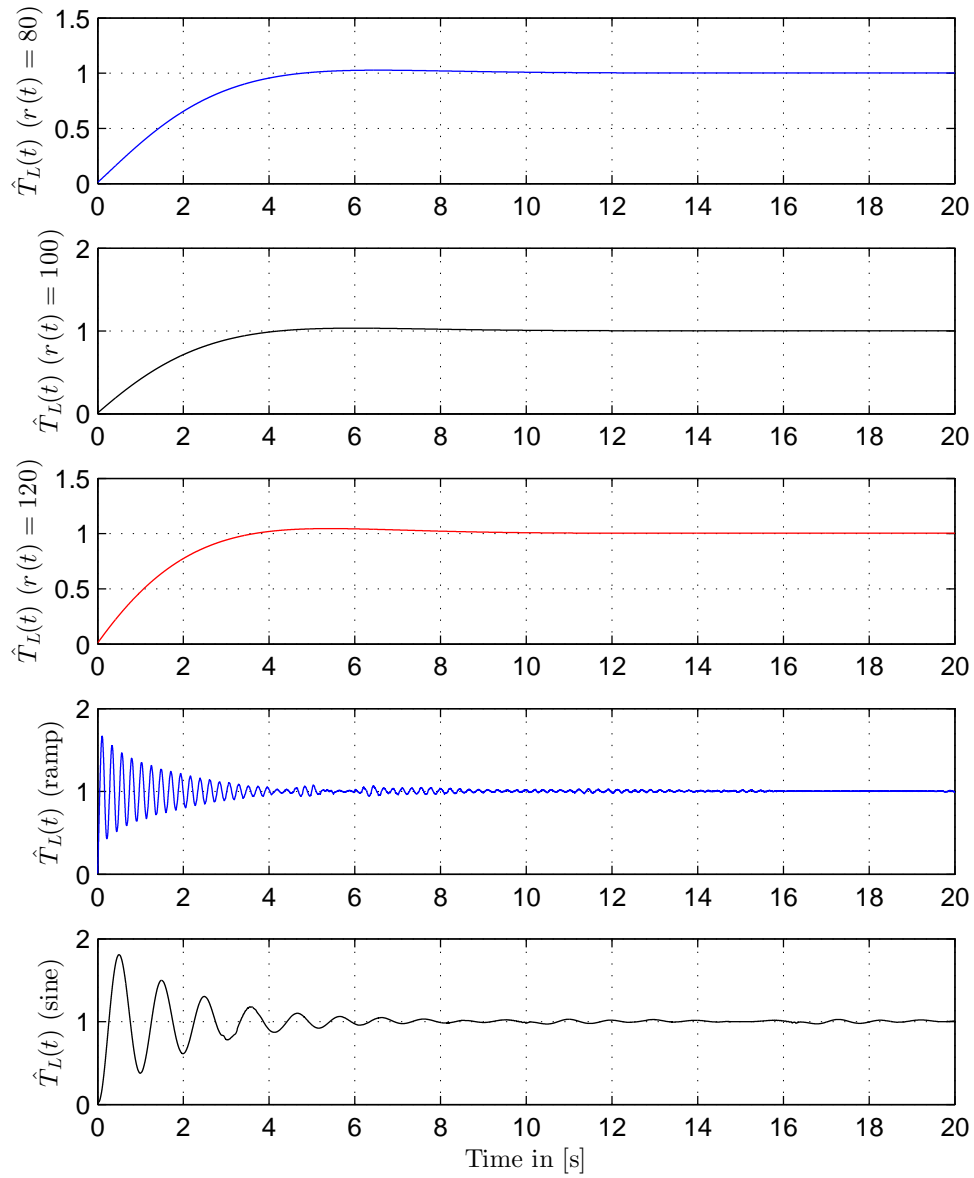


Figure 5.19: Load torque adaptive parameter \hat{T}_L performance for constant, ramp and sinusoid references respectively (symmetric dead-zone case).

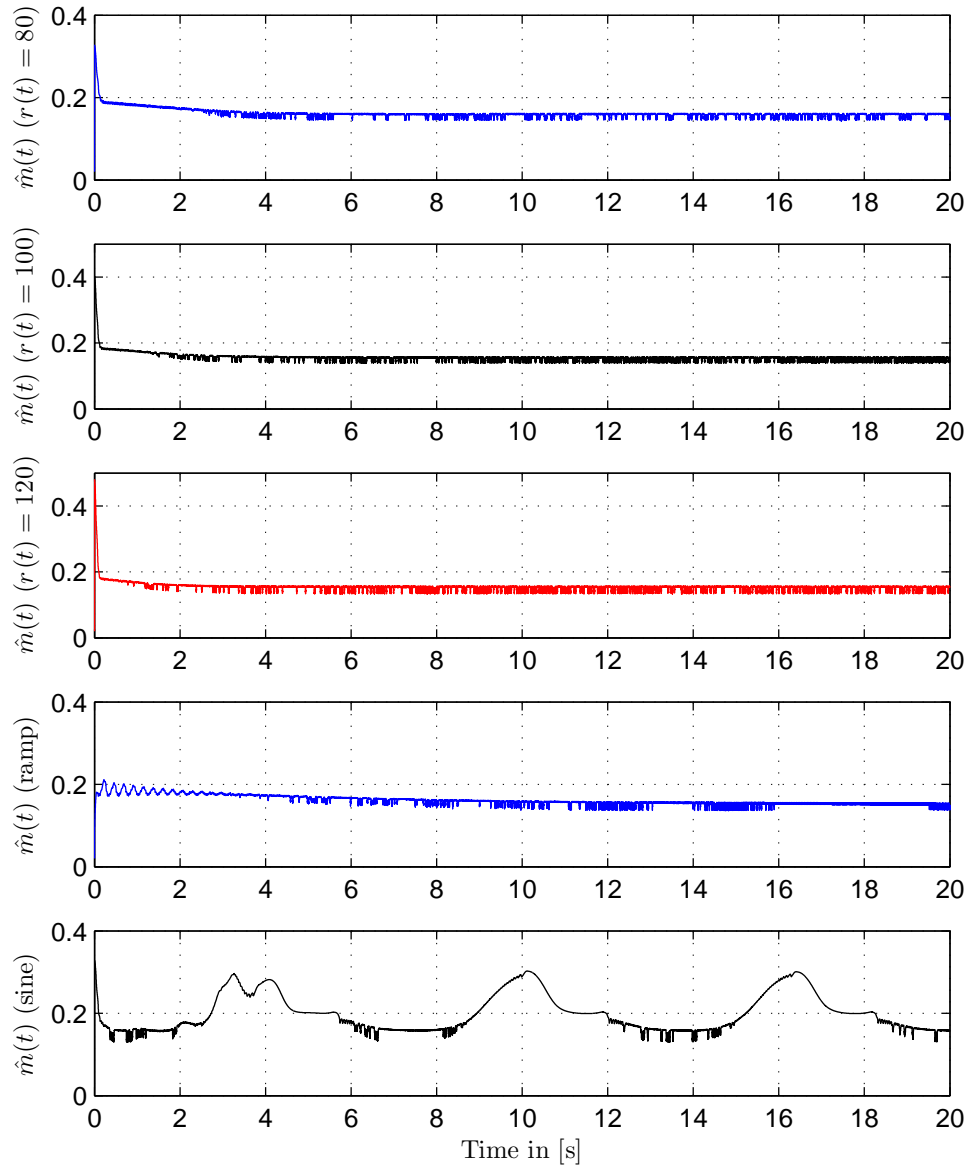


Figure 5.20: Adaptive parameter \hat{m} performance for constant, ramp and sinusoid references respectively (symmetric dead-zone case).

CHAPTER 6

IM WITH ASYMMETRIC DEAD-ZONE INPUT

This chapter explores the asymmetric dead-zone modeling, the development of the required controller for IM subject to this nonlinearity and the numerical simulations.

6.1 Asymmetric Dead-zone Modeling

The asymmetric dead-zone nonlinearity for a scalar input u is defined as [13]:

$$\Gamma(u(t)) = \begin{cases} m_r(u(t) - b_r) & \text{if } u(t) > b_r, \\ 0 & \text{if } -b_l \leq u(t) \leq b_r, \\ m_l(u(t) + b_l) & \text{if } u(t) < -b_l, \end{cases} \quad (6.1)$$

where m_r , m_l are right and left slopes respectively, b_r , b_l are right and left break points of the dead-zone respectively. Alternatively, $\Gamma(u(t))$ can also be redefined

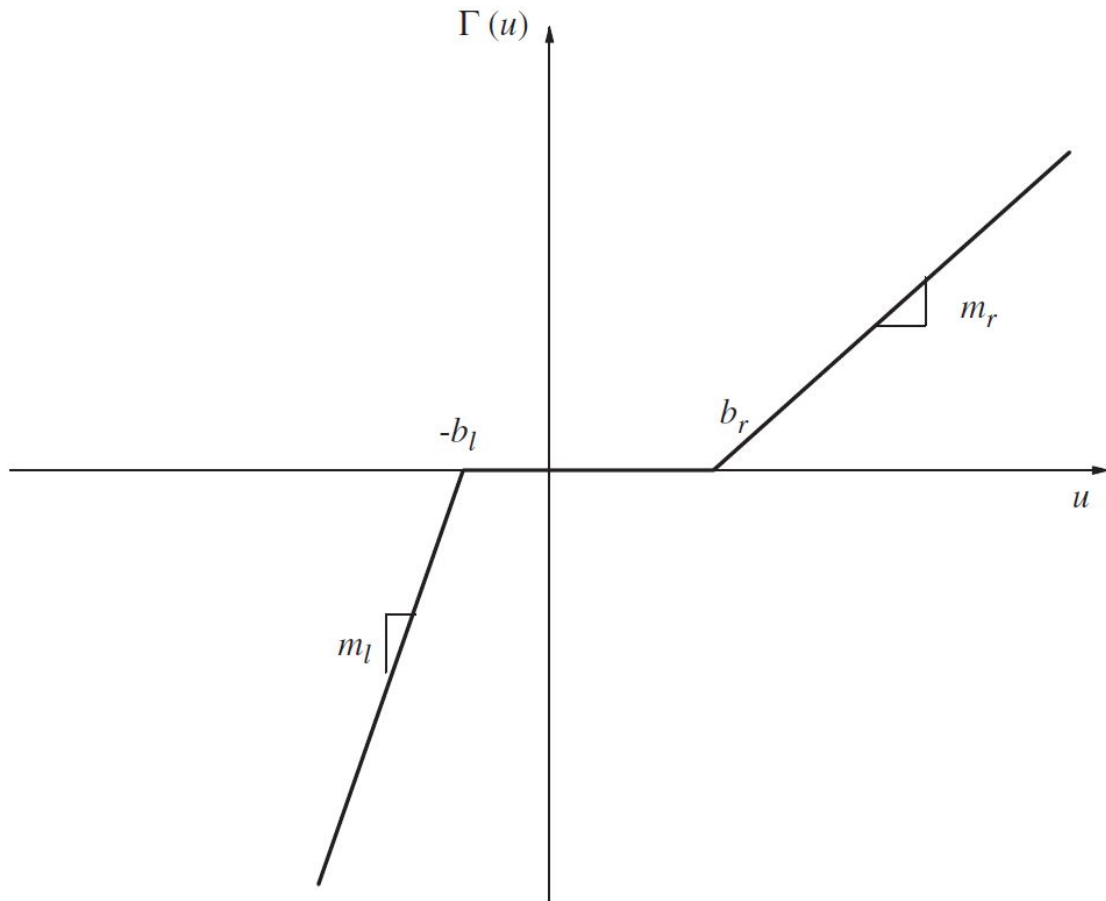


Figure 6.1: Asymmetric dead-zone nonlinearity

as a time-varying function, which depends on $u(t)$ as follows:

$$\Gamma(u(t)) = m(u(t))u(t) + \xi(u(t)), \quad (6.2)$$

where $m(u(t))$ is defined as:

$$m(u(t)) = \begin{cases} m_r & \text{if } u(t) > 0, \\ m_l & \text{if } u(t) \leq 0. \end{cases} \quad (6.3)$$

$\xi(u(t))$ is a bounded perturbation function having the following definition:

$$\xi(u(t)) = \begin{cases} -m_r b_r & \text{if } u(t) > b_r, \\ -m(t)u(t) & \text{if } -b_l \leq u(t) \leq b_r, \\ m_l b_l & \text{if } u(t) < -b_l. \end{cases} \quad (6.4)$$

Assumption 5. All dead-zone parameters, namely m_r , m_l , b_r and b_l are unknown positive constants with known positive boundaries. That is, dead-zone slopes' boundaries $\min(m_r, m_l) = m_{min}$ and $\max(m_r, m_l) = m_{max}$ and dead-zone break points boundaries $\min(b_r, b_l) = b_{min}$, $\max(b_r, b_l) = b_{max}$ and $\xi_{max} = m_{max}b_{max}$ are all known positive constants. Again, as in symmetric dead-zone case, this assumption is justified as having knowledge about the parameters boundaries seems to be a very natural assumption in practical applications.

6.2 Controller Design for Asymmetric Dead-zone Input

Now, suppose that the inputs applied to the IM stator (u_1, u_2) are subject to unknown asymmetric dead-zone. Also, recall (6.3) as well as the previously defined dead-zone slope minimum m_{min} . It can be easily seen that:

$$\frac{m(t)}{m_{min}} = 1 + q(t), \quad (6.5)$$

where $q(t)$ is a piecewise positive function. Now, let $\rho = \sup\{q(t)\}$, $\forall t \geq 0$ and define the adaptive parameter $\hat{\rho}$ associated with it. In addition, define the error $\tilde{\rho}$ as:

$$\tilde{\rho} = \rho - \hat{\rho}. \quad (6.6)$$

Note that ρ is always a positive quantity and has a maximum limit of $\rho_{max} = \frac{m_{max}}{m_{min}} - 1$. Now, the system Lyapunov function in (4.7) is updated to account for dead-zone parameter compensation as follows:

$$V = V_1 + \frac{1}{2}(e_2 + c_1 e_1)^2 + \frac{1}{2\alpha} \tilde{T}_L^2 + \frac{1}{2\delta} \tilde{\rho}^2 \geq 0, \quad (6.7)$$

where δ is a selected positive constant. Now, taking the time derivative and utilizing (4.18) result in:

$$\begin{aligned}\dot{V} = & -W + (e_2 + c_1 e_1)(\psi + k_1 k_7 x_2 \Gamma(u_2) - k_1 k_7 x_3 \Gamma(u_1)) \\ & + \frac{1}{\delta} \tilde{\rho} \dot{\tilde{\rho}}.\end{aligned}\tag{6.8}$$

Choose the inputs to be:

$$u_1 = \frac{-x_3 v}{m_{min} k_1 k_7 (x_2^2 + x_3^2)}, \quad u_2 = \frac{x_2 v}{m_{min} k_1 k_7 (x_2^2 + x_3^2)}.\tag{6.9}$$

Substituting (6.2) and (6.9) in (6.8), results in:

$$\begin{aligned}\dot{V} = & -W + (e_2 + c_1 e_1)(\psi + k_1 k_7 x_2 \left(\frac{x_2 v}{m_{min} k_1 k_7 (x_2^2 + x_3^2)} m(t)\right) \\ & + \xi(u_2)) - k_1 k_7 x_3 \left(\frac{-x_3 v}{m_{min} k_1 k_7 (x_2^2 + x_3^2)} m(t) + \xi(u_1)\right) \\ & + \frac{1}{\delta} \tilde{\rho} \dot{\tilde{\rho}}.\end{aligned}\tag{6.10}$$

Note that:

$$\dot{\tilde{\rho}} = -\dot{\rho}.\tag{6.11}$$

Manipulating (6.10) and using (6.5) and (6.11), \dot{V} can be bounded as:

$$\begin{aligned}
\dot{V} \leq & -W + (e_2 + c_1 e_1)(\psi + k_1 k_7 x_2 \frac{(1+q(t))x_2 v}{k_1 k_7 (x_2^2 + x_3^2)} \\
& + k_1 k_7 x_3 \frac{(1+q(t))x_3 v}{k_1 k_7 (x_2^2 + x_3^2)}) + k_1 k_7 |(e_2 + c_1 e_1)x_3 \xi(u_1)| \\
& + k_1 k_7 |(e_2 + c_1 e_1)x_2 \xi(u_2)| - \frac{1}{\delta} \tilde{\rho} \dot{\rho}.
\end{aligned} \tag{6.12}$$

Note that $k_1, k_7 > 0$. Now, using the fact that $|xy| \leq |x||y|$ for any $x, y \in \mathbb{R}$ and with some simplifications, the inequality is reduced to:

$$\begin{aligned}
\dot{V} \leq & -W + (e_2 + c_1 e_1)(\psi + (1+q(t))v) \\
& + k_1 k_7 |e_2 + c_1 e_1| |x_3| |\xi(u_1)| + k_1 k_7 |e_2 + c_1 e_1| |x_2| |\xi(u_2)| \\
& - \frac{1}{\delta} \tilde{\rho} \dot{\rho}.
\end{aligned} \tag{6.13}$$

Select v as:

$$v = \frac{-(1+\hat{\rho})(k_1 k_7 (|x_2| + |x_3|) \xi_{max} + |\psi|)^2 (e_2 + c_1 e_1)}{|(k_1 k_7 (|x_2| + |x_3|) \xi_{max} + |\psi|)(e_2 + c_1 e_1)| + \varphi}, \tag{6.14}$$

where φ is a sufficiently small selected positive constant. Substitute (6.14) in inequality (6.13) to get:

$$\begin{aligned}
\dot{V} &\leq -W + (e_2 + c_1 e_1)\psi + k_1 k_7 |e_2 + c_1 e_1| |x_3| |\xi(u_1)| \\
&\quad + k_1 k_7 |e_2 + c_1 e_1| |x_2| |\xi(u_2)| - \frac{1}{\delta} \tilde{\rho} \dot{\rho} \\
&\quad - \frac{((k_1 k_7 (|x_2| + |x_3|) \xi_{max} + |\psi|)(e_2 + c_1 e_1))^2 (1 + q(t))(1 + \hat{\rho})}{|(k_1 k_7 (|x_2| + |x_3|) \xi_{max} + |\psi|)(e_2 + c_1 e_1)| + \varphi}. \tag{6.15}
\end{aligned}$$

Recall the below inequality for any $Y, \varepsilon \in \mathbb{R}$ ($\varepsilon \neq -|Y|$):

$$-\frac{Y^2}{|Y| + \varepsilon} \leq -|Y| + \varepsilon. \tag{6.16}$$

Utilizing the inequality (6.16), by setting:

$$\begin{aligned}
Y &= (k_1 k_7 (|x_2| + |x_3|) \xi_{max} + |\psi|)(e_2 + c_1 e_1), \\
\varepsilon &= \varphi, \tag{6.17}
\end{aligned}$$

the following inequality is deduced:

$$\begin{aligned}
&\frac{-((k_1 k_7 (|x_2| + |x_3|) \xi_{max} + |\psi|)(e_2 + c_1 e_1))^2}{|(k_1 k_7 (|x_2| + |x_3|) \xi_{max} + |\psi|)(e_2 + c_1 e_1)| + \varphi} \\
&\leq -|(k_1 k_7 (|x_2| + |x_3|) \xi_{max} + |\psi|)(e_2 + c_1 e_1)| + \varphi. \tag{6.18}
\end{aligned}$$

Applying inequality (6.18) in (6.15), to get:

$$\begin{aligned}
\dot{V} &\leq -W + (e_2 + c_1 e_1) \psi + k_1 k_7 |e_2 + c_1 e_1| |x_3| |\xi(u_1)| \\
&\quad + k_1 k_7 |e_2 + c_1 e_1| |x_2| |\xi(u_2)| - \frac{1}{\delta} \tilde{\rho} \dot{\hat{\rho}} + (1 + q(t))(1 \\
&\quad + \hat{\rho})(-(k_1 k_7 (|x_2| + |x_3|) \xi_{max} + |\psi|)(e_2 + c_1 e_1) + \varphi). \tag{6.19}
\end{aligned}$$

Note that (6.19) is valid since the adaptive parameter $\hat{\rho}$ shall be selected later as a positive quantity. Rearrange the inequality to obtain the following:

$$\begin{aligned}
\dot{V} &\leq -W + (1 + \hat{\rho})(1 + q(t))\varphi + ((e_2 + c_1 e_1) \psi \\
&\quad - |e_2 + c_1 e_1| |\psi|) + k_1 k_7 |e_2 + c_1 e_1| (|x_2| (\xi(u_2) - \xi_{max}) \\
&\quad + |x_3| (\xi(u_1) - \xi_{max})) - q(t) |e_2 + c_1 e_1| (|\psi| + k_1 k_7 (|x_2| \\
&\quad + |x_3|) \xi_{max}) - \hat{\rho} (1 + q(t)) |e_2 + c_1 e_1| (|\psi| + k_1 k_7 (|x_2| \\
&\quad + |x_3|) \xi_{max}) - \frac{1}{\delta} \tilde{\rho} \dot{\hat{\rho}}. \tag{6.20}
\end{aligned}$$

In order to further simplify the inequality (6.20), utilize the facts that:

$$(e_2 + c_1 e_1)\psi - |e_2 + c_1 e_1||\psi| \leq 0, \quad (6.21)$$

$$k_1 k_7 |e_2 + c_1 e_1| (|x_2|(\xi(u_2) - \xi_{max}) + |x_3|(\xi(u_1) - \xi_{max})) \leq 0, \quad (6.22)$$

and

$$\begin{aligned} & -q(t)|e_2 + c_1 e_1|(|\psi| + k_1 k_7(|x_2| + |x_3|)\xi_{max}) \\ & \leq \rho |e_2 + c_1 e_1|(|\psi| + k_1 k_7(|x_2| + |x_3|)\xi_{max}), \end{aligned} \quad (6.23)$$

since $\rho > -q(t)$ as both $\rho, q(t) \geq 0$.

All these inequalities can be used to transform (6.20) into:

$$\begin{aligned} \dot{V} & \leq -W + (1 + \hat{\rho})(1 + q(t))\varphi - \frac{1}{\delta}\tilde{\rho}\dot{\hat{\rho}} \\ & + \rho|e_2 + c_1 e_1|(|\psi| + k_1 k_7(|x_2| + |x_3|)\xi_{max}) \\ & - \hat{\rho}|e_2 + c_1 e_1|(|\psi| + k_1 k_7(|x_2| + |x_3|)\xi_{max}) \\ & - q(t)\hat{\rho}|e_2 + c_1 e_1|(|\psi| + k_1 k_7(|x_2| + |x_3|)\xi_{max}). \end{aligned} \quad (6.24)$$

or simply:

$$\begin{aligned} \dot{V} & \leq -W + (1 + \hat{\rho})(1 + q(t))\varphi - \frac{1}{\delta}\tilde{\rho}\dot{\hat{\rho}} \\ & + \tilde{\rho}|e_2 + c_1 e_1|(|\psi| + k_1 k_7(|x_2| + |x_3|)\xi_{max}) \\ & - q(t)\hat{\rho}|e_2 + c_1 e_1|(|\psi| + k_1 k_7(|x_2| + |x_3|)\xi_{max}). \end{aligned} \quad (6.25)$$

Now, assign the adaptive parameter dynamics based on the below update law:

$$\dot{\hat{\rho}} = Proj(\hat{\rho}, \Psi) = \begin{cases} \delta \Psi & \text{if; } 0 < \hat{\rho} < \rho_{max}, \\ 0 & \text{Otherwise,} \end{cases} \quad (6.26)$$

where Ψ is defined as:

$$\Psi = |e_2 + c_1 e_1| (|\psi| + k_1 k_7 (|x_2| + |x_3|) \xi_{max}). \quad (6.27)$$

This update law ensures that the adaptive parameter $\hat{\rho}$ stays within previously specified boundaries and never exceed the maximum limit ρ_{max} . Note that Ψ is always positive, which makes $\hat{\rho}$ a non-decreasing function of time. Given that $\hat{\rho}(0) > 0$ and the defined projection law (6.26) is employed, this shall ensure that $\hat{\rho} > 0$ for all $t \geq 0$, which entails that:

$$-q(t)\hat{\rho}|e_2 + c_1 e_1| (|\psi| + k_1 k_7 (|x_2| + |x_3|) \xi_{max}) \leq 0. \quad (6.28)$$

Applying the adaptive law (6.26) and using result (6.28), inequality (6.25) is reduced to:

$$\begin{aligned}\dot{V} &\leq -W + (1 + \hat{\rho})(1 + q(t))\varphi \\ \Rightarrow \dot{V} &\leq -W + (1 + \rho_{max})^2\varphi, \\ &\text{since } \rho_{max} \geq \rho \geq q(t).\end{aligned}\tag{6.29}$$

By this step, the feedback design is completed. Note that by reaching (6.29) with sufficiently small φ , trajectories error boundedness is guaranteed as the system has achieved stability in the practical sense.

6.3 Simulations and Results

In this section, asymmetric dead-zones are attached to the inputs to the IM simulation model. The dead-zone has the following parameters $\{m_l = 2, m_r = 4, b_l = 2.5, b_r = 5, \xi_{max} = 25, \rho_{min} = 0.01, \rho_{max} = 10\}$. Again, simulation is conducted in two parts similar to previous chapters, starting from the same initial conditions and using a similar set of reference trajectories. The simulation is done with the feedback developed in section 6.2. In the first part, the adaptive parameter is initialized as $\hat{\rho} = 0.05$ and the simulation time is chosen to be $T = 10$ [s]. The simulation outcome shows that tracking is successfully accomplished with a decent accuracy. Referring to figure 6.2, the rise time appears to be less than 2.4[s] for constant references and negligible for ramp and sine references. In addition,

the applied feedback depicted in figures 6.3-6.4 for all cases is bounded within the range ± 30 [V]. Finally, the boundedness of the rest of the states and adaptive parameter ρ can be seen in figures 6.5-6.9. These results show the validity of the proposed feedback design.

The second part is done with an external torque of $T_L = 1$ [Nm] and with similar initial conditions, parameter settings and reference functions. The resulting performance of the adaptive controller against several reference functions is shown in figure 6.10. In worst case scenario, the rise time is reached by around [5]s (constant references) and in about 2[s] in the best case (ramp reference). In addition, the applied feedback stays within the range ± 40 [V] as seen in figures 6.11 and 6.12. The state variables of the IM system in addition to both adaptive parameters $\hat{\rho}$, \hat{T}_L are plotted in figures 6.13-6.18, all of which are bounded throughout the simulation time. In short, the illustrated outcome of both parts of the simulation achieved very similar performance as in previous chapter, which meets the design objective.

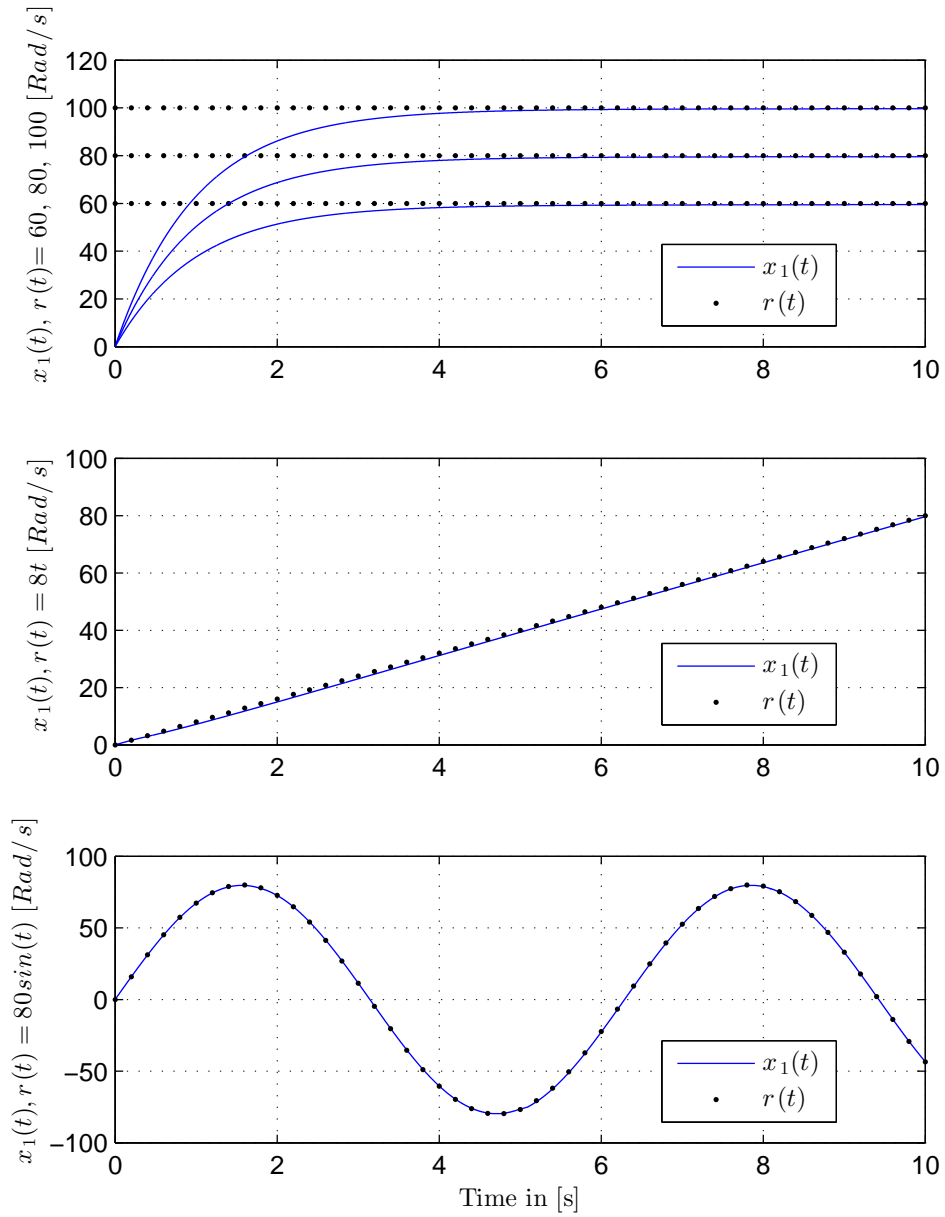


Figure 6.2: Speed tracking performance of IM (with $T_L = 0$) against constant, ramp and sinusoidal reference trajectory respectively (asymmetric dead-zone case).

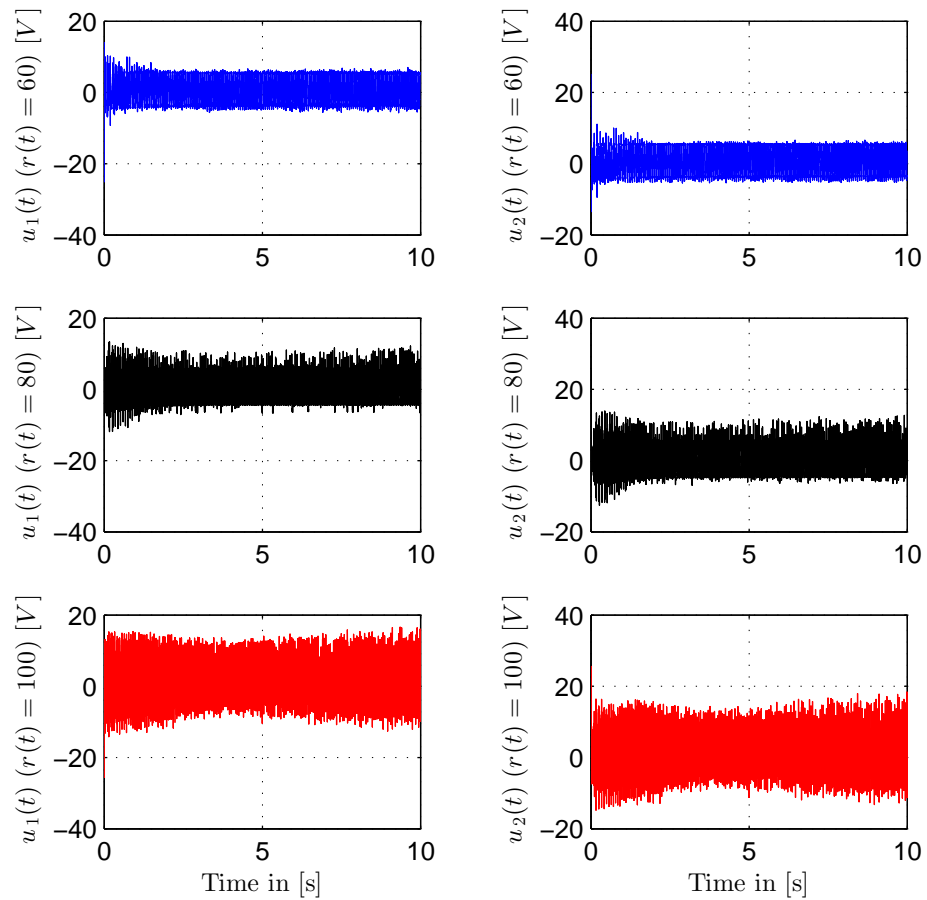


Figure 6.3: Applied control input voltages of IM (with $T_L = 0$) against various constant references (asymmetric dead-zone case).

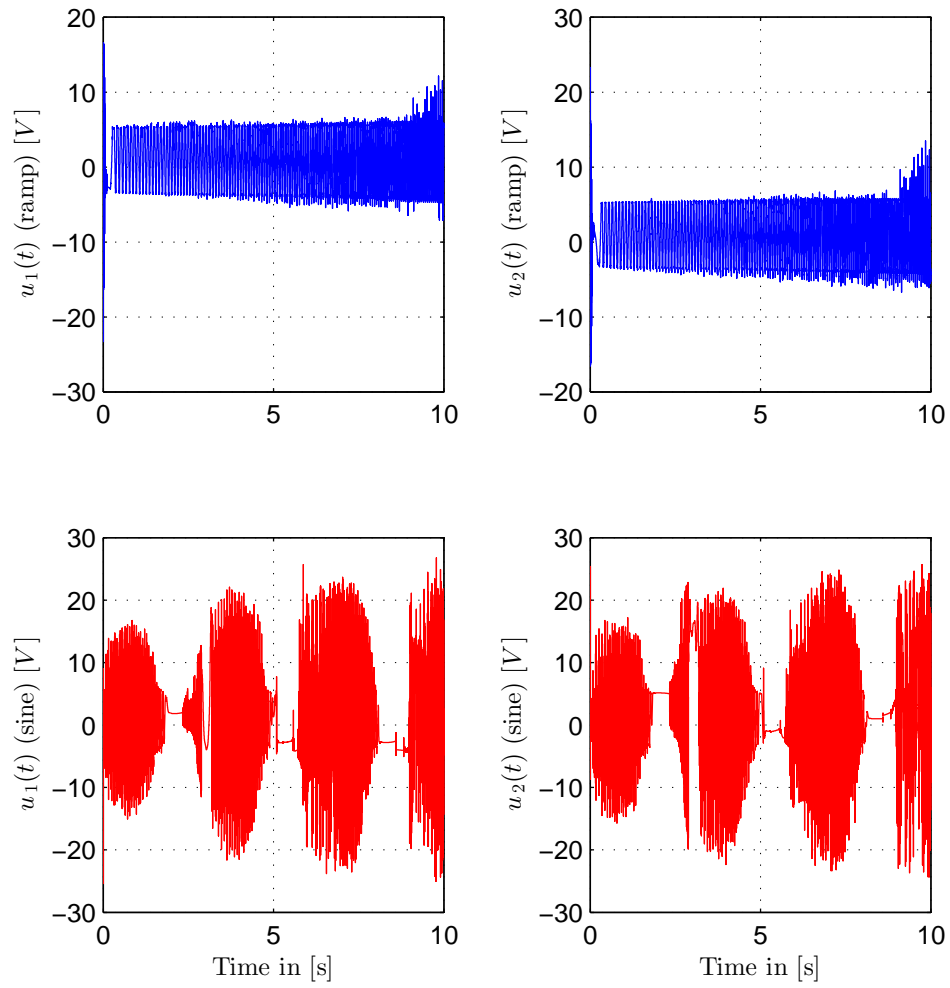


Figure 6.4: Applied control input voltages of IM (with $T_L = 0$) against ramp and sinusoid references respectively (asymmetric dead-zone case).

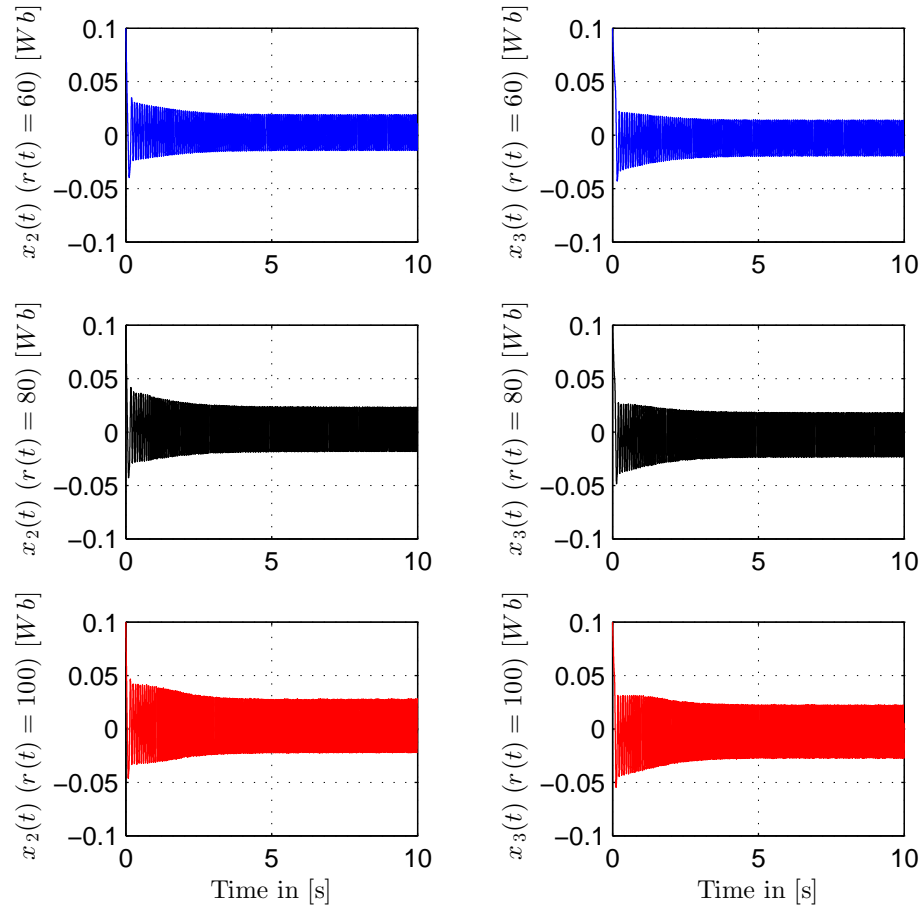


Figure 6.5: Magnetic flux components of IM (with $T_L = 0$) for various constant references (asymmetric dead-zone case).

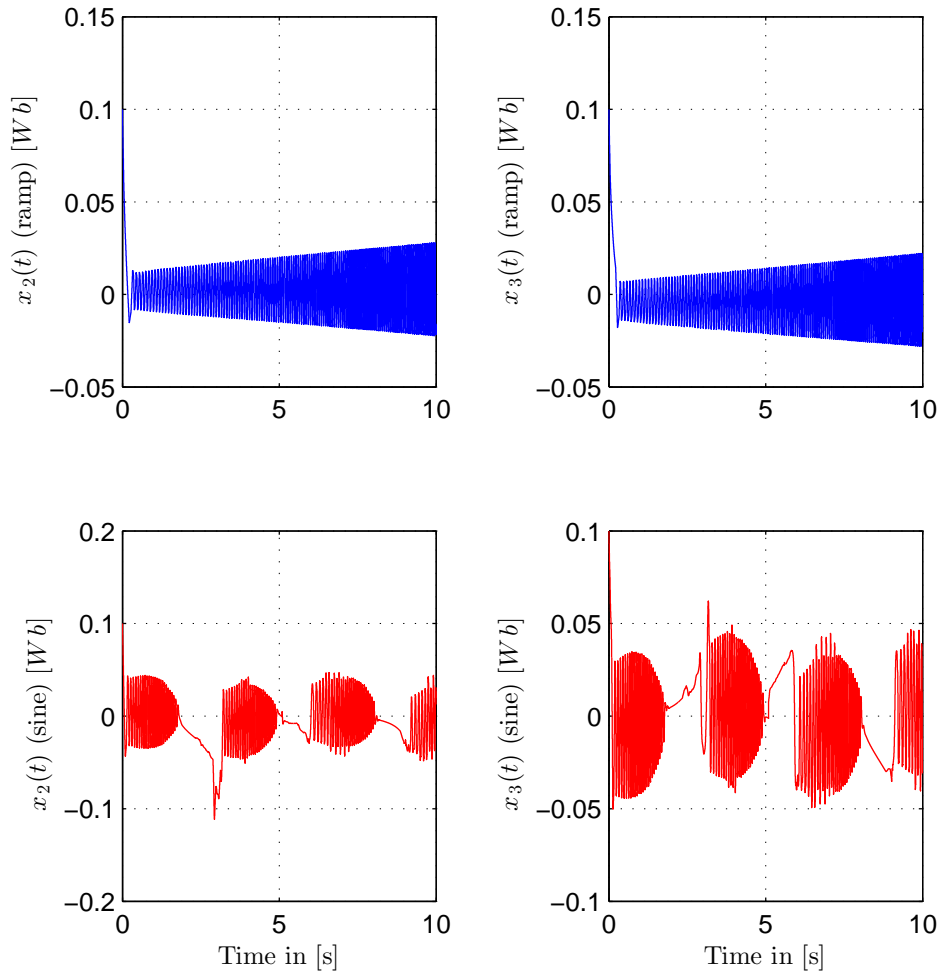


Figure 6.6: Magnetic flux components of IM (with $T_L = 0$) for ramp and sinusoid references respectively (asymmetric dead-zone case).

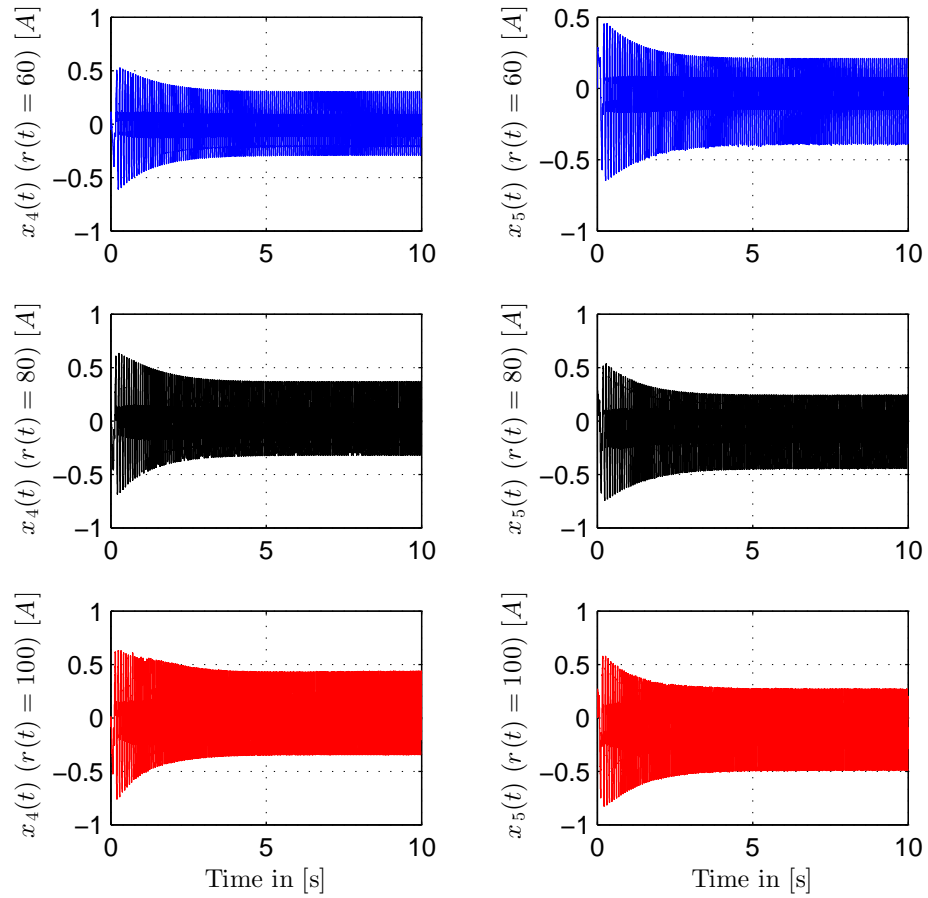


Figure 6.7: Current components of IM (with $T_L = 0$) for various constant references (asymmetric dead-zone case).

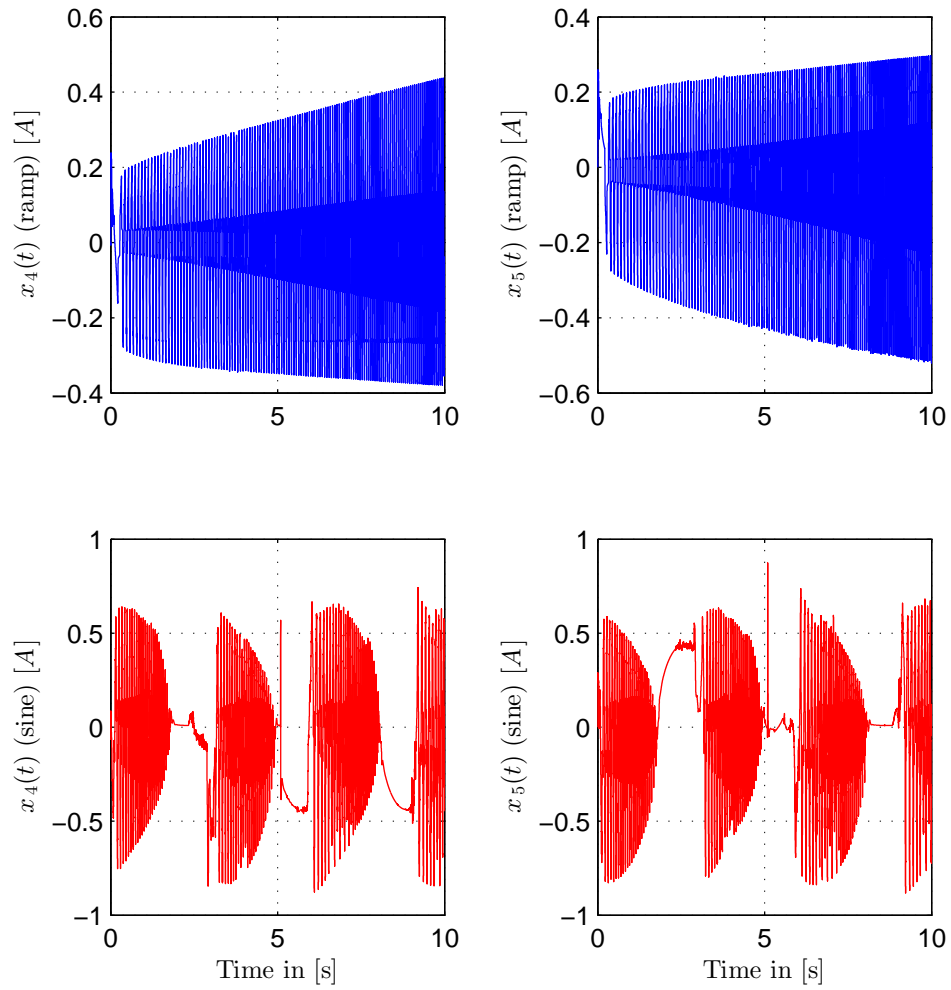


Figure 6.8: Current components of IM (with $T_L = 0$) for ramp and sinusoid references respectively (asymmetric dead-zone case).

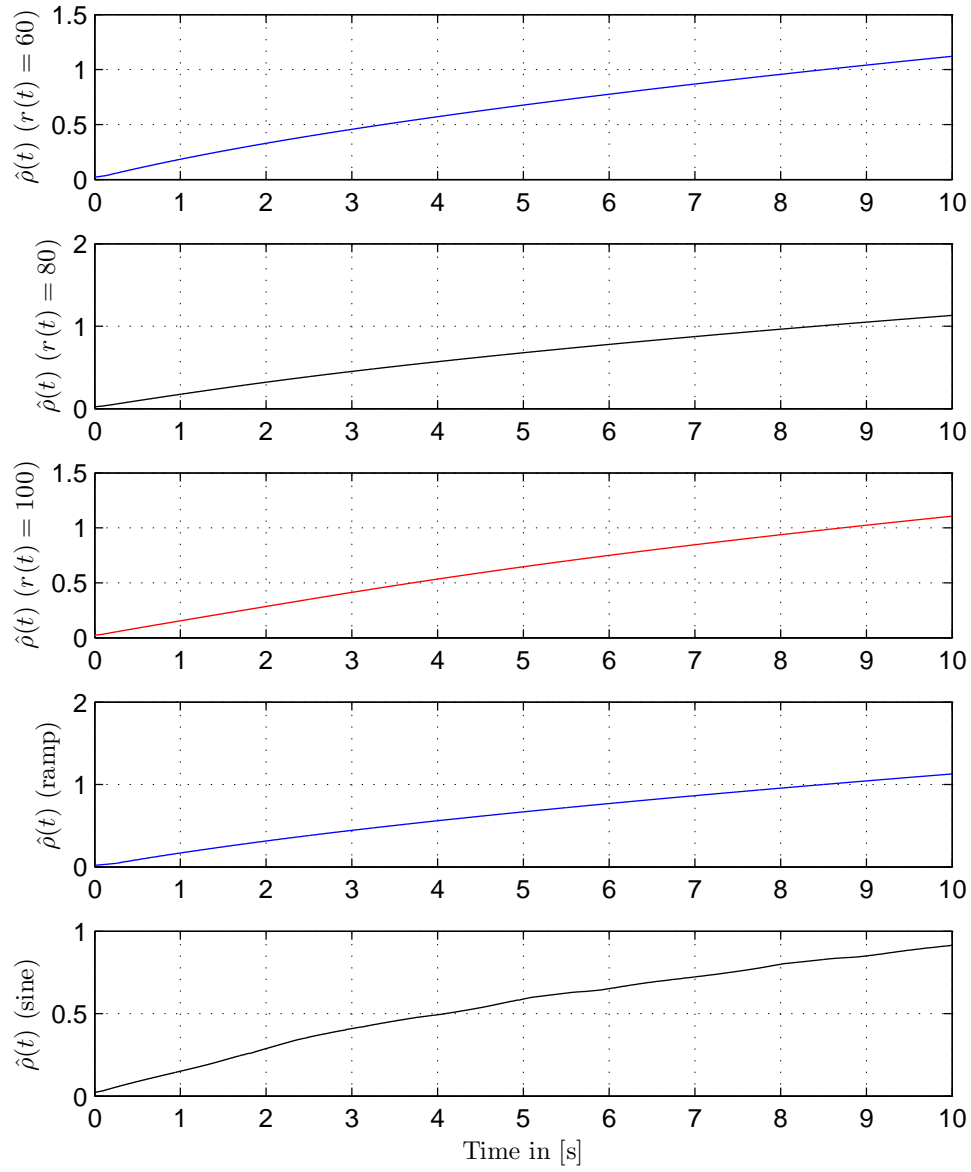


Figure 6.9: Adaptive parameter $\hat{\rho}$ performance for constant, ramp and sinusoid references respectively (asymmetric dead-zone case).

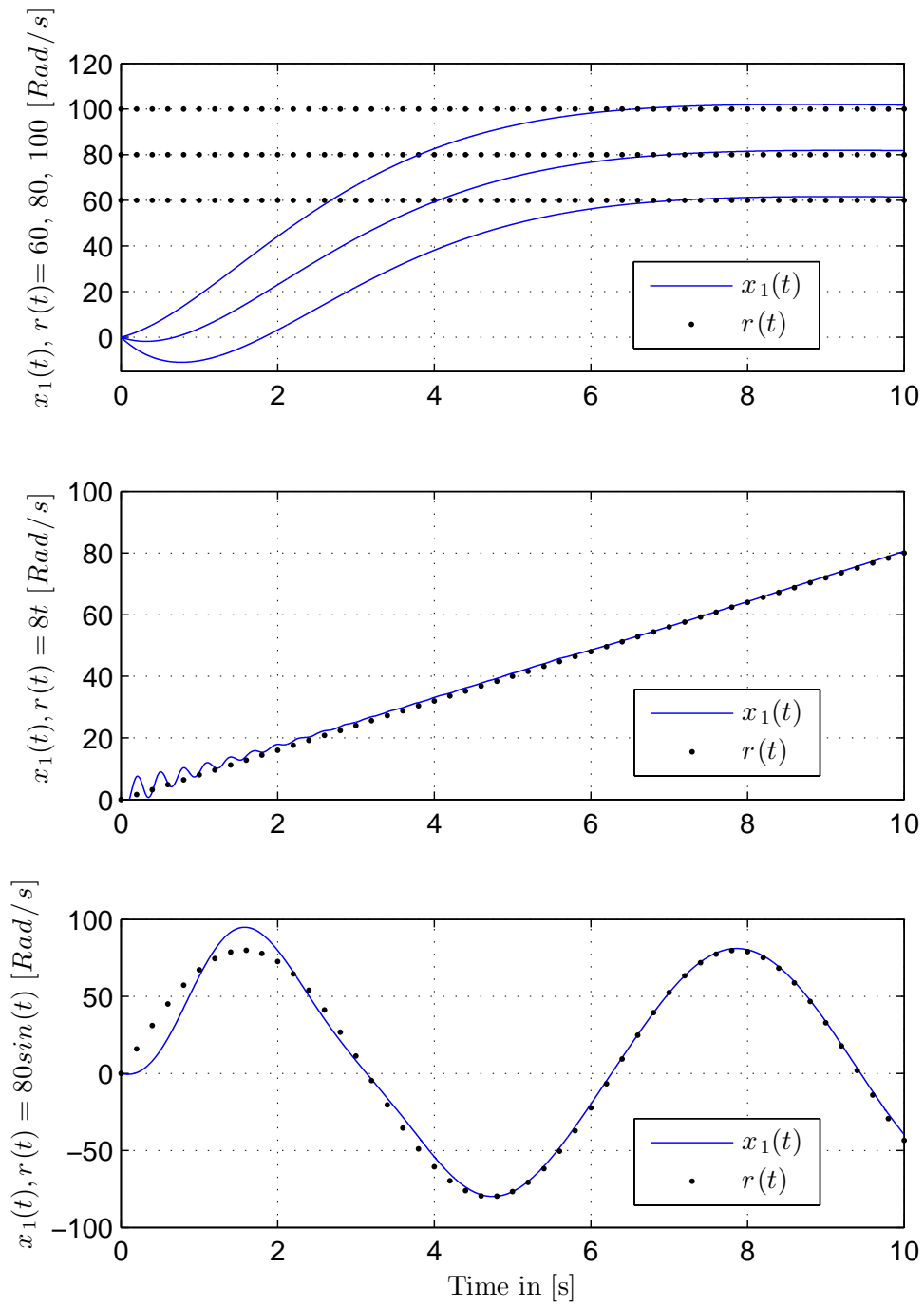


Figure 6.10: Speed tracking performance of IM (with $T_L = 1$ [Nm]) against constant, ramp and sinusoidal reference trajectory respectively (asymmetric dead-zone case).

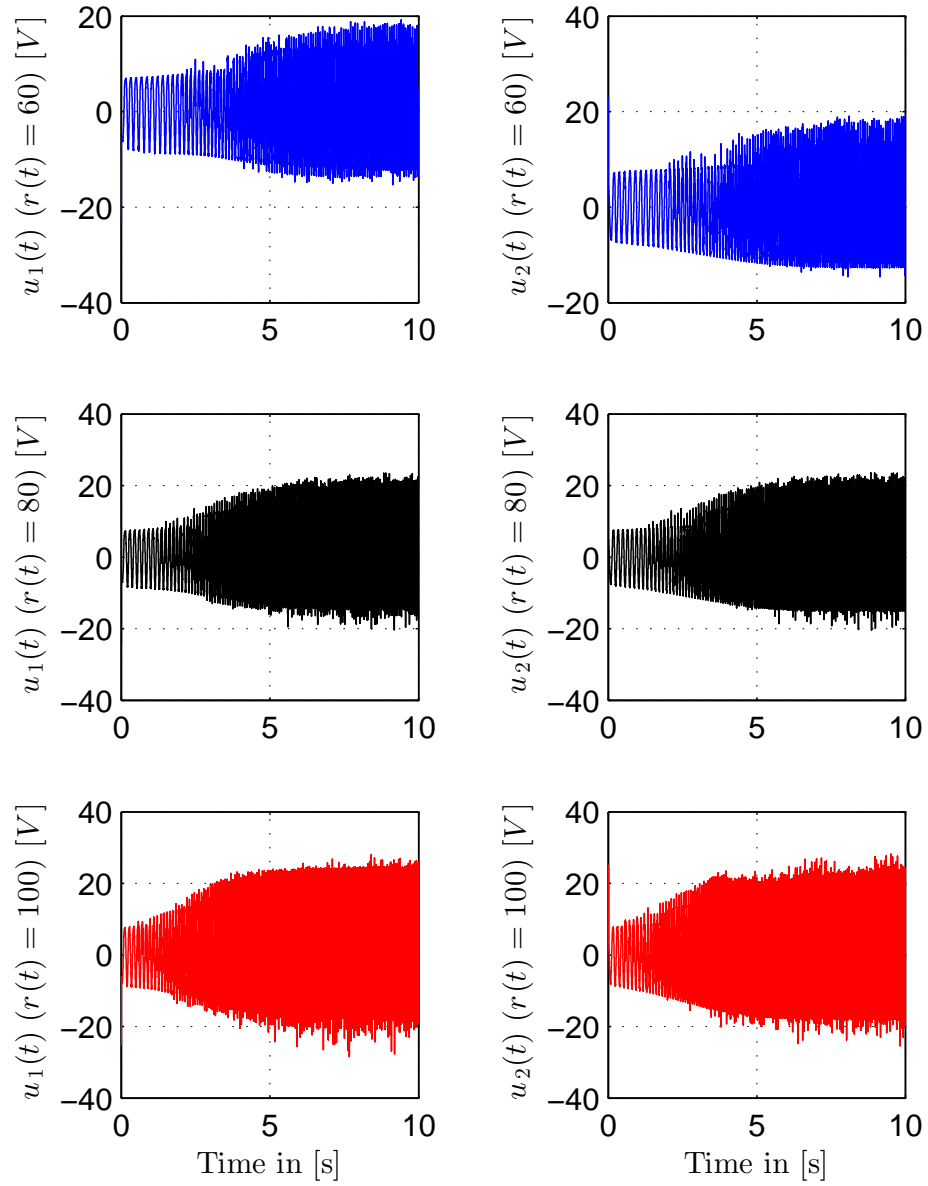


Figure 6.11: Applied control input voltages of IM (with $T_L = 1$ [Nm]) against various constant references (asymmetric dead-zone case).

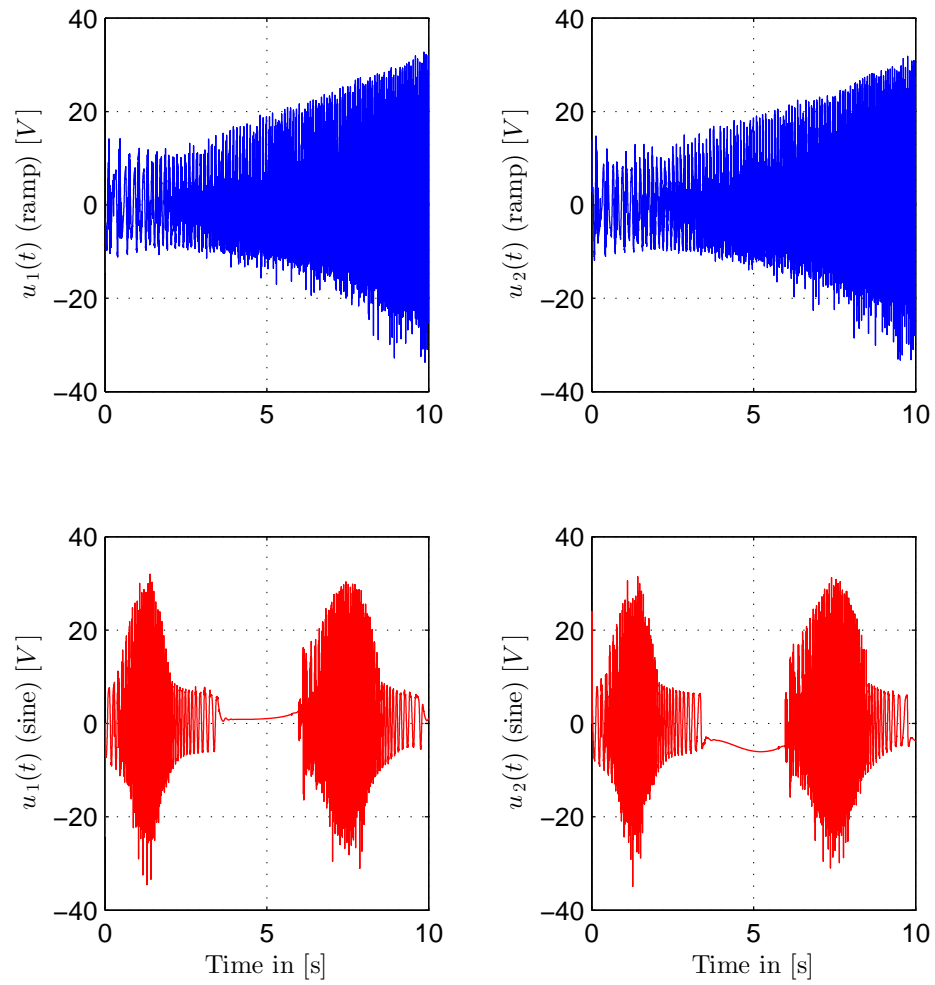


Figure 6.12: Applied control input voltages of IM (with $T_L = 1$ [Nm]) against ramp and sinusoid references respectively (asymmetric dead-zone case).

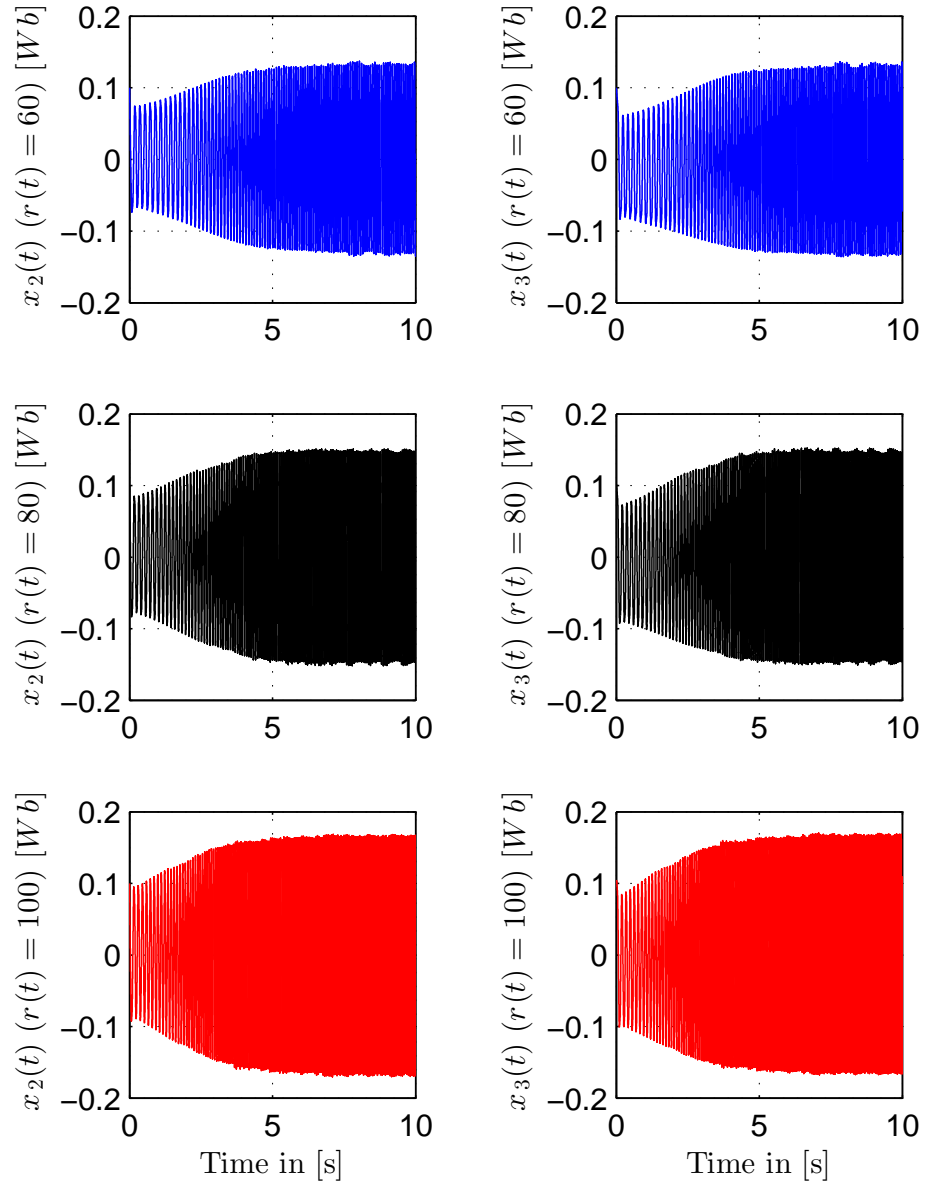


Figure 6.13: Magnetic flux components of IM (with $T_L = 1$ [Nm]) for various constant references (asymmetric dead-zone case).

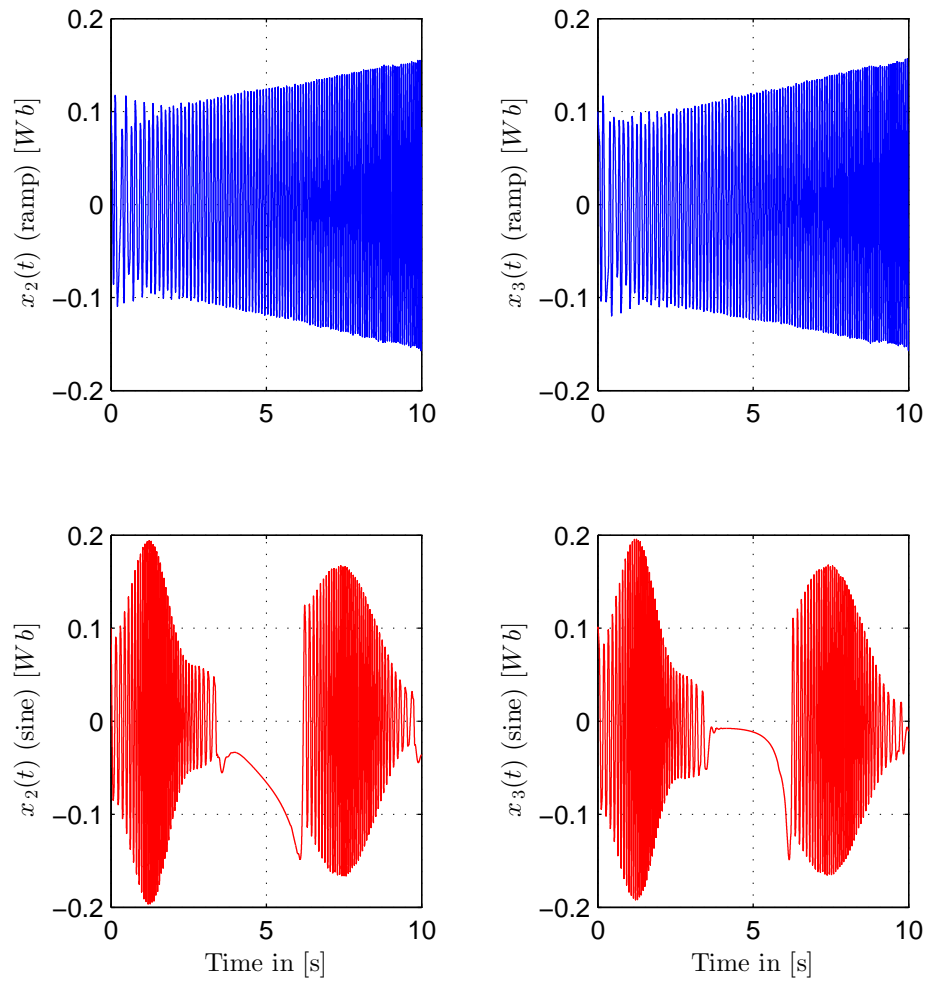


Figure 6.14: Magnetic flux components of IM (with $T_L = 1$ [Nm]) for ramp and sinusoid references respectively (asymmetric dead-zone case).

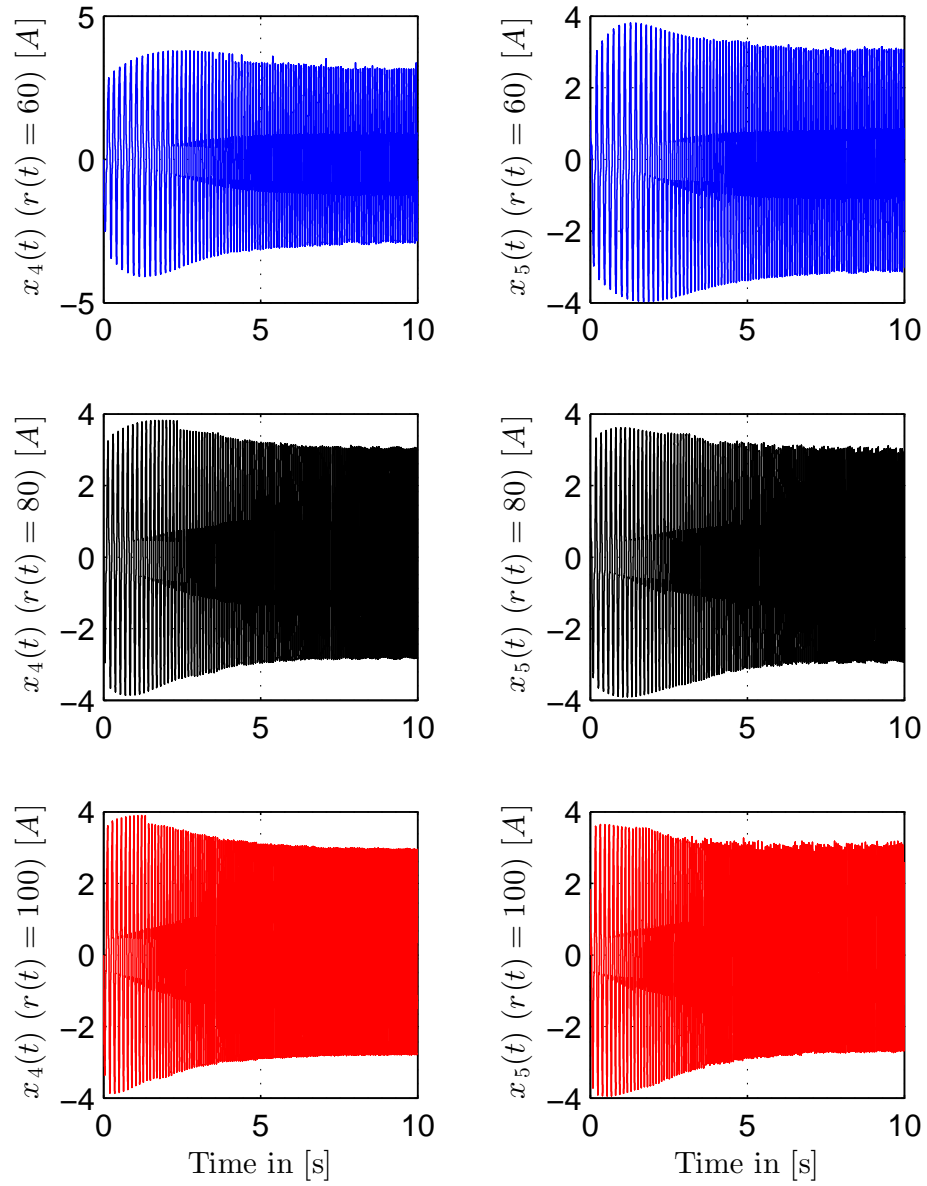


Figure 6.15: Current components of IM (with $T_L = 1$ [Nm]) for various constant references (asymmetric dead-zone case).

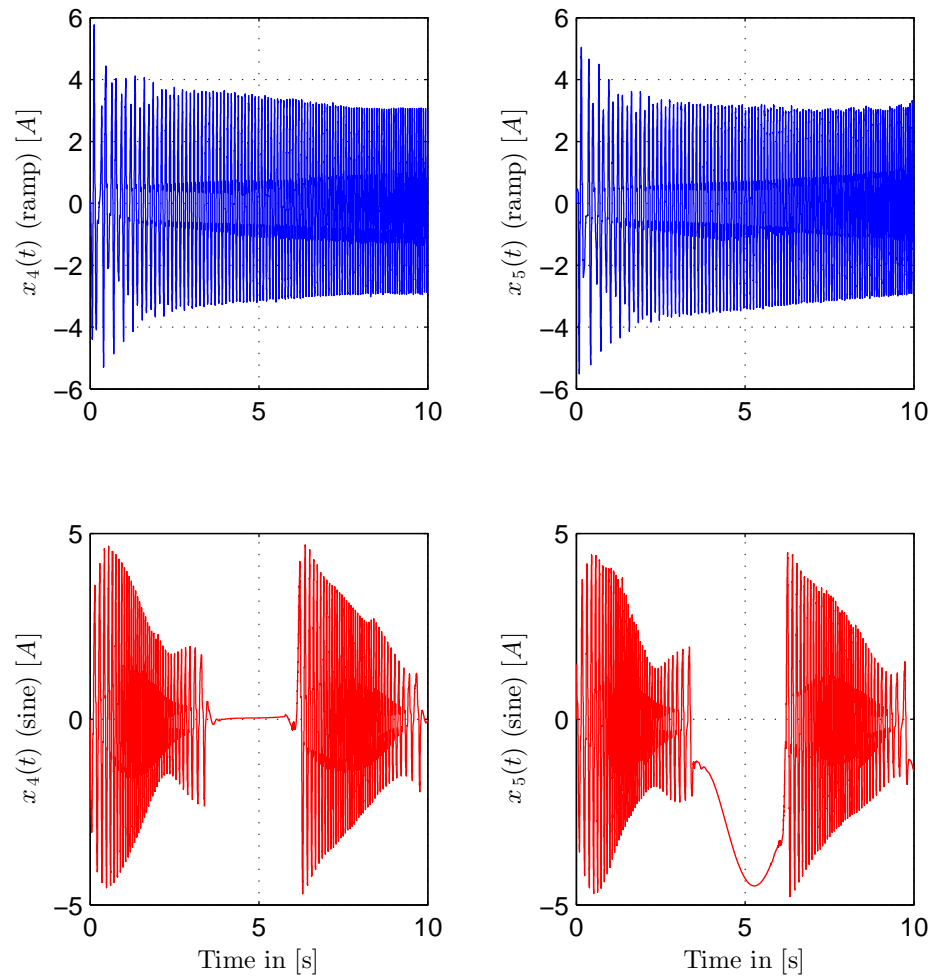


Figure 6.16: Current components of IM (with $T_L = 1$ [Nm]) for ramp and sinusoid references respectively (asymmetric dead-zone case).

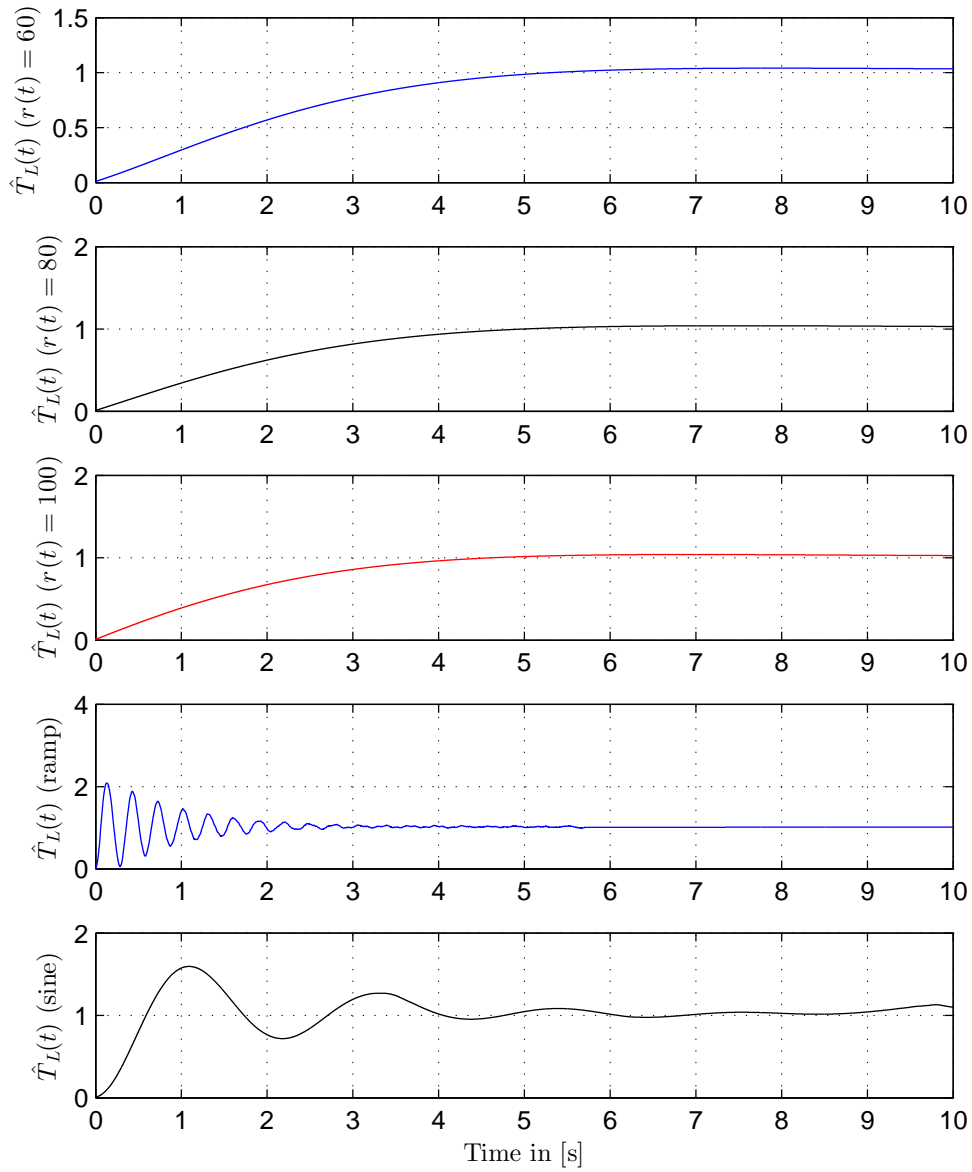


Figure 6.17: Load torque adaptive parameter \hat{T}_L performance for constant, ramp and sinusoid references respectively (asymmetric dead-zone case).

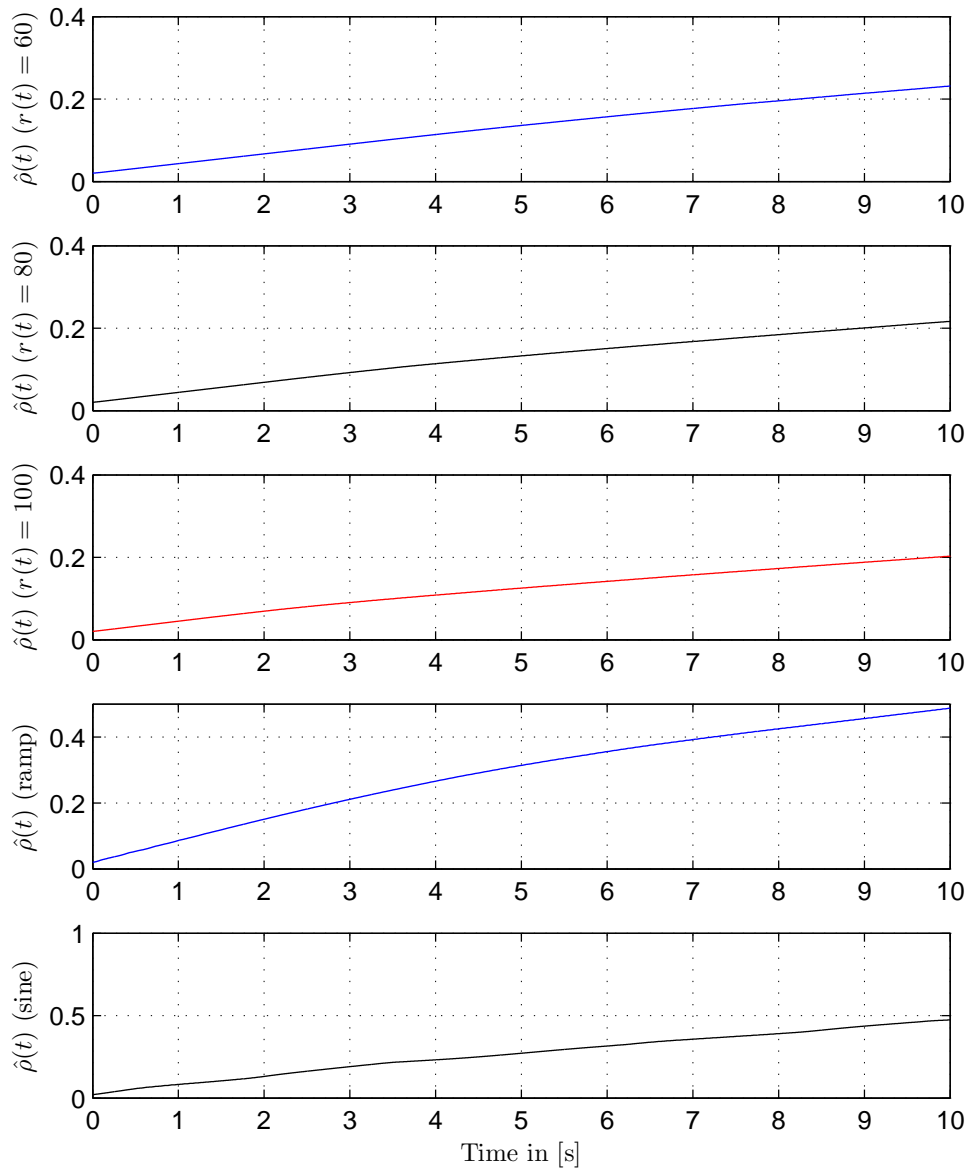


Figure 6.18: Adaptive parameter $\hat{\rho}$ performance for constant, ramp and sinusoid references respectively (asymmetric dead-zone case).

CHAPTER 7

IM WITH BACKLASH INPUT

Previous chapters has dealt with the case of IM subject to a dead-zone, a passive input nonlinearity. The control feedbacks were developed and simulated for that case. In addition, there are dynamic nonlinearities such as hysteresis, an example of which are the backlash and the Bouc-Wen hysteresis. Similar to the dead-zone chapter, the goal is to design and simulate the controller for IM after adding these effects to the inputs. The backlash case is treated in this chapter, while the Bouc-Wen case is left for next chapter.

7.1 Backlash Modeling and Controller Design

The backlash input function $B(\cdot)$ for a given scalar input u can be defined by the following model [45]:

$$B(u) = \begin{cases} h(u-d) & \text{if } \dot{u} > 0 \text{ and } B(u) = h(u-d), \\ h(u+d) & \text{if } \dot{u} < 0 \text{ and } B(u) = h(u+d), \\ B(u)^* & \text{Otherwise,} \end{cases} \quad (7.1)$$

where h and d are positive and upper bounded unknown constants. Note that $B(u)^*$ means no change occurs in $B(u)$.

Alternatively, backlash can also be represented using the following definition [37]:

$$B(u) = \alpha_r(t)h(u-d) + \alpha_l(t)h(u+d) + \alpha_s(t)u_s, \quad (7.2)$$

where u_s is a constant verifying the inequality:

$$h(u-d) \leq u_s \leq h(u+d), \quad (7.3)$$

and where

$$\alpha_r(t) = \begin{cases} 1 & \text{if } \dot{u} > 0, \\ 0 & \text{otherwise,} \end{cases} \quad (7.4)$$

$$\alpha_i(t) = \begin{cases} 1 & \text{if } \dot{u} < 0, \\ 0 & \text{otherwise,} \end{cases} \quad (7.5)$$

$$\alpha_s(t) = \begin{cases} 1 & \text{if } \dot{u} = 0, \\ 0 & \text{otherwise,} \end{cases} \quad (7.6)$$

along with below equation:

$$\alpha_r(t) + \alpha_i(t) + \alpha_s(t) = 1, \quad (7.7)$$

being valid all the times. Finally, backlash can also be described by the following combination [30]:

$$B(u) = h u + \vartheta(u), \quad (7.8)$$

where $\vartheta(u)$ is a bounded perturbation function with following representation:

$$\vartheta(u) = \begin{cases} -h d & \text{if; } \dot{u} > 0, \\ h d & \text{if; } \dot{u} < 0, \\ \varrho(u) & \text{if; } \dot{u} = 0, -h d \leq \varrho(u) \leq h d. \end{cases} \quad (7.9)$$

Assumption 6. The backlash has known parameters' boundaries. In other words, $h \in [h_{min}, h_{max}]$ and $d \in [d_{min}, d_{max}]$ with h_{min} , h_{max} , d_{min} , and d_{max} are all known positive constants. Also, the perturbation ϑ is bounded as $\vartheta_{max} = h_{max}d_{max}$, a known constant positive quantity.

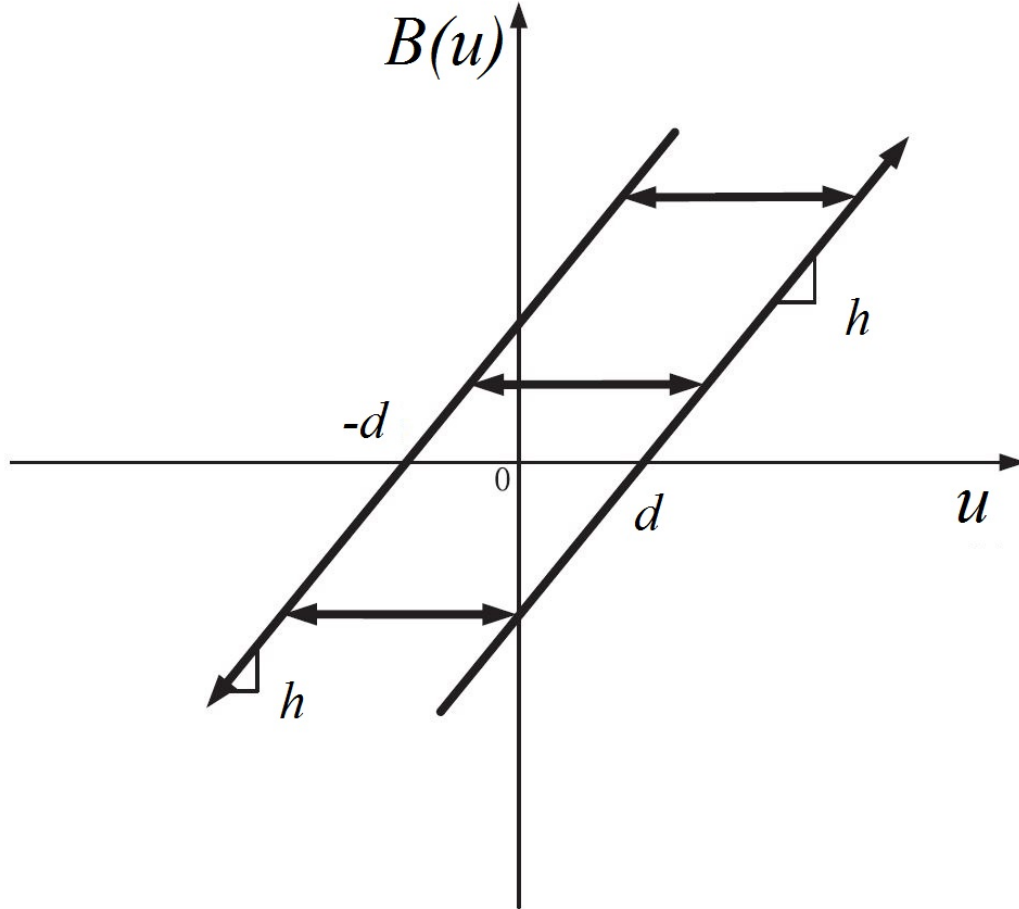


Figure 7.1: Backlash nonlinearity

Consider subjecting IM inputs to some unknown backlash, thereby replacing u_1, u_2 by $B(u_1), B(u_2)$. Let \hat{h} be the adaptive control parameter. Define the error \tilde{h} as:

$$\tilde{h} = \frac{1}{h} - \hat{h}. \quad (7.10)$$

Select a Lyapunov function similar to (5.6):

$$V = V_1 + \frac{1}{2}(e_2 + c_1 e_1)^2 + \frac{1}{2\alpha} \tilde{T}_L^2 + \frac{1}{2\tau} h \tilde{h}^2 \geq 0, \quad (7.11)$$

where τ is a selected positive constant. Now, taking the time derivative and utilizing (4.18) result in:

$$\begin{aligned}\dot{V} = & -W + (e_2 + c_1 e_1)(\psi + k_1 k_7 x_2 B(u_2) - k_1 k_7 x_3 B(u_1)) \\ & + \frac{1}{\tau} h \tilde{h} \dot{\tilde{h}}.\end{aligned}\tag{7.12}$$

Choose the inputs to be:

$$u_1 = \frac{-\hat{h}x_3(-\psi + v)}{k_1 k_7 (x_2^2 + x_3^2)}, \quad u_2 = \frac{\hat{h}x_2(-\psi + v)}{k_1 k_7 (x_2^2 + x_3^2)}.\tag{7.13}$$

Recall equations (5.3) and (7.8). Note that both the dead-zone and the backlash can be described as the combination of linear function of the input (mu or hu) and a bounded perturbation function of the input ($\eta(u)$ or $\vartheta(u)$). In both cases, according to assumptions (4) and (6), both $\eta(u)$ and $\vartheta(u)$ have known positive bounds, namely η_{max} , ϑ_{max} respectively. Now, substituting (7.8) and (7.13) in (7.12), results in:

$$\begin{aligned}\dot{V} = & -W + (e_2 + c_1 e_1)\left(\psi + k_1 k_7 x_2 \left(h \frac{\hat{h}x_2(-\psi + v)}{k_1 k_7 (x_2^2 + x_3^2)}\right.\right. \\ & \left. + \vartheta(u_2)\right) - k_1 k_7 x_3 \left(h \frac{-\hat{h}x_3(-\psi + v)}{k_1 k_7 (x_2^2 + x_3^2)} + \vartheta(u_1)\right) \\ & + \frac{1}{\tau} h \tilde{h} \dot{\tilde{h}}.\end{aligned}\tag{7.14}$$

Note that equation (7.14) is almost identical to (5.9), which can be achieved by renaming (h, \hat{h}, \tilde{h}) to (m, \hat{m}, \tilde{m}) and replacing ϑ by η . Thus, the controller of the

symmetric dead-zone scenario (5.7, 5.17) with the same adaptive projection law (5.13, 5.14) can compensate for the backlash nonlinearity effect.

7.2 Simulations and Results

In this section, simulation is conducted in a very similar manner to previous chapters. Instead of the dead-zone, backlash blocks are connected to the inputs of the IM system. The exact symmetric dead-zone controller is utilized to compensate for the effects resulting from the backlash. The backlash parameters are set as $\{h = 7, h_{min} = 0.01, h_{max} = 10, d = 1.5, \vartheta_{max} = 25\}$ in the first part with $d = .75$ in the second part of the simulation. A similar set of initial conditions and reference functions (in last chapters) is used to run the simulation. Tracking results are shown in figures 7.2 and 7.10. A reasonable performance is reached in both cases and very close to the dead-zone simulation with almost identical rise times. Also, the feedback is shown to be bounded as in figures 7.3-7.4 and 7.11-7.12. Despite the fact that the feedback exhibits different behavior and is taking different shape than that in dead-zone case, both serve the same purpose and produce similar outcome. Also, the controller performance in the first part ($T_L = 0$) is better than the second part ($T_L = 1$ [Nm]) as expected. Other system outcomes (states and adaptive parameters) are bounded as depicted in figures 7.5-7.9 and 7.13-7.18. These results validate the claim proved in section 7.2. That is, the IM subject to backlash inputs can be controlled by the exact compensating feedback developed for the dead-zone input case.

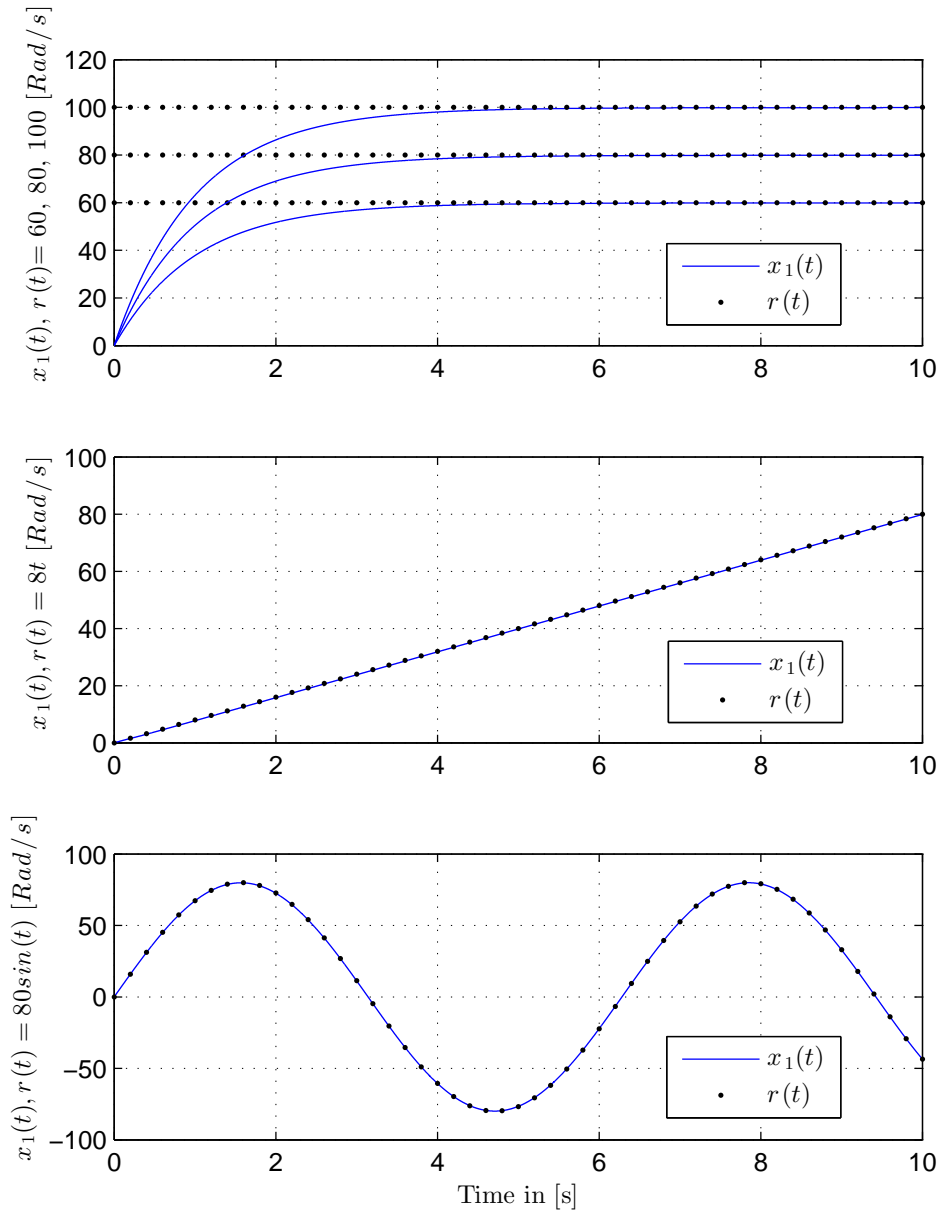


Figure 7.2: Speed tracking performance of IM (with $T_L = 0$) against constant, ramp and sinusoidal reference trajectory respectively (backlash case).

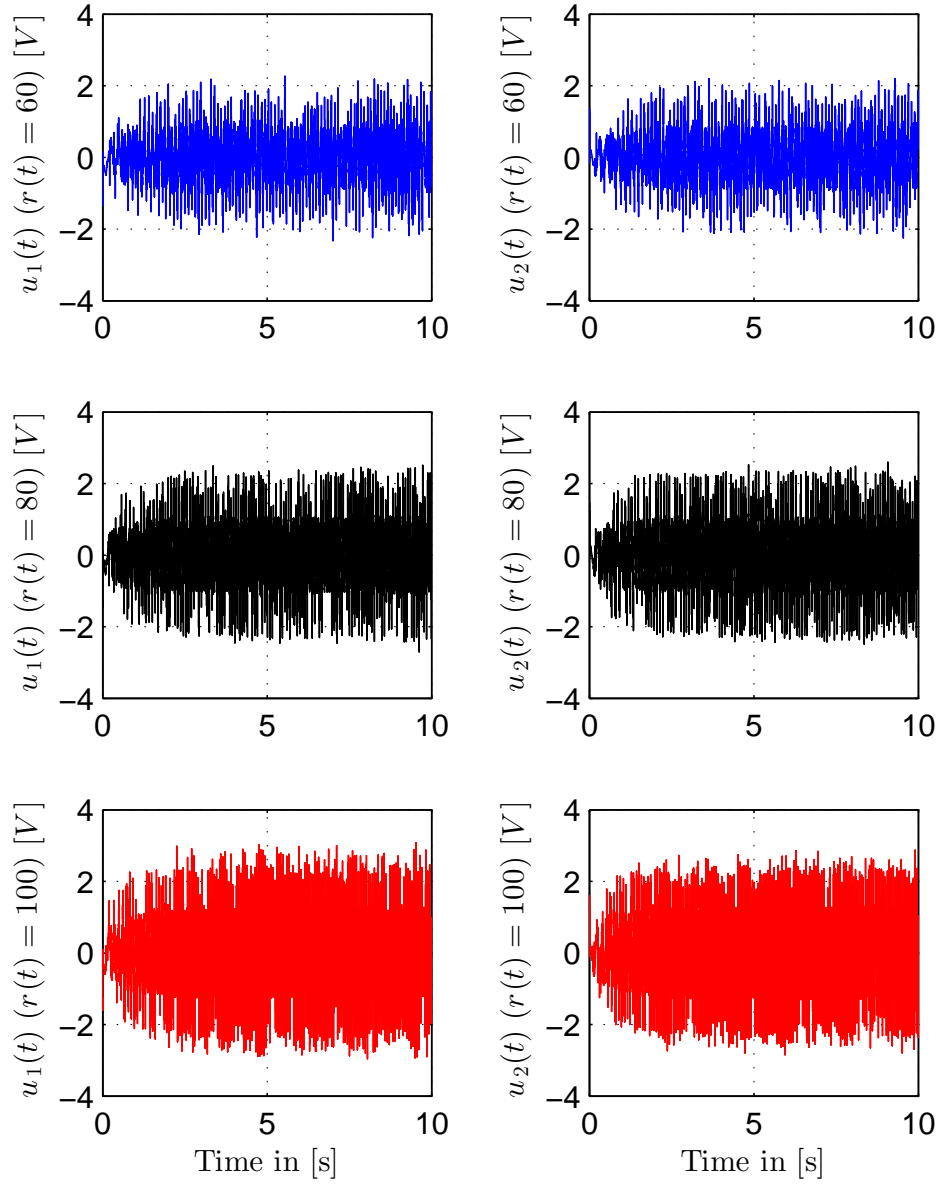


Figure 7.3: Applied control input voltages of IM (with $T_L = 0$) against various constant references (backlash case).

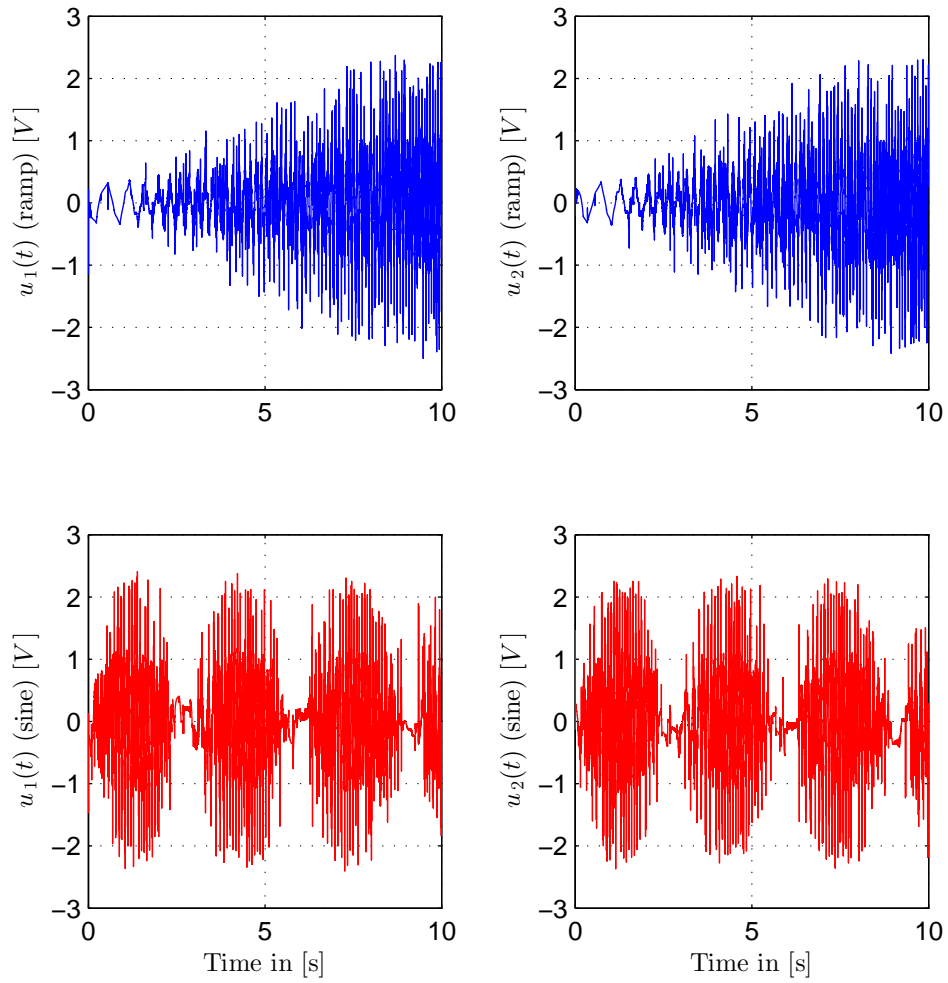


Figure 7.4: Applied control input voltages of IM (with $T_L = 0$) against ramp and sinusoid references respectively (backlash case).

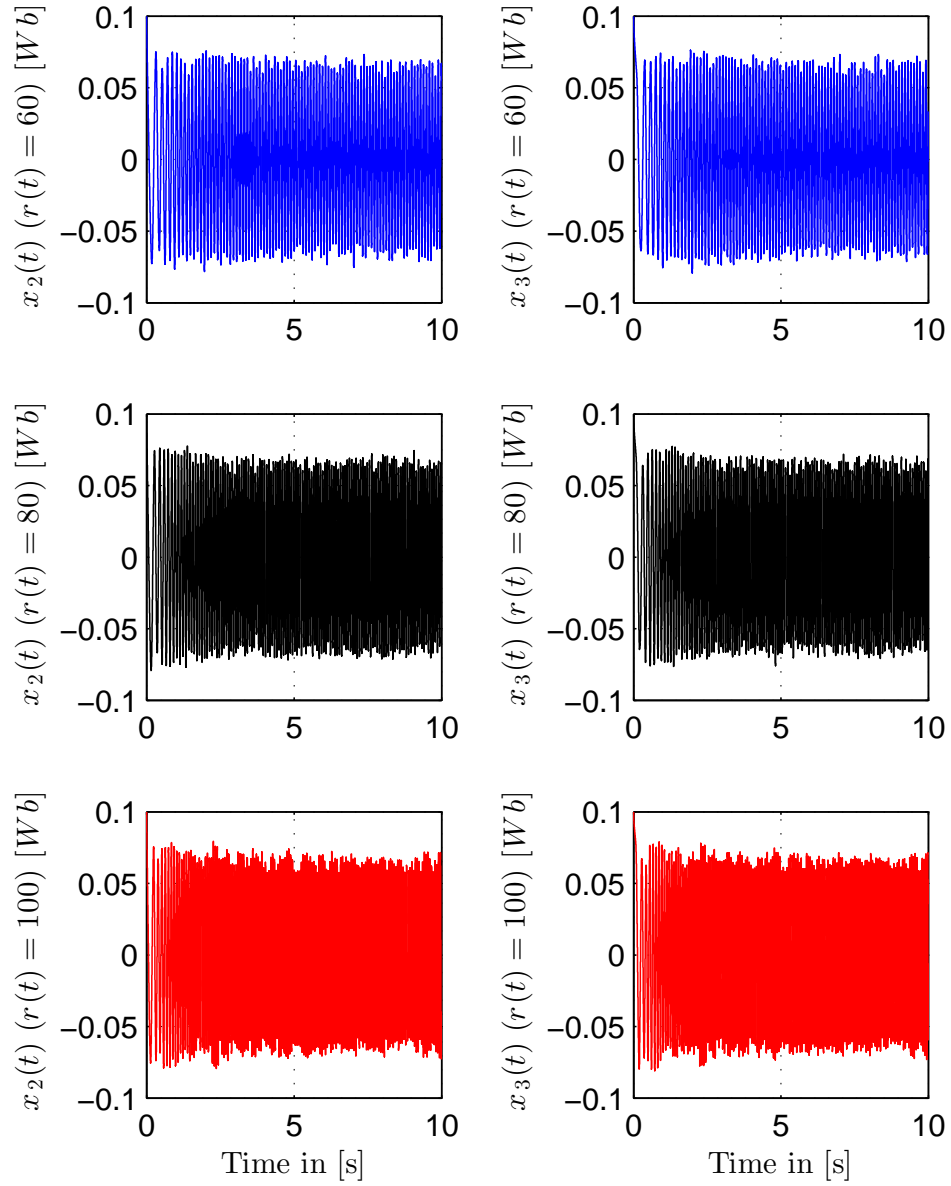


Figure 7.5: Magnetic flux components of IM (with $T_L = 0$) for various constant references (backlash case).

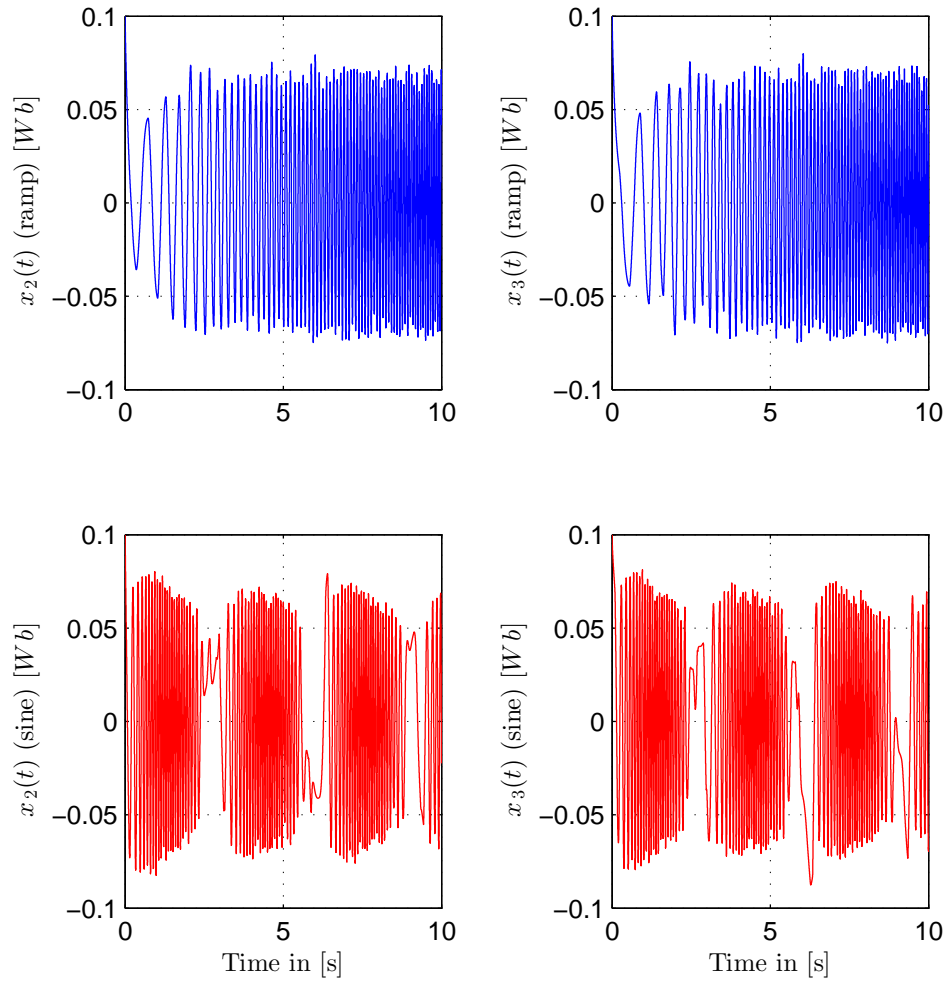


Figure 7.6: Magnetic flux components of IM (with $T_L = 0$) for ramp and sinusoid references respectively (backlash case).

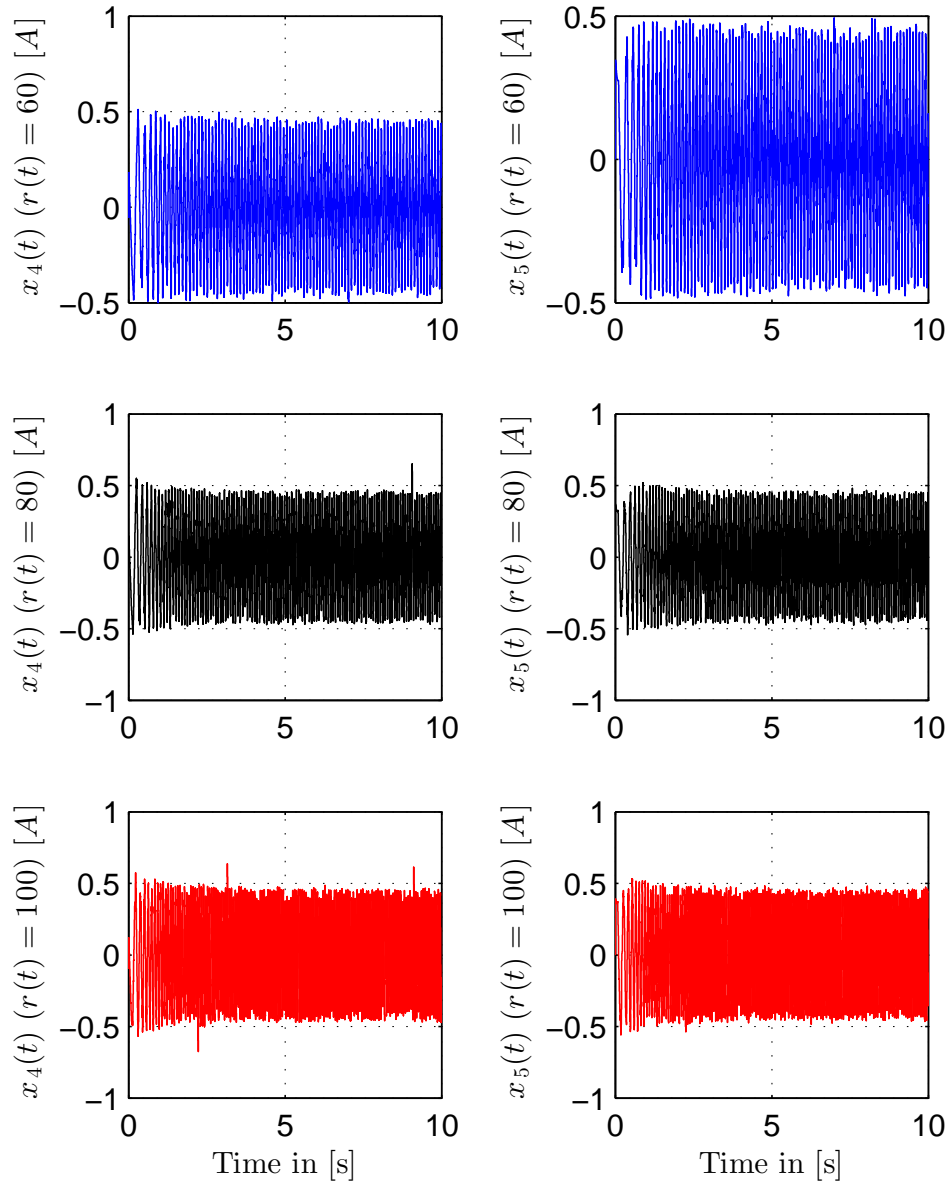


Figure 7.7: Current components of IM (with $T_L = 0$) for various constant references (backlash case).

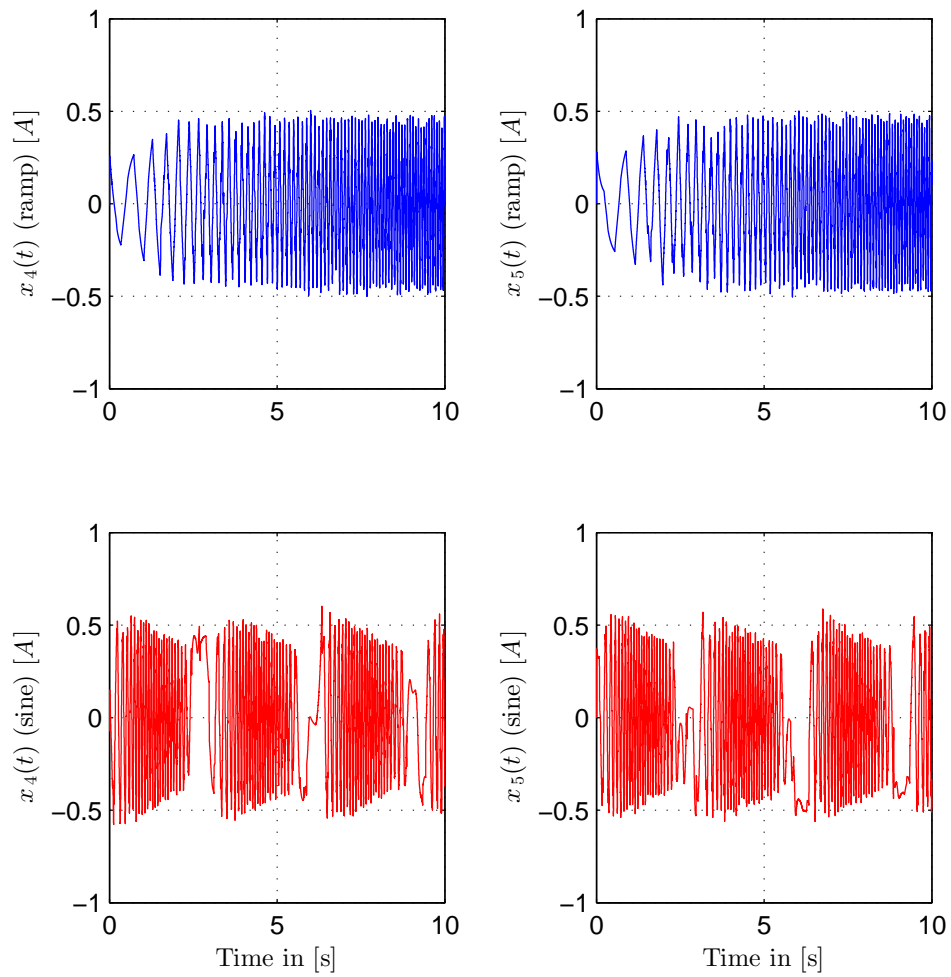


Figure 7.8: Current components of IM (with $T_L = 0$) for ramp and sinusoid references respectively (backlash case).

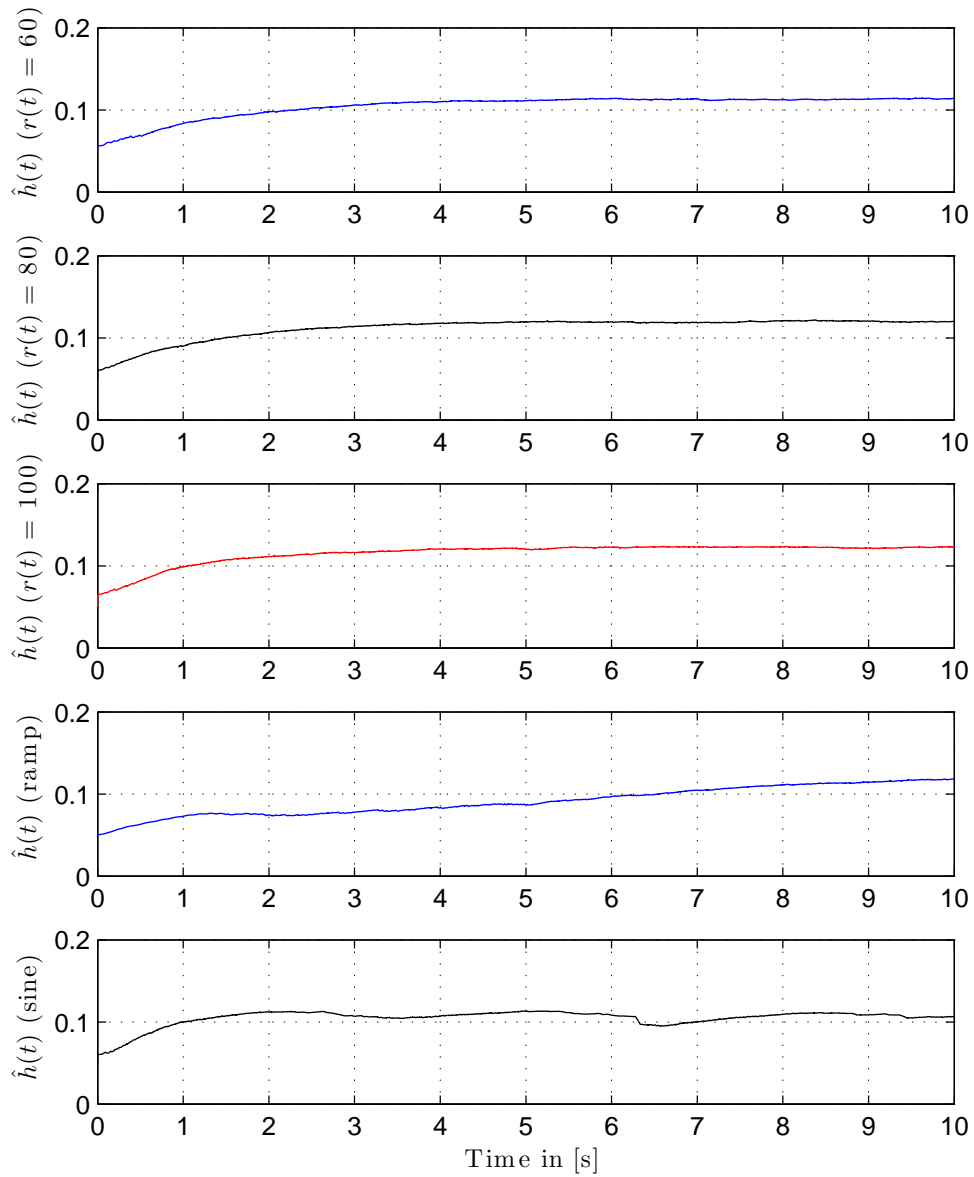


Figure 7.9: Adaptive parameter \hat{h} performance for constant, ramp and sinusoid references respectively (backlash case).

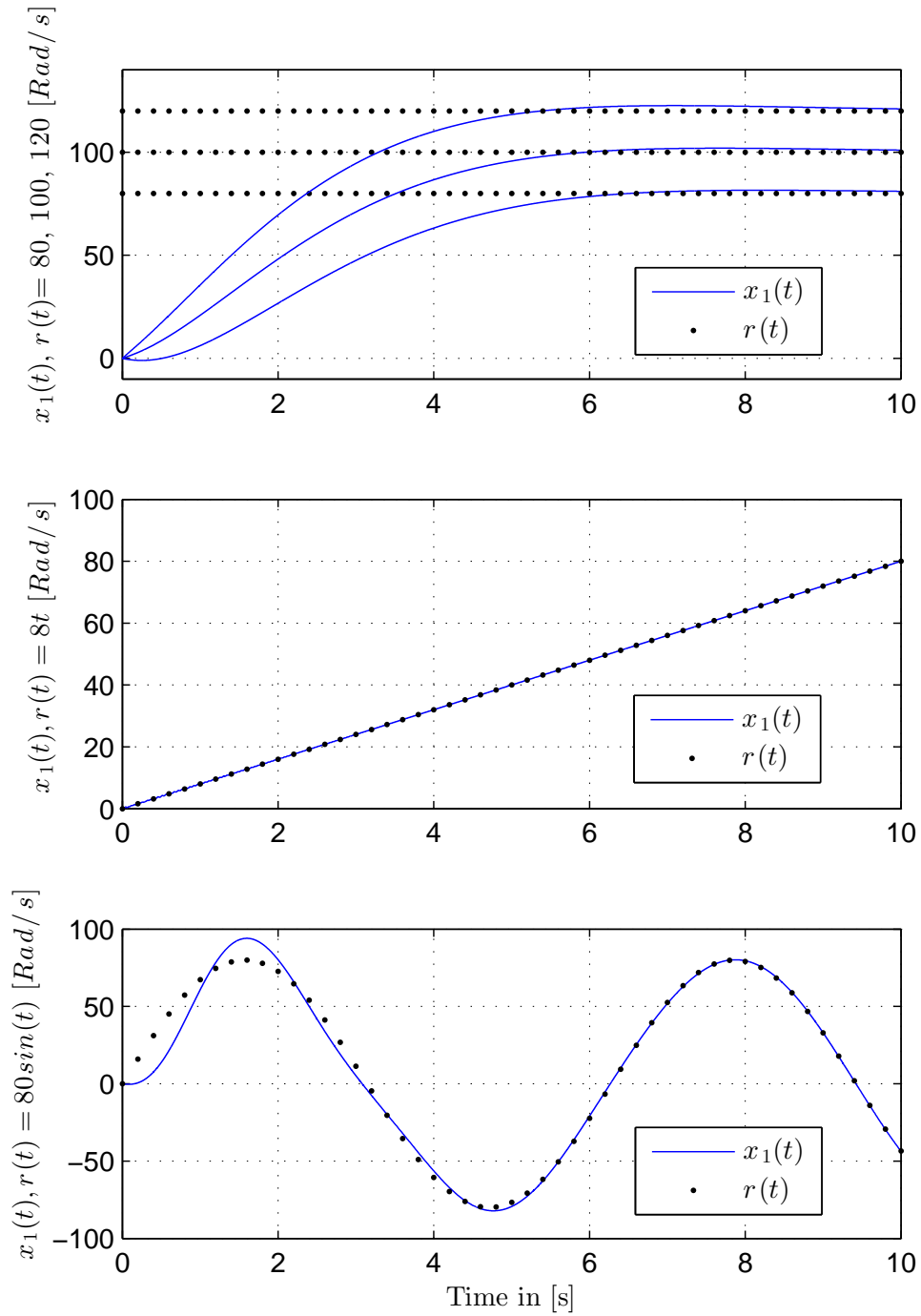


Figure 7.10: Speed tracking performance of IM (with $T_L = 1$ [Nm]) against constant, ramp and sinusoidal reference trajectory respectively (backlash case).

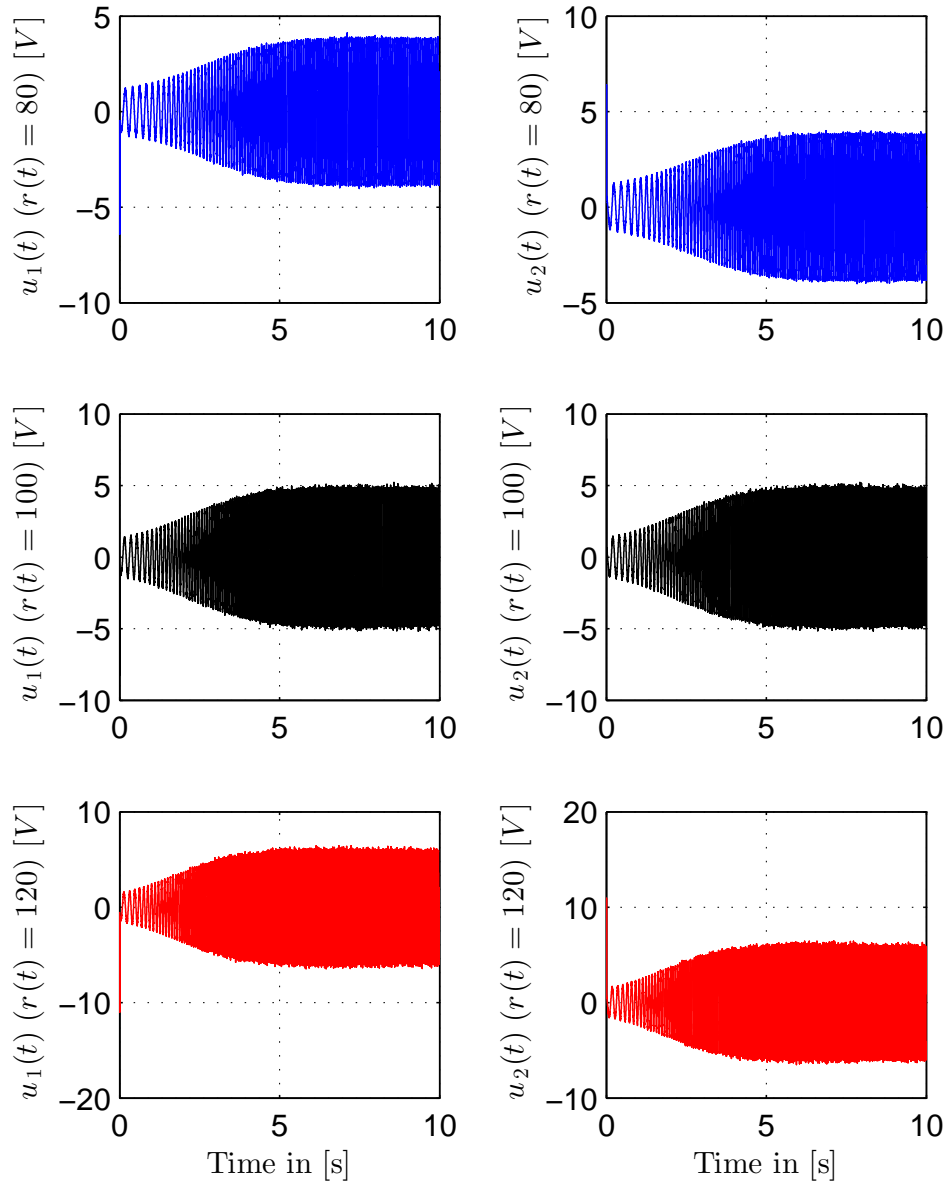


Figure 7.11: Applied control input voltages of IM (with $T_L = 1$ [Nm]) against various constant references (backlash case).

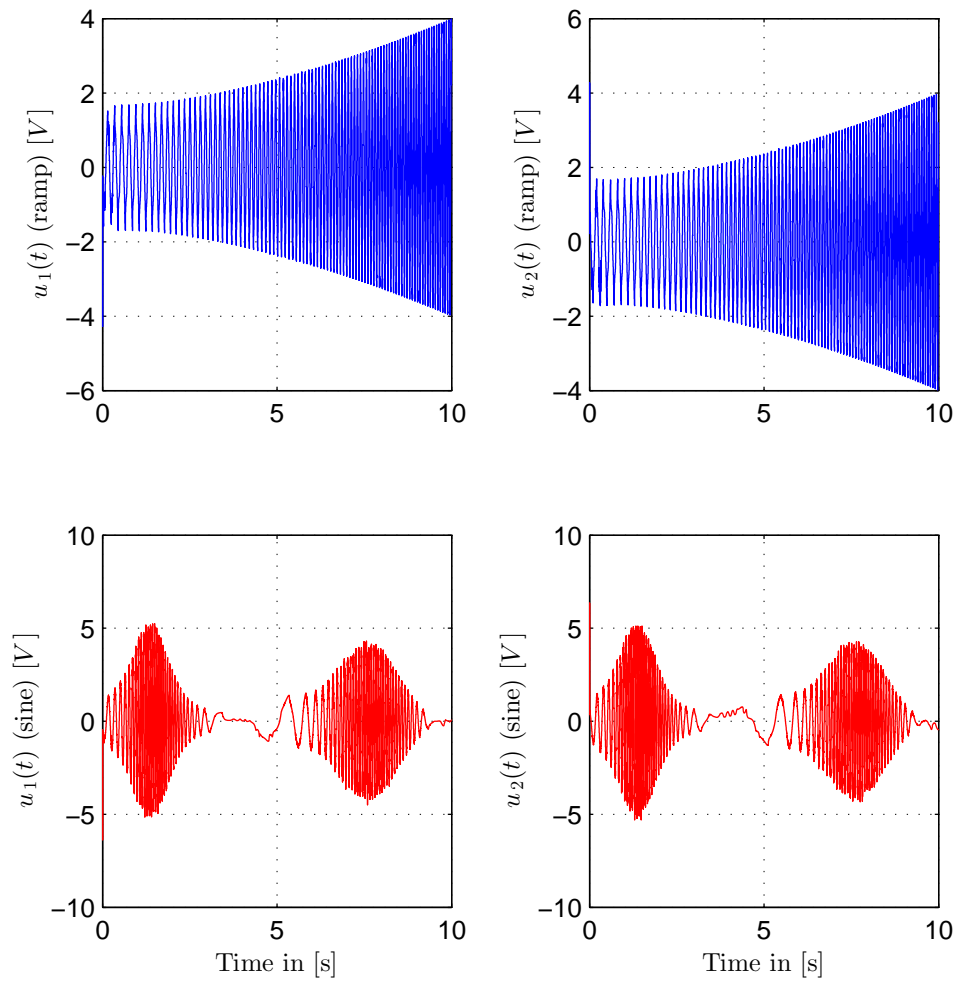


Figure 7.12: Applied control input voltages of IM (with $T_L = 1$ [Nm]) against ramp and sinusoid references respectively (backlash case).

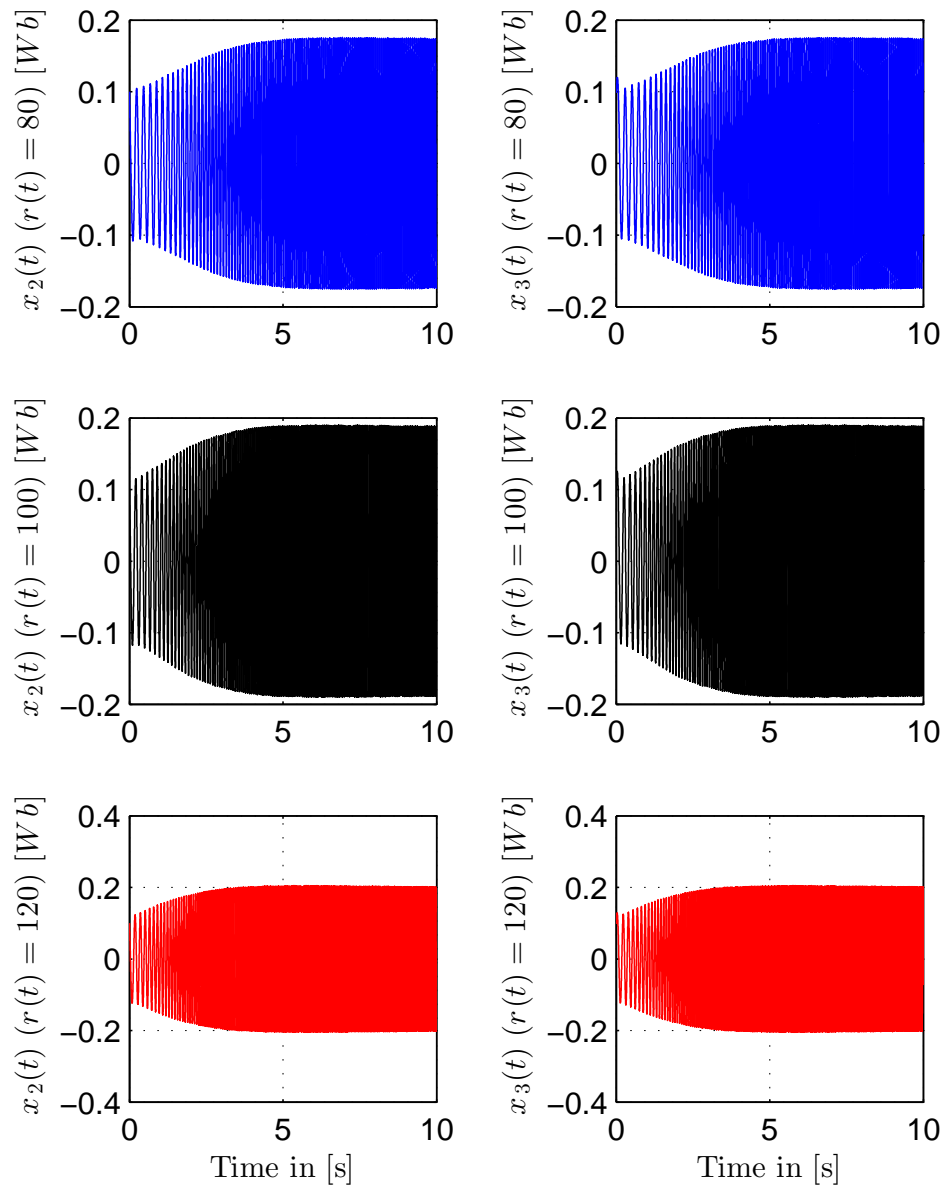


Figure 7.13: Magnetic flux components of IM (with $T_L = 1$ [Nm]) for various constant references (backlash case).

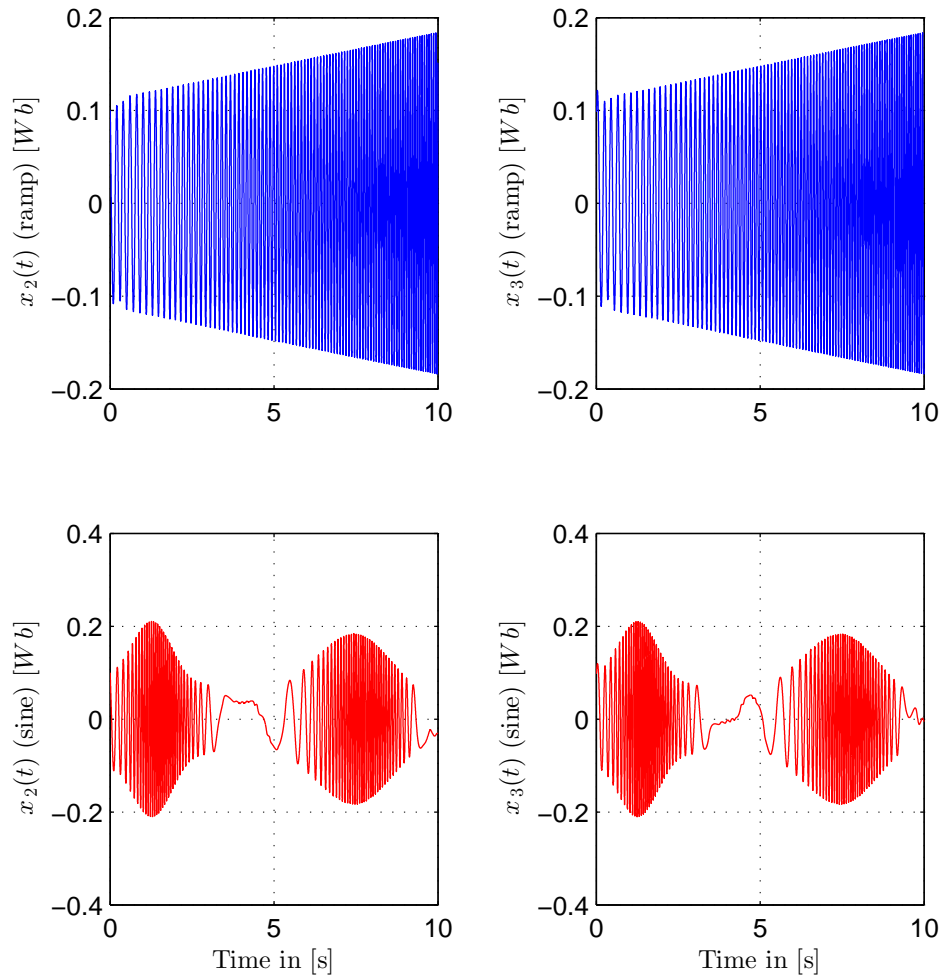


Figure 7.14: Magnetic flux components of IM (with $T_L = 1$ [Nm]) for ramp and sinusoid references respectively (backlash case).

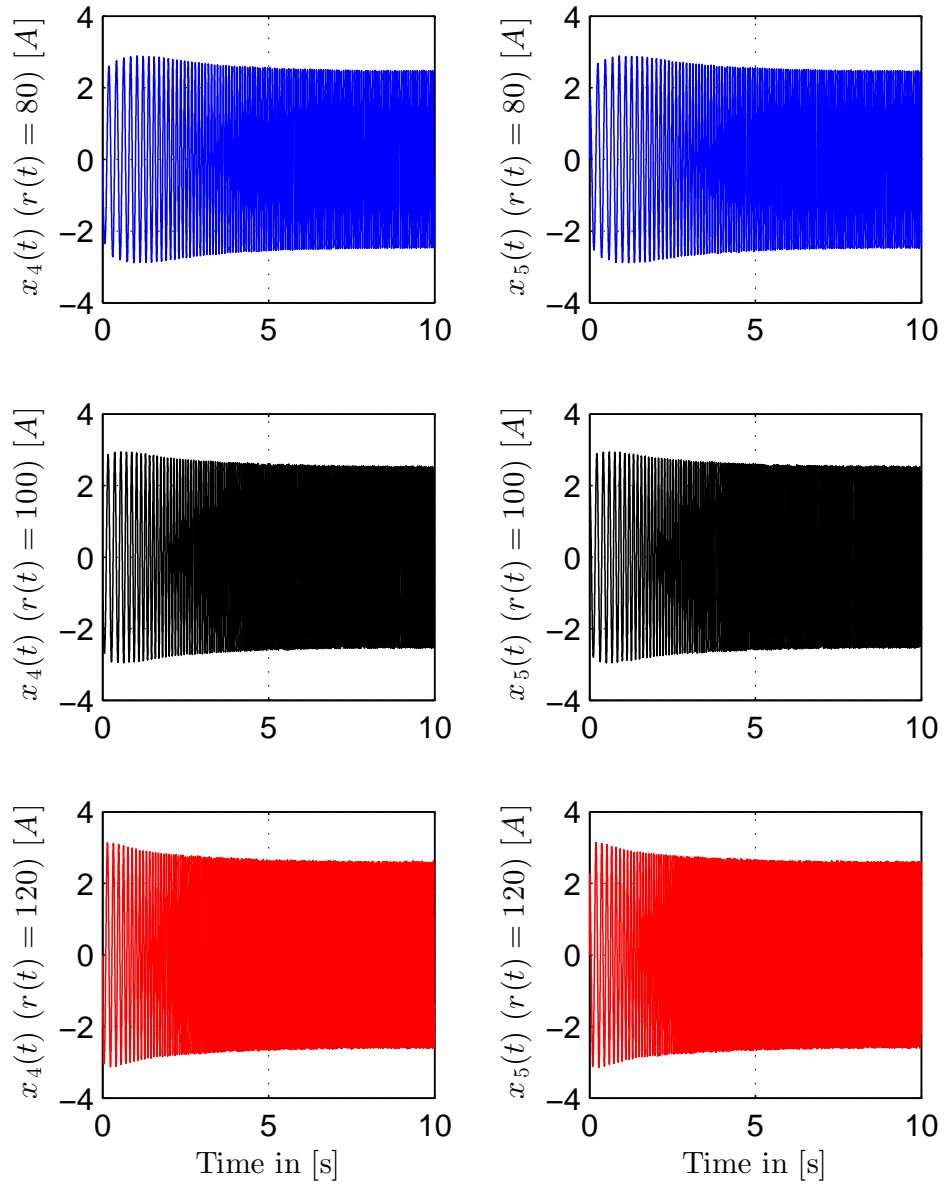


Figure 7.15: Current components of IM (with $T_L = 1$ [Nm]) for various constant references (backlash case).

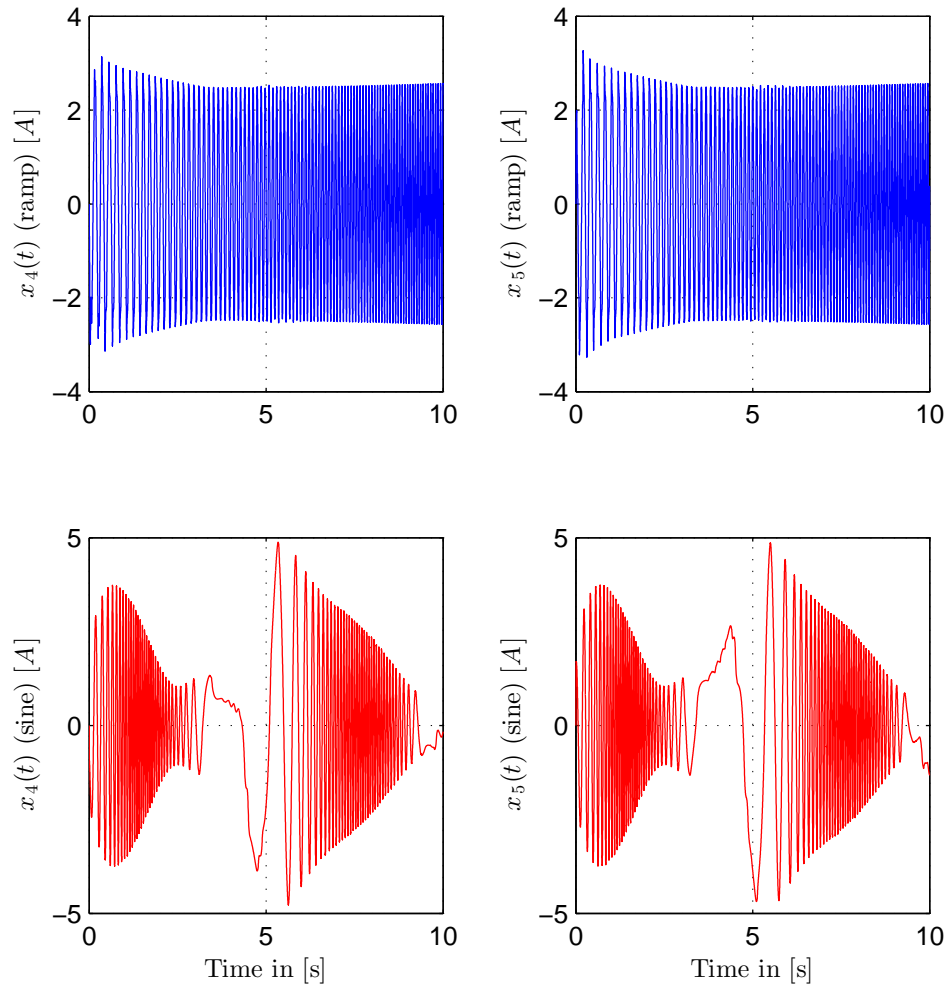


Figure 7.16: Current components of IM (with $T_L = 1$ [Nm]) for ramp and sinusoid references respectively (backlash case).

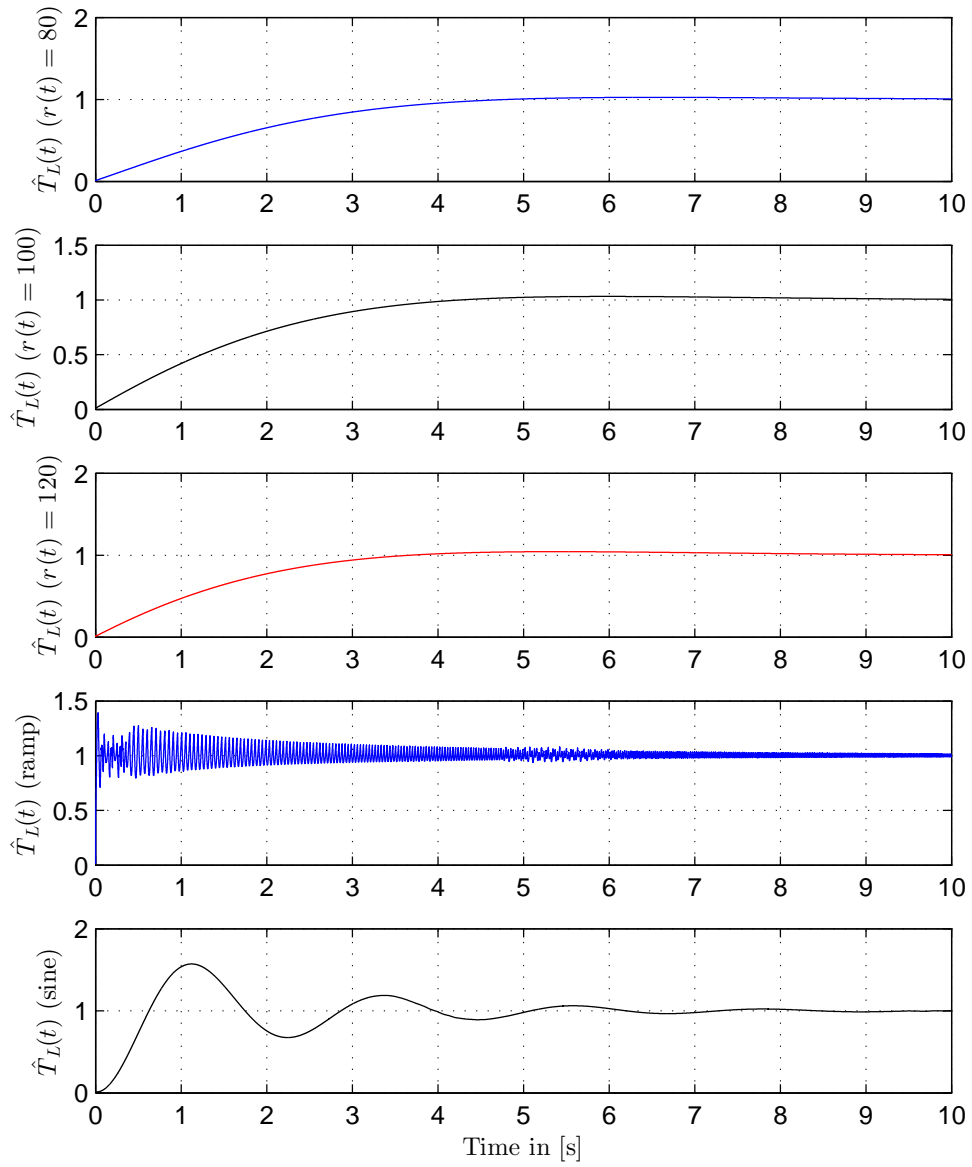


Figure 7.17: Load torque adaptive parameter \hat{T}_L performance for constant, ramp and sinusoid references respectively (backlash case).

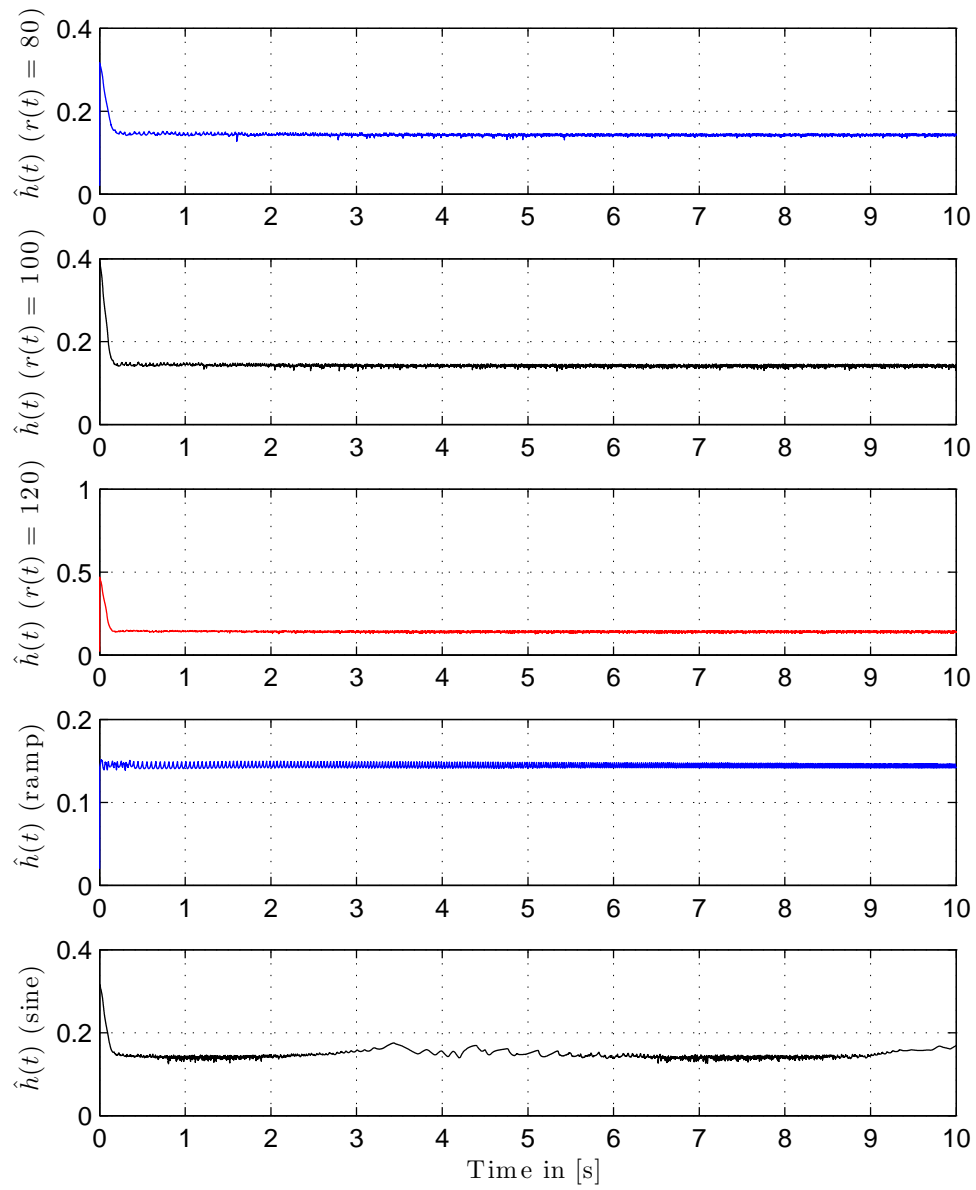


Figure 7.18: Adaptive parameter \hat{h} performance for constant, ramp and sinusoid references respectively (backlash case).

CHAPTER 8

IM WITH BOUC-WEN HYSTERESIS INPUT

8.1 Bouc-Wen Hysteresis Modeling and Controller Design

Bouc-Wen hysteresis for a scalar input u can be described by the following model:

$$H_{BW}(u(t)) = \nu K u(t) + (1 - \nu) G K z(t), \quad (8.1)$$

where, $n > 1$, $G > 0$, $0 < \nu < 1$, $u(t)$ is the input to the Bouc-Wen hysteresis and z is solution to the following nonlinear equation:

$$\dot{z} = \frac{1}{G} (A\dot{u} - \beta|\dot{u}||z|^{n-1}z - \lambda\dot{u}|z|^n), \quad (8.2)$$

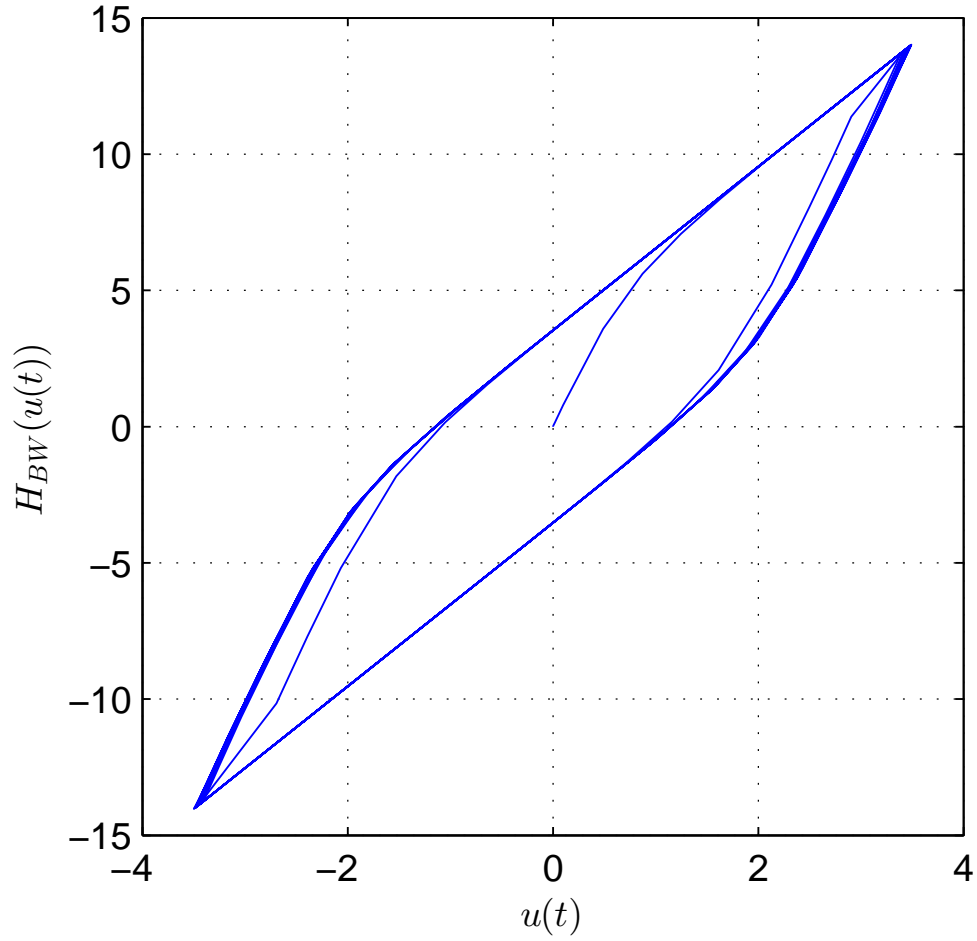


Figure 8.1: An example of Bouc-Wen hysteresis

where A, β and λ are some constants. Now, define the following constants:

$$z_0 = \sqrt[n]{\frac{A}{\beta + \lambda}}, \quad z_1 = \sqrt[n]{\frac{A}{\lambda - \beta}}. \quad (8.3)$$

Also, let Θ be the set of $z(t)$ initial conditions for which $z(t)$ is bounded for every applied piecewise continuous signals $u(t)$ and $\dot{u}(t)$.

Theorem 1. Consider the Bouc-Wen hysteresis described by (8.1) and (8.2). The hysteresis parameters (A, β and λ) can be chosen such that Θ is a nonempty set

and $z(t)$ is bounded for every applied piecewise continuous signals $u(t)$ and $\dot{u}(t)$.

Proof [57]: In order to prove the theorem, all different scenarios have to be examined. Consider the cases, starting with $A > 0$. Within this case, a total of three possibilities can be identified:

$$P_1: \beta + \lambda > 0 \text{ and } \beta - \lambda \geq 0,$$

$$P_2: \beta + \lambda > 0 \text{ and } \beta - \lambda \leq 0,$$

$$P_3: \beta + \lambda \leq 0.$$

Consider the first possibility P_1 . Use the Lyapunov function $V = \frac{1}{2}z^2$ and take the time derivative to obtain:

$$\dot{V} = \frac{z}{G}(Au - \beta|\dot{u}||z|^{n-1}z - \lambda\dot{u}|z|^n), \quad (8.4)$$

Within the first possibility P_1 , four cases arise depending on the sign of z and \dot{u} .

$$\text{Case 1: } \{z \geq 0 \text{ and } \dot{u} \geq 0\}$$

By (8.4), the below is obtained:

$$\dot{V} = \frac{z\dot{u}}{G}(A - \beta z^n - \lambda z^n). \quad (8.5)$$

Now, $\dot{V} \leq 0 \Rightarrow A - \beta z^n - \lambda z^n \leq 0$, thus:

$$z \geq \sqrt[n]{\frac{A}{\beta + \lambda}} = z_0. \quad (8.6)$$

Case 2: $\{z \leq 0 \text{ and } \dot{u} \geq 0\}$

Starting from (8.4):

$$\begin{aligned}\dot{V} &= \frac{z\dot{u}}{G}(A - \beta|z|^{n-1}z - \lambda|z|^n) \\ &= \frac{z\dot{u}}{G}(A + \beta|z|^n - \lambda|z|^n) \\ &= \frac{z\dot{u}}{G}(A + (\beta - \lambda)|z|^n) \leq 0 \quad \forall z \leq 0.\end{aligned}\tag{8.7}$$

Case 3: $\{z \geq 0 \text{ and } \dot{u} \leq 0\}$

From (8.4):

$$\dot{V} = \frac{z\dot{u}}{G}(A + (\beta - \lambda)z^n) \leq 0 \quad \forall z \geq 0.\tag{8.8}$$

Case 4: $\{z \leq 0 \text{ and } \dot{u} \leq 0\}$

Again using (8.4):

$$\begin{aligned}\dot{V} &= \frac{z\dot{u}}{G}(A + \beta|z|^{n-1}z - \lambda|z|^n) \\ &= \frac{z\dot{u}}{G}(A - \beta|z|^n - \lambda|z|^n) \\ &= \frac{z\dot{u}}{G}(A - (\beta + \lambda)|z|^n).\end{aligned}\tag{8.9}$$

Now, $\dot{V} \leq 0 \Rightarrow A - (\beta + \lambda)|z|^n \leq 0$, thus:

$$|z| \geq \sqrt[n]{\frac{A}{\beta + \lambda}} = z_0.\tag{8.10}$$

It can be concluded from all four cases that $\dot{V} \leq 0$ for all $|z(t)| \geq z_0$. Using theorem (4.18) in [58], it can be shown that $z(t)$ is bounded for every piecewise continuous function \dot{u} and every initial condition $z(0)$. The bounds can also be computed based on the same theory and it has two cases:

- 1) If $|z(0)| \leq z_0$, then the bound is set to z_0 for all $t \geq 0$.
- 2) If $|z(0)| > z_0$, then the bound is set to $|z(0)|$ for all $t \geq 0$.

Now, consider the second possibility P_2 . This can also have four cases for all z, \dot{u} signs combinations.

Case 1: $\{z \geq 0 \text{ and } \dot{u} \geq 0\}$

Similar to case 1 in P_1 . It results in $z \geq z_0$.

Case 2: $\{z \leq 0 \text{ and } \dot{u} \geq 0\}$

$$\begin{aligned}
 \dot{V} &= \frac{z\dot{u}}{G}(A - \beta|z|^{n-1}z - \lambda|z|^n) \\
 &= \frac{z\dot{u}}{G}(A + \beta|z|^n - \lambda|z|^n) \\
 &= \frac{z\dot{u}}{G}(A + (\beta - \lambda)|z|^n).
 \end{aligned} \tag{8.11}$$

For $\dot{V} \leq 0 \Rightarrow A + (\beta - \lambda)|z|^n \geq 0$, so:

$$|z| \leq \sqrt[n]{\frac{A}{\lambda - \beta}} = z_1. \tag{8.12}$$

Case 3: $\{z \geq 0 \text{ and } \dot{u} \leq 0\}$

$$\dot{V} = \frac{z\dot{u}}{G}(A + (\beta - \lambda)z^n). \tag{8.13}$$

For $\dot{V} \leq 0 \Rightarrow A + (\beta - \lambda)z^n \geq 0$, thus:

$$z \leq \sqrt[n]{\frac{A}{\lambda - \beta}} = z_1. \quad (8.14)$$

Case 4: $\{z \leq 0 \text{ and } \dot{u} \leq 0\}$

Similar to case 4 in P_1 . It results in $|z| \geq z_0$.

Assume that $z_1 \geq z_0$ (which is the case of $\beta \geq 0$). This implies that $\dot{V} \leq 0 \forall z(t)$ such that $z_0 \leq |z(t)| \leq z_1$ regardless of the sign of \dot{u} . Again, the boundedness of $z(t)$ can be deduced (using the same theory mentioned earlier) for any piecewise continuous \dot{u} such that $|z(0)| \leq z_1$. Also, the upper bound is found to be similar to P_1 , i.e., $|z(t)| \leq \max(|z(0)|, z_0)$. Note that conditions for P_2 in this case $\{\beta + \lambda > 0, \beta - \lambda \leq 0 \text{ and } \beta \geq 0\}$ can also be re-written as $\{\beta \geq 0 \text{ and } \beta - \lambda < 0\}$.

In addition, explore the third possibility P_3 . Assume that $\dot{u} \geq 0$ and $z(t) \geq 0$ (for $z(t) < 0$, a similar analysis can be done). By (8.2):

$$\begin{aligned} \dot{z} &= \frac{\dot{u}}{G}(A - \beta|z|^{n-1}z - \lambda|z|^n) \\ &= \frac{\dot{u}}{G}(A - (\beta + \lambda)z^n) \\ &= Q_1\dot{u}(Q_2 + z^n), \end{aligned} \quad (8.15)$$

where $Q_1 = -\frac{\beta + \lambda}{G}$, $Q_2 = -\frac{A}{\beta + \lambda}$. Since $n > 1$, the below quantity is finite:

$$S = \int_{z(0)}^{\infty} \frac{dy}{Q_2 + y^n} \geq 0. \quad (8.16)$$

Now, select an increasing function $u(t)$, such that $u(0) = 0$ and as $t \rightarrow \infty$, $u(t) = \frac{S}{Q_1}$. By integrating (8.15), the below is obtained:

$$\begin{aligned} \lim_{t \rightarrow \infty} \int_{z(0)}^{z(t)} \frac{dy}{Q_2 + y^n} &= \lim_{t \rightarrow \infty} \int_{u(0)}^{u(t)} Q_1 dr \\ \Rightarrow \lim_{t \rightarrow \infty} \int_{z(0)}^{z(t)} \frac{dy}{Q_2 + y^n} &= S. \end{aligned} \tag{8.17}$$

Comparing (8.16), (8.17) shows that there exists some bounded $u(t)$ for which the corresponding output $z(t)$ is unbounded for every initial condition $z(0)$. This proves that in case of P_3 , the set of initial conditions such that $z(t)$ is bounded is the empty set ($\Theta = \emptyset$).

A similar approach can be used for the cases $A < 0$ and $A = 0$ to extract the set of initial conditions Θ as well as the upper bound on $z(t)$ in each case.

This analysis shows that $z(t)$ (verifying the parameters' inequalities with the corresponding Θ specified in table 8.1) is bounded for every piecewise continuous \dot{u} .

This result shall conclude the proof of theorem 1. \square

Now, using the result of the previous theorem, the Bouc-Wen hysteresis (verifying conditions in table 8.1) can be represented in the following form:

$$H_{BW}(u(t)) = gu(t) + \zeta(t), \tag{8.18}$$

Table 8.1: Bouc-Wen hysteresis boundedness conditions

Case	Θ	Upper bound of $\mathbf{z}(t)$
$A > 0, \beta + \lambda > 0$ and $\beta - \lambda \geq 0$	\mathbb{R}	$\max(z(0) , z_0)$
$A > 0, \beta - \lambda < 0$ and $\beta \geq 0$	$[-z_1, z_1]$	$\max(z(0) , z_0)$
$A < 0, \beta - \lambda > 0$ and $\beta + \lambda \geq 0$	\mathbb{R}	$\max(z(0) , z_1)$
$A < 0, \beta + \lambda < 0$ and $\beta \geq 0$	$[-z_0, z_0]$	$\max(z(0) , z_1)$
$A = 0, \beta + \lambda > 0$ and $\beta - \lambda \geq 0$	\mathbb{R}	$ z(0) $
Other cases	\emptyset	none

where g and ζ are chosen as:

$$g = \nu K \tag{8.19}$$

$$\zeta(t) = (1 - \nu)GKz(t) \tag{8.20}$$

Note that g is a constant and $\zeta(t)$ is a bounded perturbation function.

Assumption 7. Consider the Bouc-Wen model in (8.18). Parameter g is assumed to be an uncertain positive constant with known boundaries, g_{max} and g_{min} . Also, the magnitude of the perturbation function ζ is assumed to be unknown but has a known maximum bound of ζ_{max} .

Now, consider the scenario of IM with Bouc-Wen hysteresis input. Recall equations (5.3) and (8.18). Note that both dead-zone and Bouc-Wen hysteresis (as a result of theorem 1) can be represented by a sum of a linear function of the input and a bounded perturbation function. Using the same rationale as in section (7.1), it can be shown that the compensating feedback required for the Bouc-Wen hysteresis input case is exactly the same as in dead-zone case. That is, the control feedback described by (5.7, 5.17) with the adaptive update law (5.13, 5.14).

8.2 Simulations and Results

As done in previous chapters, the IM system is now simulated with Bouc-Wen hysteresis inputs instead. The control feedback employed in this section is the same feedback for both symmetric dead-zone and backlash cases. The Bouc-Wen model used in this simulation has the following parameters $\{\nu = \frac{3}{8}, K = 8, G = 1, A = 1, \beta = \frac{3}{2}, \lambda = \frac{1}{2}, g = 3, \zeta_{max} = 25\}$. The simulations two scenarios and as well as initial conditions, reference functions and IM model parameters are kept similar to previous chapters. The resulting tracking can be seen in figures 8.2 and 8.10. The performance is very close to both dead-zone and backlash cases. Furthermore, the applied feedback as well as the rest of the state variables and the adaptive parameters for all references and both scenarios are plotted in figures 8.3-8.9 and 8.11-8.18. All are upper-bounded and never exceed or even come close to the rating values. Overall, the performance of the controller looks very good. Again, as in backlash case, the dead-zone controller has successfully proven to be capable of compensating for the Bouc-Wen hysteresis effect and archiving the desired trajectory tracking.

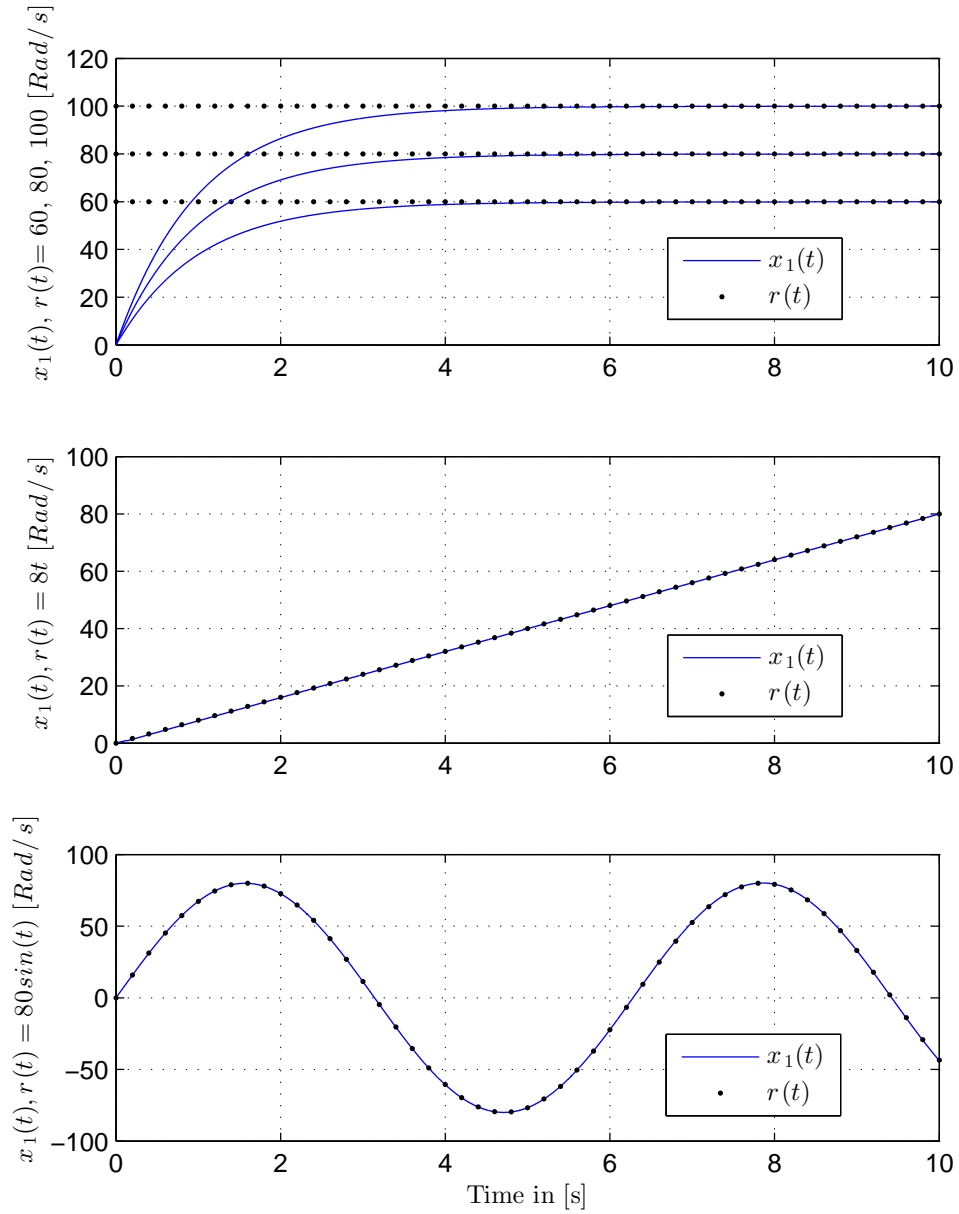


Figure 8.2: Speed tracking performance of IM (with $T_L = 0$) against constant, ramp and sinusoidal reference trajectory respectively (Bouc-Wen hysteresis case).

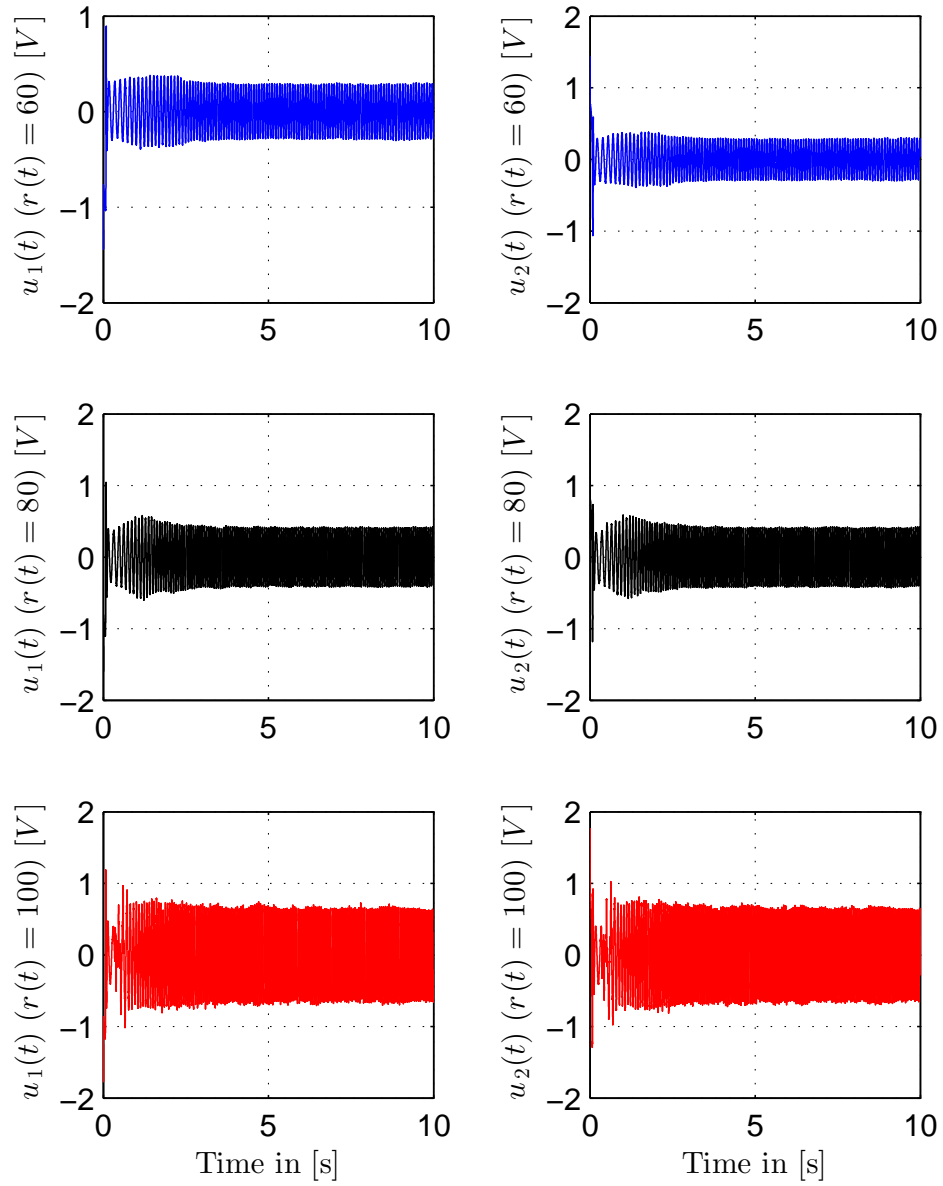


Figure 8.3: Applied control input voltages of IM (with $T_L = 0$) against various constant references (Bouc-Wen hysteresis case).

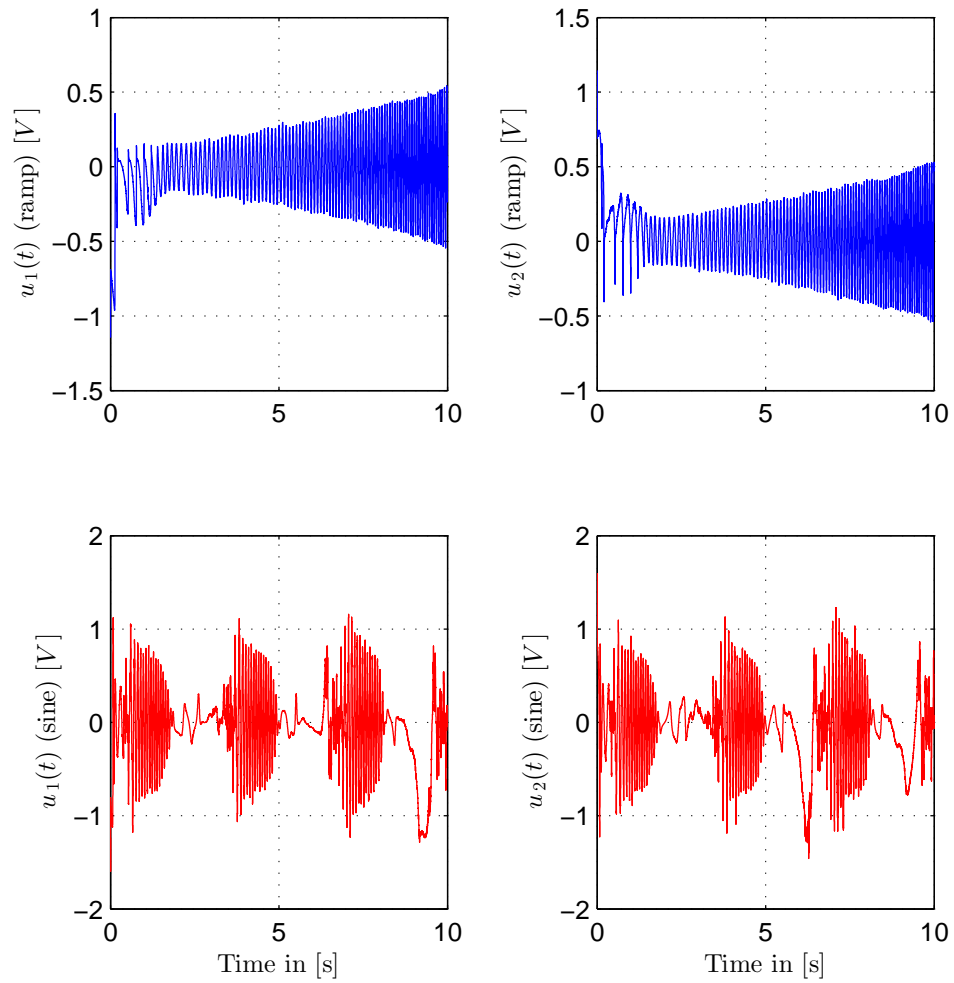


Figure 8.4: Applied control input voltages of IM (with $T_L = 0$) against ramp and sinusoid references respectively (Bouc-Wen hysteresis case).

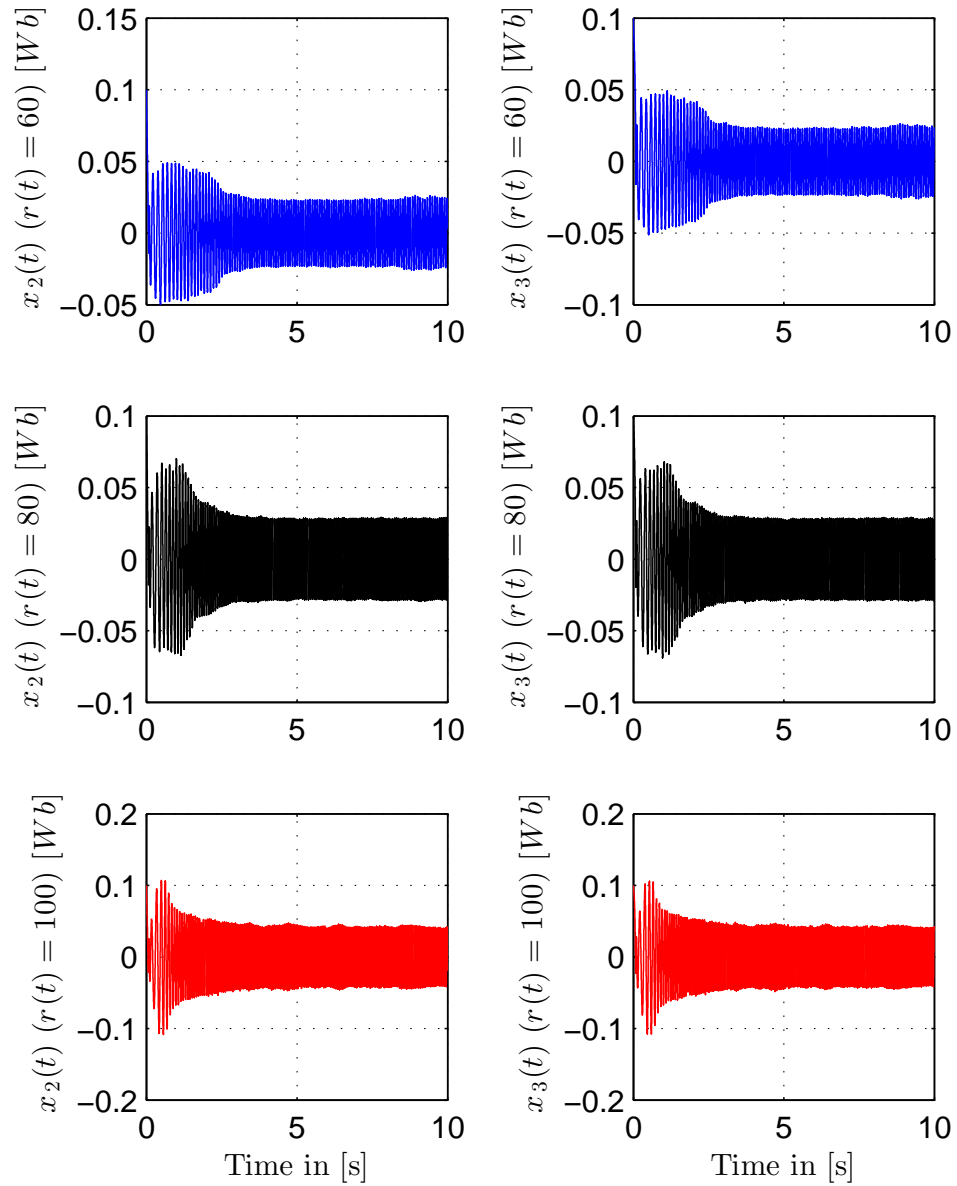


Figure 8.5: Magnetic flux components of IM (with $T_L = 0$) for various constant references (Bouc-Wen hysteresis case).

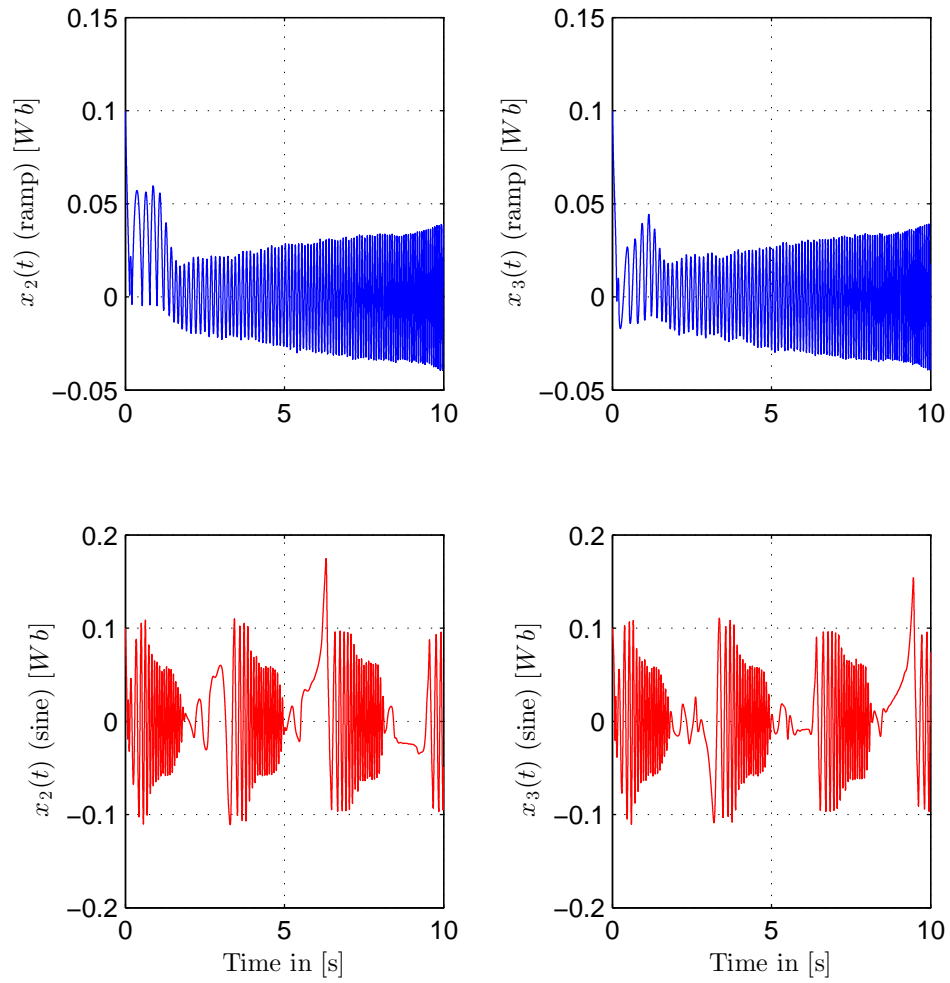


Figure 8.6: Magnetic flux components of IM (with $T_L = 0$) for ramp and sinusoid references respectively (Bouc-Wen hysteresis case).

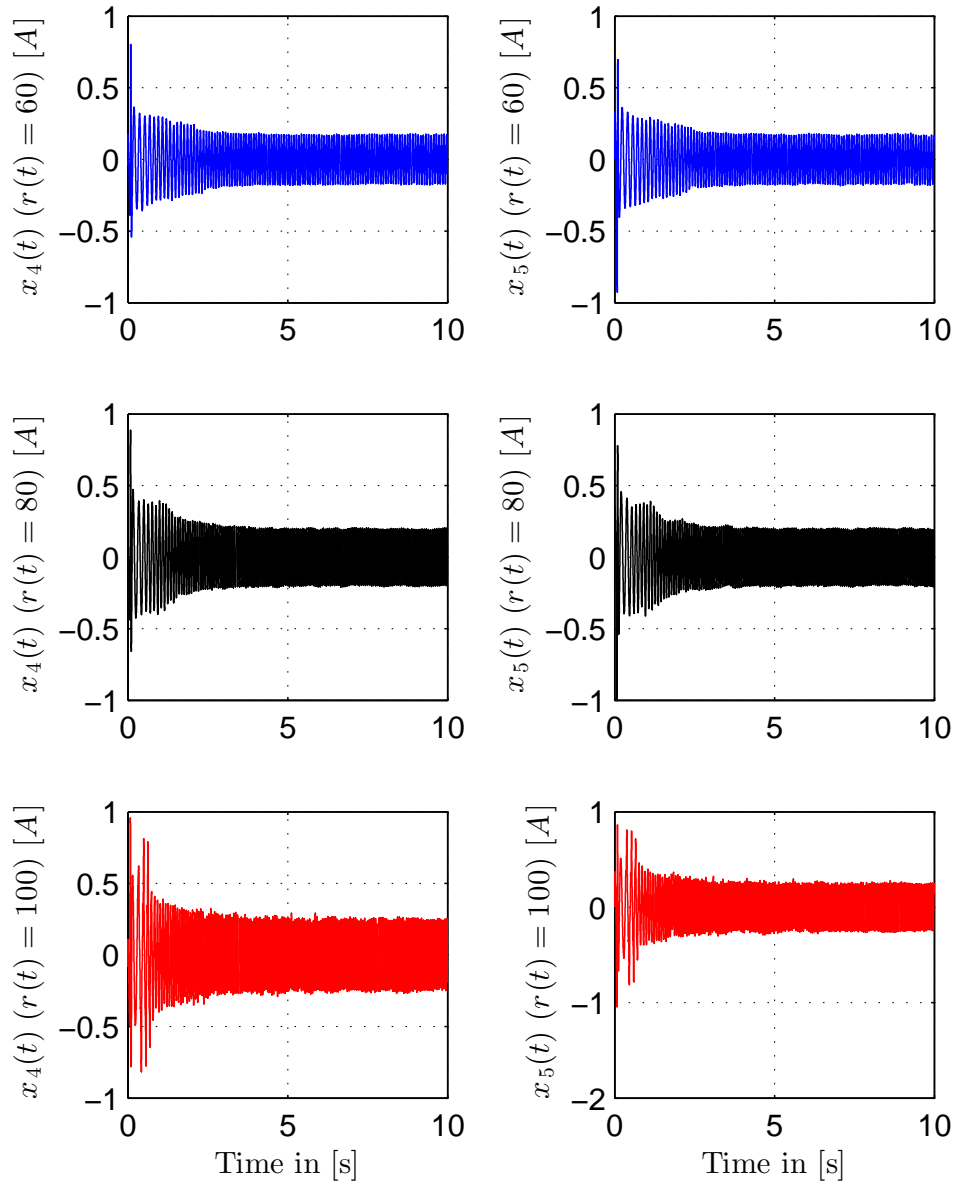


Figure 8.7: Current components of IM (with $T_L = 0$) for various constant references (Bouc-Wen hysteresis case).

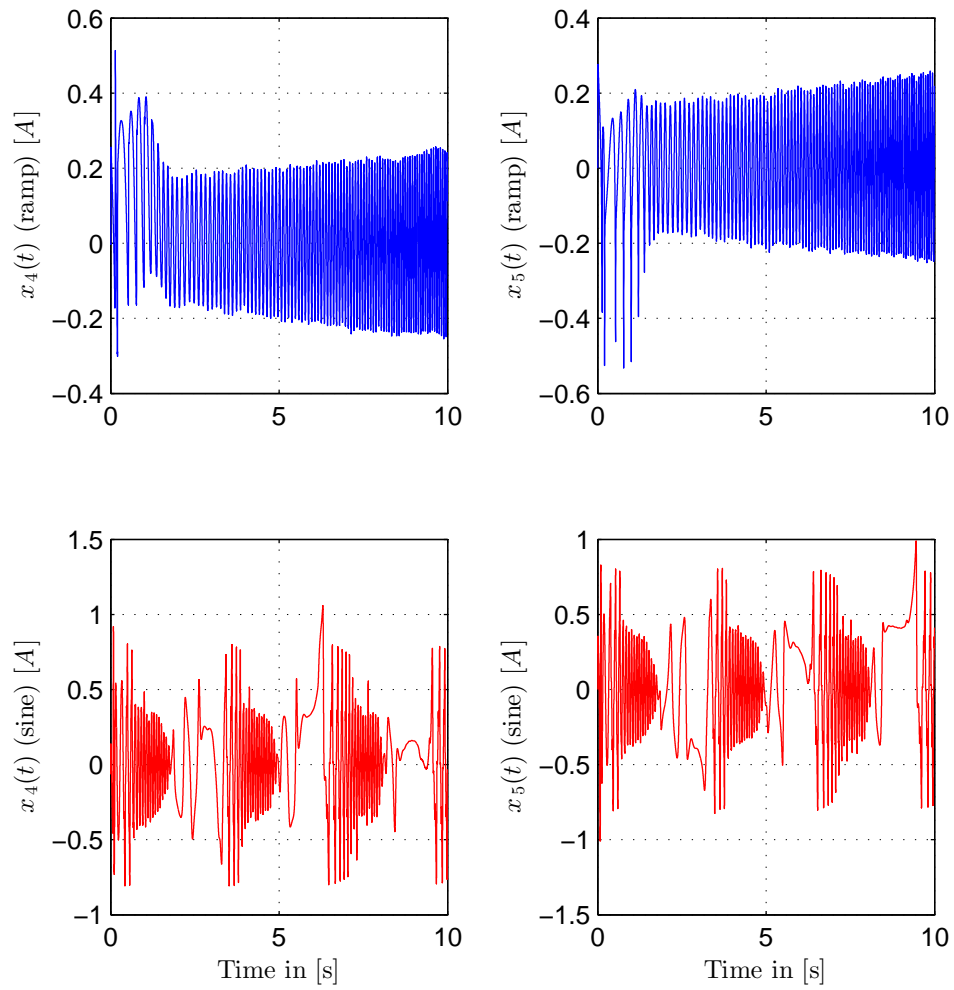


Figure 8.8: Current components of IM (with $T_L = 0$) for ramp and sinusoid references respectively (Bouc-Wen hysteresis case).

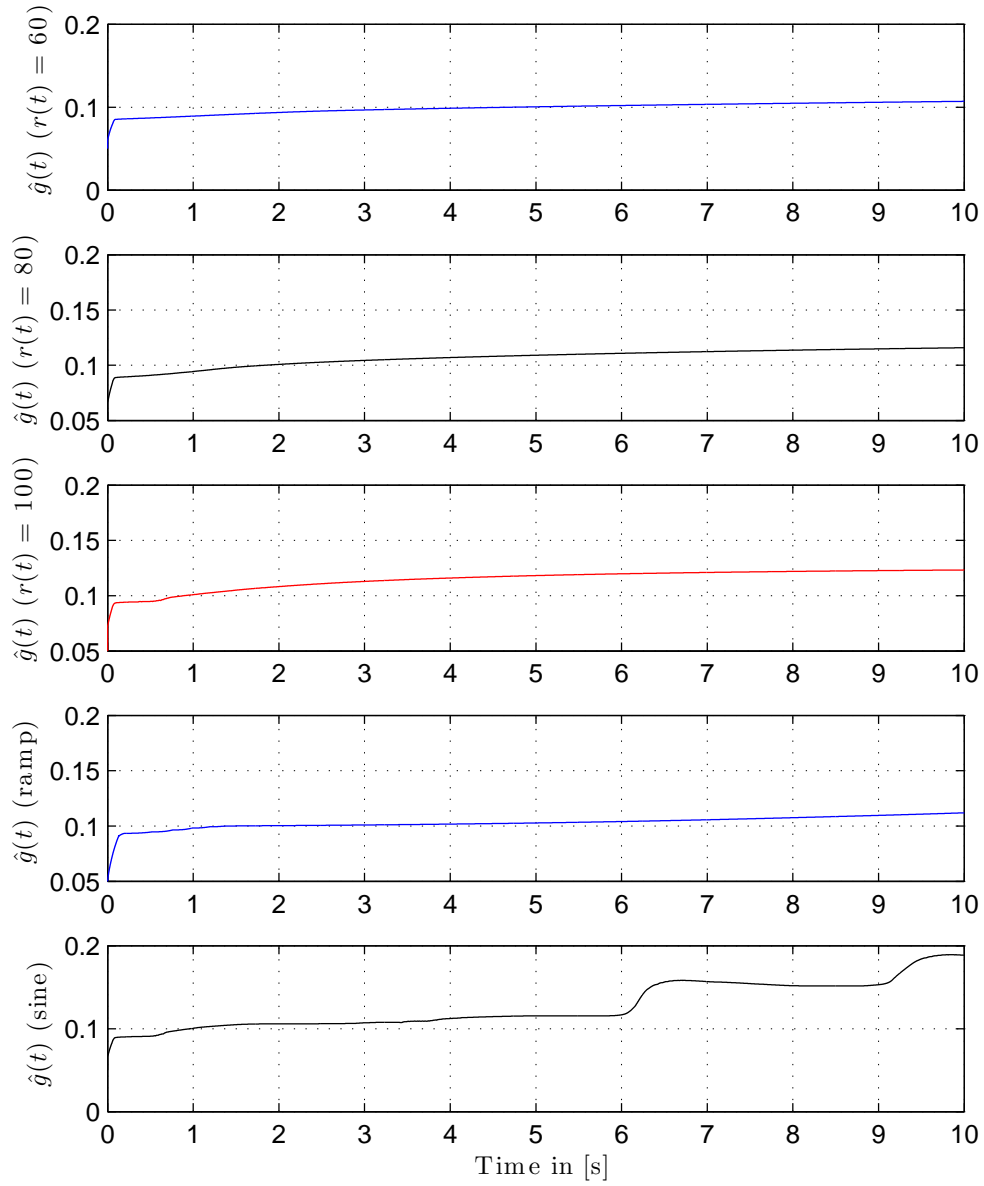


Figure 8.9: Adaptive parameter \hat{g} performance for constant, ramp and sinusoid references respectively (Bouc-Wen hysteresis case).

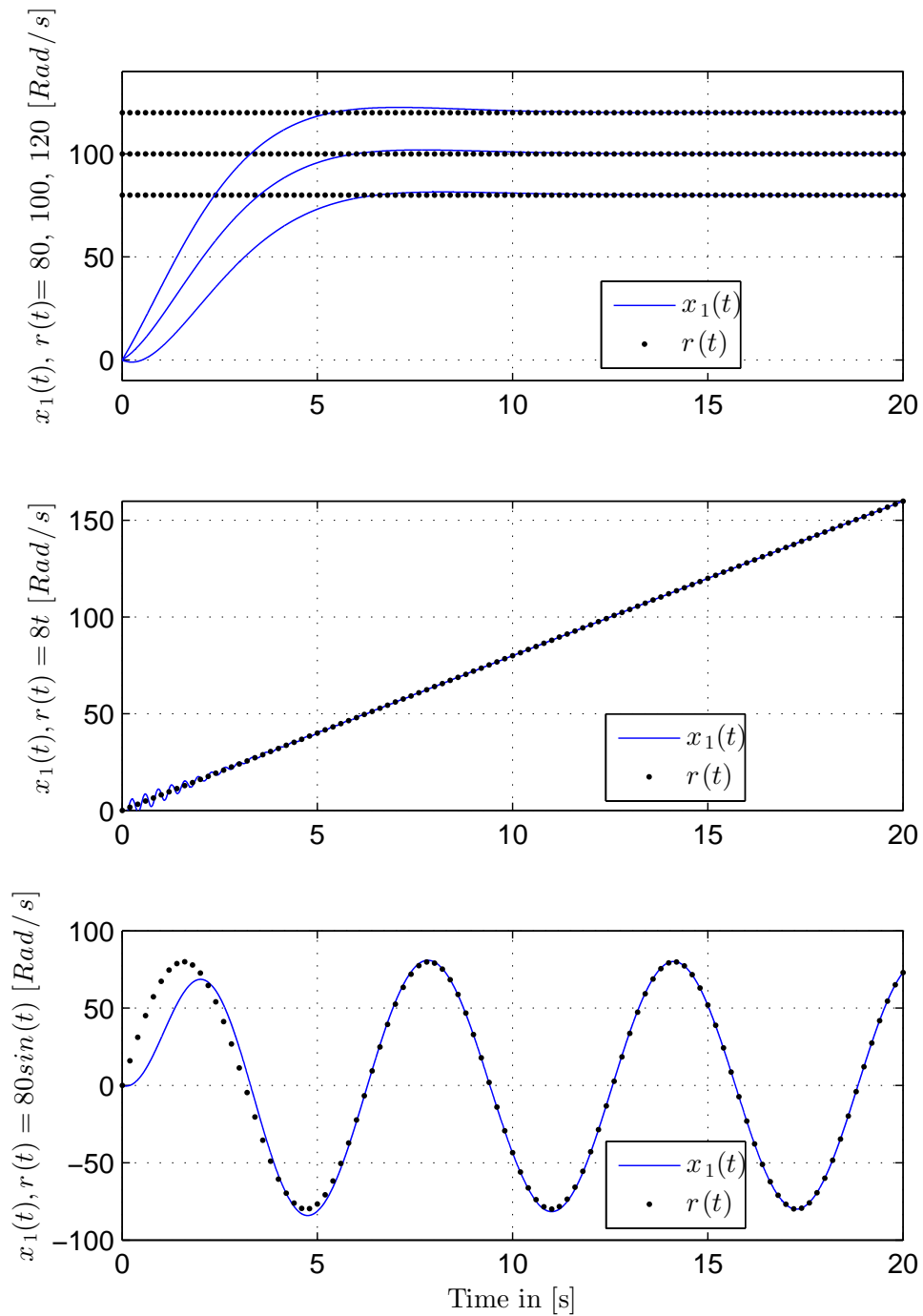


Figure 8.10: Speed tracking performance of IM (with $T_L = 1 \text{ [Nm]}$) against constant, ramp and sinusoidal reference trajectory respectively (Bouc-Wen hysteresis case).

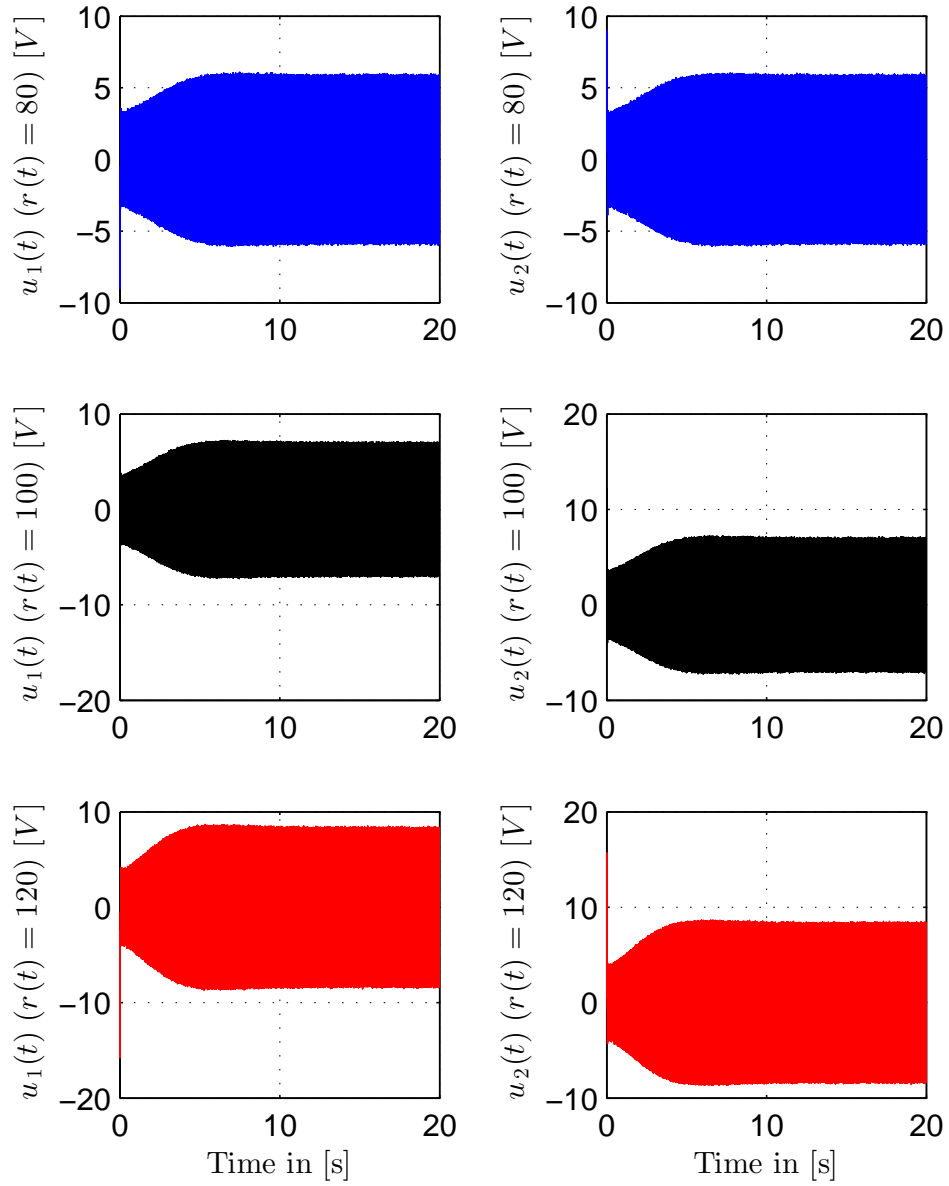


Figure 8.11: Applied control input voltages of IM (with $T_L = 1$ [Nm]) against various constant references (Bouc-Wen hysteresis case).

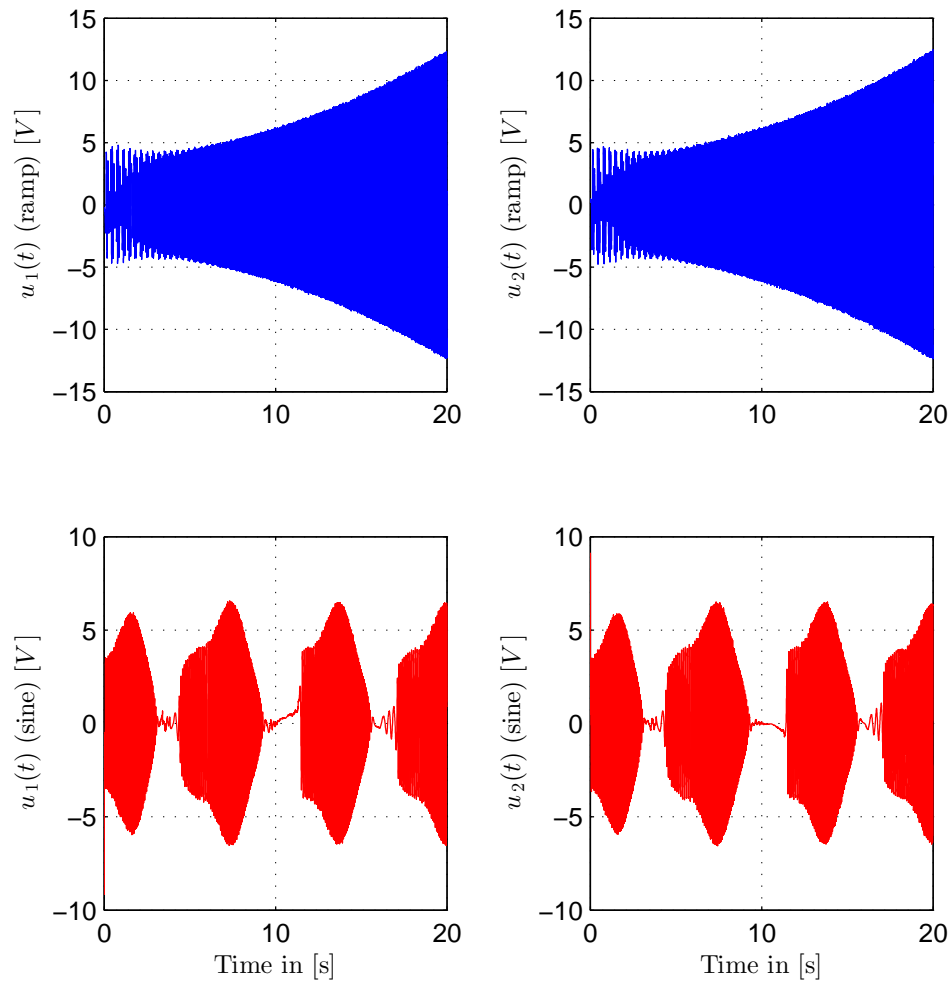


Figure 8.12: Applied control input voltages of IM (with $T_L = 1$ [Nm]) against ramp and sinusoid references respectively (Bouc-Wen hysteresis case).

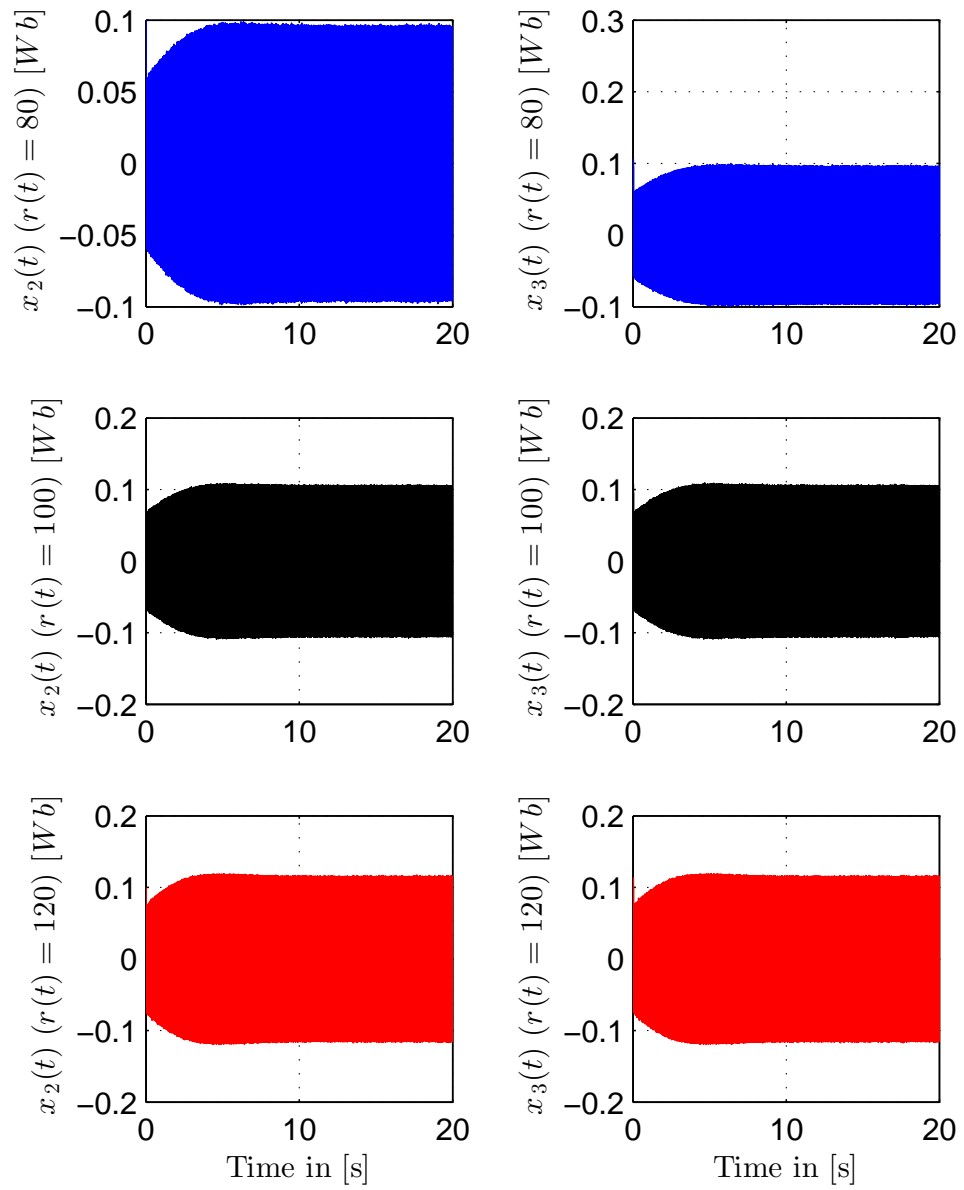


Figure 8.13: Magnetic flux components of IM (with $T_L = 1$ [Nm]) for various constant references (Bouc-Wen hysteresis case).

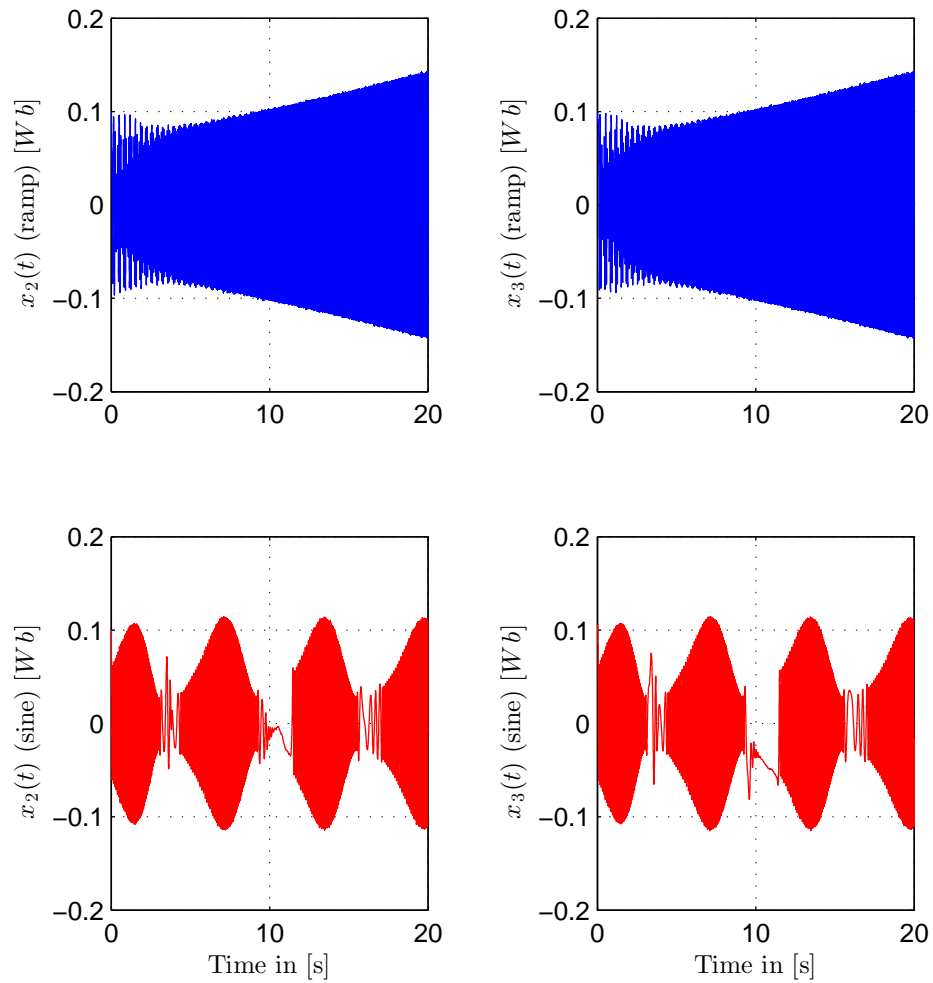


Figure 8.14: Magnetic flux components of IM (with $T_L = 1$ [Nm]) for ramp and sinusoid references respectively (Bouc-Wen hysteresis case).

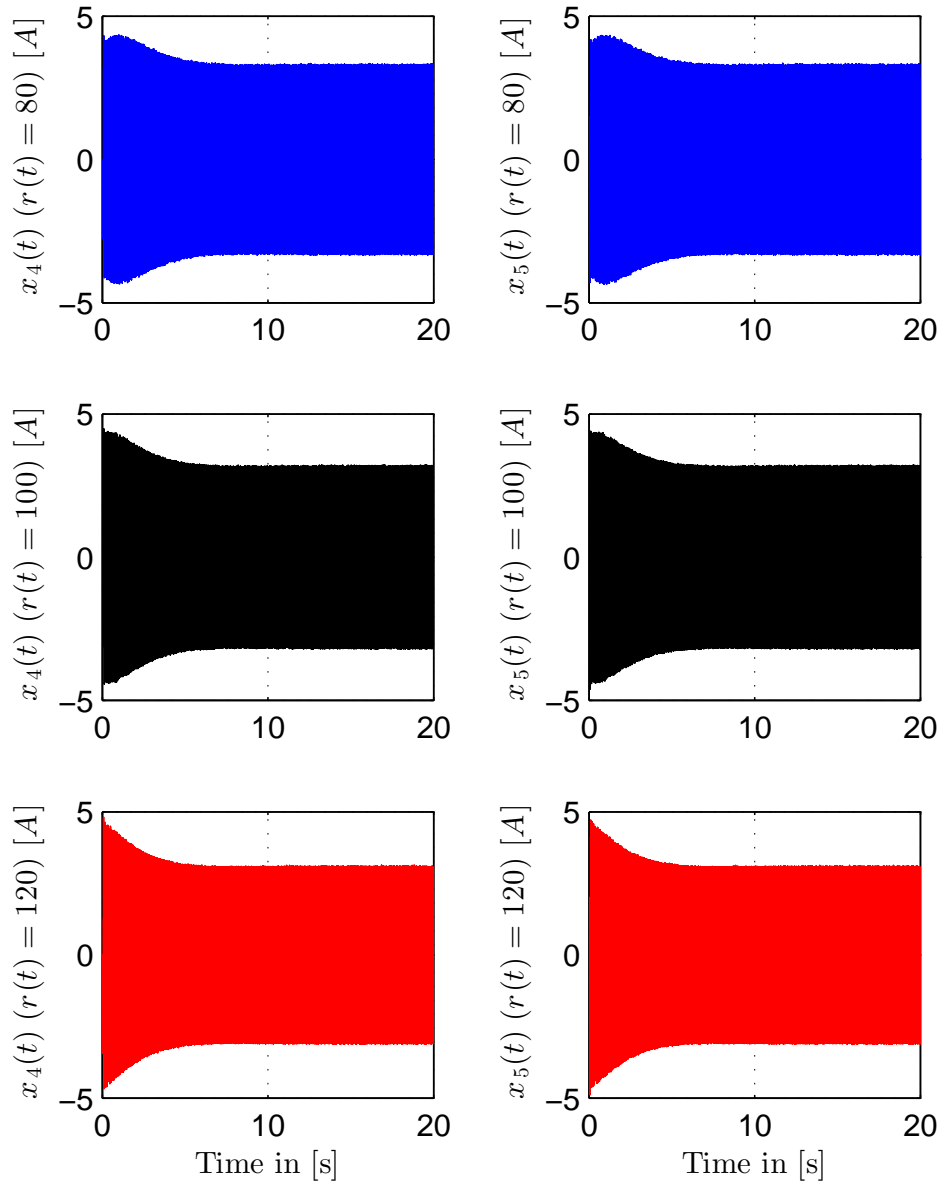


Figure 8.15: Current components of IM (with $T_L = 1$ [Nm]) for various constant references (Bouc-Wen hysteresis case).

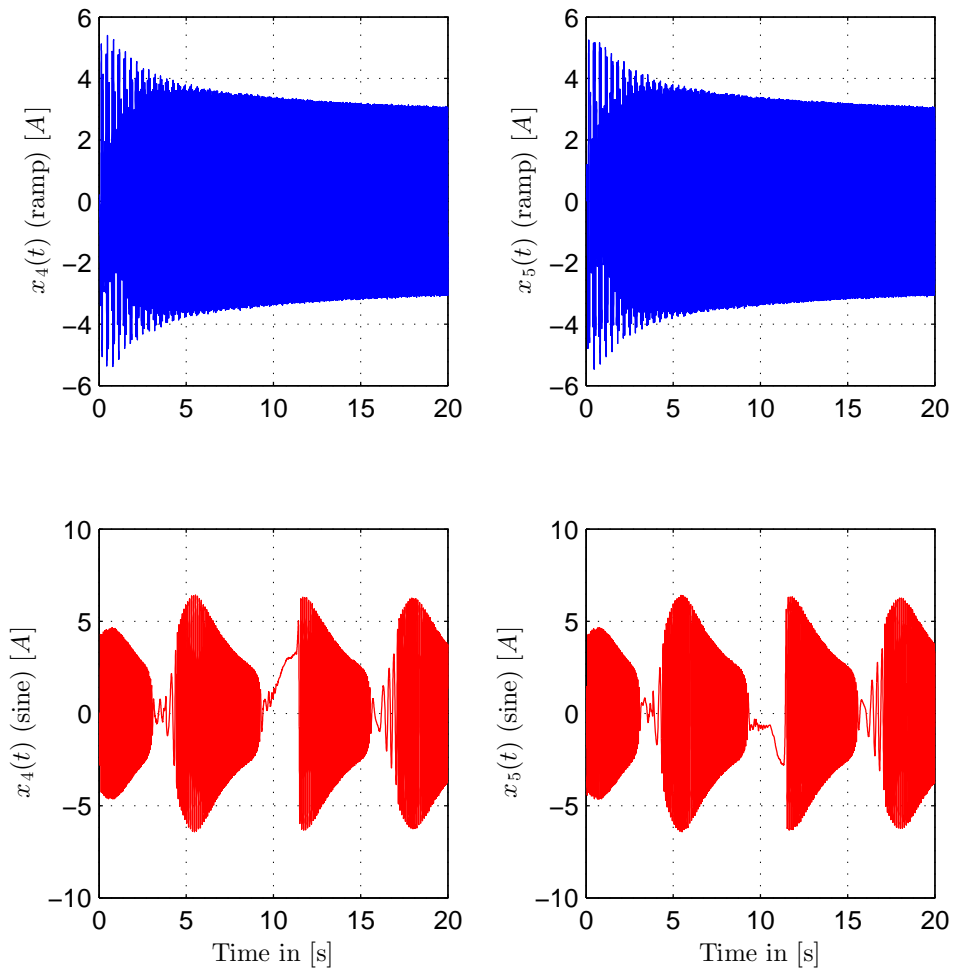


Figure 8.16: Current components of IM (with $T_L = 1$ [Nm]) for ramp and sinusoid references respectively (Bouc-Wen hysteresis case).

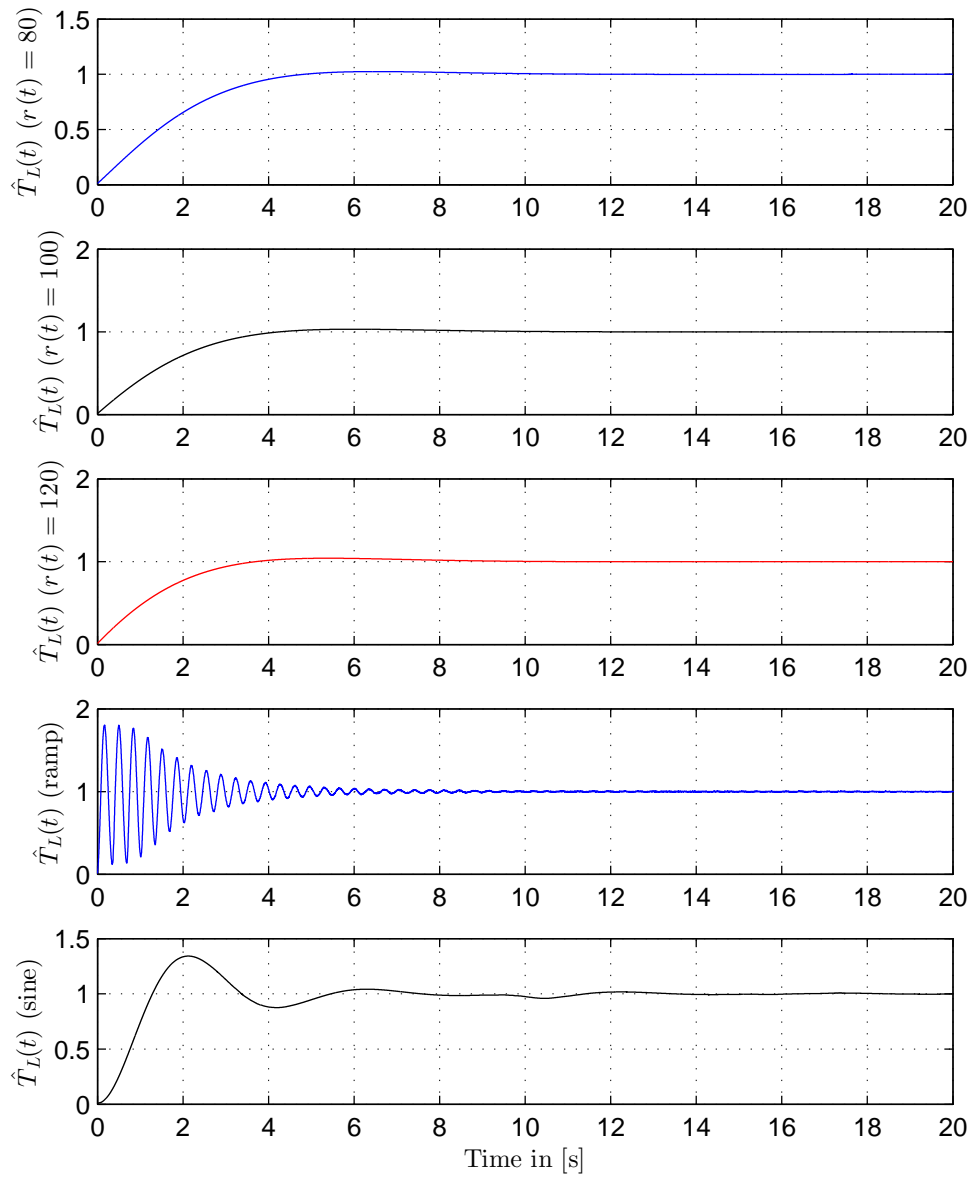


Figure 8.17: Load torque adaptive parameter \hat{T}_L performance for constant, ramp and sinusoid references respectively (Bouc-Wen hysteresis case).

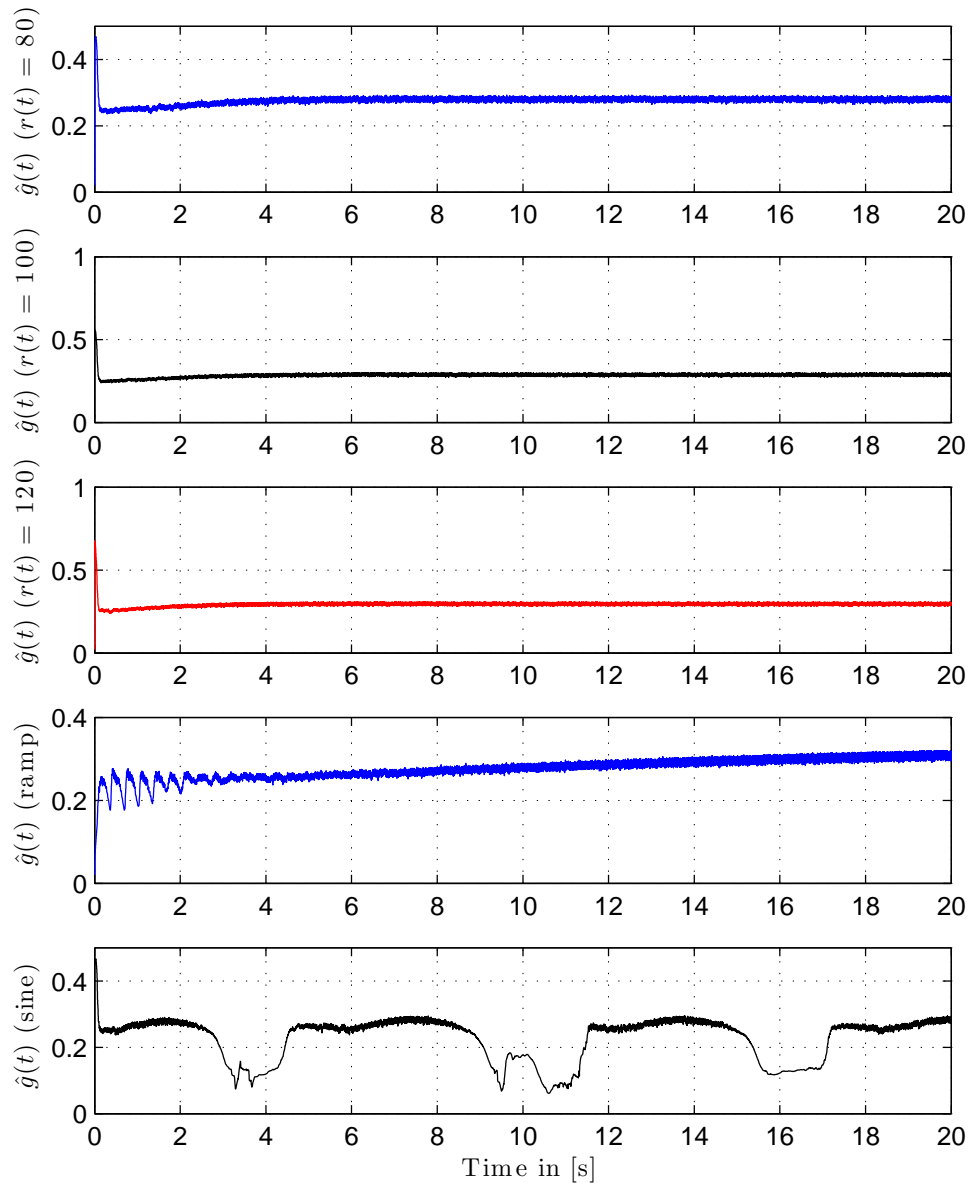


Figure 8.18: Adaptive parameter \hat{g} performance for constant, ramp and sinusoid references respectively (Bouc-Wen hysteresis case).

CHAPTER 9

CONCLUSION AND FUTURE WORK

Induction motor control problem is a very rich subject in the literature. Many IM control schemes are introduced for different objectives. On the other hand, input nonlinearity phenomena such as dead-zone and hysteresis are very common practical problems in various industrial disciplines. This thesis was developed to tackle the combined problem, i.e., IM control in presence of input nonlinearities. The work was arranged to cover the subject in a step-by-step organized manner. First, a brief background covering some aspects of the problem was introduced. Then, a survey about recently published relevant works was presented to provide an insight to the currently employed methods and to highlight many contributions made in various related applications. After that, IM models were explored and the appropriate model is selected and enhanced. Next step was introducing the proposed IM control methodology, that is, adaptive backstepping tracking control

scheme. The method began by defining a system of errors. The ultimate goal is to minimize this system in order to achieve tracking of some known reference functions. The desired feedback was designed first for IM system with regular inputs. Next step was to incorporate input nonlinearities starting by dead-zones, both symmetric and asymmetric. Introducing each of which required major modifications to the control feedback in order to provide the appropriate compensations. Then, another nonlinearity was introduced, namely the backlash and its mathematical models. IM subject to the backlash input phenomenon was considered and the corresponding compensation controller is deduced. Finally, Bouc-Wen hysteresis modeling was explored. In addition, a proof was provided to show that this nonlinearity is bounded given a specified set of initial values and parameters that satisfies some conditions. Then, the IM control feedback for IM with hysteresis input is discussed. It is worth mentioning that all the mathematical developments were supported by by extensive MATLAB SIMULINK simulations to verify the results obtained from the theory and to evaluate the performance of the controller in each case. Each simulation was done twice, without and with external load torque. Having both parts helped showing the effect of the feedback in various situations and highlighted the effect of torque estimation on the feedback overall performance. Throughout the system simulations, the control feedback has succeeded to achieve the desired target. Trajectory tracking with small rise time as well as nonlinearity compensation was observed easily from obtained results. In addition, boundedness of the rest of the states and parameters was validated

throughout the simulation time.

One of the most important contributions of this thesis is the development of a single control feedback that works for three different scenarios, IM subject to symmetric dead-zone input, backlash input and Bouc-Wen hysteresis input. Even though these nonlinearities do not exhibit the same behavior and are described by different models, the designed controller has proven to be capable of compensating for each of these phenomena and providing the desired tracking performance with minimum knowledge of each phenomenon parameters.

Now, this research can move forward by enhancing some design aspects and/or changing some of the stated assumptions. The next step might be to consider a more realistic IM model. For example, magnetic flux is typically not measurable quantity. Thus, a flux estimation can be incorporated in the IM model. In addition, iron losses can be added to the model, making it more real and useful. Other enhancement should include dealing with different references. As was the case in this work, the reference was assumed to be a differentiable function. The controller can be improved to deal with non-differentiable functions such as the step or the rectangular function. Finally, a major step can be achieved by implementing the controller in a real life scenario. That is, applying the feedback using real equipment in the lab and verifying theoretical and simulated results.

REFERENCES

- [1] Z. Shang, “Simulation and experiment for induction motor control strategies,” Master’s thesis, University of Windsor, 2011.
- [2] O. Barambones and P. Alkorta, “Vector control for induction motor drives based on adaptive variable structure control algorithm,” *Asian J. Control*, vol. 12, no. 5, pp. 640–649, 2010.
- [3] A. E. Fadili, F. Giri, A. E. Magri, R. Lajouad, and F. Chaoui, “Towards a global control strategy for induction motor: Speed regulation flux optimization and power factor correction,” *Electrical Power and Energy Systems*, vol. 43, pp. 230–244, 2012.
- [4] K. L. Shi, “Intelligent control for an induction motor,” Ph.D. dissertation, Hong Kong Polytechnic University, 2001.
- [5] A. E. Fadili, F. Giri, A. E. Magri, R. Lajouad, and F. Chaoui, “Adaptive control strategy with flux reference optimization for sensorless induction motors,” *Control Engineering Practice*, vol. 26, pp. 91–106, 2014.

- [6] S. Ibrir and C. Y. Su, “Adaptive and robust stabilization of feedforward nonlinear systems driven by symmetric and non-symmetric dead-zone inputs,” *Asian J. Control*, vol. 16, no. 5, pp. 1437–1447, 2014.
- [7] Y. Li, S. Tong, T. Li, and X. Jing, “Adaptive fuzzy control of uncertain stochastic nonlinear systems with unknown dead zone using small-gain approach,” *Fuzzy Sets and Systems*, vol. 235, pp. 1–24, 2014.
- [8] F. Wang, Z. Liu, and G. Lai, “Fuzzy adaptive control of nonlinear uncertain plants with unknown dead zone output,” *Fuzzy Sets and Systems*, vol. 263, pp. 27–48, 2015.
- [9] C. Hu, B. Yao, and Q. Wang, “Performance-oriented adaptive robust control of a class of nonlinear systems preceded by unknown dead zone with comparative experimental results,” *IEEE/ASME Trans. Mechatronics*, vol. 18, no. 1, pp. 178–189, 2013.
- [10] A. Taware, “Control of sandwich nonlinear systems,” Ph.D. dissertation, University of Virginia, 2001.
- [11] I. U. Ponce, Y. Orlov, L. T. Aguilar, and J. Alvarez, “Sensorless nonsmooth h_∞ -tracking synthesis of servosystems with backlash and coulomb friction,” *IFAC-PapersOnLine*, vol. 48, no. 11, pp. 280–285, 2015.
- [12] X. Luo, X. Wu, and X. Guan, “Adaptive backstepping fault-tolerant control for unmatched non-linear systems against actuator dead-zone,” *IET Control Theory Appl.*, vol. 4, no. 5, pp. 879–888, 2010.

- [13] S. Ibrir, W. Xie, and C.-Y. Su, "Adaptive tracking of nonlinear systems with non-symmetric dead-zone input," *Automatica*, vol. 43, pp. 522–530, 2007.
- [14] A. Smith, S. Gadoue, M. Armstrong, and J. Finch, "Improved method for the scalar control of induction motor drives," *IET Electr. Power Appl.*, vol. 7, no. 6, pp. 487–498, 2013.
- [15] T. Santos, A. Goedel, S. Silva, and M. Suetake, "Scalar control of an induction motor using a neural sensorless technique," *Electric Power Systems Research*, vol. 108, pp. 322–330, 2014.
- [16] M. Suetake, I. da Silva, and A. Goedel, "Embedded dsp-based compact fuzzy system and its application for induction-motor v/f speed control," *IEEE Trans. Ind. Electron.*, vol. 58, no. 3, pp. 750–760, 2011.
- [17] M. Allouche, M. Chaabane, M. Souissi, and D. Mehdi, "Fuzzy tracking control for indirect field-oriented induction machine using integral action performance," *IETE Journal of Research*, vol. 57, no. 5, pp. 443–451, 2011.
- [18] V. Hernandez-Guzman, V. S. ez, and R. Silva-Ortigozac, "Indirect field-oriented control of induction motors is globally asymptotically stable when used to regulate position in rigid robots," *International Journal of Control*, vol. 83, no. 10, pp. 2153–2164, 2010.
- [19] M. Hajian, J. Soltani, and G. A. Markadeh, "Non-linear direct torque control of sensorless induction motor drives with parameter identification and capable

- for very low speeds,” *Electric Power Components and Systems*, vol. 40, no. 15, pp. 1656–1675, 2012.
- [20] S. Wang, C. Tseng, C. Tseng, and C. Yeh, “Speed controller design of direct torque control system for induction motors by using adaptive supervisory fuzzy-cmac,” *Journal of the Chinese Institute of Engineers*, vol. 38, no. 1, pp. 42–56, 2015.
- [21] Y. Zhang, J. Zhu, Z. Zhao, W. Xu, and D. Dorrell, “An improved direct torque control for three-level inverter-fed induction motor sensorless drive,” *IEEE Trans. Power Electron.*, vol. 27, no. 3, pp. 1502–1512, 2012.
- [22] S. Wang, C. Tseng, C. Chang, and J. Chou, “Estimator-based fuzzy credit-assigned cerebellar model articulation controller design for vector-controlled induction motor drives,” *Journal of the Chinese Institute of Engineers*, vol. 37, no. 3, pp. 332–345, 2014.
- [23] S. Rafa, A. Larabi, L. Barazane, M. Manceur, N. Essounbouli, and A. Hamzaoui, “Implementation of a new fuzzy vector control of induction motor,” *ISA Transactions*, vol. 53, pp. 744–754, 2014.
- [24] J. F. Daya, V. Subbiah, and P. Sanjeevikumar, “Robust speed control of an induction motor drive using wavelet-fuzzy based self-tuning multiresolution controller,” *International Journal of Computational Intelligence Systems*, vol. 6, no. 4, pp. 724–738, 2013.

- [25] T. Orłowska-Kowalska, M. Dybkowski, and K. Szabat, “Adaptive sliding-mode neuro-fuzzy control of the two-mass induction motor drive without mechanical sensors,” *IEEE Trans. Ind. Electron.*, vol. 57, no. 2, pp. 553–564, 2010.
- [26] M. Khan and A. Iqbal, “Predictive adaptive model based control of a five-phase induction motor drive,” *International Journal of Modelling and Simulation*, vol. 30, no. 3, pp. 323–332, 2010.
- [27] D. Traor, J. D. Leonb, and A. Glumineau, “Adaptive interconnected observer-based backstepping control design for sensorless induction motor,” *Automatica*, vol. 48, pp. 682–687, 2012.
- [28] R. Trabelsi, A. Khedher, M. Mimouni, and F. Msahli, “Backstepping control for an induction motor using an adaptive sliding rotor-flux observer,” *Electric Power Systems Research*, vol. 93, pp. 1–15, 2012.
- [29] S. Fatemi, N. Abjadi, J. Soltani, and S. Abazari, “Speed sensorless control of a six-phase induction motor drive using backstepping control,” *IET Power Electron.*, vol. 7, no. 1, pp. 114–123, 2014.
- [30] S. Ibrir and C.-Y. Su, “Adaptive stabilization of a class of feedforward nonlinear systems subject to unknown backlash-hysteresis inputs,” *IEEE Trans. Control Syst. Technol.*, pp. 1–13, 2016.

- [31] D. Recker, P. V. Kokotovic, D. Rhode, and J. Winkelmann, "Adaptive nonlinear control of systems containing a dead-zone," *In Proceedings of the 30th IEEE Conference on Decision and Control*, pp. 2111–2115, 1991.
- [32] G. Tao and P. V. Kokotovic, "Adaptive control of plants with unknown dead-zones," *IEEE Trans. Autom. Control*, vol. 39, no. 1, pp. 59–68, 1994.
- [33] —, "Discrete-time adaptive control of systems with unknown dead-zones," *Int. J. Control*, vol. 61, no. 1, pp. 1–17, 1995.
- [34] S. Tong and Y. Li, "Adaptive fuzzy output feedback tracking backstepping control of strict-feedback nonlinear systems with unknown dead zones," *IEEE Trans. Fuzzy Syst.*, vol. 20, no. 1, pp. 168–180, 2012.
- [35] —, "Adaptive fuzzy decentralized output feedback control for nonlinear large-scale systems with unknown dead-zone inputs," *IEEE Trans. Fuzzy Syst.*, vol. 21, no. 5, pp. 913–925, 2013.
- [36] C. Hu, B. Yao, and Q. Wang, "Adaptive robust precision motion control of systems with unknown input dead-zones: A case study with comparative experiments," *IEEE Trans. Ind. Electron.*, vol. 58, no. 6, pp. 2454–2464, 2011.
- [37] J. Zhou, C. Zhang, and C. Wen, "Robust adaptive output control of uncertain nonlinear plants with unknown backlash nonlinearity," *IEEE Trans. Autom. Control*, vol. 52, no. 3, pp. 503–509, 2007.

- [38] G. Y. Gu, C. Y. Su, and L. M. Zhu, “Robust inverse compensation and control of a class of non-linear systems with unknown asymmetric backlash non-linearity,” *IET Control Theory Appl.*, vol. 9, no. 12, pp. 1869–1877, 2015.
- [39] S. Xiao and Y. Li, “Dynamic compensation and h_∞ control for piezoelectric actuators based on the inverse boucwen model,” *Robotics and Computer-Integrated Manufacturing*, vol. 30, p. 4754, 2014.
- [40] J. Zhou, C. Wen, and T. Li, “Adaptive output feedback control of uncertain nonlinear systems with hysteresis nonlinearity,” *IEEE Trans. Control Syst. Technol.*, vol. 57, no. 10, pp. 2627–2633, 2012.
- [41] Z. Liu, G. Lai, Y. Zhang, and C. Chen, “Adaptive neural output feedback control of output-constrained nonlinear systems with unknown output non-linearity,” *IEEE Trans. Neural Netw.*, vol. 26, no. 8, pp. 1789–1802, 2015.
- [42] J. Wei, Y. Hu, and M. Sun, “Adaptive iterative learning control for a class of nonlinear time-varying systems with unknown delays and input dead-zone,” *IEEE/CAA Journal of Automatica Sinica*, vol. 1, no. 3, pp. 302–314, 2014.
- [43] H. Wang, B. Chen, and C. Lin, “Adaptive fuzzy control for pure-feedback stochastic nonlinear systems with unknown dead-zone input,” *International Journal of Systems Science*, vol. 45, no. 12, pp. 2552–2564, 2014.
- [44] A. Boulkroune and M. MSaad, “A fuzzy adaptive variable-structure control scheme for uncertain chaotic mimo systems with sector nonlinearities and

- dead-zones,” *Expert Systems with Applications*, vol. 38, pp. 14 744–14 750, 2011.
- [45] W. He and C. Liu, “Vibration control of a timoshenko beam system with input backlash,” *IET Control Theory Appl.*, vol. 9, no. 12, pp. 1802–1809, 2015.
- [46] S. Tarbouriech, I. Queinnec, and C. Prieur, “Stability analysis and stabilization of systems with input backlash,” *IEEE Trans. Autom. Control*, vol. 59, no. 2, pp. 488–494, 2014.
- [47] Y. Li, S. Tong, and T. Li, “Adaptive fuzzy output feedback control of mimo nonlinear uncertain systems with time-varying delays and unknown backlash-like hysteresis,” *Neurocomputing*, vol. 93, pp. 56–66, 2012.
- [48] K. Chen, J. Wang, Y. Zhang, and Z. Liu, “Adaptive consensus of nonlinear multi-agent systems with unknown backlash-like hysteresis,” *Neurocomputing*, vol. 175, pp. 698–703, 2016.
- [49] Z. Liu, G. Lai, Y. Zhang, X. Chen, and C. Chen, “Adaptive neural control for a class of nonlinear time-varying delay systems with unknown hysteresis,” *IEEE Trans. Neural Netw.*, vol. 25, no. 12, pp. 2129–2140, 2014.
- [50] Z. Zhang, S. Xu, and B. Zhang, “Asymptotic tracking control of uncertain nonlinear systems with unknown actuator nonlinearity,” *IEEE Trans. Control Syst. Technol.*, vol. 59, no. 5, pp. 1336–1341, 2014.

- [51] R. R. elmic and F. L. Lewis, *Deadzone Compensation in Motion Control Systems Using Augmented Multilayer Neural Networks (Adaptive Control of Nonsmooth Dynamic Systems)*. Springer, 2001.
- [52] S. W. Nam, “Adaptive backstepping based online loss minimization control of an induction motor drive,” Master’s thesis, Lakehead University, 2006.
- [53] H. M. Kojabadi, “A novel mras-based adaptive observer for sensorless induction motor drive,” Ph.D. dissertation, University of New Brunswick, 2003.
- [54] K.-Y. Lian, C.-S. C. C.-Y. Hung, and P. Liu, “Induction motor control with friction compensation: An approach of virtual-desired-variable synthesis,” *IEEE Trans. Power Electron.*, vol. 20, no. 5, pp. 1066–1074, 2005.
- [55] A. B. Ebrahim, “Adaptive nonlinear induction motor control,” Ph.D. dissertation, The University of Alabama, 2007.
- [56] M. Krstic, I. Kanellakopoulos, and P. Kokotovic, *Nonlinear and adaptive control design*. John Willey & Sons, Inc., 1995.
- [57] F. Ikhouane, V. Maosa, and J. Rodellar, “Dynamic properties of the hysteretic bouc-wen model,” *Systems & Control Letters*, vol. 56, pp. 197–205, 2007.
- [58] H. K. Khalil, *Nonlinear Systems*. USA: NJ: Prentice Hall, Inc.

Vitae

- Name: Hassan M. Al-Abudib
- Nationality: Saudi
- Date of Birth: 17th of July 1987
- Email: *hassan.alabodib@gmail.com*
- Permenant Address: Qatif, Eastern Province, Saudi Arabia
- Received Bachelor of Science Degree in Electrical and Computer Engineering from the University of Colorado at Boulder in 2010.
- Started graduate program in King Fahd University of Petroleum and Minerals, Electrical Engineering Department in 2013.